

# **SPECIATION OF ACTINIDES AND LANTHANIDES: SPECTROSCOPIC AND MODELING STUDIES**

*By*

**AISHWARYA SOUMITRA KAR**  
**CHEM01200604017**

**Bhabha Atomic Research Centre, Mumbai**

*A thesis submitted to the  
Board of Studies in Chemical Sciences  
In partial fulfillment of requirements  
For the Degree of*

**DOCTOR OF PHILOSOPHY**

*of*

**HOMI BHABHA NATIONAL INSTITUTE**



**SEPTEMBER, 2013**

# HOMI BHABHA NATIONAL INSTITUTE

## Recommendations of the Viva Voce Board

As members of the Viva Voce Board, we certify that we have read the dissertation prepared by **Aishwarya Soumitra Kar** entitled “**Speciation of Actinides and Lanthanides: Spectroscopic and Modeling Studies**” and recommend that it may be accepted as fulfilling the dissertation requirement for the Degree of Doctor of Philosophy.

**Date:**

---

**Chairman:** Prof. K.L. Ramakumar

**Date:**

---

**Guide:** Prof. B. S. Tomar

**Date:**

---

**Member 1:** Prof. A. Goswami

**Date:**

---

**Member 2:** Prof. P.K. Mohapatra

Final approval and acceptance of this dissertation is contingent upon the candidate's submission of the final copies of the dissertation to HBNI. I hereby certify that I have read this dissertation prepared under my direction and recommend that it may be accepted as fulfilling the dissertation requirement.

**Date:**

**Place:**

# **STATEMENT BY AUTHOR**

This dissertation has been submitted in partial fulfillment of requirements for an advanced degree at Homi Bhabha National Institute (HBNI) and is deposited in the Library to be made available to borrowers under rules of the HBNI.

Brief quotations from this dissertation are allowable without special permission, provided that accurate acknowledgement of source is made. Requests for permission for extended quotation from or reproduction of this manuscript in whole or in part may be granted by the Competent Authority of HBNI when in his or her judgment the proposed use of the material is in the interests of scholarship. In all other instances, however, permission must be obtained from the author.

**Aishwarya Soumitra Kar**

# **DECLARATION**

I, hereby declare that the investigation presented in the thesis has been carried out by me.  
The work is original and has not been submitted earlier as a whole or in part for a degree  
/diploma at this or any other Institution / University.

**Aishwarya Soumitra Kar**

*Dedicated to*

*My Parents*

# List of Publications

## REFEREED JOURNALS

1. U(VI) sorption by silica: Effect of complexing anions, **A. S. Kar**, S. Kumar and B.S. Tomar, Colloids and Surfaces A 395 (2012) 240.
2. Time resolved fluorescence spectroscopy and modeling of Eu(III) sorption by silica in presence and absence of alpha hydroxy isobutyric acid, **A. S. Kar**, B.S.Tomar, S.V.Godbole and V.K.Manchanda, Colloids and Surfaces A : Physicochemical and Engineering Aspects 378 (2011) 44.
3. Sorption of curium by silica colloids: Effect of humic acid, **A.S. Kar**, Sumit Kumar, B.S.Tomar and V.K.Manchanda, Journal of Hazardous Materials, 186 (2011) 1961.
4. Spectroscopic investigation on europium complexation with humic acid and its model compounds, **A. Jain**, K. Yadav, M. Mohapatra, S.V. Godbole, B.S. Tomar Spectrochim Acta A 72(5) (2009)1122.
5. Time resolved fluorescence spectroscopy of Eu (III) complexation with  $\alpha$ -hydroxy isobutyric acid, **A. Jain**, M. Mohapatra, S.V. Godbole, B.S. Tomar ,Spectrochimica Acta A: 71(3) (2008) 1007.
6. Effect of humic acid on Sorption of Neptunium by hematite colloids, **Aishwarya Jain**, Sumit Kumar, Neetika Rawat, B. S. Tomar, V. K. Manchanda and S. Ramanathan, Radiochim. Acta 95 (2007) 501.
7. Cm(III) sorption by Silica: Effect of Alpha Hydroxy Isobutyric Acid, **A. S. Kar** and B.S.Tomar, Radiochim. Acta (communicated)

## **SYMPOSIUM**

1. Cm(III) sorption by silica: Effect of alpha hydroxy isobutyric acid, **A.S. Kar** and B.S. Tomar, Nuclear and Radiochemistry Symposium, February 19-23 (2013), Govt. Model Science College, R.D. University, Jabalpur, Madhya Pradesh, pp. 605.
2. U(VI) sorption by silica: Effect of citrate **A. S. Kar**, Sumit Kumar, and B. S. Tomar, 13th International Conference on the chemistry and migration behaviour of actinides and Fission products in geosphere, Sep 18-23 (2011), Peking University, China, , pp. 222.
3. Effect of complexing anions on sorption of uranium on silica, **A. S. Kar**, Sumit Kumar and B.S. Tomar, DAE-BRNS Symposium on Nuclear and Radiochemistry, (NUCAR-2011) February 22-26 (2011), GITAM University, Visakhapatnam, pp.306.
4. Time resolved fluorescence spectroscopy of Eu enhanced dissolution of silica, **A.S.Kar**, M. Mohapatra, S.V.Godbole and B.S.Tomar, Fourth International Symposium on Nuclear Analytical Chemistry (NAC-IV), November 15-19, (2010), Bhabha Atomic Research Centre, Trombay, Mumbai, India, pp. 222.
5. Surface complexation modeling of U(VI) sorption by silica, **A.S.Kar**, Sumit Kumar, B.S.Tomar and V.K.Manchanda Application of Radiotracers in Chemical, Environmental and Biological Sciences, (ARCEBS), Nov. 7-13 (2010), Saha Institute of Nuclear Physics, Kolkata, pp. 143.
6. Time resolved Fluorescence Spectroscopy of Eu(III) sorption by Silica in Presence and Absence of Alpha Hydroxy Isobutyric Acid, **A.S.Kar**, B.S.Tomar, S.V.Godbole and V.K.Manchanda, 12<sup>th</sup> International Conference on the Chemistry and Migration behaviour of Actinides and Fission Products in the Geosphere, Sep 20-25 (2009), Kennewick, WA, USA, pp. 173.

7. Sorption of Curium by silica colloids: Effect of humic acid, **A. S. Kar**, Sumit Kumar, B.S.Tomar and V.K.Manchanda, 12<sup>th</sup> International Conference on the Chemistry and Migration behaviour of Actinides and Fission Products in the Geosphere during September 20-25 (2009), Kennewick, WA, USA, pp. 255.
8. Sorption of Eu(III) onto Silica: A Time Resolved Fluorescence Spectroscopic study, **Aishwarya Jain**, B.S.Tomar, V.Sudarsan, R.K.Vatsa, S.V.Godbole and V.K.Manchanda, DAE-BRNS Symposium on Nuclear and Radiochemistry (NUCAR), Mithibai College, Mumbai, Jan 7-10 (2009) pp. 627.
9. Time Resolved Laser Fluorescence Spectroscopy of U(VI) sorbed onto Silica, **Aishwarya Jain**, B.S.Tomar, V.Sudarsan, R.K.Vatsa and V.K.Manchanda, *ibid.* pp.297.
10. Time resolved Fluorescence studies on Complexation of Eu(III) by  $\alpha$ -hydroxy isobutyric acid, **Aishwarya Jain**, Manoj Mahopatra S.V.Godbole and B.S. Tomar Asian Spectroscopic Conference, Jan 29- Feb 3 (2007), Indian Institute of Science, Bangalore, pp. 160.
11. Sorption of Neptunium on Hematite Colloids, **Aishwarya Jain**, Neetika Rawat, Sumit Kumar, B.S. Tomar, V.K.Manchanda and S.Ramanathan, DAE symposium on Nuclear and Radiochemistry (NUCAR), Feb 14-17 (2007), M.S. University, Baroda, pp. 621.
12. Thermodynamic study of Np(V) - humate complexation, Neetika Rawat, **Aishwarya Jain**, Sumit Kumar, B.S. Tomar and V.K. Manchanda, *ibid.* pp. 217.
13. Time resolved fluorescence studies on complexation of Eu(III) by  $\alpha$ -hydroxy isobutyric acid, **Aishwarya Jain**, S.V.Godbole and B.S. Tomar *ibid.* pp. 331.

# ACKNOWLEDGEMENTS

This thesis would not have been accomplished without the support and encouragement of numerous people including my well wishers, my friends and colleagues who contributed in many ways to the successful completion of this thesis.

First and Foremost, I would like to express my sincere gratitude to my research guide Dr. ***B.S. Tomar*** for the continuous support, patience, motivation, and enthusiasm. Whatever I learnt in the field of actinide speciation is because of him. His encouragement, immense knowledge and experience helped me in overcoming all the hurdles not only during the course of my Ph.D but in all spheres of life. I owe my deep sense of gratitude for his unimaginable support and inspiration. I could not have imagined having a better guide and mentor for my Ph.D. study.

Besides my advisor, I would like to thank members of my doctoral committee; ***Prof. K.L. Ramakumar, Prof. V.K. Manchanda, Prof. A. Goswami, and Prof. P.K. Mohapatra*** for their time, encouragement, thoughtful ideas and critical evaluation during the course of Ph.D. My sincere thanks are due to ***Dr. Neetika Rawat, Dr. Sumit Kumar, and Ms. Sharayu Kasar*** for all their precious help, simulating discussions and cooperation.

I am heartily thankful to my collaborators at ***Shri M. Mohapatra, Dr. S.V. Godbole*** (RCD), ***Dr. S. Ramanathan*** (MSD), ***Dr. R. K. Vatsa, Dr V. Sudersan*** (CD) for their help, cooperation and suggestions during the course of the work. I would also like to thank my colleagues ***Dr. M. S. Murali, Dr. P. N. Pathak, Dr. A. Bhattacharyya, Dr. S. Ansari, Dr. S. Sodye, Shri D. R. Prabhu, Shri A.S. Kanekar, Shri. S. K. Gupta, Shri. K.K. Yadav, Ms. Neelam, Ms. Sanhita, Ms Priya, Ms. Ruma, all members of RACD with Dr. R. M. Sawant, Dr. Ankita, Ms. Manjulata, Shri. Rammohan*** in particular, ***Shri T. V. Vithal Rao*** for their help, encouragement and support during the course of the research work.

I am blessed to have friends who are constant source of laughter, joy and support. I would like to thank all my friends *Vinita, Dheeraj, Renu, Raj Kishore, Sangeeta, Chhavi, Shankar, Sachin and Parimal* who always stood by me and lend constant encouragement and support. I would also like to thank all *my training school batch mates* for their warm friendship which helped in sailing through all hardships.

I would like to acknowledge all the *teachers*; I learnt from since my childhood, I would not have been here without their guidance, blessings and support.

Finally, I would like to acknowledge the people who mean the world to me, *my family*. I would like to thank *my parents* for their unconditional love, support, faith, encouragement and confidence in me. They have been my driving force and inspiration in all pursuits of life. I owe all my accomplishments to them. My *sister (Parul)* and *brother (Bharat)* have been constant source of love and confidence and their belief and hope helped in overcoming all hurdles of my life. I would like to thank my *parents in laws* for their unconditional support and faith. I would also like to thank my *sister in laws (Sonali, Shweta & Sneha)* and *brother in laws (Vipin & Somendra)* for constant encouragement and support. I run short of words in expressing my gratitude towards my husband *Soumitra* who always stood by me and encouraged me up at every step of life. He has faith in me and my intellect which helped me to keep things in perspective. He is everything for me, without his love and understanding I would not have been able to make it. I would like to express thanks to my *daughter Arunima* who in her own way geared me up to reach the goal. Thanks are due to my *nephews (Divit and Homi)* and my *niece (Aadya)* for their love which gave me strength to pursue my Ph.D.

Lastly, I would like to thank everybody who was important in the successful realization of this thesis, as well as apologize that I could not mention everyone personally.

*Aishwarya Soumitra Kar*

## LIST OF ABBREVIATIONS

Low Level Waste	<b>LLW</b>
Intermediate Level Waste	<b>ILW</b>
High Level Waste	<b>HLW</b>
Low Molecular Weight Carboxylic Acid	<b>LMCA</b>
Humic Substances	<b>HS</b>
Fulvic Acid	<b>FA</b>
Humic Acid	<b>HA</b>
Time Resolved Laser Induced Fluorescence spectroscopy	<b>TRLFS</b>
Extended X-ray Absorption Fine Structure	<b>EXAFS</b>
X-ray Photoelectron Spectroscopy	<b>XPS</b>
Nuclear Magnetic Resonance	<b>NMR</b>
Time Resolved Fluorescence Spectroscopy	<b>TRFS</b>
Surface Complexation Modeling	<b>SCM</b>
Distribution Coefficient	<b>K<sub>D</sub></b>
Alpha Hydroxy Isobutyric Acid	<b>HIBA</b>
Succinic Acid	<b>SA</b>
Phthalic Acid	<b>PA</b>
Mandelic Acid	<b>MA</b>
X-Ray Diffraction	<b>XRD</b>
Brunauer- Emmett- Teller	<b>BET</b>
Inductively Coupled Plasma-Atomic Emission Spectroscopy	<b>ICP-AES</b>
Total Organic Carbon	<b>TOC</b>
Bhabha Atomic Research Center	<b>BARC</b>
Photo Multiplier Tube	<b>PMT</b>
High Purity Germanium Detector	<b>HPGe</b>
Time Correlated Single Photon Counting	<b>TCSPC</b>
Constant Fraction Discriminator	<b>CFD</b>
Time-to-Amplitude Converter	<b>TAC</b>
Linear Additive Modeling	<b>LAM</b>
Constant Capacitance Model	<b>CCM</b>
Diffuse Layer Model	<b>DLM</b>
Dissolved Organic Matter	<b>DOM</b>
Coordination Environment diagram	<b>CE diagram</b>

# CONTENTS

	Page No.
<b>SYNOPSIS</b>	<b>1</b>
<b>LIST OF FIGURES</b>	<b>14</b>
<b>LIST OF TABLES</b>	<b>22</b>
 <b>CHAPTER-I</b>	
<b>INTRODUCTION</b>	
<b>1.1. Historical perspective of actinides</b>	<b>24</b>
<b>1.2. Sources of actinides in the environment</b>	<b>26</b>
<i>1.2.1. Natural occurrence</i>	<b>26</b>
<i>1.2.2. Nuclear weapon testing and accidents</i>	<b>28</b>
<i>1.2.3. Disintegration of Nuclear powered satellites</i>	<b>28</b>
<i>1.2.4. Nuclear power plants</i>	<b>29</b>
<i>1.2.4.1. Mining and milling</i>	<b>29</b>
<i>1.2.4.2. Nuclear fuel reprocessing</i>	<b>30</b>
<b>1.3. Classification and management of radioactive waste</b>	<b>31</b>
<i>1.3.1. Solid radioactive waste</i>	<b>31</b>
<i>1.3.2. Gaseous radioactive waste</i>	<b>32</b>
<i>1.3.3. Liquid radioactive waste</i>	<b>32</b>
<i>1.3.3.1. Exempt waste</i>	<b>32</b>
<i>1.3.3.2. LLW</i>	<b>32</b>
<i>1.3.3.3. ILW</i>	<b>33</b>
<i>1.3.3.4. HLW</i>	<b>33</b>
<i>1.3.3.4.a. Vitrification of HLW in Glass Matrix</i>	<b>34</b>
<i>1.3.3.4.b. Interim storage of solidified waste</i>	<b>34</b>
<i>351.3.3.4.c. Disposal in deep geological repositories</i>	<b>34</b>
<b>1.4. Actinide Chemistry in natural water systems</b>	<b>36</b>
<i>1.4.1. General Actinide Chemistry</i>	<b>36</b>
<i>1.4.1.1. Electronic Configuration</i>	<b>36</b>
<i>1.4.1.2. Oxidation State</i>	<b>39</b>
<i>1.4.1.3. Ion types</i>	<b>40</b>

1.4.1.4. Lanthanide and actinide contraction: Effect on ionic radius	40
1.4.2. Environmental Actinide Chemistry	41
1.4.2.1. Oxidation States of Actinides in solution	42
1.4.2.2 Hydration	45
1.4.2.3. Hydrolysis of actinide cations	46
1.4.2.4. Complexation of actinides	49
1.4.2.4. (a) Complexation by inorganic anions	50
1.4.2.4.(b) Complexation by organic anions	52
1.4.2.5. Colloid formation	56
1.4.2.5. (a) Intrinsic Colloids	57
1.4.2.5. (b) Pseudo Colloids	58
1.4.2.6. Reactions at the mineral/water interface	59
1.5. Need for Spectroscopic techniques to study actinide speciation	61
1.6. Need of Modeling Actinide Sorption using Geochemical Codes	63
1.7. Motivation for the present work	64
1.8. Scope of the thesis	66
<b>CHAPTER-II</b>	
<b>Experimental Methods and Techniques</b>	
2.1. Introduction	68
2.2. Preparation and Purification of Radiotracers:	68
2.2.1. Neptunium tracer	68
2.2.2. Uranium tracer	69
2.2.3. Curium tracer	69
2.2.4. Europium tracer	70
2.3. Synthesis of hematite	70
2.4. Radiometric Techniques	70
2.4.1. Liquid Scintillation Counter	70
2.4.2. NaI(Tl) Scintillation Counter	71
2.4.3. HPGe	72
2.5. XRD	73
2.6. BET Surface Area Analyser	74
2.7. UV-Visible Spectrophotometry	75
2.8. ICP-AES	77

<b>2.9. Determination of Zeta potential</b>	<b>78</b>
<b>2.10. TOC Analyser</b>	<b>80</b>
<b>2.11. TRFS</b>	<b>81</b>
<b>2.11.1. Principle of TRFS</b>	<b>82</b>
<b>2.11.2. Instrumentation</b>	<b>84</b>
<b>2.11.2.1. Xenon flash lamp</b>	<b>84</b>
<b>2.11.2.2. Monochromator</b>	<b>84</b>
<b>2.11.2.3. TCSPC</b>	<b>85</b>
<b>2.11.2.4. CFD</b>	<b>87</b>
<b>2.11.3. Data treatment and Error analysis</b>	<b>88</b>
<b>2.12. <math>K_D</math> determination of radionuclides</b>	<b>91</b>
<b>2.12.1. Experimental Details</b>	<b>92</b>
<b>2.12.2. Error determination on sorption data</b>	<b>93</b>
<b>2.13. Modeling of sorption data</b>	<b>93</b>
<b>2.13.1. LAM</b>	<b>94</b>
<b>2.13.2. SCM</b>	<b>95</b>
<b>2.13.2.1. CCM</b>	<b>97</b>
<b>2.13.2.2. DLM</b>	<b>97</b>
<b>2.13.3. FITEQL 4.0</b>	<b>100</b>
<b>2.13.4. MINTEQA2</b>	<b>101</b>

## ***CHAPTER-III***

### **Europium Complexation with LMCA and HA**

<b>3.1. Introduction</b>	<b>102</b>
<b>3.2 Experimental</b>	<b>109</b>
<b>3.2.1. Reagents used</b>	<b>109</b>
<b>3.2.2. Preparation of stock solutions</b>	<b>109</b>
<b>3.2.2.1. Eu(III) stock solution</b>	<b>109</b>
<b>3.2.2.2. LMCA stock solutions</b>	<b>109</b>
<b>3.2.3. Preparation of samples</b>	<b>110</b>
<b>3.2.3.1. Eu-HIBA</b>	<b>110</b>
<b>3.2.3.2. Eu-PA</b>	<b>110</b>
<b>3.2.3.3. Eu-MA</b>	<b>110</b>

3.2.3.4. Eu-SA	111
3.2.3.5. Eu-HA	111
3.3. Relationship between lifetime and the coordinated water molecules	111
3.4. Results and Discussion	113
3.4.1. Eu –HIBA	113
3.4.1.2. Determination of Stability constants from Intensity ratio( $I_{616}/I_{592}$ )	116
3.4.2. Eu-PA	122
3.4.3. Eu-MA	124
3.4.4. Eu-SA	125
3.4.5. Eu-HA	127
3.5. Conclusions	131

## ***CHAPTER-IV***

### **Sorption of Trivalent Actinides/Lanthanides: Effect of Complexing Anions**

4.1. Introduction	132
4.2. Experimental	137
4.2.1 Materials and characterization	137
4.2.2. Batch Sorption Experiments	137
4.2.3. Silica dissolution studies	139
4.2.4. Sorption of HIBA by silica	139
4.2.5. TRFS measurements	139
4.3. Results and discussion	140
4.3.1 Characterization of Silica	140
4.3.2. Silica Dissolution Studies	140
4.3.3. Speciation Calculations	141
4.3.4. Kinetics study of sorption of Cm (III) by silica colloids	146
4.3.5. Sorption of Cm (III) by silica: Effect of HA	148
4.3.5.1. LAM of ternary system	151
4.3.6. Sorption of Cm (III) by silica: Effect of ionic strength	152
4.3.7. Sorption of Cm (III) by silica: Effect of HA concentration	155
4.3.8. Sorption of Cm (III) by silica: Effect of HIBA concentration	155

4.3.9. SCM	157
4.3.9.1. SCM of binary systems	158
4.3.9.2. SCM of ternary systems	158
4.3.9.2. (a) Silica-Cm-HIBA(I) system ([HIBA] =10 <sup>-5</sup> M)	159
4.3.9.2. (b) Silica-HIBA(I)-Cm system ([HIBA] =10 <sup>-5</sup> M)	160
4.3.9.2. (c) Silica-Cm-HIBA(II) system ([HIBA] =10 <sup>-3</sup> M)	160
4.3.9.2. (d) Silica-HIBA(II)-Cm system ([HIBA] =10 <sup>-3</sup> M)	161
4.3.10. Sorption of Eu(III) by silica: Effect of HIBA concentration	163
4.3.10. 1. TRFS	165
4.3.10.2. SCM	170
4.3.11. Comparison of Silica-Cm(III) and Silica-Eu(III) systems	172
4.3.12. Comparison of Silica-HIBA(I)-Cm and Silica-HA-Cm systems	175
4.4. Conclusions	176

## **CHAPTER-V**

### **Sorption of uranium by silica: Effect of Complexing anions**

5.1. Introduction	178
5.2. Experimental	182
5.2.1. Materials	182
5.2.2. Batch Sorption Studies	182
5.2.3. Silica dissolution studies	183
5.2.4. TRFS	183
5.3. Results and Discussion	183
5.3.1. Sorption data	183
5.3.1.1. Effect of U(VI) concentration and ionic strength	183
5.3.1.2. Effect of complexing anions	186
5.3.2. Silica dissolution studies	187
5.3.3. Speciation calculations	188
5.3.4. TRFS	192
5.3.4.1. Determination of number of water molecules	197
5.3.5. SCM	198
5.3.5.1. SCM of binary systems	199
5.3.5.2. SCM of ternary systems	206

5.4. Conclusions	208
------------------	-----

## **CHAPTER-VI**

### **Sorption of Neptunium on Hematite: Effect of HA**

6.1. Introduction	209
6.2. Experimental	214
6.2.1. Synthesis and characterization of hematite colloids	214
6.2.2. Characterization of HA	214
6.2.3. Preparation of <sup>239</sup> Np tracer	214
6.2.4. Measurement of the stability constant of Np-HA complex	215
6.3 Sorption Experiments	216
6.3.1. Sorption of Np(V) on hematite under aerobic condition	216
6.3.2 Sorption of HA on hematite	216
6.3.3. Sorption of neptunium on hematite under anaerobic condition	217
6.4 Results and Discussion	217
6.4.1. Characterization of hematite	217
6.4.2. Determination of stability constant of Np-HA complex	219
6.4.3. Sorption of HA on hematite	221
6.4.4. Sorption of Neptunium on hematite colloids in aerobic conditions: Effect of HA	221
6.4.4.1. LAM of sorption data	224
6.4.5. Sorption of Neptunium on hematite colloids in anaerobic conditions: Effect of HA	224
6.5. Conclusions	226

## **CHAPTER-VII**

<b>Summary &amp; Conclusions</b>	227
----------------------------------	-----

<b>BIBLIOGRAPHY</b>	232
---------------------	-----

## **SYNOPSIS**

Nuclear energy is envisaged to have a significant share of the total electricity consumption in the coming decades as the other fossil fuel based energy sources, viz., coal, oil and gas start depleting. However, the expansion of the nuclear energy programmes would bring in the challenge of maintaining the growing nuclear wastes in the confines of their repositories, so that the future generations are not adversely affected by the radiations emitted by the actinides and long lived fission products. Hence if the nuclear energy has to achieve wider acceptance as a viable major alternative to the other major energy sources, it has to satisfy the stringent regulations on the level of radioactivity in the biosphere [1].

Actinides and long lived fission products can enter into the biosphere through various modes of human activity, such as, (i) atmospheric as well underground nuclear tests by the nuclear weapon countries over the past seven decades, (ii) accidental release of radioactivity from operating nuclear power and spent fuel reprocessing plants, and (iii) reentry of nuclear powered ( $^{238}\text{Pu}$  bearing) satellites into the earth's atmosphere [2]. However, the largest source of radioactivity which will remain in the geosphere for hundreds of thousands of years is the spent nuclear fuel after it has been removed from the nuclear reactor. Some of the major nuclear powered countries, viz., USA, Britain, do not reprocess the spent nuclear fuel and store it as such and propose to bury it in a deep geological repository in the future. In some countries, such as France and India, the spent nuclear fuel is reprocessed to recover the plutonium and unburnt uranium for use in the next stage of their atomic energy programme, viz., fast breeder reactors. The HLW generated during the reprocessing of the spent nuclear fuel is at present being stored in interim storage facilities and will essentially be buried in deep geological repositories, so that the long lived radionuclides do not enter the biosphere

even after hundreds of thousands of years. Thus the deep geological repositories will be housing the major proportion of the spent nuclear fuel and /or high level radioactive waste depending upon whether the spent fuel is stored as it is or reprocessed [3].

In order to ensure the safety of the future generations from the ionizing radiations emitted by actinides and long lived fission products present in the geosphere in different forms, mentioned above, it is essential to predict their migration behavior from their origin to the biosphere. Performance assessment of the deep geological repository, in retaining the actinides and long lived fission products, is an important exercise towards this objective. The studies carried out as a part of this thesis, form a part of these exercises and help in understanding the migration behavior of actinides and long fission products from the repository to the surrounding aquatic environment and thereby to the sphere of human activity.

The actinide isotopes of concern from the point of view of their impact on the biosphere are, the long lived isotopes of trans-uranium elements, namely, neptunium ( $^{237}\text{Np}$ ), plutonium ( $^{239,240,242}\text{Pu}$ ), americium ( $^{241,243}\text{Am}$ ) and curium ( $^{245}\text{Cm}$ ), which are formed during the burning of uranium based fuels in the nuclear reactors [4]. The future nuclear reactors, based on thorium will also produce long lived isotopes of uranium ( $^{233}\text{U}$ ) and protactinium ( $^{231}\text{Pa}$ ). The long lived fission products, which will be present in the HLW even after hundreds of thousands of years, constitute  $^{99}\text{Tc}^g$ ,  $^{129}\text{I}$ ,  $^{135}\text{Cs}$ , etc.

During the last two decades extensive studies have been carried out worldwide to understand the migration behavior of these long lived radionuclides in the environment, the compilation of which has recently appeared in the form of

comprehensive review [5]. The different pathways through which the actinides and long lived fission products can migrate into the environment are [6]:

(i) Precipitation in the form of hydroxides under the conditions of ground water, viz.,  $\text{Pu}(\text{OH})_4$ , which has extremely low solubility product ( $\sim 10^{-58}$ ). Precipitation will result in the retardation of the radionuclides in the environment. In fact, it is estimated that the bulk of the plutonium used in nuclear weapon tests in the oceans has been deposited at the ocean bed as hydroxide [7].

(ii) Complexation with inorganic and organic anions present in ground water, e.g., carbonate, oxalate, citrate, humate, fulvate, etc. The soluble complexes will enhance the migration of the long lived radionuclides. For instance uranium is present in carbonate complex form, e.g.,  $\text{UO}_2(\text{CO}_3)_2^-$ , which is the dominant soluble complex of uranium in sea water [8].

(iii) Colloid formation: Higher valent actinides and fission products, e.g., Pu(IV), Th(IV), Tc(IV), etc., upon entry into water get hydrolysed and form species, such as,  $\text{M}(\text{H}_2\text{O})_{n-1}(\text{OH})^{3+}$ , which undergo further hydrolysis and subsequently aggregate to form polymeric species and ultimately form colloidal particles depending upon the total metal ion concentration. These intrinsic colloids have been found to be highly mobile and hence are considered to be one of the important pathways for the radionuclide migration. Alternatively, the radionuclides may get adsorbed onto the colloidal particles made of mineral oxides of silicon, aluminium, titanium, iron, etc. and form pseudo-colloids. Migration of plutonium in the Nevada deserts from the nuclear test site to nearby underground water was found to have been facilitated by colloids formation [9].

(iv) Adsorption by sediments and rocks in the vicinity of the water bodies is another pathway for the radionuclides in the aquatic environment. This process will

significantly retard the radionuclide migration in aquatic environment. In fact high retention property of certain clays and rocks enables them to be used as a part of the engineered barrier in the deep geological repository [10].

The study of different species in which the actinides and long lived fission products are present in the environment is called as speciation, which is a frontier area of research in the field of radiochemistry, particularly with regard to actinides. The speciation studies consist of identifying the physical state (solid, soluble or gaseous state), and chemical state (oxidation state and structure of the species) of the radionuclide. As the migration behavior of actinides and long fission products is highly dependent upon their speciation, extensive studies have been devoted on the investigation of speciation of these elements under the different environmental conditions in the laboratory as well as under field conditions.

**Literature review:** The migration behavior of radionuclides in the aquatic environment had previously been studied using the  $K_D$  approach, wherein the  $K_D$  of the radionuclides between the ground water and the soil/sediment was used to deduce the retention factor, which is a measure of the mobility of the radionuclide in the geosphere [11-12]. However, the  $K_D$  approach does not provide a realistic assessment of the migration behavior of the radionuclides as the species sorbed onto the soil/sediment varies depending upon the concentration of the element, pH, ionic strength and presence of complexing anions in the ground water, thereby resulting in wide variation in the  $K_D$  depending upon the site [13]. During the past one decade, SCM has gained much popularity and acceptance among the geochemical community to infer about the radionuclide migration in the geosphere [14]. In this model, the complexation of the metal ion with the surface sites as well as with the complexing anions present in water are considered explicitly along with the correction for

electrostatic interaction between the charged species [15]. Therefore, the model can provide quite reliable data on the migration behavior of the radionuclides once the composition of the soil/sediment and the ground water are known. The validation of the SCM is usually done by characterization of the complexes and the sorbed species using the spectroscopic techniques. The common spectroscopic techniques that have been employed for the characterization of the complexes and sorbed species are TRFS, EXAFS, XPS, etc [16-20].

**Motivation for the present work:** Though a large number of studies have been carried out during the past decade on the speciation of actinides and long lived fission products [21-23], the mechanistic understanding of even the sorption of the radionuclides by the simple mineral oxides is not yet completely understood, owing to the complexity of the surface sites, the difference between the metal ion concentrations at which the sorption experiments and spectroscopic studies can be carried out [24,25]. In addition, some of the natural organic complexing anions, viz., humate and fulvate have complex structure and binding sites, which are a challenge to understand fully even now [26,27]. Further, whether the small organic molecules, having similar binding sites as humate, fulvate, can be used as model compounds for these large macromolecules is still not resolved.

With this in view, attempt was made in the present dissertation work to investigate, (i) the complexation of trivalent actinides, using Eu(III) as a chemical analogue, by small carboxylate and hydroxyl carboxylate complexing anions as well as by HA by TRFS, (ii) effect of HA on the sorption of neptunium by hematite under varying conditions of pH, (iii) effect of HA on the sorption of curium by silica under varying conditions of pH, ionic strength and addition order of metal ion and the complexing anion, (iv) effect of HIBA on the sorption of Cm(III) and Eu(III) by silica

under varying experimental conditions of pH, metal ion concentration and addition order of the metal ion and the ligand, and (v) effect of carbonate and citrate on the sorption of U(VI) by silica under varying conditions of pH. The sorption data have been modeled using the SCM and wherever possible the surface species have been characterized by the spectroscopic techniques, mainly TRFS. The thesis has been divided into seven chapters. A brief description of the different chapters is given below.

**Chapter 1:** In this chapter the historical background of the growing demand for the nuclear energy is given, which is followed by the challenges faced by the nuclear scientists in mitigating the adverse effects of ionizing radiations emitted from the actinides and long lived fission products to reach the public domain. The subject of actinide speciation is dealt with in detail to highlight the scientific pursuit which the radiochemists world-wide are following to understand the mechanism of the interaction of the actinides and long lived fission products with the different components of the geospheres. This is followed by a review of the existing literature in the field of actinide speciation, in general, and the complexation of actinides by the environmentally important ligands as well as their sorption by the simple mineral oxides of Si, Al, Fe, etc, in particular. The chapter ends with the motivation for the work carried out as a part of the present thesis.

**Chapter-2:** In this chapter, the various experimental methods and theoretical models used in the present thesis have been described. Mainly TRFS has been used for the complexation studies of Eu(III) as a chemical analogue of Am(III) and Cm(III). The excitation source in the form of xenon flash lamp is used to excite the metal ion and the spectral and temporal profiles are measured using the spectrometer system. Batch method using radiotracers has been used for studying the sorption of actinides by

different mineral oxides. In some cases, other techniques, such as, ICP-AES has also been used, particularly for studying the dissolution of the mineral oxides. TRFS has also been used for the characterization of sorbed species. Modeling of the sorption data has been carried out using SCM.

**Chapter 3:** In this chapter the studies on the complexation of Eu(III) by carboxylate and hydroxy carboxylate ligands using TRFS technique have been discussed. Fluorescence emission spectrum of  $\text{Eu}^{3+}$  ion contains the emission lines at 580, 592, 616, 650 and 700 nm due to the de-excitation of the  $^5\text{D}_0$  excited state to the  $^7\text{F}_j$  states, with  $j=0-4$ . The transition at 592 nm ( $^5\text{D}_0 \rightarrow ^7\text{F}_1$ ) is magnetic dipole in nature and hence is insensitive to the change in the chemical environment around the metal ion. On the other hand the transition at 616 nm ( $^5\text{D}_0 \rightarrow ^7\text{F}_2$ ) is of electric dipole type and hence is sensitive to the change in the chemical environment around the metal ion. Thus the ratio of the intensity of 616 to 592 nm peaks, commonly called as the asymmetry ratio is a measure of the extent of complexation of Eu(III) by the ligand. This fact has been utilized in the present work to determine the stability constant of the Eu(III)-complexes with HIBA, SA, PA and MA [28,29]. The intensity ratio data were corroborated by the life time data to arrive at the number of water molecules bound to the metal ion and thereby the stoichiometry of the complex. Attempt was also made to investigate the complexation of Eu(III) by HA, but the data were affected by the quenching of the Eu(III) fluorescence by HA, particularly at the higher HA concentrations.

**Chapter 4:** In this chapter, the results of the sorption of Cm(III) and Eu(III) by silica in presence of complexing anions such as HA and HIBA have been described.  $^{244}\text{Cm}$  and  $^{152}\text{Eu}$  were used as the tracers for the respective metal ions. In the case of Cm(III)-HA-silica system, the sorption of Cm(III) by silica was strongly influenced

by the presence of HA both at low and high pH regions. While, in the low pH range (4-6) the sorption was enhanced in presence of HA, it was strongly decreased at higher pH (7-8). This was explained in terms of the sorption behaviour of HA by silica. HA is strongly sorbed by silica at low pH values and the sorption decreases with increasing pH. At lower pH the mineral bound HA complexes the metal ion in the solution thereby enhancing the sorption, while at higher pH HA is predominantly in the solution and hence complexation of Cm(III) by HA in solution results in decreased sorption at these pH values. Interestingly, the effect of HA was different in the different addition order of Cm(III) and HA to the silica suspension. When HA was added before Cm(III), the decrease in the Cm(III) sorption was much more than that when Cm(III) was added first. This was explained in terms of the incorporation of Cm(III) in the silica matrix, which results in slow kinetics of desorption of sorbed Cm(III) by the HA in the solution [30]. With a view to compare the effect of HA and HIBA on the sorption behavior of Cm(III) by silica, similar experiments were also carried out in presence HIBA [31]. It was observed that the effect of HIBA was quite different from that of HA, indicating the small organic molecules behave differently than the large macromolecules, such as, HA. The sorption data were also fitted with the help of SCM using the computer code FITEQL to determine the nature of the sorbed species. Further, the spectroscopic characterization of the sorbed species was also carried out using TRFS with Eu(III) as a probe [32].

**Chapter 5:** In this chapter, the results of the studies on the sorption of U(VI) by silica in presence of two complexing anions, namely, carbonate and citrate has been described. Citrate was found to strongly decrease the sorption of U(VI) by silica at lower pH values, unlike carbonate which did not have significant effect at least up to the pH value 8. The batch sorption data were modeled using the SCM. Attempts have

also been made to characterize the sorbed species by TRFS [33]. The observations of the present work have been discussed in the light of the existing literature on similar systems. Some of the literature data have also been modeled and the results are consistent with that obtained in the present work.

**Chapter 6:** In this chapter the results of the sorption of neptunium by hematite under normal and reducing conditions have been described.  $^{239}\text{Np}$  was used as a tracer for neptunium owing to its gamma lines and short half life. Hematite was synthesized in-house and was characterized by XRD, dynamic light scattering and BET surface area. Under normal atmospheric conditions neptunium exists as Np(V) in pH range, which in presence of reducing agents, such as, sodium dithionate, was reduced to Np(IV), which has a strong tendency to sorb on the mineral oxides. It was observed that Np(IV) is much more strongly sorbed by hematite compared to Np(V) at all pH values. Further, in presence of HA, the sorption of Np(IV) was enhanced at low pH, which was explained in terms of the sorption of HA by hematite and the complexation of the metal ion by HA. At higher pH values, HA does not affect the sorption of Np(IV) on hematite [34].

**Chapter 7:** In this chapter the results of the work carried out as a part of the thesis have been summarized. TRFS was successfully used for determination of the stability constants of Eu(III)-complexes with carboxylate and hydroxyl carboxylate anions. The complexation behavior of small organic molecules towards Eu(III) was found to be different from that of HA. This was observed in complexation as well as in sorption studies. The order of addition of metal ion and the HA was found to have distinctly different effect on the sorption behavior of Cm(III) by silica. The study revealed the role of dissolved silica in governing the sorption behavior of Cm(III) by silica.

**References:**

1. K.D. Crowley, Nuclear waste disposal: The technical challenges, *Physics Today*, 50 (1997) 32.
2. L. R. Morss, N. M. Edelstein, J. Fuger, *The Chemistry of the Actinides and Transactinide Elements*, Fourth edition, 2010, Springer, The Netherlands.
3. Moving forward with geological disposal of Radioactive waste- A collective statement by the NEA Radioactive Waste Management Committee, OECD/NEA No. 6433 (2008).
4. K. H. Lieser, Radionuclides in the Geosphere: Sources, Mobility, Reactions in Natural waters and Interactions with Solids, *Radiochim. Acta* 70/71 (1995) 355.
5. H. Geckeis, J. Lützenkirchen, R. Polly, T. Rabung, M. Schmidt, Mineral–Water Interface Reactions of Actinides, *Chem. Rev.* 113, (2013) 1016.
6. R. J. Silva and H. Nitsche, Actinide environmental chemistry, *Radiochim. Acta* 70/71, (1995) 377.
7. G.R. Choppin, Actinide speciation in aquatic systems, *Mar. Chem.* 99 (2006) 83.
8. G.R. Choppin, Soluble rare earth and actinide species in sea water. *Mar. Chem.* 28 (1989) 19.
9. A. B. Kersting, D. W. Efur, D. L. Finnegan, D. J. Rokop, D. K. Smith, J. L. Thompson, Migration of plutonium in ground water at the Nevada Test Site. *Nature* 397 (1999) 56.
10. J. I. Kim, Significance of actinide chemistry for the long-term safety of waste disposal, *Nucl. Eng. Technol.* 38(2006) 459.
11. R. G. Wilhelm, Understanding variation in partition coefficients,  $K_D$ , values, Volume III: Review of Geochemistry and Available  $K_D$  Values for Americium,

- Arsenic, Curium, Iodine, Neptunium, Radium, and Technetium, EPA 402-R-04-002C (2004).
12. M. Sutton, Review of Distribution Coefficients for Radionuclides in Carbonate Minerals, LLNL-SR-415700 (2009).
  13. W. Stumm and J. J. Morgan, Aquatic chemistry: Chemical equilibria and rates in natural waters, Third edition, 996, John Wiley & Sons, New York, USA.
  14. J. Westall, H. Hohl A comparison of electrostatic models for the oxide/solution interface. *Adv. Coll. Int. Sci.* 12 (1980) 265.
  15. D. A. Dzombak, F. M. Morel, Surface Complexation Modeling: hydrous ferric hydroxide, Wiley-Interscience, New York, 1990.
  16. Th. Rabung, M.C. Pierret, A. Bauer, H. Geckeis, M.H. Bradbury, B. Baeyens, Sorption of Eu(III) / Cm(III) on Ca-montmorillonite and Na-illite. Part 1: Batch sorption and time-resolved laser fluorescence spectroscopy experiments, *Geochim. Cosmochim. Acta* 69 (2005) 5393.
  17. Th Rabung, Th. Stumpf, H. Geckeis, R. Klenze, J.I. Kim, Sorption of Am(III) and Eu(III) onto  $\gamma$ -alumina: experiment and modeling, *Radiochim Acta* 88 (2000) 711.
  18. M.L. Schlegel, I. Pointeau, N. Coreau, P. Reiller, Mechanism of europium retention by calcium silicate hydrates: An EXAFS study, *Environ. Sci. Technol.* 38 (2004) 4423.
  19. T. Stumpf, H. Curtius, C. Walther, K. Dardenne, K. Ufer, T. Fanghanel, Incorporation of Eu(III) into hydrotalcite: A TRLFS and EXAFS study, *Environ. Sci. Technol.* 41 (2007) 3186.
  20. F. Mercier, C. Alliot, L. Bion, N. Thomat, P. Toulhoat, XPS study of Eu(III) coordination compounds: Corelevels binding energies in solid mixed-oxo-compounds  $\text{Eu}_m\text{X}_x\text{O}_y$ . *J. Electron Microsc. Rel. Phenom.* 150 (2006) 21.

21. M. D. Siegel and C. R. Bryan, Environmental Geochemistry of radioactive contamination, Handbook of geochemistry, 206, 2004.
22. J. Bruno and V. Montoya, From aqueous solution to solid solutions: A process oriented review of the work performed within the FUNMIG project, App. Geochem., 27 (2012) 444.
23. B. E. Johnson, P. H. Santschi, C. Y. Chuang, S. Ootosaka, Collection of lanthanides and actinides from natural waters with conventional and nanoporous Sorbents, Environ. Sci. Technol. 46 (2012) 11251.
24. S. Kumar, S. V. Godbole and B. S. Tomar, Speciation of Am(III)/Eu(III) sorbed on  $\gamma$ -Alumina: effect of metal concentration, Radiochim. Acta 101 (2013) 73.
25. S. Kumar, A.S. Kar, B. S. Tomar, D. Bhattacharya, XAFS Spectroscopy study of Eu(III) sorption products on amorphous silica and  $\gamma$ -alumina: Effect of pH and substrate, Polyhedron, 33 (2012) 33.
26. Choppin, G.R., Role of humics in actinide behaviour in ecosystem. In Chemical Separation technologies and related methods of nuclear waste management, eds. G.R. Choppin and M.Kh Khankhasayev, Kluwer Academic Publishers 1999, p247.
27. N. D. Bryan, L. Abrahamsen, N. Evans, P. Warwick, G. Buckau, L. Weng, W. H. Van Riemsdijk, The effects of humic substances on the transport of radionuclides: Recent improvements in the prediction of behaviour and the understanding of mechanisms, Appl. Geochemistry, 27 (2012) 378.
28. A. Jain, M. Mohapatra, S.V. Godbole, B.S. Tomar, Time resolved fluorescence spectroscopy of Eu(III) complexation with  $\alpha$ -hydroxy isobutyric acid, Spectrochim. Acta A 71 (2008) 1007.

29. A. Jain, K. Yadav, M. Mohapatra, S.V. Godbole, B.S. Tomar, Spectroscopic investigation on europium complexation with humic acid and its model compounds, *Spectrochim. Acta A* 72 (2009) 1122.
30. A. S. Kar, S. Kumar, B.S. Tomar, V.K. Manchanda, Sorption of curium by silica colloids: Effect of humic acid, *J. Hazard. Mat.* 186 (2011) 1961.
31. A S. Kar and B. S. Tomar, Cm(III) sorption by Silica: Effect of Alpha Hydroxy Isobutyric Acid, *Radiochim. Acta* (communicated).
32. A.S. Kar, B.S. Tomar, S.V. Godbole, V.K. Manchanda, Time resolved fluorescence spectroscopy and modeling of Eu(III) sorption by silica in presence and absence of alpha hydroxy isobutyric acid, *Colloids Surf., A* 378 (2011) 44.
33. A. S. Kar, S. Kumar, B.S. Tomar, U(VI) sorption by silica: Effect of complexing anions, *Colloids Surf., A* 395 (2011) 240.
34. A. Jain, N. Rawat, S.Kumar, B. S. Tomar, V. K. Manchanda, S. Ramanathan, Effect of humic acid on sorption of neptunium on hematite colloids, *Radiochim. Acta* 95 (2007) 501.

## LIST OF FIGURES

	Page No.
<b>CHAPTER-I</b>	
<b>Figure 1.1</b> Production of transuranium radionuclides in the reactor ( <i>Kim, 2006</i> )	26
<b>Figure 1.2</b> Naturally occurring $^{238}\text{U}$ and $^{232}\text{Th}$ in lithosphere and oceans, their ratios between the two compartments ( <i>Kim, 2006</i> )	27
<b>Figure 1.3</b> Worldwide accumulation of spent fuel and plutonium produced from nuclear power plants ( <i>Kim, 2006</i> )	29
<b>Figure 1.4</b> Nuclear fuel cycle	30
<b>Figure 1.5</b> Cross section of disposal pit of deep geological repository showing components of engineered barrier system	35
<b>Figure 1.6</b> Approximate relative energies of the $f^{n-1}d^1s^2$ and $f^n s^2$ electron configurations ( <i>Huheey et al., 2006</i> )	38
<b>Figure 1.7</b> Ionic radii of lanthanides and actinides for +3 and +4 oxidation states	41
<b>Figure 1.8</b> Redox potentials of U, Np and Pu at pH = 0, 8, and 14 ( <i>Choppin, 2005</i> )	42
<b>Figure 1.9</b> Speciation of Plutonium in natural waters ( <i>Runde, 2000</i> )	44
<b>Figure 1.10</b> Stability constants of actinides of different oxidation states with common aquatic ligands ( <i>Runde and Neu, 2006</i> )	52
<b>Figure 1.11</b> Different routes of formation of HS in environment	54
<b>Figure 1.12</b> Classification of HS based on solubility	55

<b>Figure 1.13</b> Proposed Structure of HA	<b>56</b>
<b>Figure 1.14</b> Chemical properties of HS	<b>56</b>
<b>Figure 1.15</b> Conceptual illustration of the inner- (I.S.) and outer-sphere (O.S.) surface complexes of Eu <sup>3+</sup> with kaolinite ( <i>Ishida et al., 2012</i> )	<b>60</b>

## **CHAPTER-II**

<b>Figure 2.1</b> Schematic diagram of a basic UV-Vis spectrophotometer	<b>77</b>
<b>Figure 2.2</b> Schematic of ICP-AES	<b>78</b>
<b>Figure 2.3</b> Schematic showing Electrical double layer and Zeta potential	<b>79</b>
<b>Figure 2.4</b> Schematic of TOC analyser	<b>81</b>
<b>Figure 2.5</b> Jablonski diagram depicting photo physical processes	<b>83</b>
<b>Figure 2.6</b> Principle of TCSPC depicting excitation pulse and decay profile ( <i>Lakowicz, 2006</i> )	<b>86</b>
<b>Figure 2.7</b> Block diagram of TCSPC set up for fluorescence experiments	<b>87</b>
<b>Figure 2.8</b> Constant fraction discrimination in TCSPC.(a): Timing error due to pulse height variations (b): Operation of CFD ( <i>Lakowicz, 2006</i> )	<b>87</b>
<b>Figure 2.9</b> Photograph of the CD-920 time resolved fluorescence spectrometer	<b>88</b>
<b>Figure 2.10</b> Interactions between metal cations (M), HA molecules and the surface of the solid	<b>95</b>
<b>Figure 2.11</b> Conceptual representation of surface charge development in: A) DLM B) CCM ( <i>Hayes et al., 1991</i> )	<b>97</b>

## **CHAPTER-III**

<b>Figure 3.1</b> Structure of LMCA studied for determination of complexation	
---	--

constants	103
<b>Figure 3.2</b> Energy level diagram of Eu(III) along with typical emission spectrum( Tan et al., 2010)	105
<b>Figure 3.3</b> Eu(III ) fluorescence quenching by the vibrational energy levels of O–H, O-D oscillators. Semi-circles denote the lowest luminescent levels. Curved arrows denote the most likely vibrational overtone for the non-radiative decay processes ( <i>Choppin and Peterman, 1998 a</i> )	106
<b>Figure 3.4</b> Excitation spectrum of Eu(III) aqueous solution ( $\lambda_{em} = 592$ nm)	114
<b>Figure 3.5</b> Fluorescence emission spectra of solutions with different Eu:HIBA ratio	115
<b>Figure 3.6</b> Plot of $I_{616}/I_{592}$ vs [HIBA]/[Eu]	115
<b>Figure 3.7</b> (a) Lifetime vs. [HIBA] / [Eu], (b) Number of water molecules vs. [HIBA]/[Eu]	120
<b>Figure 3.8</b> Schematic CE diagram indicating areas corresponding to the characteristics of the interactions between Eu(III) and ligands. Plots in zones A and B are attributable to outer-sphere and inner sphere coordination, respectively ( <i>Ozaki et al. 2002</i> )	121
<b>Figure 3.9</b> CE diagram for varying [HIBA]/[Eu(III)]	121
<b>Figure 3.10</b> $I_{616}/I_{592}$ of Eu vs. [PA] / [Eu]	123
<b>Figure 3.11</b> (a) Lifetime vs. [PA] / [Eu], (b) Number of water molecules vs. [PA] / [Eu]	123
<b>Figure 3.12</b> $I_{616}/I_{592}$ of Eu vs. [MA] / [Eu]	124
<b>Figure 3.13</b> (a) Lifetime vs. [MA] / [Eu], (b) Number of water molecules	125

vs. [MA] / [Eu]	
<b>Figure 3.14</b> $I_{616}/I_{592}$ of Eu vs. [SA] / [Eu]	<b>126</b>
<b>Figure 3.15</b> (a) Lifetime vs. [SA] / [Eu] (b) Number of water molecules vs. [SA] / [Eu]	<b>126</b>
<b>Figure 3.16</b> Excitation spectrum of HA	<b>127</b>
<b>Figure 3.17</b> $I_{616}/I_{592}$ of Eu vs [HA] / [Eu]	<b>128</b>
<b>Figure 3.18</b> (a) Lifetime vs [HA] / [Eu], (b) Number of water molecules vs [HA] / [Eu]	<b>129</b>
<b>Figure 3.19</b> CE diagram for Eu(III)-HA system	<b>130</b>
 <b>CHAPTER-IV</b>	
<b>Figure 4.1</b> Potentiometric titration of silica suspension (6 g /L) in 0.1 M NaClO <sub>4</sub> .	<b>140</b>
<b>Figure 4.2</b> Speciation of Cm(III) in (a) absence and (b) presence of (2 mg/L) HA. [Cm(III)] = $2.2 \times 10^{-10}$ M, I = 0.1 M	<b>144</b>
<b>Figure 4.3</b> Curium speciation in absence (a) and presence (b and c) of HIBA. [Cm(III)] = $2.2 \times 10^{-10}$ ; [HIBA] = $1 \times 10^{-5}$ M in (b) and $1 \times 10^{-3}$ M (c). Ionic strength = 0.1 M NaClO <sub>4</sub> . Cm <sup>3+</sup> (□), Cm(IBA) <sup>2+</sup> (□), Cm(IBA) <sub>2</sub> <sup>+</sup> (□), [Cm(OSi(OH) <sub>2</sub> )] <sup>2+</sup> (o) and [Cm(OSi(OH) <sub>3</sub> ) <sub>2</sub> ] <sup>+</sup> (□).	<b>145</b>
<b>Figure 4.4</b> Europium speciation in absence (a) and presence (b) of HIBA. [Eu(III)] = $5.0 \times 10^{-5}$ M; [HIBA] = $2.5 \times 10^{-3}$ M. Ionic strength = 0.1 M NaClO <sub>4</sub> . Eu <sup>3+</sup> (o), Eu(IBA) <sup>2+</sup> (□), Eu(IBA) <sub>2</sub> <sup>+</sup> (□), [Eu(OSi(OH) <sub>3</sub> ) <sub>2</sub> ] <sup>2+</sup> (□) and [Eu(OSi(OH) <sub>3</sub> ) <sub>2</sub> ] <sup>+</sup> (□).	<b>146</b>
<b>Figure 4.5</b> Kinetics of sorption of Cm by silica. pH = 6.5, [Cm(III)] = $2.2 \times 10^{-10}$ M, I = 0.1 M (NaClO <sub>4</sub> ), [Silica] = 5 g/l	<b>147</b>

<b>Figure 4.6</b> Plot of kinetic data showing pseudo second order kinetics	<b>148</b>
<b>Figure 4.7</b> Sorption of Cm by silica: Effect of addition order. [Cm(III)]= $2.2 \times 10^{-10}$ M, I=0.1 M (NaClO <sub>4</sub> ), [Silica]=5g/l, [HA]=2 mg/L. The dash and dotted lines are the LAM fits of silica-HA-Cm(III) systems	<b>150</b>
<b>Figure 4.8</b> Effect of ionic strength on sorption of Cm by silica colloids. pH = 6.5, [Cm(III)] = $2.2 \times 10^{-10}$ M, [Silica] = 5g/l	<b>153</b>
<b>Figure 4.9</b> Speciation of Cm(III) as a function of ionic strength at pH=6.5.	<b>154</b>
<b>Figure 4.10</b> Sorption of Cm by silica as a function of [HA]. (pH = 6.0)	<b>155</b>
<b>Figure 4.11</b> Sorption of Cm(III) on silica in presence and absence of HIBA. [Cm(III)] = $2.2 \times 10^{-10}$ M; Silica = 5 g/L; [HIBA(I)] = $1 \times 10^{-5}$ M, ; [HIBA(II)] = $1 \times 10^{-3}$ M; I = 0.1 M (NaClO <sub>4</sub> ).	<b>156</b>
<b>Figure 4.12</b> SCM of Cm(III) sorption by Silica in presence of HIBA (a) binary Silica-Cm system; (b) Silica-Cm-HIBA(I) system ; (c) Silica- HIBA(I)-Cm system; [Cm(III)] = $2.2 \times 10^{-10}$ M; Silica = 5 g/L; [HIBA] = $1 \times 10^{-5}$ M.	<b>159</b>
<b>Figure 4.13</b> SCM of Cm(III) sorption by Silica in presence of HIBA (a) Silica-Cm-HIBA(II) system; (b) Silica-HIBA(II) - Cm system; [Cm(III)] = $2.2 \times 10^{-10}$ M; Silica = 5 g/L; [HIBA] = $1 \times 10^{-3}$ M.	<b>162</b>
<b>Figure 4.14</b> Sorption of Eu(III) on silica in presence and absence of HIBA. [Eu(III)] = $5.0 \times 10^{-5}$ M; Silica = 10 g/L; [HIBA] = $2.5 \times 10^{-3}$ M, I=0.1 M (NaClO <sub>4</sub> ).	<b>164</b>
<b>Figure 4.15</b> Time resolved fluorescence emission spectra of Eu(III) sorbed on silica in absence (a) and presence (b) of HIBA. [Eu(III)] = $5.0$ $\times 10^{-5}$ M; Silica = 10 g/L; [HIBA] = $2.5 \times 10^{-3}$ M.	<b>166</b>

- Figure 4.16** Comparison of the fluorescence decay curve of Eu(III) sorbed on silica at pH = 8.06 to that of bare silica. **167**
- Figure 4.17** Fluorescence life time data of Eu(III) sorbed on silica in absence (a) and presence (b) of  $\alpha$  – hydroxy isobutyric acid. [Eu(III)] =  $5.0 \times 10^{-5}$  M; Silica = 10 g/L; [HIBA] =  $2.5 \times 10^{-3}$  M. **168**
- Figure 4.18** Lifetime data of Eu(III) sorbed on silica as function of equilibration time. [Eu(III)] =  $5.0 \times 10^{-5}$  M; Silica = 10 g/L. **169**
- Figure 4.19** SCM of Eu(III) sorption by Silica in absence (a) and presence of HIBA(b). [Eu(III)] =  $5.0 \times 10^{-5}$  M; Silica = 10 g/L; [HIBA] =  $2.5 \times 10^{-3}$  M.  $L = \text{OSi(OH)}_3^-$ . **172**
- Figure 4.20** Sorption of Cm(III) and Eu(III) on silica in absence (a) and presence (b) of HIBA. For Silica-Cm(III) system :For Silica-Cm(III) system :Silica = 5 g/L, [Cm(III)] =  $2.2 \times 10^{-10}$  M, [HIBA] =  $1 \times 10^{-3}$  M and I = 0.1 M (NaClO<sub>4</sub>). For Silica-Eu(III) system :Silica = 10 g/L [Eu(III)] =  $5 \times 10^{-5}$  M, [HIBA] =  $2.5 \times 10^{-3}$  M and I = 0.1 M (NaClO<sub>4</sub>) (*Kar et al. 2011 b*). **173**
- Figure 4.21** Sorption of Cm(III) on silica in presence of HIBA and HA. Silica = 5 g/L; [Cm(III)] =  $2.2 \times 10^{-10}$  M; I = 0.1 M (NaClO<sub>4</sub>);[HIBA] =  $1 \times 10^{-5}$  M and [HA] = 2 mg/L. **176**

## CHAPTER-V

- Figure 5.1** Sorption of U(VI) on silica at varying U(VI) concentration. [U(VI)] =  $4.47 \times 10^{-7}$  M -  $4.47 \times 10^{-4}$  M; Silica = 5 g/L; I = 0.1 M (NaClO<sub>4</sub>). **184**
- Figure 5.2** Sorption of U(VI) on silica at varying ionic strength. [U(VI)] **185**

=  $4.47 \times 10^{-6}$  M; Silica = 5 g/L; I = 0.01, 0.1 M (NaClO<sub>4</sub>).

**Figure 5.3** Sorption of U(VI) on silica in presence and absence of citrate/carbonate. [U(VI)] =  $4.47 \times 10^{-6}$  M; Silica = 5 g/L; [CIT] =  $10^{-3}$  M; [CO<sub>3</sub><sup>2-</sup>] =  $10^{-3}$  M; I = 0.1 M (NaClO<sub>4</sub>). 186

**Figure 5.4** Silica dissolution in presence and absence of U(VI) as function of pH. [U(VI)] =  $4.47 \times 10^{-4}$  M; Silica = 5 g/L; I = 0.1 M (NaClO<sub>4</sub>). 188

**Figure 5.5** (a) U(VI) speciation in presence of silicic acid as function of pH. (a) [U(VI)] =  $4.47 \times 10^{-7}$  M; I = 0.1 M NaClO<sub>4</sub>. (b) [U(VI)] =  $4.47 \times 10^{-5}$  M; I = 0.1 M NaClO<sub>4</sub>. (c) [U(VI)] =  $4.47 \times 10^{-4}$  M; I = 0.1 M NaClO<sub>4</sub>. UO<sub>2</sub><sup>2+</sup> (□), UO<sub>2</sub>H<sub>3</sub>SiO<sub>4</sub> (○), (UO<sub>2</sub>)<sub>4</sub>(OH)<sub>7</sub><sup>+</sup> (◀), (UO<sub>2</sub>)<sub>3</sub>(OH)<sub>7</sub><sup>-</sup> (Δ), UO<sub>2</sub>(OH)<sub>3</sub><sup>-</sup> (◇), (UO<sub>2</sub>)<sub>2</sub>(OH)<sub>2</sub><sup>2+</sup> (▲), UO<sub>2</sub>OH<sup>+</sup> (▼), (UO<sub>2</sub>)<sub>3</sub>(OH)<sub>5</sub><sup>+</sup> (▶), UO<sub>2</sub>(OH)<sub>2</sub> (■). 190

**Figure 5.6** U(VI) speciation in presence of citrate and carbonate as function of pH. (a) [U(VI)] =  $4.47 \times 10^{-6}$  M; I = 0.1 M NaClO<sub>4</sub>. (b) [U(VI)] =  $4.47 \times 10^{-6}$  M; [CIT<sup>3-</sup>] =  $10^{-3}$  M; I = 0.1 M NaClO<sub>4</sub>. (c) [U(VI)] =  $4.47 \times 10^{-6}$  M; [CO<sub>3</sub><sup>2-</sup>] =  $10^{-3}$  M; I = 0.1 M NaClO<sub>4</sub>. UO<sub>2</sub><sup>2+</sup> (□), UO<sub>2</sub>H<sub>3</sub>SiO<sub>4</sub> (○), (UO<sub>2</sub>)<sub>4</sub>(OH)<sub>7</sub><sup>+</sup> (◀), (UO<sub>2</sub>)<sub>3</sub>(OH)<sub>7</sub><sup>-</sup> (Δ), UO<sub>2</sub>(OH)<sub>3</sub><sup>-</sup> (◇), UO<sub>2</sub>(OH)<sub>2</sub> (■), UO<sub>2</sub>OH<sup>+</sup> (▼), (UO<sub>2</sub>)<sub>3</sub>(OH)<sub>5</sub><sup>+</sup> (▶), UO<sub>2</sub>CIT<sup>-</sup> (⊕), UO<sub>2</sub>(CIT)<sub>2</sub><sup>2-</sup> (⊗), (UO<sub>2</sub>)<sub>2</sub>CO<sub>3</sub>(OH)<sub>3</sub><sup>-</sup> (●), UO<sub>2</sub>CO<sub>3</sub> (\*) , UO<sub>2</sub>(CO<sub>3</sub>)<sub>2</sub><sup>2-</sup> (×), UO<sub>2</sub>(CO<sub>3</sub>)<sub>3</sub><sup>4-</sup> (+). 191

**Figure 5.7** Energy level diagram of uranyl ion (*Tan et al., 2010*) 193

**Figure 5.8** Excitation spectra of U(VI) sorbed on silica 193

**Figure 5.9** Emission spectra of uranium sorbed on silica at λ<sub>ex</sub> = 230 nm 194

**Figure 5.10** Deconvoluted fluorescence emission spectra of short and

long lived component	<b>196</b>
<b>Figure 5.11</b> Correlation between $v_1$ and number of OH groups attached to uranyl ion	<b>197</b>
<b>Figure 5.12</b> SCM of U(VI) sorption by silica using Model 1 and Model 2. (a) $[U(VI)] = 4.47 \times 10^{-7} \text{ M}$ ; $m/v = 5 \text{ g/L}$ ; $I = 0.1 \text{ M NaClO}_4$ . (b) $[U(VI)] = 4.47 \times 10^{-5} \text{ M}$ ; $m/v = 5 \text{ g/L}$ ; $I = 0.1 \text{ M NaClO}_4$ . (c) $[U(VI)] = 4.47 \times 10^{-4} \text{ M}$ ; $m/v = 5 \text{ g/L}$ ; $I = 0.1 \text{ M NaClO}_4$ .	<b>200</b>
<b>Figure 5.13</b> SCM of U(VI) sorption by silica in presence and absence of complexing anions. (a) $[U(VI)] = 4.47 \times 10^{-6} \text{ M}$ ; $m/v = 5 \text{ g/L}$ ; $I = 0.1 \text{ M NaClO}_4$ using Model 1 and Model 2. (b) $[U(VI)] = 4.47 \times 10^{-6} \text{ M}$ ; $m/v = 5 \text{ g/L}$ ; $[CO_3^{2-}] = 1 \times 10^{-3} \text{ M}$ ; $I = 0.1 \text{ M NaClO}_4$ . (c) $[U(VI)] = 4.47 \times 10^{-6} \text{ M}$ ; $m/v = 5 \text{ g/L}$ ; $[CIT] = 1 \times 10^{-3} \text{ M}$ ; $I = 0.1 \text{ M NaClO}_4$	<b>202</b>
<b>Figure 5.14</b> SCM of U(VI) sorption by silica using Model 1 and Model 2 along with sorption data. (a) $[U(VI)] = 5 \times 10^{-5} \text{ M}$ ; $m/v = 3 \text{ g/L}$ ; $I = 0.2 \text{ M NaClO}_4$ . Data taken from reference ( <i>Pathak et al., 2007c</i> )	<b>205</b>
 <b>CHAPTER-VI</b> 	
<b>Figure 6.1</b> Gamma Spectrum of $^{239}\text{Np}$	<b>215</b>
<b>Figure 6.2</b> Plot of zeta potential of hematite colloids as a function of pH	<b>218</b>
<b>Figure 6.3</b> Surface saturation of hematite by $H^+$ (top) and $OH^-$ (bottom)	<b>219</b>
<b>Figure 6.4</b> Complexation of Np(V) by HA at pH 8 (TRIS buffer)	<b>220</b>
<b>Figure 6.5</b> Fraction of mineral bound HA as a function of pH	<b>221</b>
<b>Figure 6.6</b> Sorption of Np(V) on hematite: Effect of HA	<b>222</b>
<b>Figure 6.7</b> Sorption of neptunium on hematite in presence of HA under reducing conditions	<b>225</b>

## LIST OF TABLES

	<b>Page No.</b>
<b>CHAPTER-I</b>	
<b>Table 1.1</b> Long lived radionuclides present in nuclear reactor [Data taken from ( <i>Silva and Nitsche, 1995</i> )]	<b>26</b>
<b>Table 1.2</b> Classification of Solid and Gaseous Waste as per Atomic Energy Regulatory Board, India ( <i>Raj et al.,2006</i> )	<b>32</b>
<b>Table 1.3</b> Electronic configurations of lanthanide and actinide elements	<b>37</b>
<b>Table 1.4</b> Oxidation states of actinide elements ( <i>Ahrland et al.,1973</i> )	<b>39</b>
<b>Table 1.5</b> Approximate detection limits of actinides in oxidation state speciation ( <i>Choppin, 2006</i> )	<b>62</b>
 <b>CHAPTER-III</b>	
<b>Table 3.1</b> Stability Constants of Eu with SA, PA and MA	<b>119</b>
 <b>CHAPTER -IV</b>	
<b>Table 4.1</b> Dissolved Si (ppm) in silica suspensions (10 g/L) in presence of Eu(III) ( $5.0 \times 10^{-05}$ M) measured after different time of equilibration.	<b>141</b>
<b>Table 4.2</b> Log $\beta$ used for calculating the aqueous speciation	<b>143</b>
<b>Table 4.3</b> Optimized parameter values as obtained from FITEQL for Cm-silica and Cm-silica-HIBA systems	<b>163</b>
<b>Table 4.4</b> Optimised parameter values as obtained from FITEQL for Eu-silica and Eu-silica-HIBA	<b>171</b>
 <b>CHAPTER-V</b>	
<b>Table 5.1</b> Stability Constants for aqueous complexes	<b>189</b>

*List of Tables*

<b>Table 5.2</b> Lifetime data of uranium sorbed on silica	<b>195</b>
<b>Table 5.3</b> Peak maxima of two components for $\text{UO}_2^{2+}$ sorbed on silica	<b>196</b>
<b>Table 5.4</b> $\Delta\nu$ ( $\text{cm}^{-1}$ ) and $N(\text{OH}/\text{UO}_2^{+2})$ of uranium sorbed on silica at different pH	<b>198</b>
<b>Table 5.5</b> Optimized parameter values as obtained from FITEQL fit of $\text{UO}_2^{2+}$ -silica and $\text{UO}_2^{2+}$ -complexing anion – silica system	<b>201</b>

## **Chapter I**

# **Introduction**

### 1.1. Historical perspective of actinides

The natural uranium and thorium, discovered more than 200 years ago, were of fundamental interest only, until Henry Becquerel discovered radioactivity in 1895. The discovery of radioactivity aroused significant interest in physical and chemical properties of early actinides. However, the discovery of neutron by James Chadwick in 1932 marked the beginning of a new era which witnessed the very complex radioactive transformations of the naturally occurring elements.

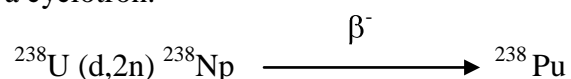
In 1930's Enrico Fermi suggested the use of neutron bombardment to synthesize new radioactive elements and carried out series of neutron induced reactions on a range of target elements. He also proposed that uranium after capturing a neutron must be converted into heavier beta-radioactive uranium isotope, which on decay should give birth to new transuranium element 93. Soon in 1940, Edwin McMillan and Philip Abelson (Berkeley Radiation Laboratory, University of California) discovered  $^{239}\text{Np}$  (element 93) as a result of  $^{239}\text{U}$  decay formed through neutron irradiation of  $^{238}\text{U}$ , which led to the validation of hypothesis by Fermi.



The discovery of nuclear fission by Hahn and Strassmann in 1939 opened new avenues in field of nuclear research related to uranium, which could lead to construction of powerful nuclear weapons.



Subsequently, in 1941 Glenn T. Seaborg, Edwin McMillan, Joseph Kennedy and Arthur Wahl (Berkeley, California) discovered element 94 ( $^{238}\text{Pu}$ ) after deuteron bombardment of  $^{238}\text{U}$  in a cyclotron.



Soon after, they discovered  $^{239}\text{Pu}$  which was produced by the bombardment of uranium with slow neutrons and found that its nuclear properties supported initiation of a chain reaction similar to  $^{235}\text{U}$ .



Seaborg and his coworkers made significant contributions towards the discovery of transuranic elements by identifying thirteen new elements (element 94-106) in a span of 30 years (1944-1974). In 1944 Seaborg gave the actinide concept which postulated that the fourteen actinides, including the first eleven transuranic elements, would form a transition series analogous to the rare-earth series of lanthanide elements and therefore led to the prediction of the chemical properties and placement of these heavier elements below lanthanides in the periodic table (*Seaborg, 1949; Seaborg and Katz, 1954*). Thus, the discovery of actinides opened the gateway of nuclear age to human civilization.

The capability of fissile isotopes of U and Pu to sustain chain reaction has been employed in the production of nuclear energy, by burning these radionuclides in nuclear reactor, which in turn is used in generation of electricity. However, this reactor operation results in the formation of transuranic elements by neutron capture and beta decay as shown in figure 1.1 (*Kim, 2006*). The long lived radionuclides are depicted by grey background and their half-lives are given in Table 1.1.

Thus, the benefit of nuclear energy production is related to the inevitable problem of generation of long lived radionuclides. For the nuclear fuel reprocessing and formulation of strategy of safe nuclear disposal, knowledge of the sources of actinide elements in the environment is of utmost importance.

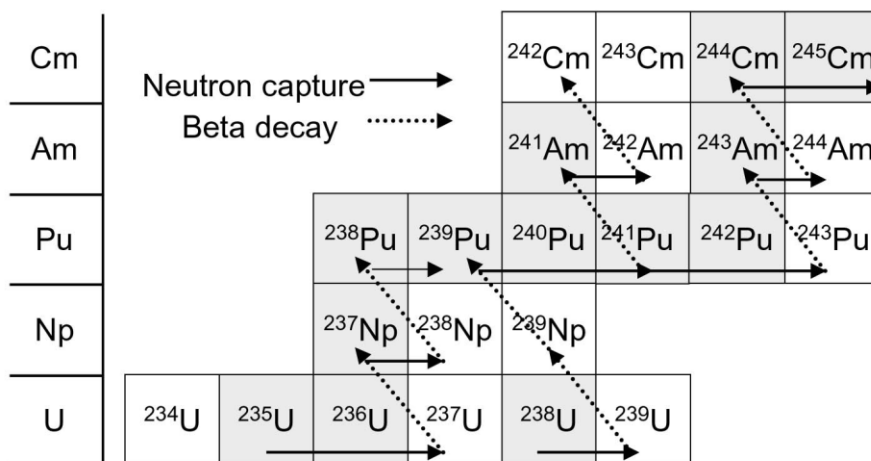


**Figure 1.1** Production of transuranium radionuclides in the reactor (Kim, 2006)

**Table 1.1** Long lived radionuclides present in nuclear reactor [Data taken from (Silva and Nitsche, 1995)]

Radioisotope	Half-life (years)	Radioisotope	Half-life (years)
$^{235}\text{U}$	$7.0 \times 10^8$	$^{241}\text{Pu}$	14.4
$^{238}\text{U}$	$4.47 \times 10^9$	$^{242}\text{Pu}$	$3.76 \times 10^5$
$^{237}\text{Np}$	$2.14 \times 10^6$	$^{241}\text{Am}$	432.6
$^{238}\text{Pu}$	87.7	$^{243}\text{Am}$	$7.38 \times 10^3$
$^{239}\text{Pu}$	$2.41 \times 10^4$	$^{244}\text{Cm}$	18.11
$^{240}\text{Pu}$	$6.56 \times 10^3$	$^{245}\text{Cm}$	$8.5 \times 10^3$

## 1.2. Sources of actinides in the environment:

All the members of actinide series are radioactive. The production and use of actinides has increased tremendously since last century which resulted in entry of actinides into the environment through different pathways. The various sources by which actinides intrude into the environment are discussed below:

### 1.2.1. Natural occurrence:

Large quantities of naturally occurring uranium ( $4.7 \times 10^{13}$  tons) and thorium ( $1.8 \times 10^{14}$  tons) have existed in lithosphere and oceans since the creation of the earth

as shown in figure 1.2 (Kim, 2006). These radionuclides have been formed in the process of nucleogenesis and are termed as primordial radionuclides. Actinium (Ac) and protactinium (Pa) found in trace quantities, have been produced as a result of decay of naturally occurring uranium and thorium. Naturally occurring Pu and Np, present in ultra-trace level, are generated by neutron capture in environment (Kim, 1986).

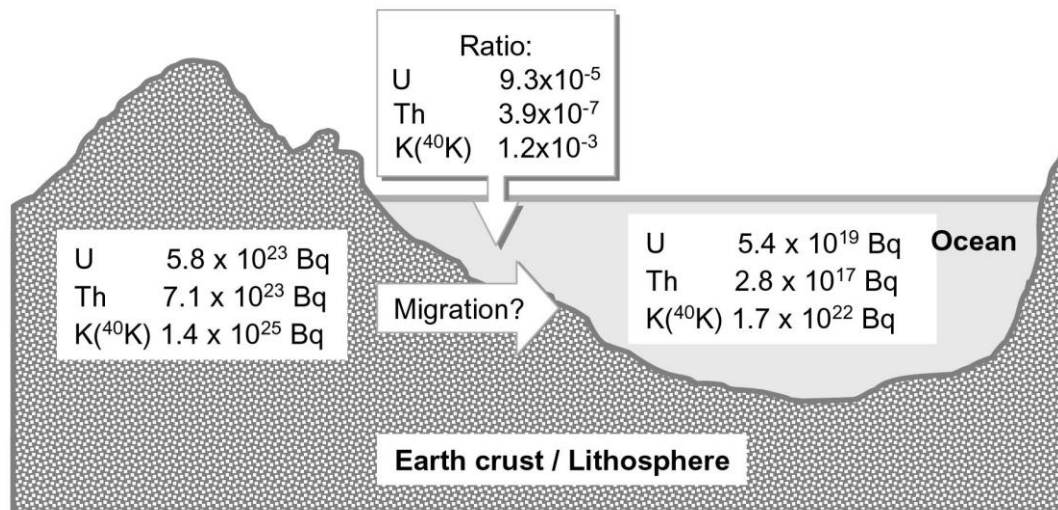


**Figure 1.2** Naturally occurring  $^{238}\text{U}$  and  $^{232}\text{Th}$  in lithosphere and oceans, their ratios between the two compartments (Kim, 2006)

Here it is worth mentioning the specific case of OKLO natural nuclear reactor. The isotopic ratio analysis of uranium deposits revealed that self-sustaining nuclear chain reaction occurred about  $2 \times 10^9$  years ago in course of which large quantities of transuranic elements were produced. However, most of them have decayed but plutonium remained in the environment (Degueudre, 2006). Thus, natural nuclear reactor existed long before man conceived the idea of nuclear fission.

### 1.2.2. Nuclear weapon testing and accidents:

Nuclear weapon testing is the main anthropogenic source which is responsible for widespread occurrence of radioactivity in the environment. The tests have been conducted underground, underwater, in atmosphere and exo atmosphere all over the world which resulted in release of  $2 \times 10^{20}$  Bq of radioactivity into the environment (*Choppin and Wong, 1998 b*). It is estimated that  $1.6 \times 10^{16}$  Bq of plutonium has been deposited in aquatic systems as a result of nuclear tests. However, the concentration of plutonium in ocean water ( $10^{-5}$  Bq/kg) is found to be extremely low due to extremely low solubility of plutonium and incorporation in the sediments (*Choppin, 2006*). The accidental release of radioactivity from nuclear power plants is also one of the sources of radioactive contamination of the environment. There have been many nuclear accidents worldwide but the prime example is Chernobyl disaster in 1986 during which reactor core got damaged, resulting in release of large amount of radioactive isotopes to the geosphere. Recently, the Fukushima Daiichi nuclear disaster took place in 2011 in which large quantity of radioactive materials was released at the Fukushima I Nuclear Power Plant, following the Tohoku earthquake and tsunami (*Strickland, 2011*). It is the largest nuclear disaster since the Chernobyl disaster.

### 1.2.3. Disintegration of Nuclear powered satellites:

$^{238}\text{Pu}$  is used as heat source in batteries of satellites. 10% of 942 kCi of  $^{238}\text{Pu}$ , containing 700 Ci of  $^{239}\text{Pu}$ , has been associated with three in-flight aborts. One of these three flights containing 17 kCi of  $^{238}\text{Pu}$  got burned on re-entry in to the atmosphere and subsequently the resulting effluent dispersed in the upper atmosphere of the southern hemisphere while the remains of the second one are lying in pacific ocean and third one (34.4 kCi of  $^{238}\text{Pu}$ ) was recovered safely (*Kim, 1986*).

#### 1.2.4. Nuclear power plants:

Today about 12.3 % of the world's electricity is generated by 435 nuclear power plants operating worldwide (Amano, 2012). Over the years, the increase in the number of nuclear power plants has resulted in subsequent increase in generation of spent fuel and production of plutonium as shown in figure 1.3 (Kim, 2006). The nuclear fuel cycle involving a series of different stages e.g., milling and mining, fuel preparation, reactor operation and fuel reprocessing (figure 1.4) results in the generation of radioactive waste at each stage.

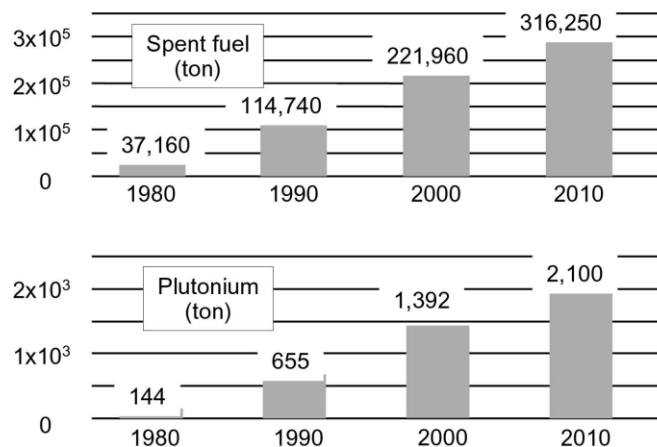


**Figure 1.3** Worldwide accumulation of spent fuel and plutonium produced from nuclear power plants (Kim, 2006)

##### 1.2.4.1. Mining and milling:

The mined uranium ore after crushing, grinding and dewatering is subjected to beneficiation followed by acid or alkali leaching and is finally precipitated to obtain ammonium diuranate (yellow cake). The yellow cake is processed to obtain uranium oxide which is used for fuel fabrication. The production and processing of large quantities of ore results in large volume of mill tailings, containing large quantities of

naturally occurring radionuclides of U, Th, Ra, Po, Bi and Pb, which are dumped in well-engineered barrier called mill tailing ponds. With the passage of time, these radionuclides may migrate from the tailing ponds and intrude into the adjoining environment (Patra *et al.* 2013).

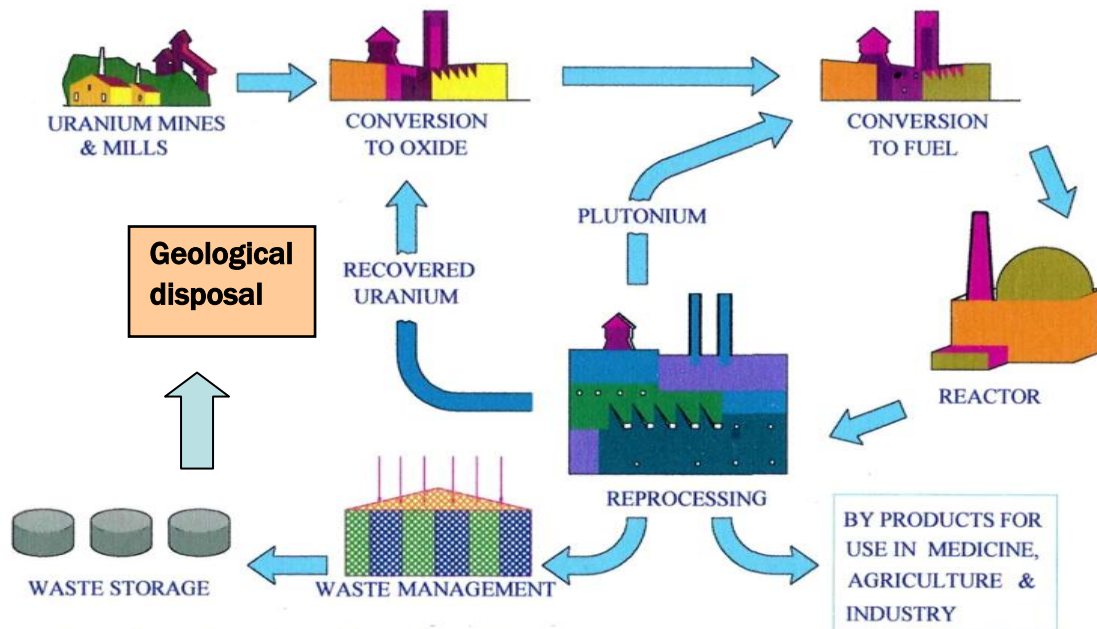


**Figure 1.4** Nuclear fuel cycle

#### 1.2.4.2. Nuclear fuel reprocessing:

The spent nuclear fuel containing uranium, plutonium, minor actinides, fission products and activation products is given a suitable cooling period for the decay of short lived radionuclides and to reduce the activity of  $^{131}\text{I}$  ( $t_{1/2} = 8$  days) to manageable levels. The PUREX process which is employed in fuel reprocessing has been its workhorse for the last few decades. In PUREX process, after interim cooling and chemical or mechanical decladding of fuel, dissolution of fuel is done in nitric acid followed by feed clarification and chemical conditions adjustment of solution for solvent extraction which is carried out using 30% tributyl phosphate (TBP) in dodecane. The U(VI) and Pu(IV) are co-extracted into TBP leaving majority of

fission products in aqueous phase which is concentrated, conditioned and is called as HLW. The separation of uranium and plutonium is achieved by selective reduction of Pu(IV) to Pu(III) which goes in aqueous phase and both uranium and plutonium are subjected to further purification to obtain desired purity (*Dey and Bansal, 2006*). The nuclear fuel reprocessing plants generate waste in all categories and thus understanding about the classification of radioactive waste is integral part of nuclear waste management.

### **1.3. Classification and management of radioactive waste:**

Classification of radioactive waste is extremely important from the point of view of nuclear waste management. While classifying the radioactive waste, its physical, chemical, radiological and biological properties must be taken into consideration. The radioactive waste classification is a useful tool in segregation, waste treatment selection, storage and disposal. Radioactive waste is generated in various forms in entire fuel cycle viz., solid, liquid or gaseous.

#### ***1.3.1. Solid radioactive waste:***

Solid radioactive wastes, depending upon their physical and chemical nature, are classified as combustible, non-combustible, compressible and non-compressible. They are further categorized depending upon the radioactivity content as shown in Table 2. It typically comprises of resins, chemical sludges, and reactor components as well as reprocessing equipments. The majority of solid waste has low activity and is either combustible or compressible. The combustible waste is burn in specially designed incinerators to achieve a volume reduction of about 50 while low active non-combustible waste is compressed by using hydraulically operated baling press to obtain volume reduction of five (*Raj et al., 2006*).

### 1.3.2. Gaseous radioactive waste:

The classification of gaseous radioactive wastes according to their activity level is listed in Table 1.2. It includes gaseous fission products generated due to radiolysis. The gaseous waste is managed either by using high efficiency particulate air filter or by chemically impregnated activated charcoal.

**Table 1.2** Classification of Solid and Gaseous Waste as per Atomic Energy Regulatory Board, India (*Raj et al.,2006*)

Category	Solid	Gaseous
	Surface Dose (mGy/hr)	Activity Level(Bq/M <sup>3</sup> )
I	< 2	< 3.7
II	2-20	3.7- 3.7x 10 <sup>4</sup>
III	>20	> 3.7 x 10 <sup>4</sup>
IV	Alpha bearing	

### 1.3.3. Liquid radioactive waste:

The classification of radioactive waste obtained during reprocessing of spent fuel on the basis of level of radioactivity is given below (*Raj et al.2006*):

**1.3.3.1. Exempt waste:** Waste which satisfies the criteria of regulatory control for radiation protection purposes for clearance, exemption or exclusion.

**1.3.3.2. LLW:** When the radioactivity level of the waste is in the range 37 Bq/L - 3.7 X 10<sup>6</sup> Bq/L then the waste is termed as LLW. It is generated as the effluent from resorcinol formaldehyde polycondensate resin used in the treatment of ILW and as the result of evaporation and concentration of secondary liquid waste during nuclear fuel reprocessing. The treatment of LLW involves the precipitation of the majority of radionuclides using suitable reagents (*Banerjee et al. 2006*). The solid residue is

stored in a near surface repository and the supernatant is monitored and then discharged after dilution.

**1.3.3.3. ILW:** When the radioactivity level of the waste is in the range  $3.7 \times 10^6$  Bq/L -  $3.7 \times 10^{11}$  Bq/L then the waste is termed as ILW. It is obtained as the condensate during the evaporation and concentration of HLW. The ILW is treated with resorcinol formaldehyde polycondensate resin and iminodiacetic acid resin to remove  $^{137}\text{Cs}$  and  $^{90}\text{Sr}$  respectively (*Kumar et al. 2008*). After use, these resins are immobilized in cement matrix.

**1.3.3.4. HLW:** When the radioactivity level of the waste is above  $3.7 \times 10^{11}$  Bq/L then the waste is termed as HLW. HLW comprises only about 3% of the total volume of all the radioactive wastes but it contains more than 99% of the total radioactivity generated in the nuclear fuel cycle. The major amount of HLW is generated in first extraction step of PUREX process. HLW contains left over uranium and plutonium, minor actinides, activation products and fission products. The disposal of HLW is challenging owing to the radiotoxicity associated with the minor actinides which have half lives ranging from few hundred to millions of years (Table 1). To ensure the isolation of waste effectively from the biosphere, till its radio toxicity reduces to innocuous levels, three step approach is being followed in India for the management of HLW (*Alexander and McKinley, 2007*).

- (a) Vitrification of waste in stable and inert solid matrix, viz., glass
- (b) Interim storage of solidified waste with continuous cooling
- (c) Disposal in deep geological repositories

**1.3.3.4.(a) Vitrification of HLW in Glass Matrix:**

Borosilicate glass matrix has been adopted for vitrification of HLW in India (Kaushik *et al.*, 2006). The glass matrix has been chosen as it has all the desired characteristics, viz., high radiation and thermal stability, mechanical strength, chemical durability and homogeneity. In vitrification process, pre-concentrated waste along with glass-forming additives is fed to a metallic processing vessel located in the induction furnace. A series of thermal and chemical conversions take place inside the vessel that is evaporation of water and nitric acid, drying and decomposition of nitrates to oxides, reaction of oxides with glass-forming additives and finally fusion of the mixture to form molten glass. The molten glass is poured into stainless steel canisters where it solidifies slowly and sealing of canister is done remotely. Three such canisters are further encased in a stainless steel container known as an over-pack.

**1.3.3.4.(b). Interim storage of solidified waste:**

The radioactivity level of overpacks is of the order of  $10^6$ Ci which generates decay heat of about 3 - 4 kW. Therefore, continuous cooling is required to maintain centerline glass temperature in order to minimize devitrification (Raj *et al.* 2006). The waste forms need to be cooled until disposal in deep geological repositories becomes viable.

**1.3.3.4.(c). Disposal in deep geological repositories:**

After interim storage the overpacks containing waste are proposed to be placed inside deep geological repositories which are designed to isolate these waste forms from biosphere for hundreds of thousands of years so as to ascertain that the residual radioactivity reaching the biosphere has negligible concentration compared to the natural radioactivity persisting in the environment. In order to ensure complete

isolation of the radioactive waste, repositories are designed using multi barrier system which comprises of engineered barrier system and natural geological barrier. Engineered barrier system includes waste form, cansisters, overpack, buffer and backfill material while natural geological barrier is provided by host rock and its surroundings as shown in figure 1.5. The host rock should have several characteristics, viz., high strength, high thermal conductivity, low thermal expansion, high sorption capacity, no ingress of water from surrounding and minimum interaction with cansister and fluid (if any). The backfill/buffer material should possess high swelling potential, high radionuclide retention capacity, low hydraulic conductivity and low gas permeability. In India crystalline granitic rocks are being considered as probable host rock while bentonite clays as the buffer/backfill materials (*Pusch, 1998*).

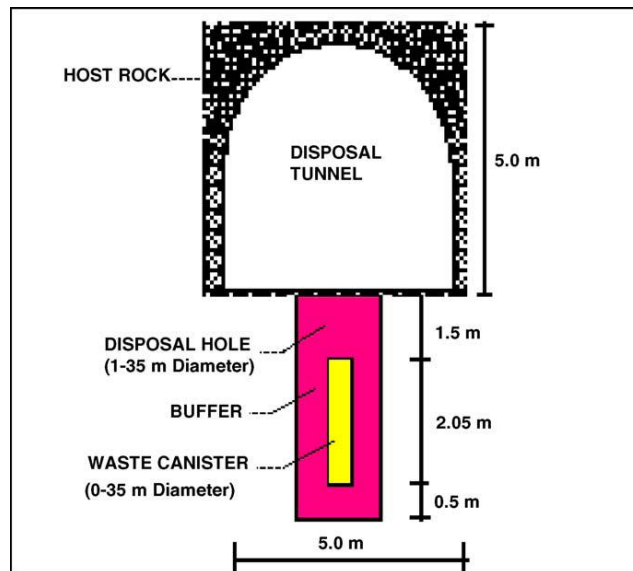


**Figure 1.5** Cross section of disposal pit of deep geological repository showing components of engineered barrier system.

Although the release of the radionuclides from the repository to biosphere is expected to be prevented by multi barrier system, radionuclides may diffuse out of the

glass matrix due to their decay heat, corrosion of canisters and/or natural calamities such as earth quakes, volcanic eruptions, followed by their dispersion and dissolution, which can ultimately lead to their release in biosphere. Therefore, it is imperative to have detailed knowledge about the behaviour of these radionuclides, which are mainly actinides, in the aquatic environment. Thus fundamental understanding of aquatic actinide chemistry is entailed by long term safety assessment of deep geological repositories.

#### **1.4. Actinide Chemistry in natural water systems:**

The chemistry of actinides in natural water systems is different and complex as compared to their known chemistry in solution owing to presence of dissolved heavy metal elements, variety of complexing organic and inorganic anions, natural water colloids, suspended material and sediment, mineral and soil surrounding water. Thus actinides are involved in multi component reactions which are dependent on their chemical properties as well as that of given water. Before having a detailed insight of the phenomena influencing actinide speciation in natural waters, few basic concept of general actinide chemistry have been discussed.

##### **1.4.1. General Actinide Chemistry:**

###### **1.4.1.1. Electronic Configuration:**

The actinide series of elements, from actinium ( $Z = 89$ ) to lawrencium ( $Z = 103$ ), have been placed in the periodic table on the basis of the actinide concept proposed by Seaborg in 1944 according to which each successive element is obtained by sequential filling of inner 5f orbitals. The lanthanide series, encompassing elements from lanthanum ( $Z = 57$ ) to lutetium ( $Z = 71$ ), also results from filling of 4f orbitals. In both the series f-shells are sequentially getting populated and therefore the

similarities and differences in the physical and chemical properties of corresponding elements of two series provide insight in to the contribution of f-electrons in determining these properties. Thus, comparative aspects of the properties of both the series have been presented. Table 1.3 gives the ground state gas phase neutral atom electronic configuration of actinide and lanthanide series (*Edelstein et al. 2006 a*).

**Table 1.3** Electronic configurations of lanthanide and actinide elements

Lanthanides			Actinides		
Elements	Atomic number	Electronic configuration	Elements	Atomic number	Electronic configurations
La	57	$5d^1 6s^2$	Ac	89	$6d^1 7s^2$
Ce	58	$4f^1 5d^1 6s^2$	Th	90	$6d^2 7s^2$
Pr	59	$4f^3 6s^2$	Pa	91	$5f^2 6d^1 7s^2$
Nd	60	$4f^4 6s^2$	U	92	$5f^3 6d^1 7s^2$
Pm	61	$4f^5 6s^2$	Np	93	$5f^4 6d^1 7s^2$
Sm	62	$4f^6 6s^2$	Pu	94	$5f^6 7s^2$
Eu	63	$4f^7 6s^2$	Am	95	$5f^7 7s^2$
Gd	64	$4f^7 5d^1 6s^2$	Cm	96	$5f^7 6d^1 7s^2$
Tb	65	$4f^9 6s^2$	Bk	97	$5f^9 7s^2$
Dy	66	$4f^{10} 6s^2$	Cf	98	$5f^{10} 7s^2$
Ho	67	$4f^{11} 6s^2$	Es	99	$5f^{11} 7s^2$
Er	68	$4f^{12} 6s^2$	Fm	100	$5f^{12} 7s^2$
Tm	69	$4f^{13} 6s^2$	Md	101	$5f^{13} 7s^2$
Yb	70	$4f^{14} 6s^2$	No	102	$5f^{14} 7s^2$
Lu	71	$4f^{14} 5d^1 6s^2$	Lr	103	$5f^{14} 6d^1 7s^2$

It is evident from the table that filling of electrons in f-shell in actinides preceding americium is not as systematic as observed in case of lanthanides which can be attributed to smaller energy difference between 5f, 6d and 7s orbitals in case of

actinides. In case of all the transition series, the relative energy of the orbital being occupied become lower as successive electrons are added and thus the energy of 5f orbital become lower than 6d orbital in the elements beyond thorium. The relative energies of electronic configurations of actinides that can interchange 5f and 6d electrons are shown in figure 1.6 (Huheey et al., 2006). The inversion from one electronic configuration to other, for the elements in which 5f-orbitals extend closer to 6d and 7s orbital, is inevitable. Therefore, early actinides up to americium ( $Z = 95$ ) show variable valancy. On the contrary, in lanthanides the large energy differences between 4f and 5d orbitals do not favour the interchange of electrons among them and consequently all the lanthanides exhibit predominantly single valancy.

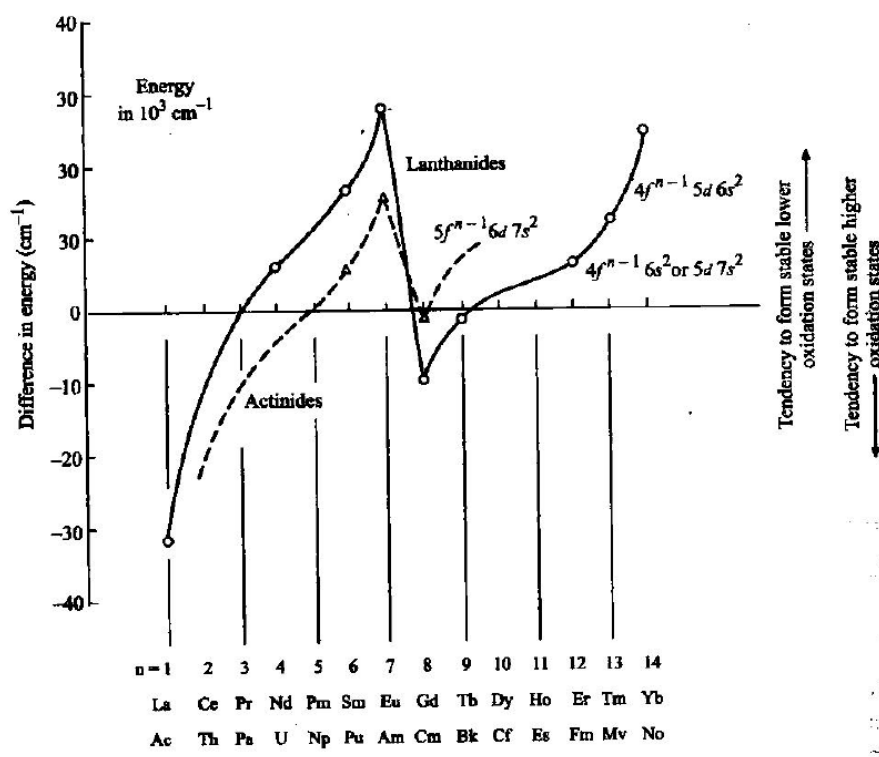


**Figure 1.6** Approximate relative energies of the  $f^{n-1}d^1s^2$  and  $f^n s^2$  electron configurations (Huheey et al., 2006)

### 1.4.1.2. Oxidation State:

Actinides, especially early members of the series, exhibit multiple oxidation states owing to the close proximity of 5f, 6d and 7s orbitals. Ionization energy and hydration energy are responsible in facilitating the conversion of one oxidation state to another in aqueous solution, and a combination of these two energies will decide the most stable oxidation state for a given metal ion. As the f orbitals are less stabilized in early actinides, f-electrons having low ionization energy result in  $f^0$  as the most stable configuration for actinides up to uranium.

With increase in atomic number, f orbital becomes more stabilized compared to 6d and 7s orbital and therefore actinides beyond americium exhibit +3 as the most stable oxidation state except nobelium for which +2 state is most stable owing to stability of full filled 5f shell. Table 1.4 lists the oxidation states of the actinides and lanthanides (*Ahrland et al.,1973*).

**Table 1.4** Oxidation states of actinide elements (*Ahrland et al.,1973*)

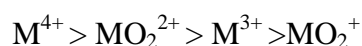
89	90	91	92	93	94	95	96	97	98	99	100	101	102	103
Ac	Th	Pa	U	Np	Pu	Am	Cm	Bk	Cf	Es	Fm	Md	No	Lr
						(2)		(2)				2	2	
<b>3</b>	(3)	(3)	3	3	3	<b>3</b>	3	<b>3</b>						
	<b>4</b>	4	4	4	<b>4</b>	4	4	4						
		<b>5</b>	5	<b>5</b>	5	5								
			<b>6</b>	6	6	6								
				7	7									
57	58	59	60	61	62	63	64	65	66	67	68	69	70	71
La	Ce	Pr	Nd	Pm	Sm	Eu	Gd	Tb	Dy	Ho	Er	Tm	Yb	Lu
			(2)		2	2						(2)	2	
<b>3</b>														
	4	(4)						4						

Bold: most stable oxidation state, in parenthesis: oxidation state not known in solution

In contrast, +3 oxidation state is predominant in lanthanides series owing to the large difference in binding energy of 4f and 5d, 6s electrons. However, +2 (Eu and Yb) and +4 (Ce and Tb) oxidation states also exist which corresponds to vacant or enhanced stability of half-filled or full filled 4f configuration. Thus, later members of actinides series behave like lanthanides and exhibit +3 as the most stable oxidation state.

#### 1.4.1.3. Ion types:

All actinides, essentially, have same structure in same oxidation states. In trivalent and tetravalent oxidation states, actinide ions exist as hydrated ions in acidic solutions. In higher oxidation states, owing to very high ionic potential, actinide ions immediately accept electron from donor atoms in solvent medium and form oxygenated species of the type  $\text{MO}_2^+$  and  $\text{MO}_2^{2+}$  which are termed as actinyl ions. The actinyl ions are highly stable and act as a single entity during chemical transformation but their formation decreases the effective charge on central actinide atom. The effective charge on the metal ion is  $3.3 \pm 0.1$  and  $2.3 \pm 0.2$  in  $\text{MO}_2^{2+}$  and  $\text{MO}_2^+$  respectively which is greater than the ionic charge on molecular entity and therefore coordinating field in the case of molecular ion is proportionately stronger (*Choppin and Allard, 1985*) The order of effective charge, which affects the different chemical properties, for different oxidation states is



#### 1.4.1.4. Lanthanide and actinide contraction: Effect on ionic radius:

In lanthanides and actinides, as the atomic number increases, electrons sequentially enter f orbitals which provide incomplete shielding of the outer shell electrons from the steadily increasing nuclear charge due to their diffused character.

Therefore, a steady decrease in the radius is observed in both the series. The phenomena are termed as the lanthanide and actinide contraction for lanthanide and actinide series respectively. Similar trend is observed in ionic radii of the elements of both the series. Figure 1.7 shows the variation of ionic radius for +3 and +4 oxidation states of lanthanides and actinides. The sufficiently small change in charge density, as a result of slight decrease in ionic radius, accounts for almost identical chemical properties of all elements across the series. Moreover for a given oxidation state, the actinides and lanthanides having similar ionic radius exhibit similar chemical properties for instance the elution of trivalent actinides and lanthanides with similar ionic radius from dowex 50 using ammonium  $\alpha$ -hydroxyisobutyrate is observed at similar position (Nash *et al.*, 2006). Thus, lanthanides are often used as the analogue of homologous actinides.

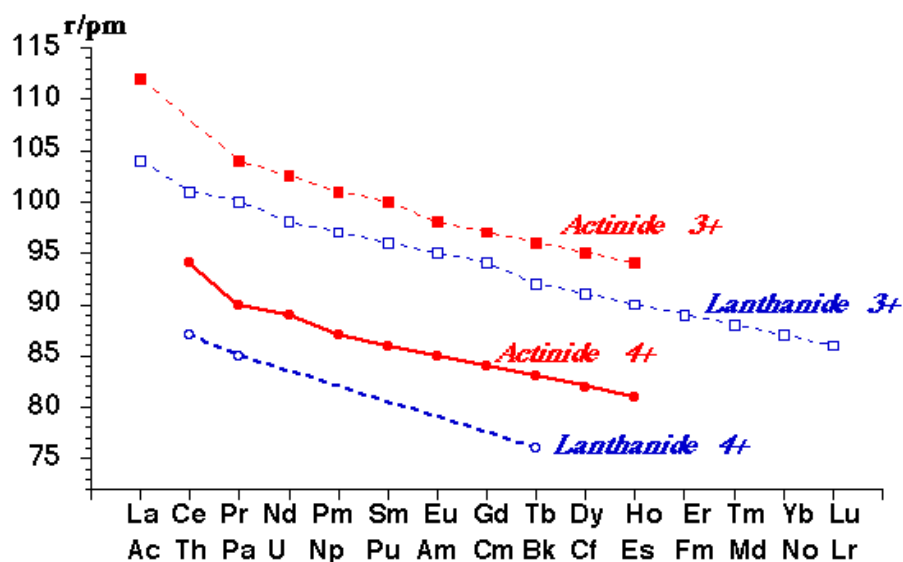


**Figure 1.7** Ionic radii of lanthanides and actinides for +3 and +4 oxidation states

#### 1.4.2. Environmental Actinide Chemistry:

For understanding the chemical behaviour of actinides in natural waters, the basic knowledge of their potential chemical reactions occurring in these aquatic

systems is indispensable. In this section, the chemical properties of actinides, with particular reference to natural waters, have been discussed.

#### 1.4.2.1. Oxidation States of Actinides in solution:

The variety of oxidation states (Table 1.4) exhibited by actinide cations and their coexistence in solution for a particular actinide, owing to small difference in redox potentials (Figure 1.8), complicate the prediction of actinide behavior in geochemical conditions with changes in  $Eh$ , pH, ligand concentrations, etc. Some of the actinides of environmental interest (e.g., Am(III), Cm(III), Th(IV)) exhibit single oxidation state but others (e.g. U, Np, Pu) can exist in several states in solution. The higher oxidation states are favoured with increasing pH and/or  $Eh$ .

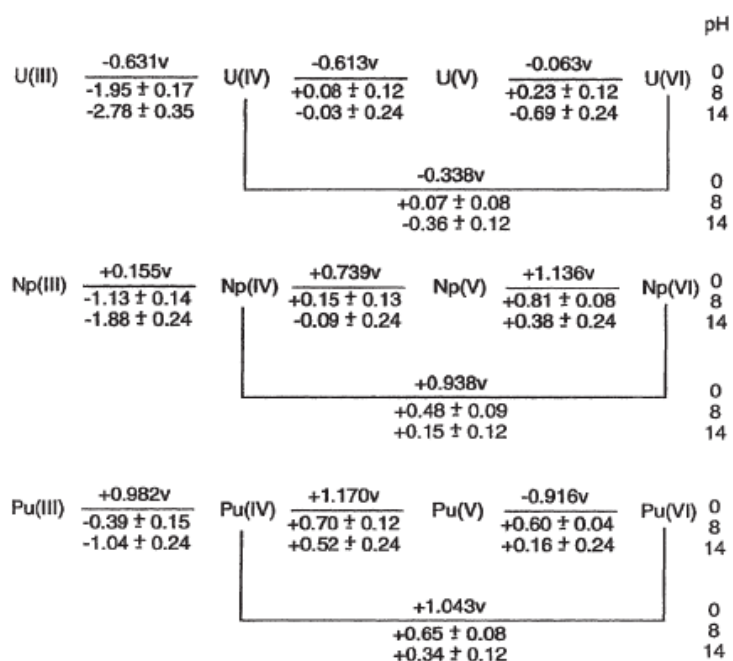
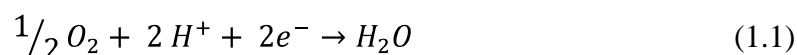


**Figure 1.8** Redox potentials of U, Np and Pu at pH = 0, 8, and 14 (*Choppin, 2005*)

Since in natural systems, water is dominant transport medium, predominant actinide oxidation states and actinide species are determined by water conditions.

Thus, for predicting the behaviour of actinides in aqueous solutions, thermodynamic equilibrium diagrams (Eh vs. pH), called Pourbaix diagrams serve as a useful tool in which stability areas are presented as a function of pH and electrochemical potential scales. For constructing the Pourbaix diagrams for any radionuclide, it is first essential to define the chemical stability area of water.

The potential when the oxygen generation starts on the anode is defined as the upper stability limit of water. It is specified by the reaction:



By use the Nernst equation, the relationship between potential and pH

$$E = E_0 - \frac{2.303RT}{nF} \log \left( \frac{1}{[H^+]^2 pO_2^{\frac{1}{2}}} \right) \quad (1.2)$$

With  $E_0 = 1.299$  V,  $T = 298^0\text{K}$ ,  $R = 8.134$  J/  $^0\text{K} \cdot \text{mol}$ ,  $F = 96500$  C/ mol and  $pO_2 = 1$  bar

$$E = 1.299 - 0.0591 \text{ pH} \quad (1.3)$$

The potential where hydrogen gas is evolved from the surface of an immersed electrode defines the lower stability limit of water. It is defined by the reaction



Applying Nernst equation to above equilibrium, the relationship between potential and pH

$$E = 0.059 \text{ pH} \quad (1.5)$$

The effective overall boundaries of the Pourbaix diagrams determined by the stability field for water are given by equation (1.3) and (1.5). The dashed lines in figure 1.9 define the area of water stability. Thus water offers its solutes only a small electropotential window of stability. Outside these limits, solute-solvent redox reactions alter the solution chemistry and oxidation-state stability. Within the stability

zone of water, the distribution of different oxidation state and species of a particular actinide can be obtained by considering all its redox and complexation reactions. Figure 1.9 shows Eh-vs-pH diagram calculated for plutonium in water containing hydroxide, carbonate, and fluoride ions. Higher Eh values stabilize redox-sensitive actinides like plutonium in the higher oxidation states V and VI. The points labeled 1, 2 and 3 in figure 1.9 are triple points where plutonium can exist in three different oxidation states. The solid black outline depicts the range of Eh/pH values found in natural waters. In ocean water or in groundwater, plutonium is likely to exist as Pu(IV), while in rainwater or streams, plutonium can assume the V state (Runde, 2000). Thus, Pourbiax diagrams are used to predict transport and mobility of actinides. In most ocean or groundwater environments U(VI), Np(V), Pu(IV), Am(III) and Cm(III) are the prevalent oxidation states.

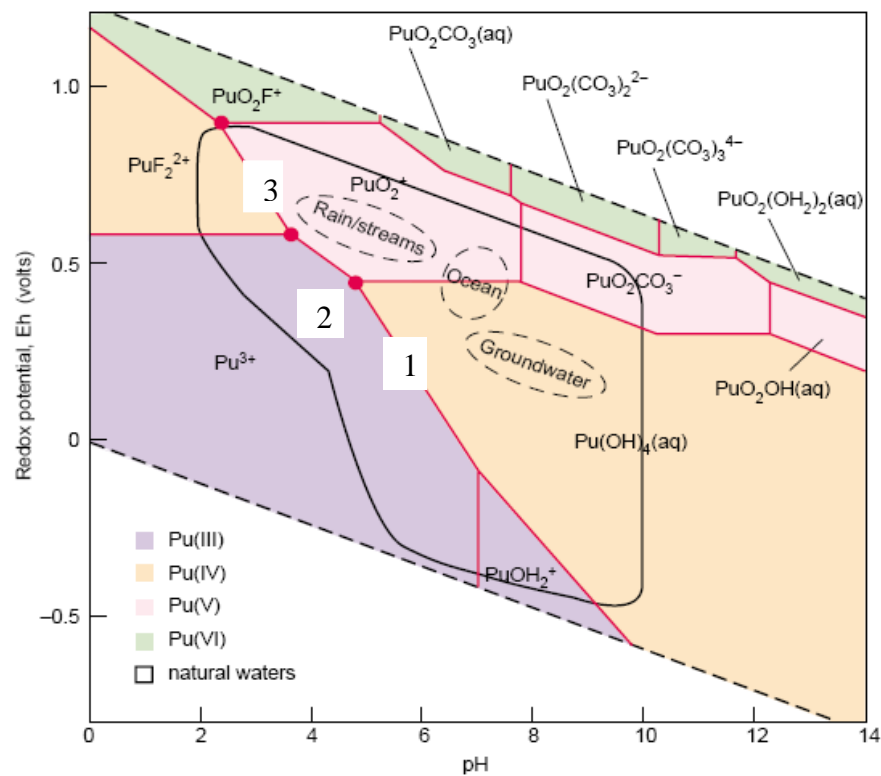


**Figure 1.9** Speciation of Plutonium in natural waters (Runde, 2000)

#### 1.4.2.2. Hydration:

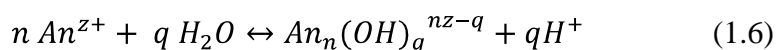
The hydration of actinides is one of the most important factors in determining the structural and chemical properties of actinides. All actinides exist as hydrated ions owing to strong interaction between actinides and water molecules. Two terminologies which are used to quantify hydration are total hydration number (h) and primary hydration number ( $N_{H_2O}$ ). Total hydration number refers to all the water molecules that feel the effect of cation over concentric hydration sphere whereas primary hydration number refers to the water molecules which are directly bonded to the cation. The hydration number can be measured using variety of methods viz., X-ray and neutron diffraction, X-ray absorption fine structure (XAFS) measurements, luminescence decay, NMR relaxation measurements, optical absorption spectroscopy. The value of h and  $N_{H_2O}$  for  $Am^{3+}$  are 13.6 and 9.0 respectively. The  $N_{H_2O}$  of trivalent actinides gradually changes from 9 to 8 across the actinide series while opposite trend is observed for h. For example the  $N_{H_2O}$  value decreases from 9 to 8 between  $Am^{3+}$  and  $Cf^{3+}$  while h increases from  $\sim 12.6$  to  $\sim 14$  (Choppin and Jensen, 2006). The higher value of h for later members of the series is attributed to increase in charge density with increase in atomic number.

While the hydration number and coordinated water molecules for the trivalent actinides have been studied extensively, for other oxidation states (+4, +5, +6) only limited studies have been carried out. The  $N_{H_2O}$  and h for actinide hydrates in +4 oxidation states lies in the range 8-10 and 20-22 respectively (Choppin and Jensen, 2006). The pentavalent and hexavalent actinides are relatively less hydrated, in comparison to trivalent and tetravalent actinides, due to the formation of actinyl ion. XAFS measurements of solution containing  $NpO_2^+$  gave  $N_{H_2O}$  value of 5 which is consistent with value obtained by optical absorption spectra. The Raman studies of

aqueous uranyl  $[UO_2^{2+}]$  solutions revealed the presence of six water molecules in the plane perpendicular to O=U=O axis thereby resulting  $N_{H_2O}$  value of 6 for hexavalent actinides (Choppin and Jensen, 2006).

#### 1.4.2.3. Hydrolysis of actinide cations:

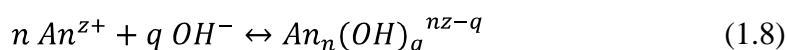
In aqueous solution, all actinide ions interact with water molecules and exist as aquo ions. More is the effective charge on the metal ion, greater is the extent of interaction with the water molecules. These hydrated cations act as hard acid thereby polarizing the water molecules sufficiently enough to release protons. This phenomenon of release of proton from water molecule under the influence of metal ion is termed as hydrolysis. Actinides undergo hydrolysis in weakly acidic to alkaline solutions in the +3, +4 and +6 oxidation states. The hydrolysis reaction can be represented as



The hydrolysis constant  $\beta_{nq}^*$  is given by

$$\beta_{nq}^* = [An_n(OH)_q^{nz-q}][H^+]^q/[An^{z+}]^n \quad (1.7)$$

The hydrolysis reaction can also be defined as the complexation with hydroxide ion



The stability constant for the above reaction is given by

$$\beta_{nq} = [An_n(OH)_q^{nz-q}]/[An^{z+}]^n[OH^-]^q \quad (1.9)$$

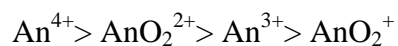
The ionic product of water ( $K_w$ ) is defined as

$$K_w = [H^+][OH^-] \quad (1.10)$$

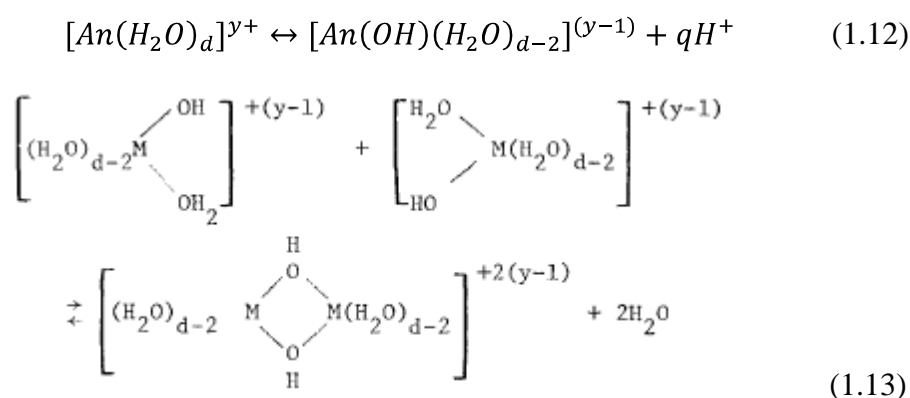
Thus,

$$\beta_{nq} = \beta_{nq}^* / K_w^q \quad (1.11)$$

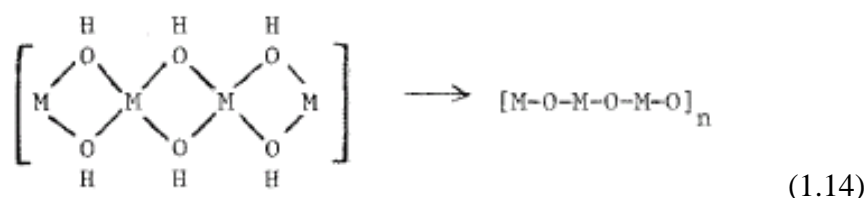
The order of hydrolysis is



which is in accordance with effective charge possessed by the actinide ions in different oxidation states. The hydroxo complexes thus formed, prior to complete hydrolysis, can undergo condensation reactions to form polynuclear species in which metal ions are linked through hydroxo (M-OH-M) and oxo (M-O-M) bridges as described by equations below



In reactions such as this, a solvating water molecule around one cationic species is replaced by a hydroxyl group. The hydroxyl ion is shared by the two metal atoms forming polynuclear hydroxyl-bridged aggregates. Under appropriate conditions, like high temperature, prolonged aging, and/or high pH, irreversible elimination of more water is accompanied by the formation of oxygen bridges between the metal atoms.



The measurements of hydrolysis constant are challenging as actinide hydroxides are quite insoluble and sorb to surfaces. Therefore, the sensitive techniques such as TRLFS which allows the measurements at very low concentrations have been used for their determination. For example, the hydrolysis constants of Cm

(III) have been determined by Fanghanel and Kim (1994) using TRIFS.

Out of all the oxidation states, the tetravalent actinides are most prone to hydrolysis and polymerisation. The tetravalent actinides undergo hydrolysis even in acidic solutions with  $\text{pH} \geq 0$ . The hydrolysis of tetravalent actinides has been studied using  $\text{Th}^{4+}$ , which is often used as a model for  $\text{Np(IV)}$  and  $\text{Pu(IV)}$ , but there exist significant differences in the extent of hydrolytic reactions as compared to other tetravalent actinides owing to its higher ionic radius. The formation of complexes of high nucleation has been confirmed by diffraction measurements that yielded Th-Th bond distance of  $3.99\text{\AA}$  which is exactly same as in the solid  $\text{Th}_2(\text{OH})_2(\text{NO}_3)_6(\text{H}_2\text{O})_8$  that contains dimer joined by hydroxo bonds (Choppin and Jensen, 2006). In case of  $\text{Pu(IV)}$ , preparation and maintenance of only  $\text{Pu}^{4+}$  in solution is a challenge and thus the data on hydrolysis constants available in the literature are not consistent. Moreover,  $\text{Pu}^{4+}$  has high tendency to form intrinsic colloids which must be removed using suitable ultra-filter to avoid improper estimation of hydrolysis constants.

The low effective charge (+ 2.2) on actinides in +5 oxidation state make them least prone to hydrolysis. It has been observed that  $\text{NpO}_2^+$  does not hydrolyze even up to  $\text{pH} = 8$ . The actinides in +6 oxidation state undergo hydrolysis to an appreciable extent. For the actinyl(VI) ions, hydrolysis decreases with increase in atomic number opposite to the trend expected based on charge to size ratio.  $\text{UO}_2^{2+}$  forms mononuclear hydrolyzed species  $\text{UO}_2(\text{OH})_q^{2-q}$  at lower ( $< 10^{-6}$  M) concentrations, while at higher concentrations, polynuclear species are formed, depending upon the pH and metal ion concentration, which are small entities containing fewer than five uranium atoms. The tendency to form polymers of colloidal dimensions appears to be diminishing in actinides in +6 oxidation state as compared to actinides in +4 oxidation state (Choppin and Jensen, 2006).

The natural waters have pH in the range 5-9 at which extensive hydrolysis is observed in case of actinides. These hydrolytic reactions constrain the solubility of actinides and facilitate the generation of colloids thereby modifying their speciation in natural aquatic systems (Kim, 1986).

#### 1.4.2.4. Complexation of actinides:

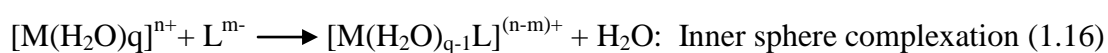
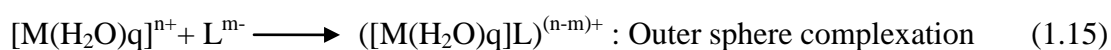
In all common solution oxidation states (+2 to +6), actinide ions act as hard Lewis acids and thus prefer to bind with the hard Lewis base donor atoms such as oxygen and fluorine. The actinide-ligands bonds are predominantly ionic in nature, kinetically labile and non-directional. Electrostatic interaction and steric interferences are the primary factors in determining the bond strength in actinide complexes. The electrostatic interaction is a function of the effective charges of the metal ion and ligand and actinide–ligand distance. The steric constraint arises due to the properties of the actinide cation and that of the ligand viz., ionic size of actinide cation and presence or absence of actinyl oxygen atoms, number and spatial relationship of donor atoms, size of chelate ring and flexibility of ligand conformations.

Considering no steric constraints, the strength of complexation of a given ligand for actinides in different oxidation states is given by



Moreover across the actinide series, for a given oxidation state the strength of complexation increases owing to the increasing charge density of actinide ions. Increase in charge density of ligands also favours complexation. However, steric constraints become important generally in case of actinyl ions as the ‘-yl’ oxygen atoms restrict the ligand to bond in the equatorial plane.

Although, most of the actinide complexes are ionic in nature, some of them, unlike lanthanides, do exhibit covalent character especially in the case of ligands with soft donor atoms, viz., N, S etc. This behaviour observed in case of actinides can be attributed to greater spatial extension of 5f orbitals than that of 4f orbitals which increases the covalent bonding in actinides as compared to lanthanides. The increased covalency in actinides, resulting in their higher affinity for soft electron donors, such as 'S' donor ligands, has been exploited to separate lanthanide and actinide elements (*Bhattacharyya et al., 2006*). Actinides form inner sphere and outer sphere complexes depending upon the basicity of the ligands. The inner sphere complexes refer to the species in which the bonding involves direct contact between cation and ligand where as in outer sphere complex, the ligand does not enter the primary coordination sphere of cation and is separated by solvent molecules. In aqueous solution, actinide cations exist as hydrated ions of the type  $[M(H_2O)_q]^{n+}$  which on interaction with the ligand ( $L^{m-}$ ) results in the formation of an outer sphere complex or inner sphere complex represented by the following equations



Thermodynamic parameters of complexation can be used to distinguish between the inner sphere and outer sphere complex formation.

In natural waters wide variety of complexing anions are present which can be broadly classified into two categories namely inorganic and organic anions.

#### 1.4.2.4. (a) Complexation by inorganic anions:

The common inorganic complexing anions present in natural waters are carbonate ( $CO_3^{2-}$ ), sulphate ( $SO_4^{2-}$ ), phosphate ( $PO_4^{3-}$ ), chloride ( $Cl^-$ ), fluoride ( $F^-$ ), nitrate ( $NO_3^-$ ) and silicate (*Silva et al. 1995*). The concentration of these inorganic

anions is dependent upon the source of water. For instance, ocean water contains very high concentration of  $\text{SO}_4^{2-}$ . The actinide solubility increases, as a result of complexation with inorganic anions, as opposed to the hydrolysis reactions. Figure 1.10 shows the stability constants ( $\beta_1$ ) for the formation of 1:1 actinide complexes with common complexing anions present in natural waters for different oxidation states. The hydrolysis (complexation by  $\text{OH}^-$ ) and carbonate complexation are usually predicted to be the most dominant in natural waters owing to their high concentration in natural waters and strong complexing tendencies. Therefore, the species formed as the result of carbonate complexation of actinides, in different oxidation states, are discussed in detail.

Above  $\text{pH} > 6$ , trivalent actinides form  $\text{AnCO}_3^+$ ,  $\text{An}(\text{CO}_3)_2^-$  and  $\text{An}(\text{CO}_3)_3^{3-}$  as major species in carbonate rich waters. The relative concentration of the three carbonate complexes is dependent on  $\text{pH}$  of water under consideration (*Silva and Nitsche, 1995*). Actinides in +3 oxidation state tend to precipitate as hydroxy carbonate, of the type  $\text{An}(\text{OH})\text{CO}_3$ , which governs their solubility equilibria in presence of carbonate. In case of tetravalent actinides, hydrolysis is more dominant which leads to the formation of insoluble  $\text{An}(\text{OH})_4$  species. Therefore,  $\text{An}^{4+}$  do not form carbonate complexes in significant levels (*Choppin, 2005*). However, like trivalent actinides,  $\text{An}^{4+}$  tend to precipitate as hydroxo carbonate complexes ( $\text{An}(\text{OH})_2\text{CO}_3$ ) which limit their solubility in carbonate rich waters (*Kim et al. 1986*). Carbonate complexes of the type  $\text{AnO}_2(\text{CO}_3)^-$ ,  $\text{AnO}_2(\text{CO}_3)_2^{3-}$  and  $\text{AnO}_2(\text{CO}_3)_3^{5-}$  are known for pentavalent actinides whereas hexavalent actinides form  $\text{AnO}_2(\text{CO}_3)$ ,  $\text{AnO}_2(\text{CO}_3)_2^{2-}$  and  $\text{AnO}_2(\text{CO}_3)_3^{4-}$  complexes. The strong carbonate complexation in case of hexavalent actinides is responsible for 90-100% of dissolved uranium in oceans (*Choppin, 2007*).

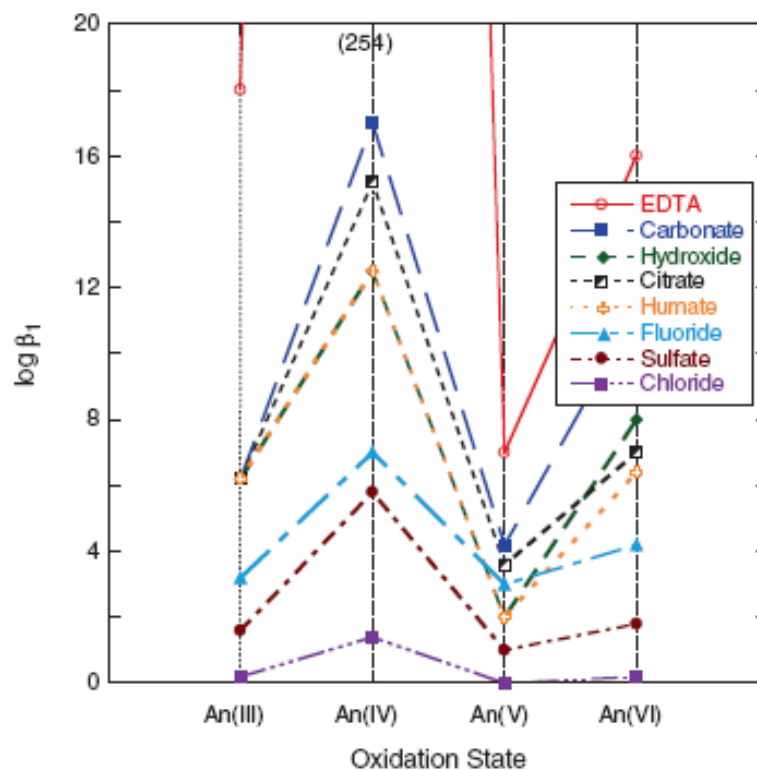


**Figure 1.10** Stability constants of actinides of different oxidation states with common aquatic ligands (*Runde and Neu, 2006*)

#### 1.4.2.4.(b) Complexation by organic anions:

The organic compounds identified in natural waters are HS and LMCA viz. citric, butyric, valeric, pyruvic, lactic, succinic, adipic, malonic, tartaric and malic (*Choppin and Allard, 1985*).

##### (i) LMCA:

LMCA are a group of organic compounds containing one or more carboxylate functions (-COOH) and a short hydrocarbon group which can be aliphatic, aromatic, saturated or unsaturated, straight chain or branched, and substituted with hydroxyl- or keto-, or any other group in their structure. The occurrence of LMCA in the environment is outcome of natural processes as well as from anthropogenic emissions. Organic acids are excreted by many organisms, including bacteria, fungi and algae as

well as higher plants and animals. Moreover, the degradation of dead biomass releases significant amounts of organic acids (*Fischer, 2002*). Residues and byproducts from different industries viz., agriculture and food processing, sewage, chemical, textile and metallurgic industries are important anthropogenic emission sources (*Abdel daiem et al., 2012*). Since all the factors contributing towards the concentration of LMCA may operate up to different extents, their concentration may vary from source to source (*Strobel, 2001*). Complexation of actinides with LMCA can increase their mobility in the environment, thus it should be understood in detail.

**(ii) HS:**

HS are formed as a result of decay of plant and animal remains in the soil. The formation of HS has been postulated using several theories as shown in figure 1.11. According to lignin theory (pathway 1) HS represent modified lignin, which is incompletely utilized by microorganism and the residuum becomes part of the soil humus. Another approach proposes the formation of either phenolic, aldehydes and acids from lignin (pathway 3) or polyphenols from cellulose (pathway 2), which undergo enzymatic conversion to quinones which polymerize in the presence or absence of amino compounds to form humic like macromolecules. Sugar-amine condensation theory (pathway 4) involves the formation of reducing sugars and amino acids, formed as by-products of microbial metabolism, which undergo nonenzymatic polymerization to form HS. In practice all four pathways must be considered as likely mechanisms for the synthesis of HS in nature. All these four pathways may operate in all soils but to different extent depending upon their geographical, climatic, physical and biological conditions.

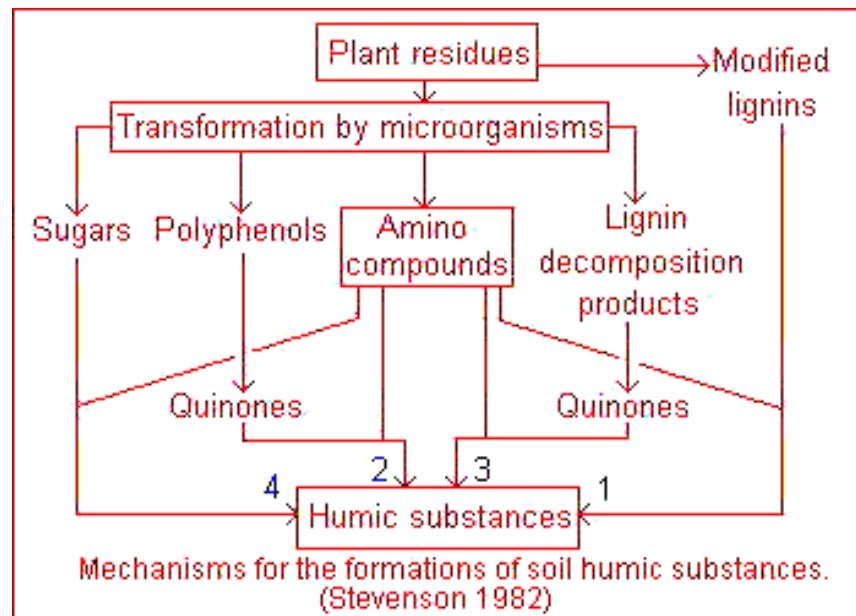


**Figure 1.11** Different routes of formation of HS in environment

As there exist large variety in original material and decomposition stage, HS are far from a ‘simple molecule’, instead, it consists of a heterogeneous mixture of complex molecules. Their properties are dependent on the ecosystem in which they are formed (Stevenson, 1982). HS are classified as FA, HA, and humins, depending upon their solubility in water as shown in figure 1.12 (Pena-Mendez et al., 2005). The hypothetical structure for HA proposed by Stevenson (1982) contains free and bound phenolic groups, quinone structure, nitrogen and oxygen as bridging units and carboxylic groups variously placed on aromatic rings as shown in figure 1.13.

The different properties of HS are depicted in figure 1.14. It is evident that carbon and oxygen contents, acidity and degree of polymerization all change systematically with increasing molecular weight. The low molecular weight FA has higher oxygen but lower carbon contents than the high molecular weight HA. Another striking difference is that while the oxygen in FA can be accounted for largely in

known functional groups (COOH, OH, C=O), a high portion of the oxygen in HA seems to occur as a structural component of HA.

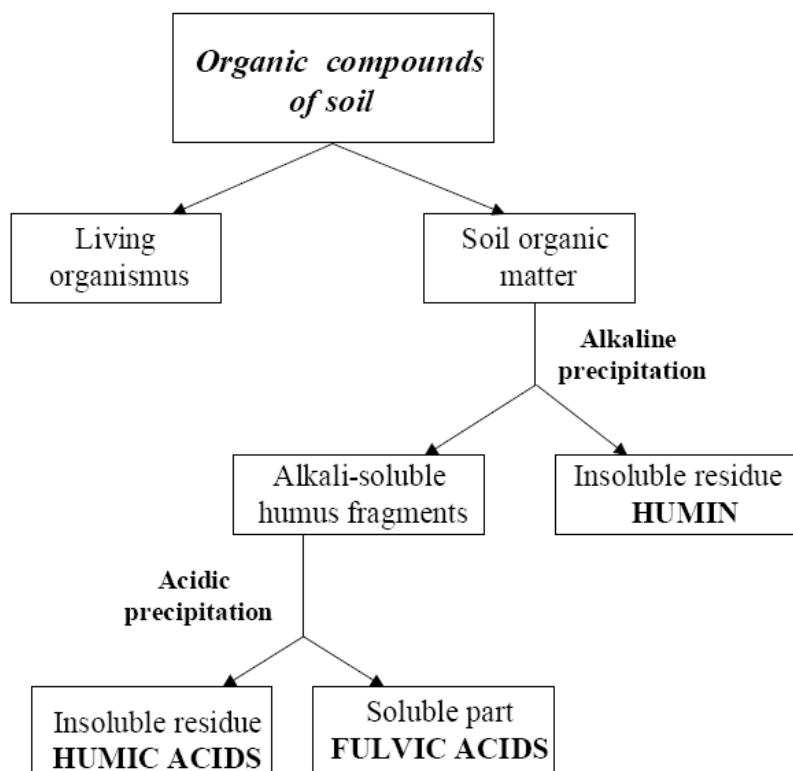


**Figure 1.12** Classification of HS based on solubility

HS constitute large fraction of dissolved organic matter. Their concentration varies from 0.1 mg/L in deep groundwater to 50 mg/L in swamp waters compared to 0.5–1.2 ppm in world's oceans (Stevenson, 1982). They are anionic macromolecules with heterogeneity in terms of physical and chemical properties and may be dissolved, colloidal, or may be bound to the surface of an inorganic colloid. They have the ability to form chelate with radionuclides via carboxylate groups, phenolic and/or amino groups. Since the deprotonation of these functional groups is pH dependent, the stability constant of these complexes vary with pH and degree of dissociation. The typical log  $K$  values of humate complexes of Am(III), Pu(IV), Np(V) and U(VI) at pH

7 are nearly 12, 16, 5 and 8 respectively (Silva and Nitsche, 1995). Hence, despite of their low concentration, they influence the transport, bioavailability and fate of radionuclides in the environment (Boggs et al., 1985).

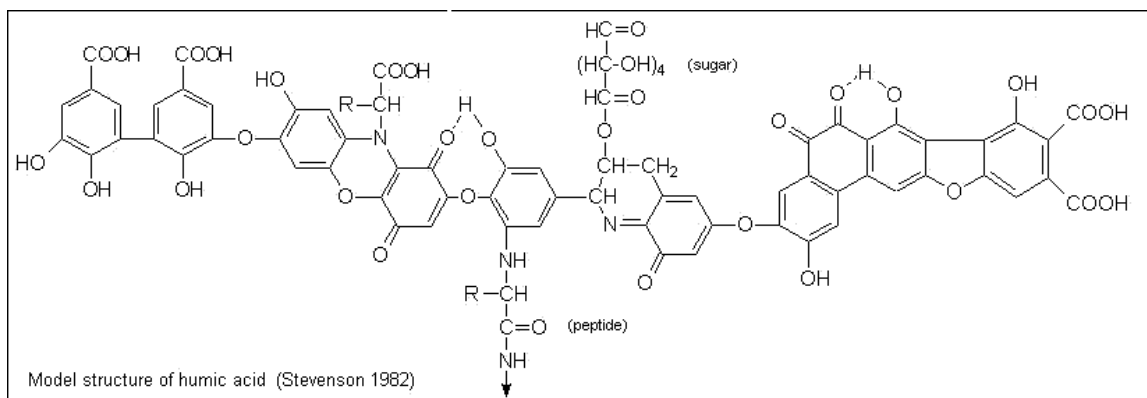


Figure 1.13 Proposed Structure of HA

Humic substances (pigmented polymers)				
Fulvic acid		Humic acid		Humin
Light yellow	Yellow brown	Dark brown	Grey-black	Black
<p>————— increase in intensity of colour —————&gt;</p> <p>————— increase in degree of polymerization —————&gt;</p> <p>2 000 ————— increase in molecular weight —————&gt; 300 000</p> <p>45% ————— increase in carbon content —————&gt; 62%</p> <p>48% ————— decrease in oxygen content —————&gt; 30%</p> <p>1 400 ————— decrease in exchange acidity —————&gt; 500</p> <p>————— decrease in degree of solubility —————&gt;</p>				
Chemical properties of humic substances. (Stevenson 1982)				

Figure 1.14 Chemical properties of HS

#### 1.4.2.5. Colloid formation:

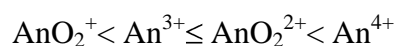
Colloids are ubiquitous in natural waters and therefore it is imperative to understand their role in actinide migration. The term colloid refers to any particles or

entities having diameter between 1 nm and 1  $\mu\text{m}$  which remain stable in suspension over long time periods unless coagulation occurs to form larger aggregates or deposition onto surfaces of larger grains (*Dozol and Hagemann, 1993*). The colloidal particles possess very large specific surface area and, therefore, are important sorbents for environmental contaminants. There are mainly two types of colloids present in natural waters namely inorganic colloids, formed by weathering and geochemical alteration of rocks and minerals, and organic colloids (HS) (*Zachara et al., 1994*). Moreover, inorganic colloids covered with organic colloids and microbes stabilized by hydrophilic coatings also come in category of colloids present in natural water (*Kessler, 1999*).

Colloids associated with actinides in ground water can be broadly classified as:

#### 1.4.2.5. (a) *Intrinsic colloids:*

Intrinsic colloids are formed by condensation of actinides ions or molecules as a result of hydrolytic or precipitation processes. The mechanism of intrinsic colloid formation resembles that of precipitation. Thus, it is expected that when actinide concentration is large enough to exceed the solubility product of the solid phase, intrinsic colloids are formed (*Ramsay, 1988; Kepak, 1971*). The intrinsic colloids formation can be thought to be the gradual transition from ions to hydrolyzed ions followed by a series of nucleation and polymerization processes. Owing to extremely low solubility of actinide oxides, hydroxides, carbonates and hydroxycarbonates, these compounds can serve as building block of intrinsic colloid formation. The order of tendency of different oxidation state of actinides to form intrinsic colloid is



It has been established that the stability of intrinsic colloids increases with time due to the enhancement in crystallinity (*Rai and Ryan, 1982*) which ultimately

results in quasi-stable species with a concentration in solution that can significantly exceed the thermodynamically calculated solubility of actinide oxides or hydroxides significantly (*Rai et al., 1980; Neck et al., 2007*). As intrinsic colloids of tetravalent actinides possess high stability, resistance to disintegration on dilution with water, and ability to increase the actinide concentration in solution, they are of major concern while predicting actinide migration. While Pu(IV) intrinsic colloids are the most studied in literature (*Rai et al., 1980, 1982; Neck et al., 2007*), similar generation of intrinsic colloids have been reported for Th(IV) and Np(IV) in recent years (*Altmaier et al., 2004; Neck et al., 2001*).

#### 1.4.2.5. (b) Pseudo Colloids

Every aquatic system contains colloids varying in nature, form and size. The type and concentration of colloids present in natural waters are dependent on the associated geological structure and hydrogeochemical transformations (*Degueldre et al., 2000*). In addition to natural processes, alteration processes in man-made materials are also responsible for the colloid formation in natural waters. For example dissolution of high-level waste glass and spent nuclear fuel may generate clay (mainly smectite) and silica colloidal material (*CRWMS 2000*). The inorganic colloids exhibit high sorption capacities to sorb actinides, owing to large surface area and high density of surface functional groups, which is responsible for generation of actinide bearing pseudo colloids. Extensive studies have been carried out in well-defined laboratory conditions with synthetic colloids to understand the fundamental behavior of actinide-bearing colloids (*Keeney-Kennicutt and Morse, 1985; Sanchez et al., 1985; Nagasaki et al., 1997; Novikov et al., 2006; Kalmykov et al., 2007; Farr et al., 2000; Lu et al., 2003*). Apart from inorganic colloids, HS and inorganic colloids covered with HS can also form pseudo colloids with actinides. In order to avoid underestimation of the

mobility of actinides, the consideration of colloid borne actinides in aquatic systems is necessary (*Schafer et al., 2012; Kersting et al., 1999*). In addition to the knowledge regarding extent of formation of colloids, the velocity of colloids in water which is a function their charge and size has to be taken into account to predict actinide mobility in aquatic systems (*Ramsay, 1988*).

#### **1.4.2.6. Reactions at the mineral/water interface:**

In natural environments there exist a wide variety of functional groups viz., hydroxyl, carbonate, silicate and phosphate that can strongly bind actinide ions on rocks, sediments and minerals. Sorption of radionuclides on mineral surfaces is regarded as one of the dominant retardation processes in the near and far-fields of nuclear waste repositories (*Geckeis and Rabung, 2008*). The sorption is used to describe the uptake of an ion or compound on solid surfaces, resulting in the transfer of this species from the liquid to the solid phase. Sorption includes large number of chemical processes viz., adsorption, absorption, incorporation, recrystallization, ion exchange and surface precipitation (*Schafer et al. 2012*) of which the former two processes are relevant to present work. Sorption involves the attachment of the metal ion to the mineral surface either physically via electrostatic interactions (dipole-dipole, ion-dipole, Vander Waals interactions) or chemically via a chemical bond between the ion and the mineral surface (*Stumm and Morgan, 1996*). The former process is termed as physiosorption and latter is called chemisorption. In physiosorption, formation of an outer sphere complex take place in which the metal ion retains its hydration sphere upon attachment to the surface while chemisorption results in the formation of inner sphere complex where the metal ion loses parts of its hydration shell to allow chemical bond formation between the sorbate and the sorbent. Incorporation however, involves uptake of the ion within the mineral structure which

is generally the outcome of the direct substitution of the metal ion with one of the mineral's structural components (*Stumm and Morgan, 1996; Ishida et al., 2012*).

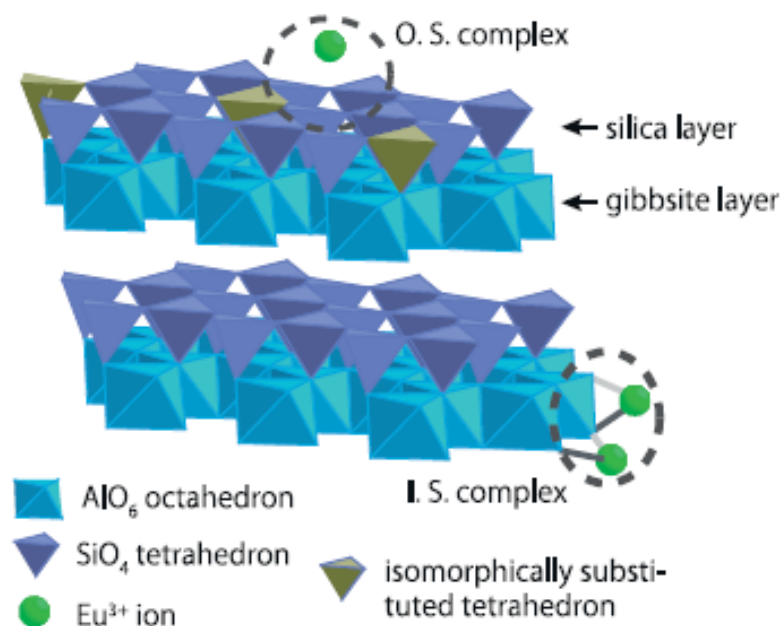


**Figure 1.15** Conceptual illustration of the inner- (I.S.) and outer-sphere (O.S.) surface complexes of  $\text{Eu}^{3+}$  with kaolinite (*Ishida et al., 2012*)

Since physisorption, chemisorption and incorporation reactions involve different interactions at solid/solution interface (figure 1.15), it is imperative to distinguish between them as they will affect the mobility of actinides to different extent in geologic media. The influence of one of the parameters of surrounding solution i.e ionic strength on physisorption and chemisorption has been discussed briefly to illustrate the inherent differences in nature of complexes formed as the result of two sorption processes. The outer sphere complexation on solid surface is very sensitive to variations in the ionic strength of the surrounding solution (*Dzombak and Morel, 1990*).

Thus, an increase in ionic strength only, may cause the outer sphere complex

to desorb from the surface. On the other hand inner sphere complexes, bound strongly to the surface owing to the chemical bond formation between the metal ion and the solid surface, does not undergo desorption with change in ionic strength. Although, desorption can take place in case of chemisorption, with increase of complexing ligands, such as HS, citrate,  $\text{CO}_3^{2-}$ ,  $\text{SO}_4^{2-}$ , and  $\text{H}_4\text{SiO}_4$  in the surrounding media (*Kar et al., 2011a, 2011b, 2012*). However, these complexes can form ternary surface complexes and thus may not increase the mobility of the radionuclides in the geosphere (*Fernandes et al., 2010*). Extensive studies have been carried out to investigate the sorption of actinides on mineral oxides and clay minerals in which spectroscopic techniques (*Rabung et al., 2000, 2005;* *Fouchard et al., 2004a;* *Takahashi et al., 2006;* *Hartmann et al., 2008;* *Ishida et al., 2009;* *Schlegel et al., 2004;* *Stumpf et al., 2007;* *Denecke, 2006;* *Geipel, 2006*) and SCM (*Bradbury and Baeyens, 2002, 2006, 2009a, 2011;* *Bradbury et al., 2005;* *Grambow et al. 2006;* *Gaskova and Bukaty, 2008*) have been employed to understand the sorption mechanism in addition to the determination of  $K_D$ . Hence, reactions at mineral/water interface are one of the dominant factors which control mobility of actinides in the environment.

### **1.5. Need for Spectroscopic techniques to study actinide speciation:**

Initially the focus of geochemists was to obtain  $K_D$  of actinides as input data for performance assessment modeling related to actinide transport in the environment. Later on, it was realized that for the development of appropriate geochemical sorption models, required for reliable description and prediction of actinide environmental behaviour, molecular level understanding of reaction mechanisms is needed which can be obtained by using spectroscopic techniques which are generally non-invasive and provide information about the oxidation state and chemical environment of the

measured species. Laser based spectroscopic systems are very sensitive and allow study of systems containing sub-molecular concentrations of some actinide ions. The spectroscopic techniques, such as TRLFS, EXAFS, Raman or infrared spectroscopy, Laser-Induced Photoacoustic Spectroscopy, Laser-Induced Thermal Lensing Spectroscopy, NMR, UV-Visible Absorption Spectroscopy and XPS are being used to understand the sorption mechanisms and actinide speciation at molecular level (Zaera, 2012; Tan et al., 2010). The detection limits of actinides for different spectroscopic methods which are dependent on the element and its oxidation state are listed in table 1.5.

**Table 1.5** Approximate detection limits of actinides in oxidation state speciation  
(Choppin, 2006)

Technique	Approximate detection limits
NMR	$10^{-1}$ – $10^{-4}$ M
X-ray Absorption Spectroscopy	$10^{-1}$ – $10^{-4}$ M
UV-Visible Absorption Spectroscopy	$>10^{-5}$ M
LIPAS	$10^{-5}$ – $10^{-9}$ M
Laser-Induced Thermal Lensing Spectroscopy	$10^{-5}$ – $10^{-9}$ M
TRLFS	$10^{-5}$ – $10^{-9}$ M

Out of the above mentioned spectroscopic techniques, EXAFS and TRLFS are the most widely used to study the actinide speciation. EXAFS is one of the most versatile spectroscopic techniques which provide information about oxidation state and the number and type of nearest neighbour surrounding the absorbing atom and thus molecular structure of the actinide species. The only limitation with EXAFS is that the detection limit for this spectroscopic tool is very high (Table 1.5). In contrast TRLFS, comprises of characteristic luminescence spectral properties arising from f–f

electron transitions of some actinide ions mainly Cm(III) and U(VI), exhibit extremely high sensitivity (*Chung et al., 1998; Edelstein et al., 2006b; Simoni, 2002; Klenze et al., 1991; Choppin and Peterman, 1998a*) and allows for molecular-level speciation even at trace concentrations as listed in table 1.5. Thus, spectroscopic techniques enable the characterization of actinide species in solution as well as at solid solution interface which, in turn, is helpful in constructing geochemical sorption models.

### **1.6. Need of Modeling Actinide Sorption using Geochemical Codes:**

The conditional  $K_D$  was initially employed to describe the radionuclide uptake on geologic media. The prime limitation of  $K_D$  values is that they are valid only to the specific experimental conditions for which they have been estimated. Since, neither sorption mechanism, nor solution and surface speciation is considered while determining  $K_D$ , they cannot account for changes in solution conditions that are imperative in natural systems. The use of SCM has advantage over conditional  $K_D$ , as in SCM, surface chemical reactions are represented by a set of mass balance equations, analogous to aqueous systems, and thermodynamic constants thus obtained are independent of changes in solution conditions (*Dzombak and Morel, 1990*). The detailed knowledge obtained by spectroscopic techniques about the sorption process is helpful in validation of SCM and increases confidence in their reliability. SCM are capable of modeling the actinide sorption on mineral oxides, clays (*Bradbury et al. 2005; Gaskova and Bukaty, 2008; Bradbury and Baeyens, 2002, 2009a, 2011*). They have the potential of serving as useful tools in predicting actinide behaviour at solid/solution interface.

**1.7. Motivation for the present work:**

Deep geological repositories have been designed so as to ensure isolation of the fission products and transuranics for sufficiently long time and to minimize the risk of radionuclide migration in the biosphere. However, a thorough nuclear safety assessment has to be performed to access and predict radionuclide migration in case of possible release scenarios which requires fundamental understanding of speciation of radionuclides in the environment. Thus intense research in this field is need of hour which has opened up challenging research avenues for scientists worldwide. The main mode of transport for radionuclides from deep geological repositories towards the biosphere is the aquatic environment. The speciation of radionuclides and their migration is directly related to parameters of natural aquatic systems such as pH, redox potential (Eh), the presence of dissolved inorganic and organic species and the surrounding geologic media. Consequently, the geochemistry of radionuclides requires comprehensive knowledge of their chemical interaction with components of aquatic environment. The formation of complexes with inorganic and organic ligands, intrinsic colloids formation, radionuclide interaction with colloids and the sorption of radionuclides on surrounding geologic media affect radionuclide migration in the geosphere. A sound understanding of these solid/water interface reactions is of fundamental importance for the safety assessment of nuclear waste repositories. Thus work carried out as a part of this thesis deals with the two aspects of actinide speciation in natural waters:

**(i) Complexation of actinides and lanthanides with LMCA and HA:**

The actinide migration is influenced by presence of complexing anions (inorganic and organic) present in the aquatic environment. Therefore, it is imperative to understand the complexation of actinides with these ligands. The organic

complexants such as HS and LMCA have high affinity for actinides and can also form strong complexes with actinides and hence enhance their transport. Thus, fundamental understanding of the complex formation and determination of stability constants with these ligands is of utmost importance in order to predict the actinide migration in the environment. Though the stability constants of actinides with the common carboxylic acids have been determined in literature, the mechanism of binding of actinides with these ligands needs to be understood in detail which can be done by probing such systems using spectroscopic techniques.

With this in view complexation of Eu(III), chemical analogue of Am(III) and Cm(III), with different LMCA and HA have been studied by TRFS and the log  $K$  as well as the stoichiometry of the complexes has been determined for LMCA (*Jain et al., 2008, 2009*).

**(ii) Sorption of actinides and lanthanides on mineral oxides: Effect of complexing anions:**

The interaction of actinides at the solid/solution interface is one of the most dominant pathways for controlling their migration in the environment and therefore it has attracted the attention of geochemist during recent years. Depending on geochemical conditions and the type of mineral, sorption can be physiosorption, chemisorption or incorporation into the matrix. In addition, sorption mechanisms and the extent of sorption are dependent on pH, Eh, total actinide ion concentration as well as the composition of the aquatic environment in contact with mineral. Initially, it was thought that only the determination of  $K_D$  values at solid solution interface were sufficient for performance assessment modeling of deep geological repositories but soon it was realized that detailed understanding of sorption mechanism is imperative to construct geochemical sorption database and models. It is, therefore,

essential to investigate the sorption of actinides on to mineral and study influence of pH, actinide concentration, presence of complexing anions (inorganic and organic) on sorption, in depth, using spectroscopic techniques and surface complexation models.

With this in view, sorption of actinides (U(VI), Cm(III) and Np(IV,V) ) on mineral oxides (silica, hematite) and influence of complexing anions (HA, citrate, HIBA, carbonate), pH, ionic strength, actinide concentration has been investigated. The spectroscopic studies have been carried out, wherever possible, to delineate species responsible for sorption and to validate SCM (*Kar et al., 2011 a, 2011 b, 2012; Jain et al., 2007; Kar et al.,(communicated)*).

### **1.8. Scope of the thesis:**

The complexation and sorption of actinides on mineral oxides are important in understanding migration of actinide ions in aquatic environment. The actinide sorption is dependent on the various organic and inorganic ligands present in the surrounding media. HA and small complexing anions are prevalent in aquatic systems and hence their complexation with actinides and their influence on actinide sorption has been investigated in this thesis.

In the present work pertaining to complexation studies, Eu(III), the rare earth element having good fluorescence yield, has been used as an analogue of trivalent actinides to study the complexation of Eu(III) by different carboxylates, namely, HIBA, SA, PA, MA and HA using TRFS and the stability constant and stoichiometry of the Eu(III)- carboxylate complexes has been deduced.

In the studies pertaining to sorption, four different systems have been investigated.

a) The effect of pH, ionic strength, HA concentration and order of addition of Cm(III) and HA on curium sorption by silica colloids has been studied. LAM qualitatively

reproduced the profile of the Cm(III) sorption by silica in presence of HA.

b) Sorption of Eu(III) by silica and the effect of HIBA has been studied by batch sorption as well as TRFS. The speciation calculations of Eu(III) using MINTEQA2 and the SCM of the binary and ternary systems using FITEQL4.0 has been carried out. The surface complexes postulated have been validated using TRFS. Similar studies were performed with Cm(III) in order to demonstrate the differences, if any, between Eu(III) and Cm(III) with regard to sorption.

c) Sorption of neptunium on hematite colloids has been studied under aerobic and anaerobic conditions at varying pH in absence and presence of HA. The stability constant of Np(V)-humate complex was determined by solvent extraction method. Under anaerobic conditions Np(IV) sorption on hematite was studied and drastic difference in sorption behaviour were observed in aerobic and anaerobic conditions.

d) Sorption of U(VI) on silica surface was investigated as function of pH, ionic strength, and U(VI) concentration by employing batch sorption experiments and SCM. The effect of complexing anions viz., carbonate and citrate on U(VI) sorption was also studied. SCM and TRFS were satisfactorily able to explain the sorption phenomena in all the systems.

**Chapter II**

**Experimental Techniques**

**&**

**Methods**

**2.1. Introduction:**

The focus of the present studies is to understand the influence of LMCA and HA on complexation and sorption of actinides and lanthanides. The complexation studies entail the measurement of the stoichiometry of the complexes and their stability constants while sorption studies deal with  $K_D$  determination followed by spectroscopic characterization and SCM. In the present chapter, brief description of the methodology of sample and radiotracer preparation, their characterization and assay by different techniques viz., XRD, BET surface area analysis, zeta potential measurement, UV-Visible Spectroscopy, ICP-AES, TOC content, TRFS, Radiometry and the data analysis has been provided. In addition, aqueous speciation of radionuclides, linear additive and SCM used to model sorption phenomenon have been discussed in detail.

**2.2. Preparation and Purification of Radiotracers:**

The sorption studies on metal ions reported in the present thesis were carried out with radiotracers. Procurement, preparation as well as purification of various radiotracers are as follows:

**2.2.1. Neptunium tracer:**

$^{239}\text{Np}$ , the short lived (2.35 days)  $\beta/\gamma$ -emitting isotope of neptunium was used as the tracer for neptunium in sorption studies. 15 mg of uranium (as  $\text{U}_3\text{O}_8$ ) was irradiated in APSARA reactor at BARC having a neutron flux of  $5 \times 10^{11}$  n/cm<sup>2</sup>/s for 2 hours. After the irradiation, the uranium oxide was dissolved in 8 M HCl and the solution loaded on to a Dowex 1 X 8 anion exchange column of 3 mm diameter and 50 mm length. The column was washed with 8M HCl till all the fission products were washed from the column, which was monitored by gamma counting of the washings

using HPGe detector (Eurysis Measures, France) coupled to a 4K MCA. Subsequently neptunium was eluted with 2 mL mixture of 4 M HCl and 0.05 M HF. The radiochemical purity of  $^{239}\text{Np}$  was ascertained by counting the eluted fraction on HPGe. The solution was evaporated to dryness and then evaporated with 1M  $\text{HClO}_4$  three times and finally dissolved in 0.1 M  $\text{NaClO}_4$  solution to prepare  $10^{-11}$  M stock solution having pH  $\sim 6$ .

### **2.2.2. Uranium tracer:**

$^{233}\text{U}$  tracer ( $t_{1/2} = 1.59 \times 10^5$  years) was produced by the irradiation of  $^{232}\text{Th}$  followed by its purification (*Srinivasan et al., 1972*). Purification of  $^{233}\text{U}$  from its daughter products and Thorium was carried out from 6 M HCl using anion exchange procedure (*Rattan et al., 1981*). Uranium in 6 M HCl solution forms anionic complex which is held on the column, whereas thorium and daughter products are not retained on the column. The column was washed with excess of 6 M HCl to remove any adsorbed impurities. Finally, the loaded uranium was eluted with 0.01 M  $\text{HNO}_3$ . The radiochemical purity of  $^{233}\text{U}$  tracer was ensured by alpha spectrometry. The eluted fraction was evaporated to dryness thrice and the residue obtained was dissolved in  $\sim 0.01$  M  $\text{HClO}_4$ . The concentration of uranium in the  $^{233}\text{U}$  stock solution thus obtained was  $8.95 \times 10^{-5}$  M.

### **2.2.3. Curium tracer:**

Existing stock of  $^{244}\text{Cm}$  at Radiochemistry Division, BARC was used as a tracer for curium. The alpha spectrometric assay of the curium solution showed it to be 99%  $^{244}\text{Cm}$  and 1%  $^{245}\text{Cm}$ . The curium concentration in stock solution was  $2.2 \times 10^{-8}$  M.

#### **2.2.4. Europium tracer:**

Natural  $\text{Eu}_2\text{O}_3$  (10 mg) sealed in quartz was irradiated in Dhruva reactor at BARC having a neutron flux of  $5 \times 10^{13}$  n/cm<sup>2</sup>/s for 7 days. After cooling period of two days, the irradiated  $\text{Eu}_2\text{O}_3$  was dissolved in conc  $\text{HClO}_4$  and finally diluted to pH 2 with water to prepare the  $^{152,154}\text{Eu}$  stock solution. The concentration of Eu(III) in the stock solution was  $2 \times 10^{-4}$  M.

#### **2.3. Synthesis of hematite:**

Hematite was synthesized by neutralization of aqueous ferric chloride (AR grade, 0.5 M) solution with sodium hydroxide solution (AR grade, 0.5 M) followed by thermostating the precipitate at 800<sup>0</sup>C to transform it into granular precipitate in an air oven. It was filtered, washed repeatedly with distilled water to remove counter ions and oven dried. The dried precipitate was further heated at 300<sup>0</sup>C for one hour to form crystalline hematite. The crystalline powder was ground to sub-micron size particles in a planetary ball mill (Ms FRITSCH, Germany).

#### **2.4. Radiometric Techniques:**

Alpha emitting radionuclides e.g.  $^{244}\text{Cm}$  and  $^{233}\text{U}$  were assayed in the sorption experiments by liquid scintillation counting whereas NaI(Tl) scintillation counter and HPGe detector were used for the estimation and radionuclide purity of gamma emitting radionuclides respectively.

##### **2.4.1. Liquid Scintillation Counter:**

For quantitative analysis of alpha emitters, liquid scintillation counters are most widely used. The main advantage of these detectors is nearly 100% detection efficiency which allows assay of as low as few Bq of alpha activity with good precision. A scintillator is a material that emits luminescence in a suitable wavelength

region when ionizing radiation interacts with it. Interaction of the charged particles (alpha particles) with the scintillator results in emission of photons, which are converted into a voltage signal using a PMT. The height of the voltage signal is a measure of the energy of  $\alpha$  particle while the number of pulses gives the activity of the source. In cases, where the scintillator emits photons in UV region, a wavelength shifter is added to the scintillator in order to shift the wavelength of the emitted photons to visible region which is subsequently collected in the PMT since photo cathodes of most PMTs are compatible with visible light. The liquid scintillation counters provide data on the gross alpha activity as it cannot distinguish between alpha energies and therefore it cannot be used for alpha spectrometry. Many organic compounds are versatile scintillators for radiation measurements (*Horrocks and Peng, 1971*). The liquid scintillation cocktail comprises of a solvent like dioxane or toluene, a scintillator like PPO (2,5-diphenyl oxazole) and a wavelength shifter such as POPOP (1,4-bis-2-(5-phenyl oxazolyl)-benzene). The solvent is the main stopping medium for radiation and must be chosen so as to provide the efficient energy transfer to the scintillating solute. In the present work, the concentration of the radiotracers was kept low so as to mimic natural conditions and hence generally large volume of aqueous aliquots (1 mL) was added to scintillators. Thus di-isopropyl naphthalene based scintillators which satisfied all the requirements were employed for alpha counting. Each sample was counted for sufficient time so as to get more than 10,000 counts to minimize the statistical counting error.

#### **2.4.2. NaI(Tl) Scintillation Counter:**

Sodium iodide activated with 0.1-0.2% of thallium, NaI(Tl), is by far the most widely used inorganic scintillator for the assay of gamma emitting radionuclides. Salient features of these detectors are the low cost, ease of operation and ruggedness

(Knoll, 2000). The band gap in NaI crystal is of the order of 5-6 eV. When a charged particle (or gamma ray) falls on the detector its energy is used up either for excitation of electrons from the valence band to conduction band or for the ionization of atom. Introduction of thallium in the NaI(Tl) not only shifts the wavelength to higher value by creating intermediate levels in conduction bands but also increases the fluorescence yield of the detector. The energy resolution of NaI(Tl) detector is about 7% at 662 keV.

In the present work, a 3" x 3" well type NaI(Tl) detector coupled with a multichannel analyzer has been used for gamma counting. Nearly 100 % detection efficiency for moderate energy photons in a well type NaI(Tl) detector offers great advantages for counting of low activity samples. A suitable aliquot (1 mL) of the desired analyte solution was taken in glass counting tubes which was then placed in the cavity of detector coupled with PMT and associated electronics. Each sample was counted for sufficient time so as to get more than 10,000 counts to reduce the statistical error in counting

#### **2.4.3. HPGe:**

In the present work, HPGe detector coupled with multichannel analyzer was employed for gamma spectroscopy to check the radiochemical purity of the radionuclides. The HPGe detector is made up of exceptionally pure germanium in which the impurity level is around  $10^{10}$  atoms/cm<sup>3</sup> or less. This is referred to as high purity germanium which approaches the theoretical pure semiconductor. HPGe is the most widely used semiconductor detector for gamma spectrometry and can be called as the workhorse of gamma ray spectroscopy. The high energy resolution (typically 1.9 keV at 1332 keV) is the key feature of this detector due to low band gap (0.7 eV). The great advantage of HPGe detector is that it can be stored at room temperature

(Knoll, 2000). However, while operating it has to be cooled to liquid nitrogen temperature. In present work radiochemical purity of  $^{239}\text{Np}$  and  $^{152}\text{Eu}$  was ascertained by using HPGe.

## 2.5. XRD:

XRD is one of the non-destructive, fast and most widely used techniques to characterize single crystal, polycrystalline and amorphous materials. The ease of sample preparation and highly-accurate determination of d-spacing calculations has made XRD, a versatile tool in the field of material chemistry. In crystalline materials, due to the presence of long range periodicity, the XRD patterns are in the form of sharp peaks.

The underlying principle of XRD is based on scattering of X-rays by a crystal consisting of well-defined array of atoms, ions and molecules. Since parallel arrays of atoms of the crystal lattice are equivalent to the parallel lines of the diffraction grating, therefore inter-planar spacing could be successfully determined from the separations of bright fringes of the diffraction pattern. The wavelength of X-rays (0.5 to 2 Å) has same magnitude as interplanar spacings in the crystal lattice and therefore crystal planes act as diffraction gratings for impinging X-ray radiation. X-rays interact with the electron cloud of the atoms which act as scattering centers and the scattered X-rays from two scattering centers may undergo constructive or destructive interference. Interaction of X-rays reflected by a set of parallel planes lead to constructive interference only at a particular angle according to Bragg's Law, given by equation (2.1), which results in sharp peaks in XRD pattern and are characteristic of a particular material.

$$n\lambda = 2d \sin \theta \quad (2.1)$$

where,

$n$  is the order of diffraction

$\lambda$  is the wavelength of X-rays,

$\theta$  is the glancing angle (called as Bragg's angle),

$d$  is the inter-planar separation

In general, in most of the diffractometers Cu K $\alpha$  is used as the X-ray source and a proportional counter (Argon filled) as the detector. In present work, XRD (Stoe  $\theta$ - $\theta$  diffractometer, Germany) was used to characterize mineral oxide hematite.

## 2.6. BET Surface Area Analyser:

BET surface area analysis is an important analysis technique for the measurement of the surface area of a material. This technique is based on BET theory, given by Brunauer-Emmett-Teller, which explains the physical adsorption of gas molecules on a solid surface.

The BET theory explains multilayer adsorption by taking into consideration following hypotheses: (a) gas molecules are physically adsorb on a solid in infinite layers at saturation pressure; (b) there is no interaction between each adsorption layer; and (c) the Langmuir theory can be applied to each layer. The resulting BET equation is expressed by (2.2):

$$\frac{1}{v\left[\left(\frac{p_0}{p}\right)-1\right]} = \frac{c-1}{v_{mc}}\left(\frac{p}{p_0}\right) + \frac{1}{v_{mc}} \quad (2.2)$$

$p$  and  $p_0$  are the equilibrium and the saturation pressure of adsorbate at the temperature of adsorption,  $v$  is the volume of adsorbed gas, and  $v_m$  is the volume of adsorbed gas for monolayer formation,  $c$  is the BET constant, which is expressed by (2.3):

$$c = \exp\left(\frac{E_1-E_l}{RT}\right) \quad (2.3)$$

$E_1$  is the heat of adsorption for the first layer, and  $E_L$  is that for the second and higher layers and is equal to the heat of liquifaction.

Equation (2.2) is a BET adsorption isotherm and can be plotted as a straight line with  $1/v[(p_0/p)-1]$  on the y-axis and  $(p_0/p)$  on the x-axis. The value of the slope and the intercept are used to calculate the monolayer adsorbed gas quantity  $v_m$  and the BET constant  $c$ .

The surface area of the material can be evaluated by use of following equation:

$$S = (v_m N s) / V a \quad (2.4)$$

where

$N$  : Avogadro's number,

$s$  : adsorption cross section of the adsorbing species,

$V$ : molar volume of adsorbate gas

$a$  : mass of adsorbent (in g)

In present work, surface area of mineral oxides was determined using BET surface area analyser (Sorptomatic 1990, CE Instruments, UK).

## 2.7. UV-Visible Spectrophotometry:

UV-Visible Spectrophotometry refers to absorption spectroscopy in the ultraviolet-visible spectral region. Spectrophotometry is one of the direct methods for determining concentration of the species as the spectra obtained are characteristic of particular species. The observed spectra thus provide information about the species formed which are helpful in both qualitative and quantitative estimations.

The principle of UV-Visible Spectrophotometry is based on the Lambert – Beer law according to which equal fractions of the incident light are absorbed by

successive layers of equal thickness and equal concentration of absorbing medium.

Mathematically, Lambert – Beer law is given by equation (2.5)

$$A = \log\left(\frac{I_0}{I}\right) = \epsilon cl \quad (2.5)$$

Where,

$I_0$  = intensity of light incident on the sample

$I$  = intensity of transmitted light

$A$  = absorbance

$\epsilon$  = Molar extinction coefficient which is the characteristic of species

$c$  = concentration of species

$l$  = path length

In this technique, absorption of electromagnetic radiation results in transition from the ground state to the excited state. The wavelength, at which maximum absorption for species is observed, ( $\lambda_{max}$ ), is used for its spectroscopic analysis. The absorption spectrum is a reflection of structure of a species and therefore absorption spectra provide information about the functional groups as well as oxidation state of metal ion in a particular species. A schematic diagram of a standard spectrophotometer is given in figure 2.1.

In the present case, UV-Visible absorption spectra of the HA samples were recorded, using a Jasco V-350 UV/Vis spectrophotometer at ambient conditions, in order to determine the fraction of HA sorbed on hematite. The equipment uses deuterium lamp and halogen lamp as source of radiation for ultraviolet and visible region respectively. A PMT is used for detection of transmitted photons. The instrument has a resolution of 1 nm with wavelength accuracy of  $\pm 0.5$  nm.

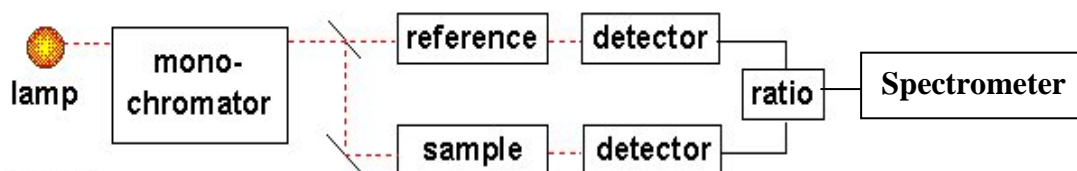


**Figure 2.1** Schematic diagram of a basic UV-Vis spectrophotometer

## 2.8. ICP-AES:

ICP-AES is one of the most common techniques for elemental analysis. Its high specificity, multi-element capability and good detection limits make this technique suitable for wide variety of applications. A plasma source is used for dissociation of the sample into its constituent atoms or ions, and their subsequent excitation to a higher energy level. They return to their ground state by emitting photons of a particular wavelength which is characteristic of the element present. This light is recorded by an optical spectrometer. When calibrated against standards the technique provides a quantitative analysis of the original sample.

A JY-50P poly scan instrument with axial ICP and operated at 40.68 MHz radio frequency (r.f) with 1.0 kW forward output r.f. power served as the spectral excitation source. The instrument known as “Panorama” model has a unique facility for simultaneous and sequential operation in the same spectrometer assembly. Thus, the spectrometer has a polychromator covering 35 elements and is also able to function as a sequential unit over a spectral range of  $\pm 2.2$  nm around each channel. The block diagram of ICP-AES is given in figure 2.

In present work, ICP-AES has been used for the determination of dissolved silica.

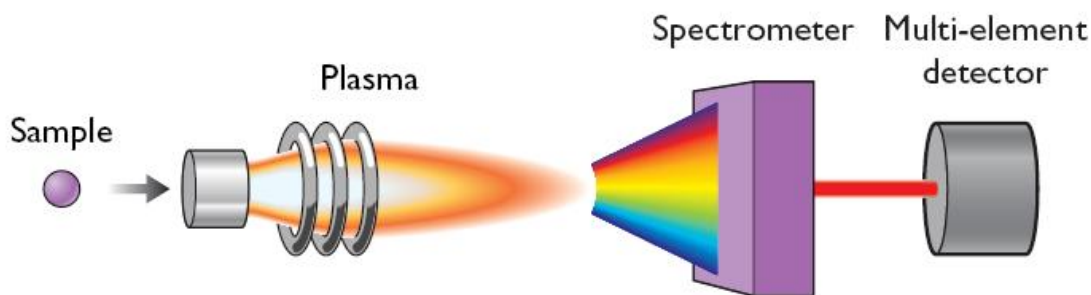


**Figure 2.2** Schematic of ICP-AES

### 2.9. Determination of Zeta potential:

The ionization of surface groups, lattice imperfection and specific ion adsorption leads to development of a surface charge at the particle surface which in turn affects the distribution of ions in the surrounding interfacial region and hence increase in concentration of counter ions close to the surface which ultimately leads to the formation of electric double layer around each particle. There exists a notional boundary within the diffuse layer inside which the ions and particles form a stable entity and move along with the particle, but any ions beyond the boundary do not travel with the particle. This boundary is termed as shear plane and the potential at this plane is known as the Zeta potential as shown in figure 2.3.

The stability of the colloidal system can be ascertained in terms of magnitude of the zeta potential. Large negative or positive zeta potential values ( $\geq \pm 30$  mV) of colloidal system generate repulsion among particles and thus avoid tendency of flocculation. Such systems are termed as stable suspensions. In contrast low zeta potential values ( $\leq \pm 30$  mV) offer low electrostatic repulsion which results in flocculation and these systems are called unstable suspensions. The point where zeta potential becomes zero is called the isoelectric point or  $\text{pH}_{\text{pzc}}$  and is one of the very important parameters used for characterizing the colloidal systems.

The zeta potential measurement involves determination of electrophoretic mobility which is defined as the velocity of a particle in an electric field. The charged particles suspended in the electrolyte are attracted towards the electrode of opposite charge on application of electric field but their movement is opposed by viscous forces acting on them. When equilibrium is attained between these two opposing forces, the particles move with constant velocity. The velocity i.e. electrophoretic mobility of the particle ( $U_E$ ) is dependent on the strength of electric field, the dielectric constant ( $\epsilon$ ) and the viscosity ( $\eta$ ) of the medium and the Zeta potential ( $z$ ). The electrophoretic mobility and zeta potential is related by Henry equation (2.6)

$$U_E = \frac{2\epsilon z f(Ka)}{3\eta} \quad (2.6)$$

$f(Ka)$  is known as Henry's function and generally have two values either 1.5 or 1.0.

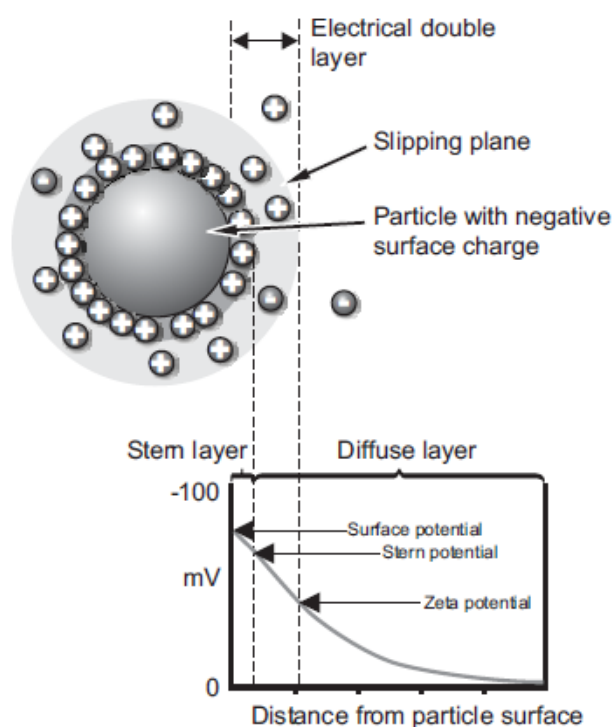


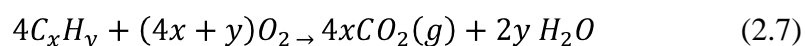
**Figure 2.3** Schematic showing Electrical double layer and Zeta potential

This velocity is measured using the technique of the Laser Doppler Velocimetry. The frequency shift or phase shift of an incident laser beam caused by these moving particles is measured as the particle mobility, and from this mobility zeta potential is determined using equation (2.6). In present studies the zeta potential determination of hematite and silica were carried out using Malvern, Zetasizer Nano ZS.

### **2.10 TOC Analyser:**

TOC is the amount of carbon bound in an organic compound. A typical analysis for TOC measures both the total carbon present as well as the so called "inorganic carbon" (IC), the latter representing the content of dissolved carbon dioxide and carbonate salts. Subtraction of IC from the total carbon yields TOC. But nowadays, direct determination of TOC can be made using photocatalytic oxidation followed by infra red detection.

Introduction of sample directly into the photocatalytic reactor allows direct mixing with the titanium dioxide (catalyst) slurry in the presence of a near-UV light source (300-400 nm). There is continuous circulation of air in a closed loop system and the reactor provides the necessary oxygen. Under these conditions any bound organic carbon present in the sample is quickly oxidized.



The carbon dioxide that is formed during this reaction is passed through a condenser and then circulated through the closed loop system. A dual wavelength Non-Dispersive Infra-Red detector measures the increase in carbon dioxide resulting

from the oxidation. The block diagram of TOC analyser is shown in Figure 2.4. For quantitative analysis of TOC, benzoic acid is used as a standard.

In present studies, Anatoc analyzer (SGE, Australia), with detection limit 0.5 ppm carbon, has been employed to determine the sorption of HIBA and citric acid on silica.

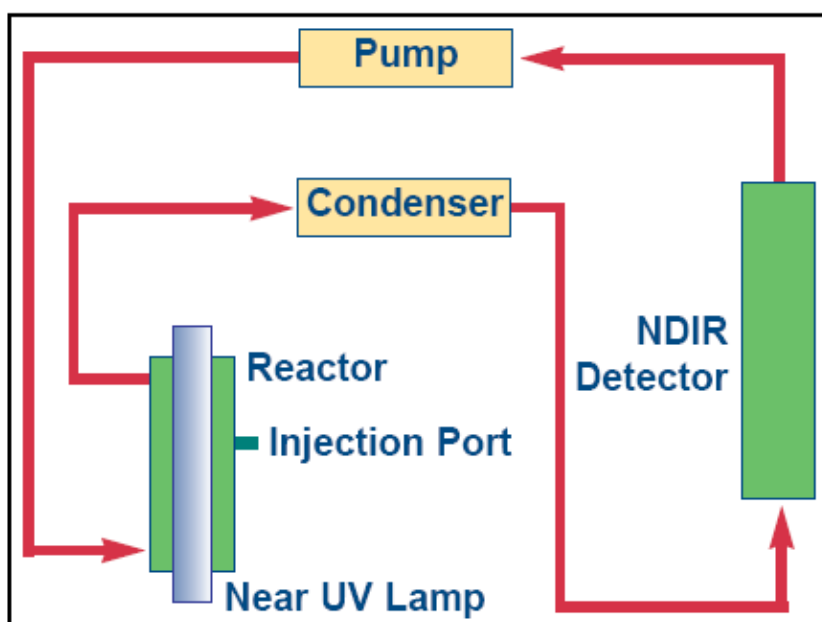


**Figure 2.4** Schematic of TOC analyser

### 2.11. TRFS:

For a comprehensive understanding of the interaction mechanisms between trivalent lanthanides/actinides and the chosen minerals and complexing ligands, TRFS have been employed. TRFS is one of the most sensitive, non-invasive and widely used spectroscopic techniques for speciation studies. The technique has triple advantage of (i) characteristic excitation wavelength, (ii) characteristic emission wavelength and (iii) characteristic lifetime which helps in accurate assignment of the complex stoichiometry and structure in both sorption as well as complexation studies

(Plancque et al., 2003). The fluorescence emission spectra are characteristic of particular species and the selective excitation helps in reduction of interferences from others species. Thus spectral characteristics and lifetime of species provide information about the important properties like oxidation states of metal ions, coordination numbers, and covalence. Due to the above mentioned advantages, TRFS has been used extensively for speciation studies.

### **2.11.1. Principle of TRFS:**

Photoluminescence is a process in which a substance absorbs photons (electromagnetic radiation) and then emits its characteristic luminescence. Quantum mechanically, this can be described as an excitation to a higher energy state and then return to a lower energy state accompanied by the emission of a photon. The various deexcitation pathways of an excited molecule can be described with the help of Jablonski diagram as shown in figure 2.5.  $S_0$ ,  $S_1$ , and  $S_2$ , depict the singlet ground, first, and second electronic states respectively. The vertical lines are used to depict transitions between different electronic states. The light absorption is instantaneous in nature ( $10^{-15}$  s). Following light absorption, several processes usually occur. A fluorophore is usually excited to some higher vibrational level of either  $S_1$  or  $S_2$  and rapidly relax to the lowest vibrational level of  $S_1$ . This process is called internal conversion and generally occurs within  $10^{-12}$  s or less. When the relaxation occurs between an excited state and the ground state of same spin multiplicity ( $\Delta S = 0$ ) the luminescence process is referred to as fluorescence. Thus, fluorescence emission generally results from a thermally equilibrated excited state, that is, the lowest energy vibrational state of  $S_1$ . Although the fluorescence is a fast process, some of the original energy is dissipated so that the emitted light photons are of lower energy than those absorbed. The generated photon in this case is said to be red shifted as the result

of loss of energy in internal conversion. Molecules in the  $S_1$  state can also undergo a spin conversion to the first triplet state  $T_1$  which is termed as intersystem crossing. Emission from  $T_1$  is termed phosphorescence, and is generally shifted to longer wavelengths (lower energy) relative to the fluorescence. Transition from  $T_1$  to the singlet ground state is quantum mechanically forbidden, which result in a slow process of radiative transition back to the singlet ground state, sometimes lasting even minutes or hours (Lakowicz, 2006). Typically, this is correlated with the relaxation time that is longer for phosphorescence than for fluorescence.

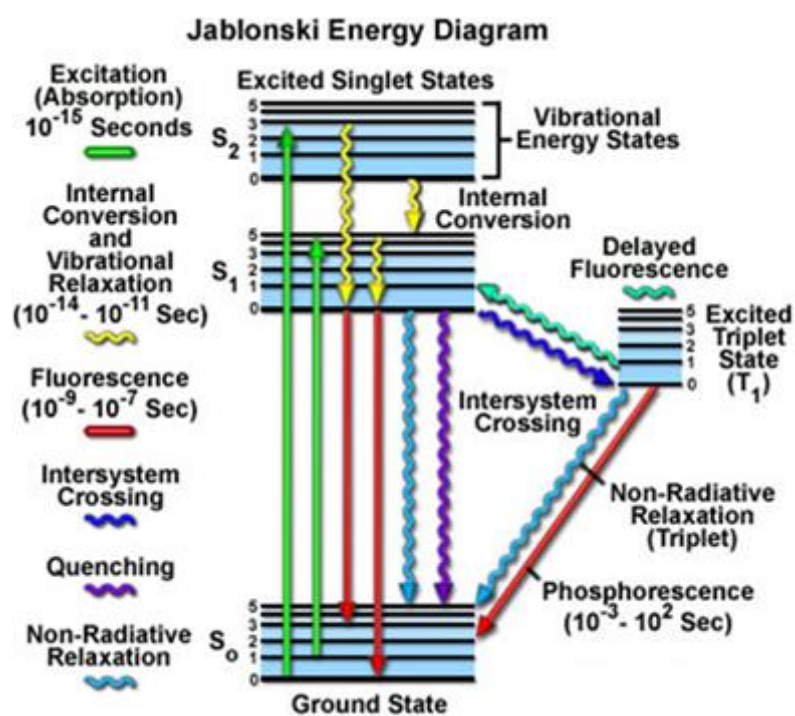


**Figure 2.5** Jablonski diagram depicting photo physical processes

Some f-elements relax through intense luminescence emission in aqueous media. Some actinide and lanthanide fluorophores are Am(III), Cm(III), Bk(III), Cf(III), Pa(IV), U(VI), Eu(III), Gd(III), and Tb(III). The characteristic optical spectra of these inner transition elements originate from f-f transitions, taking place between

the partly filled 4f (lanthanides) and 5f (actinides) energy levels (*Carnall, 1979*). The f-f transitions are sensitive to changes in the ligand field, thus, making TRFS an extremely useful tool to probe the complex speciation of these elements.

### **2.11.2. Instrumentation:**

The present TRFS studies were carried out using an Edinburgh 920 series spectrometer which works on the principle of TCSPC. The spectrometer is equipped with a Xe flash lamp and a couple of M 300 monochromators providing resolution of ~1 nm.

#### **2.11.2.1. Xenon flash lamp:**

A Xenon flash lamp is an electric arc lamp designed to produce extremely intense, incoherent, full-spectrum white light for very short durations. Flash lamp comprises a hermetically sealed glass tube, in which noble gas xenon is filled with electrodes at either end to carry electrical current. The electrodes of the lamp are usually connected to a capacitor, which is charged to a relatively high voltage (generally between 250 and 5000 volts). The gas, owing to its inert nature, exhibits extremely high resistance, and the lamp does not conduct electricity until the gas is ionized. On ionization, a spark forms between the electrodes, allowing the capacitor to discharge. The sudden surge of electric current quickly heats the gas to a plasma state, where electrical resistance becomes very low, and a high voltage pulse is generated to produce the light.

#### **2.11.2.2. Monochromator:**

The dispersion of polychromatic or white light into the various colors or wavelengths is achieved by using monochromators. In most spectrofluorimeters, the

dispersion into light of specific wavelength is attained by using diffraction gratings, an optical component with a periodic structure that splits and diffracts light into several beams travelling in different directions. The directions of these beams depend on the spacing of the grating and the wavelength of the light. The relationship between the grating spacing ( $d$ ), the angles of the incident ( $\theta_i$ ) and diffracted beams ( $\theta_r$ ) of light is known as the grating equation which is given in equation (2.11)

$$m\lambda = d(\sin \theta_i \pm \sin \theta_r) \quad (2.11)$$

where  $m$  is the order of diffraction and  $\lambda$  is the wavelength.

M300 monochromator, dispersive element in the instrument used for present studies, is a high quality general purpose grating monochromators designed for use in the UV, visible and infra-red spectral regions. All the gratings are kinematically mounted so that calibration is not lost when gratings are changed. The use of an 1800 lines/mm of 69 mm x 69 mm grating in the visible region results in a higher resolution and light gathering power.

### **2.11.2.3. TCSPC**

TCSPC technique is a digital counting technique where the photons, that are time correlated in relation to an excitation light pulse, are counted. The sample is excited with light pulse, resulting in the waveform, as shown in the figure 2.6, which excite many fluorophores and numerous photons are observed. However, the conditions for TCSPC are so adjusted that less than one photon is detected per laser pulse. In fact, the typical detection rate is 1 photon per 100 excitation pulses. The time difference between the excitation pulse and the observed photon is measured and stored in a histogram which represents the waveform of decay provided less than one photon per 100 excitation pulse is detected. The excitation pulse, in addition to sample excitation, triggers the start PMT which sends an analog signal to CFD that

generates a logic signal which represents the accurate arrival time of the pulse. This signal is passed to TAC as a start signal, which generates a linear voltage ramp with respect to time. As soon as the first fluorescence photon is observed, stop PMT detects the photon and the arrival time of the signal is accurately determined using a CFD, which sends a signal to stop the voltage ramp. The voltage contained in TAC is proportional to the time delay ( $t$ ) between the excitation and emission signals.

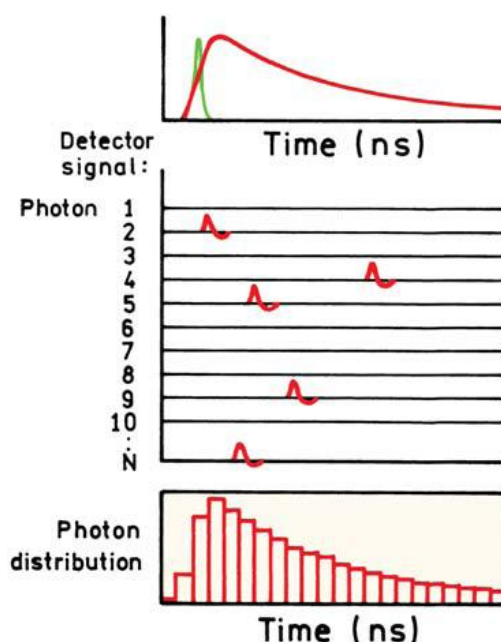


**Figure 2.6** Principle of TCSPC depicting excitation pulse and decay profile

*(Lakowicz, 2006)*

The sample is repetitively excited and a probability histogram relating the time difference between an excitation pulse (Start) and the observation of the first fluorescence photon (Stop) is obtained. The time of arrival of photon must be defined precisely and accurately in TCSPC. This precise timing information is achieved by CFD. The schematic diagram of TCSPC set up used for fluorescence investigations is shown in figure 2.7.

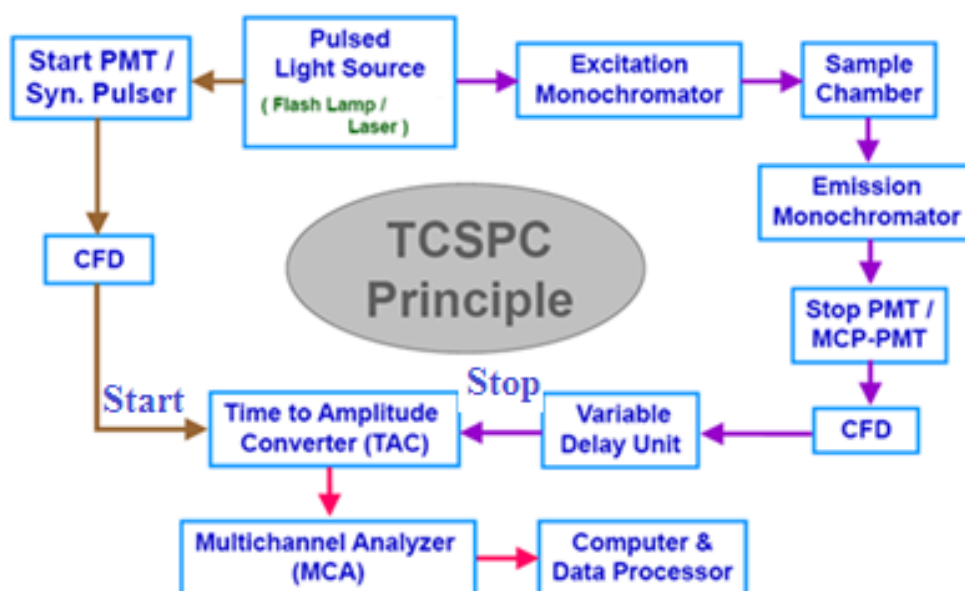


**Figure 2.7** Block diagram of TCSPC set up for fluorescence experiments

#### 2.11.2.4. CFD:

The analog signal from PMT corresponding to individual photon detection, have a significant spread in pulse height which means that timing based on amplitude threshold will result in considerable jitter as shown in figure 2.8.

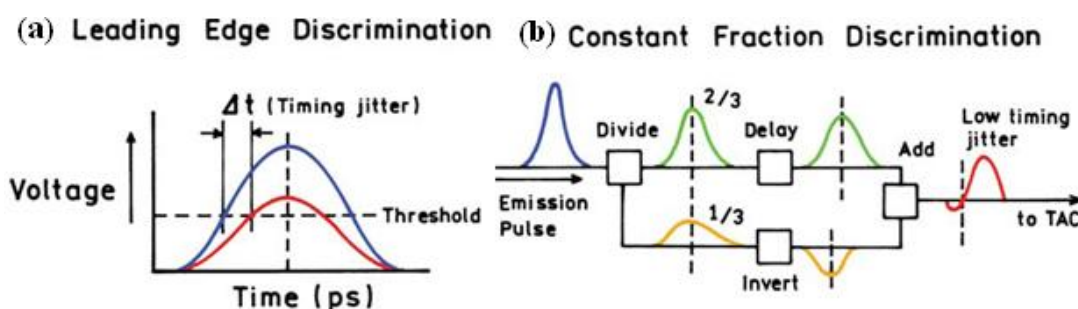
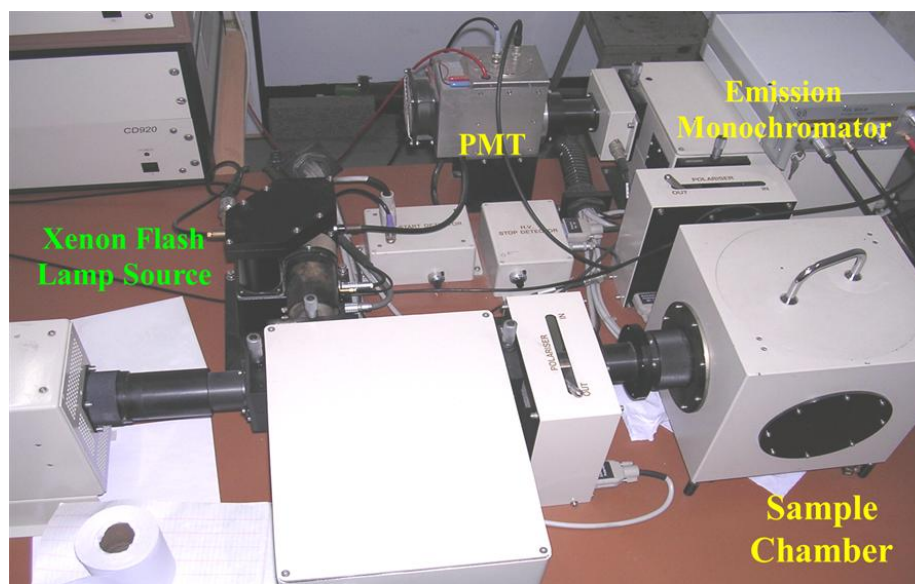


**Figure 2.8** Constant fraction discrimination in TCSPC. (a): Timing error due to pulse height variations (b): Operation of a CFD (*Lakowicz, 2006*)

The accurate timing information about a photon is obtained with the help of CFD in which input signal is split into two parts, one part is delayed by about half the

pulse width and the other part of the signal is inverted. On summing of these two parts, the zero crossing point is independent of the pulse height which accurately determines the arrival time of the signal (*Lakowicz, 2006*).

Figure 2.9 shows the TRFS setup used for present work.



Wavelength range – 180-900nm

**Figure 2.9** Photograph of the CD-920 time resolved fluorescence spectrometer

### 2.12.3. Data treatment and Error analysis:

Decay curve analysis is a very vital aspect of the TCSPC technique. In reality  $\delta$ -pulse excitation is impossible as all excitation sources have their finite pulse width and therefore measured decay is the convolution of the true decay and the excitation pulse profile. Therefore analysis of decay curve involves following steps:

- (a) Removal of distortion introduced by excitation pulse and extraction of true sample decay profile
- (b) Evaluation of parameters to ascertain goodness of fit

The first step is carried out using deconvolution procedure. The observed fluorescence decay curve is convolution of excitation pulse and decay profile of sample. Mathematically, the observed decay curve,  $F(t)$ , is given by equation (2.12)

$$F(t) = \int_0^t I(t-t')D(t')dt \quad (2.12)$$

where  $D(t')$  represents sample decay profile while  $I(t)$  represents instrument response function i.e lamp profile which is measured by replacing the sample by scattering solution and resetting the emission monochromators to the excitation monochromators.

In our analysis program, reconvolution is employed which involves convoluting a theoretical model, that is assumed to represent the sample decay, with an instrument response function and the resultant convolution integral is compared with observed decay curve. However, it is possible to do exponential fitting without reconvolution analysis by excluding instrument response function. Thus, sample decay curve,  $D(t)$ , can be represented as

$$D(t) = \sum_{i=1}^n B_i \exp(-t/\tau_i) \quad (2.13)$$

where  $n$  is the number of species in the decay curve and  $\tau$  represents the lifetime of each species and is defined as the average time the molecule spends in the excited state prior to return to the ground state.

Nonlinear least square fitting is used to compare the theoretical function and measured data. The goal of least squares is to test whether a given mathematical model is consistent with the data, and to determine the parameter values for that model which provide best match between observed and calculated decay which is achieved by minimization of the goodness-of-fit parameters. Statistical parameters which are used to judge the goodness of fit are described in brief.

(a) Chi square value ( $\chi^2$ ):

$\chi^2$  is defined as follows :

$$\chi^2 = \sum_t \left[ \frac{D(t)-F(t)}{\sigma(t)} \right]^2 \quad (2.14)$$

where  $D(t)$  is raw fluorescence data,  $F(t)$  is the fitting function and  $\sigma(t)$  is the statistical uncertainty of point  $D(t)$ . The aim is to adjust the fitting parameters such that lowest value of  $\chi^2$  is obtained. Thus, if the fitting function represents the observed decay accurately then the ratio of actual deviation to expected deviation will be equal to number of data points,  $N$ . It is not convenient to interpret the values of  $\chi^2$  as it is dependent on number of data points. Therefore, reduced  $\chi_R^2$  is used which is obtained by normalizing  $\chi^2$  by degree of freedom.

$$\chi_R^2 = \frac{\chi^2}{(n-p)} \quad (2.15)$$

where  $n$  is the number of data points,  $p$  is the number of floating parameters, and  $n - p$  is the number of degrees of freedom. For TCSPC the number of data points is typically much larger than the number of parameters so that  $(n - p)$  is approximately equal to  $n$ . Thus,

$$\chi_R^2 \approx 1 \quad (2.16)$$

(b) Weighted Residuals:

Weighted Residuals are very important means of determining the goodness of fit. The weighted residuals are the difference between the fitted function and the measured data, normalized by data uncertainty. Thus,

$$R(t) = \frac{Y(t)-F(t)}{\sigma^2(t)} \quad (2.17)$$

Hence

$$\chi^2 = \sum_t R^2(t) \quad (2.18)$$

For a good fit, weighted residuals should be randomly distributed around zero among the data channels.

### 2.12. $K_D$ determination of radionuclides:

Sorption plays an important role in reducing the mobility of radionuclides in natural systems. Initial research for modeling performance assessment related to nuclear waste repositories dealt with determination of solid/liquid  $K_D$  which is measured as the concentration ratio of radionuclides on solid and in aqueous phase under well defined set of experimental conditions of temperature, pressure, Eh, pH, ionic strength and solid/solution ratio. Thus, the  $K_D$  is expressed as

$$K_D = C_s / C_l \quad (2.8)$$

where  $C_s$  is the concentration of radionuclide per gram of solid and  $C_L$  is the concentration of radionuclide per mL of aqueous phase. Since the speciation of radionuclides is quite complex, specially for lanthanides and actinides, many species for a particular radionuclide can exist simultaneously for given set of experimental parameters but  $K_D$  represents the gross distribution of radionuclide at solid/solution interface without considering their speciation.

Another parameter, which is commonly used in surface chemistry to evaluate the distribution of radionuclide at solid /solution interface, is % sorption which is defined as

$$\% \text{ sorption} = \frac{(C_i - C_f)}{C_i} \times 100 \quad (2.9)$$

where  $C_i$  and  $C_f$  are the initial and final concentration, after sorption on solid surface, of radionuclides in aqueous phase. The % sorption and  $K_D$  are related by following equation:

$$\% \text{ sorption} = \frac{K_D}{K_D+1} \times 100 \quad (2.10)$$

Generally, batch sorption method is used for  $K_D$  determination. The design of the batch sorption experiments employed for present studies is discussed below.

### 2.12.1. Experimental Details:

Batch sorption experiments were carried out in 50 mL Oak Ridge polypropylene tubes. The mineral oxides, after characterization for surface properties, were suspended in aqueous phase of fixed ionic strength in fixed solid to liquid ratio for 12 to 24 hours.  $\text{NaClO}_4$  was used to maintain the ionic strength owing to least complexing tendency of the perchlorate ion. Subsequently appropriate quantity of radionuclide was added in order to achieve desired radionuclide concentration. The control, prepared in 0.1 M  $\text{HClO}_4$  but without mineral oxide, was taken for each of the sorption experiment in order to determine the initial concentration of radionuclide ( $C_i$ ). Thereafter, pH of the suspensions was adjusted in the range 2-10 using dil  $\text{NaOH}$  and dil  $\text{HClO}_4$ . While adjusting the pH, drop wise addition of acid/base was done so as to avoid local changes in radionuclide speciation. The pH adjustment was followed by equilibration of suspensions for a time period which was fixed based on kinetics experiments. Post equilibration, the pH of the suspensions was checked, recorded and suspensions were centrifuged at appropriate centrifuge speed for appropriate time to separate the phases. A suitable aliquot (1 mL in most of the cases) of supernatant was taken for determining the concentration of radionuclide in supernatant ( $C_f$ ) after equilibration. Once  $C_i$  and  $C_f$  were known, % sorption at varying pH was determined for radionuclides. In ternary systems, where the effect of complexing ions on radionuclide sorption is investigated, suspensions were equilibrated with complexing anions, in similar manner as mentioned above, prior to radionuclide addition. It is

worth mentioning that pH of suspensions were readjusted after radionuclide addition so that radionuclide and complexing ion equilibrate at same pH. Similar methodology was adopted for ternary systems in which radionuclide addition was preceded by addition of complexing anion.

### **2.12.2. Error determination on sorption data:**

In order to quantify the error on sorption data, it is essential to identify the sources of error. In present work radionuclides investigated are mainly lanthanides and actinides which undergo extensive hydrolysis. Therefore it is imperative to their check sorption on walls of polypropylene containers. The wall sorption was estimated by removal of suspensions from the polypropylene container and subsequently tube was rinsed with distill water followed by addition of 1.0 M HNO<sub>3</sub> in same quantity as that of aqueous phase in sorption experiments. After 24 hours, the solution was assayed so as to estimate the leached radionuclide from walls of the container. The wall sorption was quantified as the ratio of concentration of radionuclide leached into HNO<sub>3</sub> to the initial concentration of radionuclide in the sorption experiments. Negligible wall sorption was obtained in systems investigated in present work.

The other errors viz., random errors, systematic errors were taken into account by performing duplicate measurements and calculating standard deviation. Since duplicate measurements for entire range of pH is difficult, statistical error on radioactive counting was considered while calculating the error on sorption.

### **2.13. Modeling of sorption data:**

Initially,  $K_D$  approach was commonly used for modeling adsorption on solid surfaces and migration of radionuclides in geosphere. The severe weakness of the  $K_D$  approach is that all physico-chemical interactions taking place at the solid solution

interface are represented by purely phenomenological parameter. Such  $K_D$  tend to exhibit large uncertainties when inter- or extra polation to other system is required. Surface reaction mechanisms and changes in chemical environment are also neglected in  $K_D$  approach. In order to have the fundamental understanding of the type of interaction taking place at solid/solution interface and development of efficient thermodynamic sorption database, sorption models which can overcome the above mentioned short comings are required. In present work, two modeling approaches namely LAM and SCM are used, which are discussed below:

### **2.13.1. LAM:**

The LAM, a mathematical model, is used for predict the sorption of metals onto surfaces in the presence of HA. In ternary system, metal cations, HA and the solid or colloid surface coexist. The different interactions of ternary system are shown in figure 2.10.

LAM is based on the series of assumptions which are given below (*Samadfam et al., 1998,2000; Sakuragi et al., 2004; Christl and Kretzschma, . 2001*):

- a)  $K_D$  for the ternary system is a combination of the distribution coefficients of the separate binary interactions.
- b) The individual sorption coefficients are independent of the metal concentration.
- c) The sorption properties or characteristics of the mineral are not affected by the presence of HA.
- d) Different molecular weight fractions of HA are neglected and sorption of HA is considered as a whole.

- e) Affinity of metals for mineral-bound HA and for dissolved HA are considered identical.
- f) The mass of mineral is much higher than the mass of mineral-bound HA.
- g) Electrostatic interactions at the mineral-water interface are neglected.

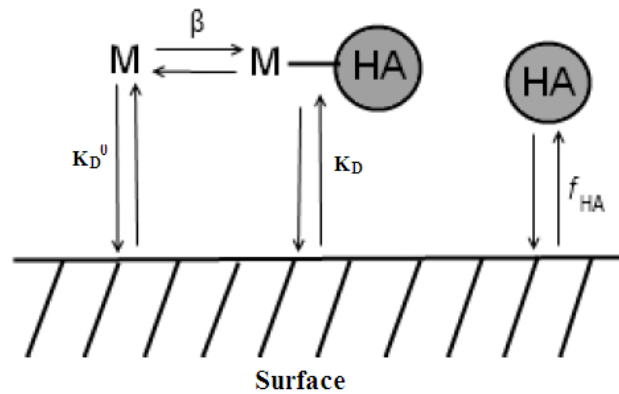


**Figure 2.10** Interactions between metal cations (M), HA molecules and the surface of the solid

In view of above assumptions,  $K_D$  for the ternary system is defined as

$$K_D = \frac{K_D^0 + (V/W)f_{HA}\beta[HA]}{1 + (1-f_{HA})\beta[HA]} \quad (2.19)$$

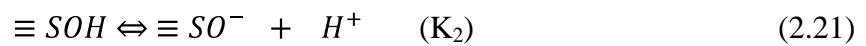
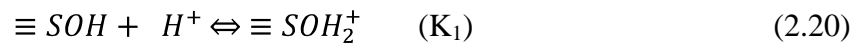
where,  $\beta$  is metal-humate stability constant,  $K_D^0$  is the distribution coefficient for the binary metal-solid surface interaction,  $f_{HA}$  is the fraction of HA sorbed onto the surface,  $V$  and  $W$  are the volume of solution and weight of solid respectively and  $[HA]$  is the concentration of HA in solution.

### 2.13.2. SCM:

SCM are used to describe the equilibrium reactions that take place at the solid/solution interface. SCM enables treatment of sorption data by taking into consideration main basic processes defining overall sorption phenomenon. It considers sorption of ions at solid/solution interface similar to complexation in

solution, and electrostatic effects at the surface-solution interface are addressed by theories describing the electrical double layer.

An accepted mechanism for oxide surfaces is to introduce the concept of amphoteric surface sites i.e. general hydrolysed species,  $\equiv\text{SOH}$ . The pH dependent surface charge arises due to the protonation/deprotonation of the hydroxylated functional groups according to the following equations



where  $\text{K}_1$  and  $\text{K}_2$  are the intrinsic equilibrium constants for the reactions 2.20 and 2.21 respectively. The mass law equations corresponding to the equations 2.20 and 2.21 are,

$$K_1 = \frac{[\text{SOH}_2^+]}{[\text{SOH}][\text{H}^+]} \exp\left(\frac{F\psi}{RT}\right) \quad (2.22)$$

$$K_2 = \frac{[\text{SO}^-][\text{H}^+]}{[\text{SOH}]} \exp\left(-\frac{F\psi}{RT}\right) \quad (2.23)$$

where  $[\text{X}]$  refers to the concentration of species X. The argument of the exponential term represents the Coulomb term that accounts for the change in electrostatic energy during the surface chemical reaction (*Dzombak and Morel, 1990*). R is the molar gas constant, T the absolute temperature (K), F is the Faraday constant and  $\psi$  represents the surface potential. In SCM, the adsorption on a surface is calculated as a function of the surface potential which cannot be determined directly. Therefore determination of surface charge density,  $\sigma$ , is done which can be related to surface potential,  $\psi$ . Several expressions have been proposed to relate  $\Psi$  to  $\sigma$ , and based on these expressions; different SCMs have been proposed viz., CCM and DLM.

### 2.13.2.1. CCM:

The CCM was developed by Schindler and coworkers (*Dzombak and Morel, 1990*). It is applicable at high ionic strength or at very low surface potential values. It also assumes that all the surface complexes are inner-sphere complexes. The relationship between surface charge density ( $\sigma_0$ ) and surface potential ( $\psi_0$ ) (where 0 indicates the surface plane), in the CCM is given by the following equation:

$$\sigma_0 = \frac{CAS}{F} \psi_0 \quad (2.24)$$

where, C is the capacitance density ( $F/m^2$ ), A is the surface area ( $m^2/g$ ), S is the sorbent density ( $g/L$ ). A diagram of the structure of the surface-solution interface for the CCM is shown in figure 2.11.

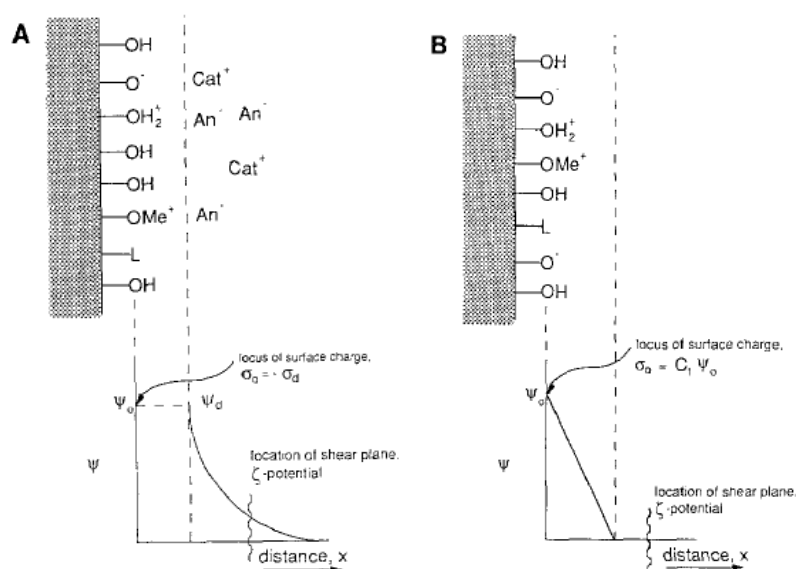


**Figure 2.11** Conceptual representation of surface charge development in: A) DLM B) CCM (*Hayes et al., 1991*)

### 2.13.2.2. DLM:

The DLM was developed by Stumm and his co-workers (*1970*). The model assumes two planes for surface charge: a surface layer (plane 0) and diffuse layer of

counter ions (plane d). A diagram of the structure of the surface-solution interface for DLM is shown in figure 2.11. The relationship between surface charge and surface potential is described with the Gouy-Chapman theory which is based on following assumptions:

- a) The ions in the solution are assumed to be point charges.
- b) Correlations between the ions in the solution are not taken into account.
- c) The surface charge is homogeneous.
- d) The liquid is homogeneous and the dielectric constant  $\epsilon$  is not affected by the electric field from the surface.
- e) The concentration of ions at any location in the electrical double layer is related to the bulk ion concentration by the Boltzmann distribution.

The relation between surface charge density ( $\sigma$ ) and surface potential ( $\psi$ ), based on above assumptions, can be derived as follows:

According to Gauss Law, the total electric flux coming out of a closed surface is equal to the charge enclosed divided by the permittivity as illustrated in equation (2.25)

$$\vec{\nabla} \cdot \vec{E} = \frac{\rho(r)}{\epsilon_0 \epsilon_r} \quad (2.25)$$

where E is the electric field,  $\epsilon_0$  is the permittivity of vacuum,  $\epsilon_r$  is the permittivity of medium and  $\rho$  is the charge density. The electric field is differential of electric potential  $\psi$ .

$$\vec{\nabla} \psi(r) = \vec{E}(r) \quad (2.26)$$

Thus, on combining equation (2.25) and (2.26), we have

$$\vec{\nabla}^2 \psi(r) = \frac{\rho(r)}{\epsilon_0 \epsilon_r} \quad (2.27)$$

For one dimension, the above equation can be written as

$$\frac{d^2\psi(x)}{dx^2} = \frac{\rho(x)}{\epsilon_0\epsilon_r} \quad (2.28)$$

Applying Boltzmann distribution for the ions in the electric double layer, we have

$$\frac{d^2\psi(x)}{dx^2} = \frac{N_A e \sum Z_i c_i \exp(-Z_i e \psi / kT)}{\epsilon_0 \epsilon_r} \quad (2.29)$$

$N_A$  is Avogadro's number;  $c_i$  is the bulk ionic concentration and  $Z_i$  is the corresponding ionic valence. For 1:1 electrolyte ( $c_+ = c_- = c$ ). Accordingly, equation (2.29) becomes

$$\frac{d^2\psi(x)}{dx^2} = \frac{2N_A Z e c}{\epsilon_0 \epsilon_r} \sinh\left(\frac{Z e \psi}{kT}\right) \quad (2.30)$$

For  $Z e \psi / kT \ll 1$ ,

$$\frac{d^2\psi(x)}{dx^2} = \frac{2N_A (Z e)^2 c}{\epsilon_0 \epsilon_r kT} \psi \quad (2.31)$$

$\frac{2N_A (Z e)^2 c}{\epsilon_0 \epsilon_r kT}$  is equal to  $\kappa^2$ , where  $\kappa$  is known as Debye Huckel parameter. Thus,

$$\frac{d^2\psi(x)}{dx^2} = \kappa^2 \psi \quad (2.32)$$

The solution of above equation is

$$\psi(x) = \psi_0 \exp(-\kappa x) \quad (2.33)$$

which is a simple exponential decay

The whole system should be electrically neutral, which is described by the electro neutrality condition.

$$\sigma = \oint_0 \rho dx = \epsilon_0 \epsilon_r \oint_0 \frac{d^2\psi(x)}{dx^2} = \left[ \epsilon_0 \epsilon_r \left(\frac{d\psi}{dx}\right) \right]_{x=0} \quad (2.34)$$

Equation (2.34) gives the relation between the surface charge density and potential on the surface. Taking value of  $\frac{d^2\psi(x)}{dx^2}$  from equation (2.30) and then solving

equation (2.34), we get the relationship between surface charge density and surface potential in accordance with Gouy Chapman Theory.

$$\sigma = (8RT \epsilon_r \epsilon_0 c \times 10^3)^{0.5} \sinh \frac{zF\psi}{RT} \quad (2.35)$$

Once  $\psi$  is known, the equilibrium constants for surface reactions can be calculated.

In present work DLM has been employed in the SCM of the sorption data. Since computing surface reaction equilibrium constants involves rigorous calculations, geochemical speciation code, FITEQL 4.0, has been used in present studies.

### 2.13.3. FITEQL 4.0

The best-fit equilibrium constants for surface equilibrium reactions were determined by modeling sorption data using the simulation code FITEQL 4.0. To solve sorption problems, laws of mass action and mass balance constraints are applied and chemical species concentrations are subjected to iteration until the difference between the calculated and observed values is minimized i.e. best fit solution of the derived set of nonlinear equations is achieved. This iterative numerical procedure, based on Newton Raphson approximation, typically computes a correct and unique solution; provided the geochemical equilibrium problem is mathematically defined in terms of adequate chemical components. The geochemical problem definition of components and species in FITEQL 4.0 is given in the form of Tableau (*Dzombak and Morel, 1990; Morel and Morgan, 1971; Morel, 1983*). In this format, every species can be represented as the product of reactions involving only components. Components are defined in such a manner that they cannot be obtained as reaction product of other components. The charge on the surface species is also defined as a component in tableau. For each convergent optimization, FITEQL 4.0 provides the

quality of fit criterion ( $V_y$ ) for a set of surface constants.  $V_y$  is the weighted sum of squares of residues (WSOS) divided by the degrees of freedom (DF), may be calculated using the equation:

$$V_y = \frac{WSOS}{DF} = \frac{\sum (Y_j/S_j)^2}{N_p N_c - N_u} \quad (2.36)$$

where DF (Degree of Freedom) = N (number of data points) – number of adjustable parameters,  $Y_j$  is the mass residual balance calculated from the deviation between the calculated and experimental mass balance for the component  $j$ ;  $S_j$  is the error calculated for  $Y_j$  from the experimental error estimates;  $N_p$  is the number of data points;  $N_c$  is the number of components for which both the total and the free concentrations are known; and  $N_u$  is the number of adjustable parameters. The value of  $V_y$  thus depends on the experimental error estimates and generally lies between 0.1– 20 for satisfactory fit of the data, when realistic error estimates are used (Dzombak and Morel, 1990; Herbelin and Westell, 1994).

#### 2.13.4. MINTEQA2:

In present work the speciation of metal ions in aqueous solution has been calculated using equilibrium speciation code MINTEQA2. A comprehensive database of components and species has been included in MINTEQA2. However, there is provision in MINTEQA2 to add new components and species. Moreover, it includes the implementation of a competitive Gaussian model for computing the complexation of metals by DOM. An ancillary program, PRODEFA2, serves as an interactive pre-processor to help produce the required MINTEQA2 input files. Like FITEQL 4.0, nonlinear optimization procedure is used to calculate speciation in MINTEQA2 (Allison et al., 1991).

**Chapter III**

**Europium Complexation**

**with LMCA and HA**

### **3.1 Introduction:**

In the present chapter the spectroscopic study of the complexation of Eu(III), an analogue of trivalent actinides, such as, Am(III), Cm(III) by various small carboxylate ligands and HA has been described.

HS and LMCA are ubiquitous in the ecosphere. Complexation of actinides/lanthanides with HS as well as LMCA is important as they influence transport and migration of actinides in the environment. HS are formed as the result of degradation of plant and animal matter whereas the occurrence of large variety of LMCA viz., citrate, phthalate, succinate, in the environment is the outcome of biological, geological, (bio) geochemical processes as well as their use in numerous industrial processes. However, the carboxylates groups are responsible for complexation in both the cases. In present study, the complexation of Eu(III) with HIBA, PA, SA, MA and HA has been investigated. The structure of different LMCA are given in figure 3.1 while that of HA in figure 1.13.

SA is an intermediate in citric acid cycle and used in polymer and food industries while MA is used in preparation of medicines. The esters of PA are used as plasticizers and anhydride of PA is used in production of dyes. HIBA is used in the manufacture of superconducting fibers, biological analysis for diabetes and urinalysis. Moreover, it is most commonly used in radiochemical separation of individual members of actinides /lanthanides series (*Choppin et al., 1956*). Thus, all LMCAs investigated in the present work are introduced in the environment as industrial effluents.

The complexation studies of actinides/lanthanides with LMCA help in understanding the structure of complexes as well as provide deep insight of the various mechanistic aspects of complexation process which in turn will be helpful in

predicting their fate in the environment. Though lot of data on stability constants of actinide/lanthanide complexes with LMCA are available in literature, reliable complexation constants are needed to know the extent to which LMCA will affect the radionuclide speciation. In spite of many years of research, complexation studies of An(III) and Ln(III) with complexing anions present in water are still being perused in order to refine the existing database of stability constants which will enable more realistic prediction of transport of long-lived radionuclides in environment. Further the structures of the complexes need to be determined to understand the mechanism of complexation.

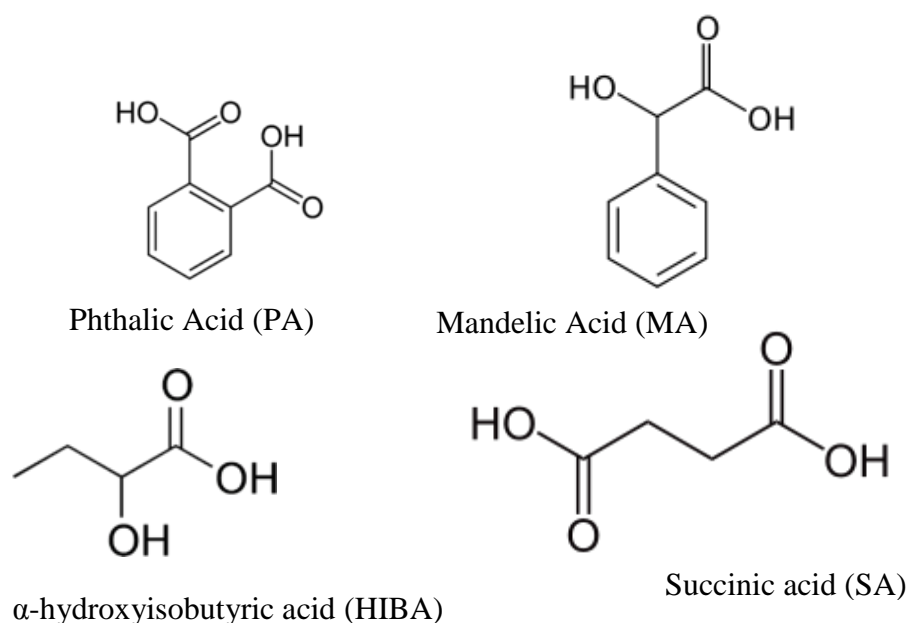


**Figure 3.1** Structure of LMCA studied for determination of complexation constants

TRFS is one of the spectroscopic methods used for determining molecular level speciation of metal ions. This technique has the advantage of triple resolution namely, excitation resolution (excitation wavelength can be unique to a particular metal ion), emission resolution (characteristic emission wavelength for a particular species) and the lifetime resolution (*Planck et al., 2003*). Moreover, TRFS is a very

sensitive tool and provides information about concentrations (based on intensities) and coordination (based on emission wave numbers and fluorescence lifetimes) of fluorescing probe (*Krepelova et al., 2007; Gabriel et al., 2001*). In addition, TRFS is a non-invasive technique and can be used directly for studying solutions and solids. Owing to the above mentioned advantages, TRFS enables the speciation of lanthanides like Eu(III) and actinides like U(VI), Am(III) and Cm(III) in aqueous solutions and on the water/mineral interfaces. However the major drawbacks of TRFS are that lanthanides/actinides that are fluorescent are limited and TRFS measurements are influenced by parameters such as temperature, pH, and method of sample preparation which should be taken into account while interpreting results of TRFS measurements (*Gabriel et al., 2001*). Recently Geipel (2006) has reviewed the actinide speciation work by laser induced spectroscopy.

In present studies, Eu(III) has been used as an analogue of the trivalent lanthanides/actinides owing to similarities in the complexation behaviour of trivalent lanthanides and actinides. The energy level diagram of Eu(III) along with the typical emission profile of Eu(III) is given in figure 3.2 (*Tan et al., 2010*).

The fluorescence emission of Eu (III) has characteristic peaks at wavelength of 580, 592, 616, 650 and 700 nm corresponding to deexcitation of  $^5D_0$  level to  $^7F_i$  levels with  $i = 0$  to 4. Since 4f-electrons are well shielded, the emission wavelength positions for  $^5D_0 \rightarrow ^7F_{0-4}$  transitions are almost independent of the chemical environment of the Eu(III) ion. The emission at 592 nm is of magnetic dipole nature and hence is insensitive to changes in the coordination sphere of the metal ion. On the other hand emission at 616 nm is hypersensitive, that means, its intensity changes with change in chemical environment around the metal ion. This hypersensitivity has been attributed to the electric dipole nature of the transition ( $^5D_0 \rightarrow ^7F_2$ ) and mixing of

quadrupole components (*Hass and Stein, 1971*). The factor  $I_{616}/I_{592}$  (intensity ratio of the 616 nm and 592 nm peaks) is known as the ‘asymmetric ratio’ and is a measure of the asymmetry in electron density around the metal ion.

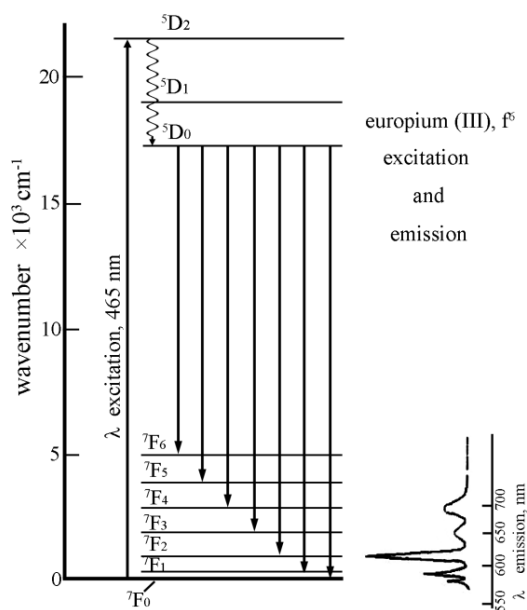


**Figure 3.2** Energy level diagram of Eu(III) along with typical emission spectrum(  
*Tan et al., 2010*).

Lanthanide ions ( $\text{Ln}^{3+}$ ) exist in aqueous solution in the form of aquo complexes. Fluorescence of lanthanides/actinides is known to be quenched by the water molecules in the first coordination sphere of the metal ions. This is due to the deexcitation of the excited state through OH vibration of the coordinated water molecule. In lanthanide aquo complexes,  $[\text{Ln}(\text{H}_2\text{O})_n]^{3+}$ , the value of  $n$  is 9 for early lanthanides while it changes to 8 for later elements due to the reduction in the ionic radius owing to lanthanide contraction. Owing to the presence of 9 water molecules in the first coordination sphere, the lifetime of the  $^5\text{D}_0$  excited state decrease from 2.5 ms in solids to 110  $\mu\text{s}$  in the aqueous solution at low pH values. The drastic reduction in the lifetime is attributed to quenching of the fluorescence by coupling with OH vibrations which provides efficient path for radiationless deexcitation of excited state.

The energy gap between the luminescent  $^5D_0$  state and the highest acceptor ( $^7F_6$ ) state  $\text{Eu}^{3+}$  is  $\sim 12000 \text{ cm}^{-1}$  while the symmetric frequency of OH vibration is  $3700 \text{ cm}^{-1}$ . Thus,  $\sim 3$  OH vibrations are required to quench the fluorescence as shown in figure 3.3.

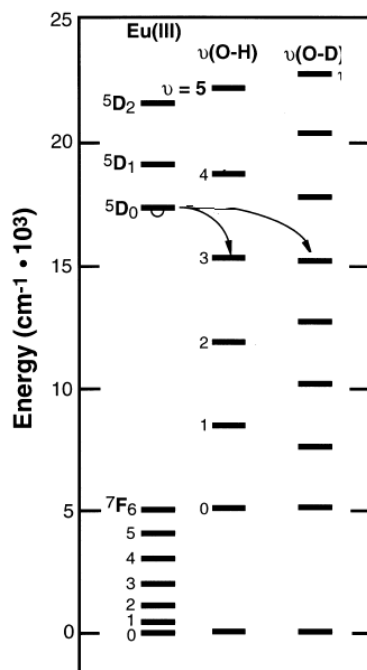


**Figure 3.3** Eu(III) fluorescence quenching by the vibrational energy levels of O–H, O–D oscillators. Semi-circles denote the lowest luminescent levels. Curved arrows denote the most likely vibrational overtone for the non-radiative decay processes

(Choppin and Peterman, 1998 a)

Moreover, the rate of deexcitation via this process is directly proportional to the number of OH oscillators in the first coordination sphere. As the water molecules in the first coordination sphere are replaced by the complexing ligands such as carboxylates, the lifetime increases to higher value than  $110 \mu\text{s}$ . The rise in  $\tau$  value is a measure of the degree of complexation. This can be used to determine the number of ligand bound to metal ion. Since the similar lifetime changes have been observed for both the bands at 592 and 616 nm, the number of water molecules coordinated to

metal ion can be determined from lifetime data measured using any of the peaks. Horrocks and Sudnick (1979) used this approach to deduce the number of water molecules coordinated to metal ion Eu(III). A number of studies were subsequently carried out to determine the number of coordinated water molecules in the complexes of Eu (III) and other rare earth ions (Barthelemy *et al.*, 1989; Kimura and Choppin, 1994; Kimura and Kato, 1998; Thomason *et al.*, 1996).

TRLFS have been used to determine stability constant by several authors (Aoyagi *et al.*, 2004; Toraiishi *et al.*, 2004; Chung *et al.*, 2005; Klenze *et al.*, 1998; Wang *et al.*, 1999; Planque *et al.*, 2005; Couston *et al.*, 2004; Moulin *et al.*, 1999; Montavon *et al.*, 2002; Dobbs *et al.*, 1989). In Eu-salicylate and Eu-5-sulfosalicylate system, static quenching of carboxylic acids was observed with increasing concentration of Eu(III) which was used to determine the stability constant of the complex using Stern Volmer equation (Aoyagi *et al.*, 2004; Toraiishi *et al.*, 2004). In addition, quenching of FA fluorescence with increasing Eu(III) concentration was used to calculate stability constant thereby demonstrating that ligand fluorescence quenching may be effectively used for the complexation study between the HS and the paramagnetic metal ions with a low fluorescence yield (Chung *et al.*, 2005). Complexation of Cm(III) with 5-sulfo-salicylic acid (SSA) was studied using TRIFS and pure spectral components and their mole fraction obtained from peak deconvolution of emission spectra were used to deduce the stability constant (Klenze *et al.*, 1998). Wang *et al.* (1999) calculated stability constants of Eu(III) with aromatic (mellitic, pyromellitic, hemimellitic, trimellitic, trimesic, phthalic, isophthalic, terephthalic and benzoic) carboxylic acids from the changes  ${}^7F_0-{}^5D_0$  excitation spectra with increasing carboxylate concentration.

Moreover, the hypersensitivity of the band at 616 nm has been used to determine the stability constant of the metal ligand complex (*Plancque et al., 2005; Couston et al., 2004; Moulin et al., 1999; Montavon et al., 2002; Dobbs et al., 1989*). The interaction of Eu(III) with small organic ligands e.g. acetic acid, glycolic acid and 4 hydroxy acetic acid has been studied by Plancque. et.al (2005) using TRLFS to deduce the information about metal ion binding to HA. The intensity ratio ( $I_{616}/I_{592}$ ) and fluorescence lifetimes were used to determine the equilibrium constant and hydration number in the Eu(III), tetraethylmalonamide (TEMA), and  $\text{NO}_3$  system. Hydration number obtained from fluorescence lifetime clearly depicted the inner-sphere location of nitrate in the  $\text{Eu}(\text{NO}_3)_2^+$  complex and the outer-sphere location of TEMA in the  $\text{Eu}(\text{TEMA})^{3+}$  complex (*Couston et al., 2004*). The complexation of Eu(III) with new micellar system (TAC8), a "diblock" surfactant cage molecule containing a cage (cyclam) as a complexation part linked to a sugar-based surfactant part, has been studied using TRLFS and the hypersensitive transition was used to estimate the complexation constant (*Moulin et al., 1999*). The complexation behaviour of Eu(III) with polymaleic acid (PMA) studied using TRLFS showed the formation of 1:1 Eu:PMA complex and the existence of at least two distinct interaction environments ("sites") of Eu with the polymer chain, whose proportions varied with the ratio of the total Eu and PMA concentrations, was proven from the lifetimes and emission spectra of Eu-PMA complexes (*Montavon et al., 2002*). Moreover, Dobbs et al. (1989) used free metal concentration, deduced from variation in intensity ratio of Eu(III) with FA concentration, as an input to continuous multiple site ligand modeling in order to describe Eu(III) complexation with FA.

In the present work, the intensity ratio of 616 and 592 nm peaks in the fluorescence emission spectra of Eu(III)-LMCA complexes was used to determine the

stability constant of the complexes. The stoichiometry of the complexes ( $ML_n$ ) has also been corroborated by lifetime data.

## **3.2 Experimental**

**3.2.1. Reagents used:** All the reagents used for the present investigation were of AR grade.  $Eu_2O_3$  (spec pure), HIBA, PA, MA and SA were obtained from Merck. HA was purchased from ACROS.

### **3.2.2. Preparation of stock solutions:**

#### **3.2.2.1. Eu(III) stock solution:**

The stock solution of Eu(III) was prepared by dissolving AR grade  $Eu_2O_3$  in conc.  $HNO_3$ . Solution was evaporated to dryness. The metal nitrates thus formed were dissolved in  $HClO_4$ . The solution was again evaporated to dryness thrice and the residue obtained was dissolved in  $\sim 0.1$  M  $HClO_4$ . The stock solution of Eu(III) was standardized by complexometric titration with EDTA using Xylenol orange as indicator. The concentration of europium stock solution was  $5.6 \times 10^{-2}$  M.

#### **3.2.2.2. LMCA stock solutions:**

2.6 g of HIBA was dissolved in 25 ml of water to prepare HIBA stock solution having concentration 1 M. For PA stock solution, 2.3269 g of PA was dissolved in 20 ml of 1.045 M NaOH which was finally made up to 25 ml. Owing to the low solubility of PA in water, NaOH was used. The final concentration of PA solution was 0.56 M. The stock solutions of MA and SA were prepared in a similar manner and the final concentration was the same, that is, 0.56 M. For stock solution of HA, 0.0108 g of HA was dissolved in 10 mL water. The proton exchange capacity of HA had been determined by the Bartya method and the value was 4.6 meq/g (*Kumar, 2012*). The

final concentration of HA was 1 g/L and accordingly the concentration of HA was in the range  $10^{-3}$  M. HA concentration represents the concentration of proton exchanging groups. Millipore water having resistivity 18 M $\Omega$ .cm was used for making all solutions.

### **3.2.3. Preparation of samples:**

**3.2.3.1. Eu-HIBA:** The solution having different HIBA to Eu(III) ratio were prepared at pH 4 by adding appropriate quantity of stock solution of HIBA to Eu(III) solution. The concentration of Eu(III) in the final solution was  $5.6 \times 10^{-3}$  M while that of HIBA was varied from 0 to 0.42 M so as to have L/M ratio from 0 to 75. In all the solutions ionic strength was maintained at 0.1 M NaClO<sub>4</sub> by using appropriate volume of 1 M NaClO<sub>4</sub>. This applies to other systems described below.

**3.2.3.2. Eu-PA:** The solutions having different PA to Eu ratio were prepared at pH 5.0 by adding appropriate quantity of stock solution of PA to Eu solution. The concentration of Eu in final solution was  $5.6 \times 10^{-4}$  M, while that of PA was varied from 0 to 0.056 M, so as to have L/M ratio from 0 to 100.

**3.2.3.3. Eu-MA:** Seventeen samples having varying ratio of concentration of Eu and MA from 1:0 up to 1:100 were prepared by mixing appropriate volume of the stock solutions and maintaining the pH of the solutions to 5.0 using dilute NaOH solution. The Eu concentration was fixed at  $5.6 \times 10^{-4}$  M while that of MA was varied up to 0.056 M. For the higher value of L/M ratio europium concentration was taken as  $5.6 \times 10^{-5}$  M.

**3.2.3.4. Eu-SA:** Different L/M solutions were prepared at pH 5.5 by adding appropriate quantity of stock solutions of SA and Eu so that the final concentration of Eu was  $5.6 \times 10^{-4}$  M, while that of SA was varied from 0-0.112 M so as to have L/M ratio from 0-200.

**3.2.3.5. Eu-HA:** The solutions having a range of L/M ratio from 0 to 10 were prepared using required amount of Eu and HA from their stock solutions. In all the solutions Eu concentration was  $5.6 \times 10^{-5}$  M whereas the HA concentration varied from 0-100 mg/l. For all the solutions, pH was fixed at 6.5.

The ligand assisted Eu(III) excitation takes place in case of PA, MA, SA and HA which allowed the complexation studies at lower concentration of Eu(III) as compared to that used for Eu(III)-HIBA system.

### **3.3. Relationship between lifetime and the coordinated water molecules:**

It is expected that lanthanides/actinides should have long lifetimes as f-f transitions, responsible for their fluorescence, are forbidden transitions. However, in aquatic environment their lifetimes are relatively short due to non-radiative relaxation of excited f levels to lower lying vibrational levels of water molecules in first coordination sphere of the lanthanides/actinides. The vibration of few OH bonds offers an alternative pathway for deexcitation of the  $^5D_0$  state of  $\text{Eu}^{3+}$  and hence can provide a possible quenching mechanism of the Eu(III) fluorescence. This radiationless deexcitation exhibits a very large isotope effect as replacement of OH by OD oscillators' results in virtual elimination of this mode of deexcitation of excited state. Since, the symmetric stretching of OD vibration is  $2600 \text{ cm}^{-1}$ , 5 OD vibrational overtones are required for radiationless transition as shown in figure 3.3. Coupling to a higher energy overtone, as required for the OD oscillator, results in less efficient

quenching of the Eu(III) excited state. Horrocks et al. established empirical relationship between lifetime ( $\tau$ ) and number of water molecules in first coordination sphere of  $\text{Eu}^{3+}$  ( $N_{\text{H}_2\text{O}}$ ) by synthesizing variety of crystalline  $\text{Eu}^{3+}$  complexes of known crystal structure having varying numbers of water molecules in the range zero to nine coordinated to the  $\text{Eu}^{3+}$  ions (*Horrocks and Sudnick, 1979*). Two series of crystals were prepared, one containing coordinated  $\text{H}_2\text{O}$  and the other coordinated  $\text{D}_2\text{O}$ . Lifetime of crystalline solids of both the series was measured. The large isotope effect was used to identify the contribution of coordinated  $\text{H}_2\text{O}$  to the rate of deexcitation of excited state. The observed exponential decay constant,  $k_{\text{obsd}}$ , is given by

$$k_{\text{obsd}} = k_{\text{nat}} + k_{\text{nonrad}} + k_{\text{H}_2\text{O}} \quad (3.1)$$

where  $k_{\text{nat}}$  is the natural rate constant for the emission of photons,  $k_{\text{nonrad}}$  is the rate constant for radiationless deexcitation processes which do not involve water, and  $k_{\text{H}_2\text{O}}$  is the rate constant for the transfer of energy to the OH vibrations of coordinated water. For any given complex,  $k_{\text{H}_2\text{O}}$  is proportional to the number of coordinated water molecules. Thus,  $k_{\text{obsd}}$  in  $\text{D}_2\text{O}$  is summation of  $k_{\text{nat}}$  and  $k_{\text{nonrad}}$ , while  $k_{\text{obsd}}$  in  $\text{H}_2\text{O}$  includes all three terms of equation 3.1. The measured difference  $\Delta k_{\text{obsd}} = k_{\text{obsd}}(\text{H}_2\text{O}) - k_{\text{obsd}}(\text{D}_2\text{O})$ , is a measure of the number of coordinated water molecules,  $q$ . Since the number of water molecules was known in case of solids, correlation between the  $\Delta k_{\text{obsd}}$  in case of solids and the known number of water molecules was deduced which was applied to a number of model chelate systems in solution and to the structurally well-characterized proteins. The close correspondence was found between the solution and solid-state results (*Horrocks and Sudnick, 1979*). The relationship between number of water molecules in the inner coordination sphere and lifetime is given by equation (*Hass and Stein, 1971; Kimura and Kato, 1998*):

$$n(\text{H}_2\text{O}) \pm 0.5 = 1.07 k - 0.62 \quad (3.2)$$

where  $n(\text{H}_2\text{O})$  is the number of water molecules in the inner hydration sphere of the Eu(III) ion. The high uncertainty,  $\pm 0.5$  in number of inner sphere water molecules was reported, due to the potential of a small degree of quenching of excited state of Eu(III) by O-H bonds in the outer coordination spheres. The number of coordination sites of Eu(III) occupied by the ligand can be calculated as the difference between 9 and  $n(\text{H}_2\text{O})$ , as fully hydrated Eu(III) ion has 9 water molecules in its primary coordination sphere (Ozaki *et al.*, 2007). Thus, fluorescence decay lifetime provides information about the chemical environment of Eu(III) complexes in solution as well as adsorbed on solid phases.

### 3.4. Results and Discussion:

#### 3.4.1. Eu –HIBA:

Figure 3.4 shows the excitation spectrum of aqueous solution of Eu(III), at  $\lambda_{\text{em}} = 592$  nm, having metal ion concentration equal to  $5.6 \times 10^{-3}$  M at pH 4.0. The interference from HIBA in the fluorescence spectra of Eu(III) was found to be negligible. Since no ligand assisted excitation was observed in case of Eu(III)-HIBA complexes,  $\lambda_{\text{ex}} = 395$  nm was used for recording spectral and temporal characteristics of Eu(III)-HIBA system.

The fluorescence emission spectra of a few solutions with varying Eu-HIBA ratio are shown in Figure 3.5. The figure shows emission peaks at 592 and 616 nm due to de-excitation of  $^5\text{D}_0$  to  $^7\text{F}_1$  and  $^7\text{F}_2$  respectively. The spectra of different solutions have been normalized to the intensity at 592 nm. It is evident from the plot that intensity of 616 nm peak increases with respect to that of 592 nm with increasing ligand to metal ratio. With increasing concentration the successive higher number of ligands replace the water molecules in the inner coordination sphere of Eu(III) which

results in change in the electric field gradient around Eu(III). Since the transition corresponding to 616 nm is electric dipole transition, its intensity increases with increasing ligand to metal ratio. In contrast, transition at 592 nm is magnetic dipole transition and its intensity remains unaffected on changing electric field gradient around metal ion.

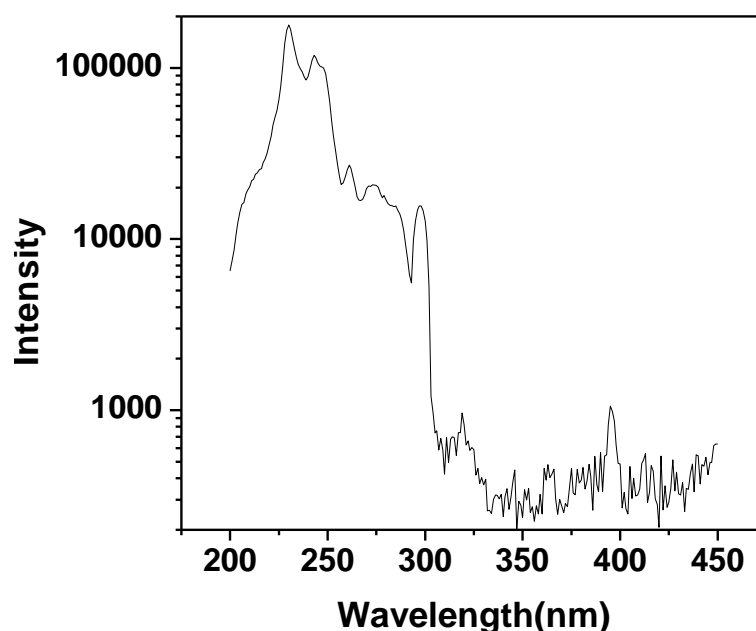


**Figure 3.4** Excitation spectrum of Eu(III) aqueous solution ( $\lambda_{em} = 592$  nm)

Figure 3.6 shows the plot of intensity ratio  $I_{616/592}$  as a function of  $[HIBA]/[Eu]$ . The plot shows stepwise increase of  $I_{616/592}$  with  $[HIBA]/[Eu]$  indicating the formation of Eu-HIBA complexes having different stoichiometry. The intensity plot can be resolved into different regions for systems in which the complexes are formed between the ligands and metal ion. The first region can be defined by  $[L] : [M] < 2$ , in which formation of  $ML$  species takes place, while the second region, occurring for  $[L] : [M]$  ratio between 2 and 10, accounts for the formation of the  $ML_2$  species. Similarly, the formation of  $ML_3$  occurs when the  $[L] : [M]$  ratio is between 10 and 75.

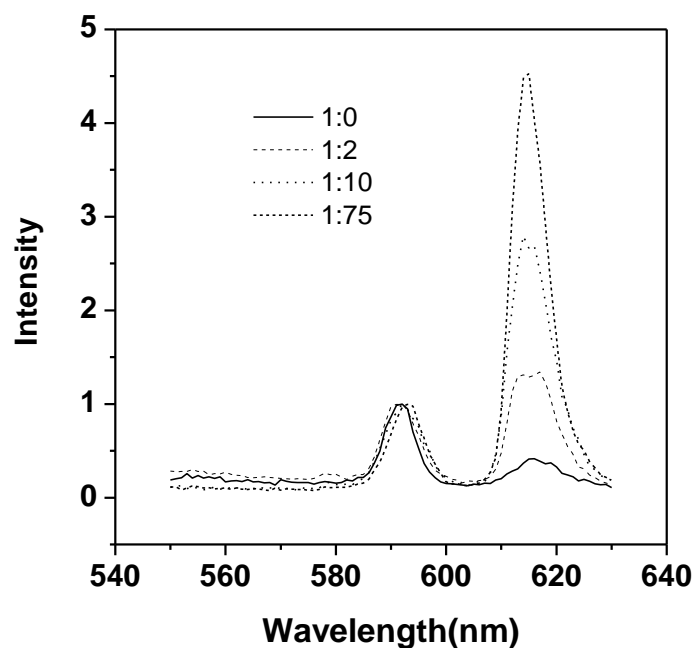


Figure 3.5 Fluorescence emission spectra of solutions with different Eu : HIBA ratio

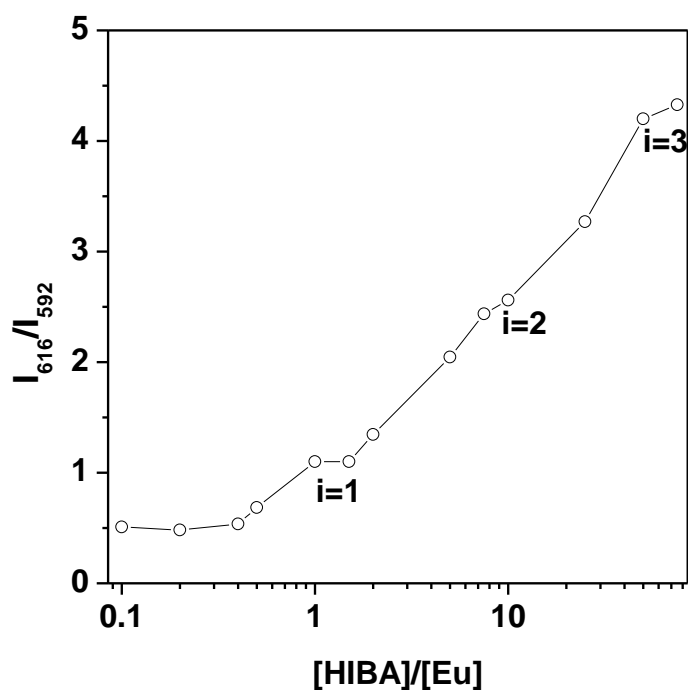


Figure 3.6 Plot of  $I_{616}/I_{592}$  vs  $[HIBA]/[Eu]$

It is worth mentioning that segregation of intensity ratio plot into different regions is possible as plateau (constant value for intensity ratio) is attained for every region which indicates that the metal ion is not binding to an additional ligand even

though the [L] : [M] ratio continues to increase. Therefore, three different regions defined above were selected to compute stability constants of Eu(III)-HIBA complexes as described below

### 3.4.1.2. Determination of Stability constants from Intensity ratio ( $I_{616}/I_{592}$ ):

The stability constant of Eu –LMCA complex  $ML_i$  ( $i= 1-3$ ) were determined from the data of  $I_{616}/I_{592}$  as a function of ligand concentration using the following procedure:

$$I_{592} = X[M] + X \sum_{i=1}^3 [ML_i] \quad (3.3)$$

$$I_{616} = Y[M] + Y \sum_{i=1}^3 k_i [ML_i] \quad (3.4)$$

$$\frac{I_{616}}{I_{592}} = \frac{Y[M] + Y \sum_{i=1}^3 k_i [ML_i]}{X[M] + X \sum_{i=1}^3 [ML_i]} \quad (3.5)$$

where X be the fluorescence contribution factor for the emission band at 592 nm. This factor is the same for both the metal terms since the intensity of this band is not influenced by the metal-ligand complex. The corresponding intensity contribution factor for band at 616 nm is Y. Since band at 616 nm is hypersensitive transition, therefore fluorescence contribution factor for metal and metal complexes is not equal. Hence for metal complexes constant k is introduced which is defined as the enhancement in the fluorescence intensity of the complex at 616 nm with respect to uncomplexed metal ion.

$\frac{Y}{X}$  can be obtained from the ratio  $[R_0]$  for the sample containing no ligand i.e.

when  $\sum ML_i = 0$

$$R_0 = Y/X \quad (3.6)$$

Likewise k for ML can be obtained from the ratio  $R_b$  for the sample having highest concentration of ligand that is when  $[M] \ll [ML]$ , therefore  $[M] \approx 0$

$$R_b = (Y/X)k \quad (3.7)$$

From equation (3.6) & (3.7)

$$R_b = R_0k \quad (3.8)$$

Considering the formation of 1:1 complex between Eu and the ligand, the stability constant  $\beta_{11}$ , defined by equation (3.9), can be obtained by placing R values before the first plateau in equation (3.5) and using the mass balance equation for the total metal and ligand concentration.

$$\beta_{11} = \frac{[ML]}{[M][L]} \quad (3.9)$$

[ML], obtained from the R values for the intermediate [L], is given by

$$[ML] = \frac{[M_T](R-R_0)}{R_0(1-k)} \quad (3.10)$$

Free ligand concentration is given by

$$[L] = [L]_T - [ML] \quad (3.11)$$

In the case of free ligand concentration, the  $pK_a$  of the acid must be taken into account.

The free metal concentration is given by

$$[M] = [M]_T - [ML] \quad (3.12)$$

Substituting the value of [ML], [L] and [M] from equation (3.10, 3.11, 3.12) respectively into equation (3.9) the stability constant can be determined. In the case of  $ML_2$  the stability constant was determined by solving the following three equations

$$\frac{I_{616}}{I_{592}} = \frac{Y\{[M] + k_1[ML_1] + k_2[ML_2]\}}{X\{[M] + [ML_1] + [ML_2]\}} \quad (3.13)$$

$$[M]_T = [M] + [ML_1] + [ML_2] \quad (3.14)$$

$$[L]_T = [L] + [ML_1] + 2[ML_2] \quad (3.15)$$

Likewise in case of  $ML_3$  following equations were used

$$\frac{I_{616}}{I_{592}} = \frac{Y\{[M] + k_1[ML_1] + k_2[ML_2] + k_3[ML_3]\}}{X\{[M] + [ML_1] + [ML_2] + [ML_3]\}} \quad (3.16)$$

$$[M]_T = [M] + [ML_1] + [ML_2] + [ML_3] \quad (3.17)$$

$$[L]_T = [L] + [ML_1] + 2[ML_2] + 3[ML_3] \quad (3.18)$$

where  $k_1, k_2, k_3$  were taken from the R values at the corresponding plateaus in the plot of  $I_{616}/I_{592}$  vs. L/M. Thus, by dividing the intensity ratio data into various segments, the stability constants were deduced. The stability constants of Eu(III) – HIBA complexes are given in Table 3.1. The  $\log \beta_1$  and  $\log \beta_2$  values for Eu(III)-HIBA complexes obtained in present study are in conformity with literature data (*Martell and Smith, 1977*), in which potentiometry was used for determination of stability constants, while  $\log \beta_3$  values are lower. The lower experimental temperature in case of reported data may be the reason for the difference in the observed and reported values.

The plot of lifetime ( $\tau$ ) as a function of [HIBA]/[Eu] is shown in Figure 3.7 (a). The mono-exponential fit for all [HIBA]/[Eu] indicates fast exchange of ligand between free metal ion and the complex. The life time increases from 110  $\mu$ s for the aquo complex  $\text{Eu}(\text{H}_2\text{O})_n$  to 346.4  $\mu$ s for the highest concentration of [HIBA]. This is due to the replacement of the water molecules in the primary coordination sphere of Eu(III) by HIBA upon complexation.

The coordinated water molecules provide alternative non-radiative pathway for the  ${}^5\text{D}_0 \rightarrow {}^7\text{F}_1$  transitions, through OH stretching vibrations. The number of water molecules coordinated to Eu(III) at different values of [HIBA]/[Eu] are also shown in figure 3.7 (b). The  $n(\text{H}_2\text{O})$  for Eu-aquo complex was found to be 9 which is in agreement with the literature data (*Horrocks and Sudnick, 1979*). Considering that HIBA acts as a bidentate ligand, each HIBA molecule will replace two water

molecules from Eu-aquo complex. This is evident from figure 3.5 which shows plateaus at 7, 5 and 3 thus suggesting the formation of ML, ML<sub>2</sub>, ML<sub>3</sub> type of complexes with increasing HIBA concentration.

**Table 3.1** Stability Constants of Eu with HIBA, SA, PA and MA

Ligand (pka <sub>1</sub> ,pka <sub>2</sub> )	Log β <sub>1</sub>	Log β <sub>2</sub>	Log β <sub>3</sub>	Remarks
HIBA (3.79)	3.32 ± 0.04	5.5 ± 0.07	6.62 ± 0.13	Present work
	3.09	5.54	7.32	(Martell and Smith, 1977)
SA (4.00, 5.24)	2.9 ± 0.1	5.1 ± 0.2		Present work
	3.0 ± 0.01	4.9 ± 0.02		(Wang et al., 2000)
PA (2.75,4.93)	3.7 ± 0.3	5.8 ± 0.3		Present work
	3.5 ± 0.02	5.17 ± 0.08		(Wang et al., 1999)
MA (3.19)	2.9 ± 0.2	4.9 ± 0.4		Present work
	2.70	4.89		(Manning, 1967)

Ozaki et al. (2002) constructed CE diagram for a variety of Eu(III) complexes by plotting intensity ratio ( $I_{616}/I_{592}$ ) against  $\Delta N_{H_2O}$  ( $9-n(H_2O)$ ) as shown in Figure 3.8. According to this diagram when Eu(III) forms an outer sphere complex with the ligands,  $I_{616}/I_{592}$  increases whereas  $\Delta N_{H_2O}$  remains close to zero. Thus, outer sphere complexes are depicted by a narrow zone 'A' in the CE diagram as shown in Figure 3.8. In contrast when inner-sphere complexes are formed, an increase in intensity ratio is accompanied by the expulsion of water molecules. Hence a much wider zone 'B', compared to zone A, has been assigned to inner sphere complexes. Thus  $I_{616}/I_{592}$  vs  $\Delta N_{H_2O}$  diagrams help in understanding of the coordination environment of Eu(III) by predicting the formation of inner sphere and outer sphere complexes.

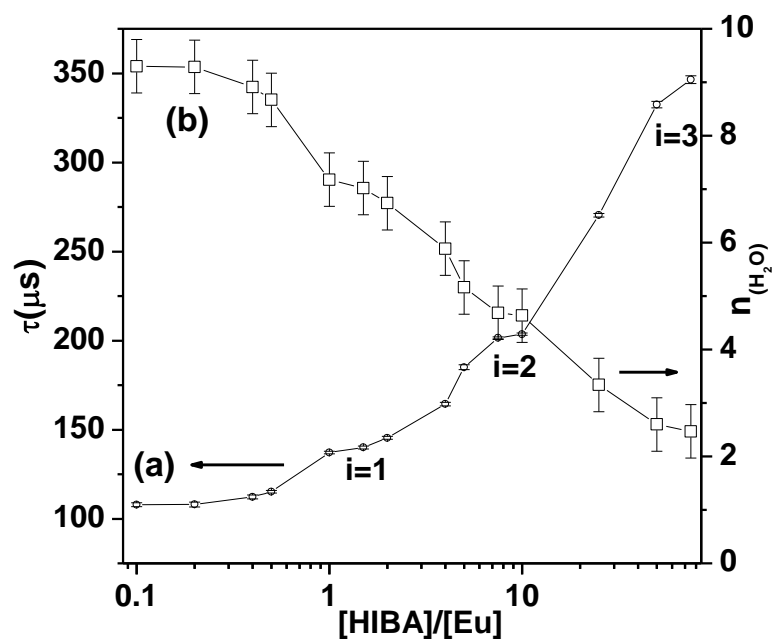


**Figure 3.7** (a) Lifetime vs.  $[HIBA]/[Eu]$ , (b) Number of water molecules vs.  $[HIBA]/[Eu]$

In present work the CE diagram is constructed by plotting  $I_{616}/I_{592}$  for varying  $[HIBA]/[Eu(III)]$  against corresponding  $\Delta N_{H_2O}$  as shown in figure 3.9.  $\Delta N_{H_2O}$ , which represents the number of coordination sites occupied by the ligands in the place of water molecules in the inner sphere of Eu(III), increases with  $I_{616}/I_{592}$ . Initially when  $[HIBA]$  concentration is extremely small, Eu(III) aquo complexes dominate and hence value of  $\Delta N_{H_2O}$  is close to zero. The  $I_{616}/I_{592}$  for all Eu(III)-HIBA complexes are greater than 1 (figure 3.6) and the corresponding  $\Delta N_{H_2O}$  are greater than 2, hence all these complexes lie in the zone B (figure 3.8) which correspond to the formation of inner sphere complexes. Thus CE diagram reveals the gradual change in the coordination of Eu(III) ion for varying  $[HIBA]/[Eu(III)]$  and validate the formation of inner sphere complexes.

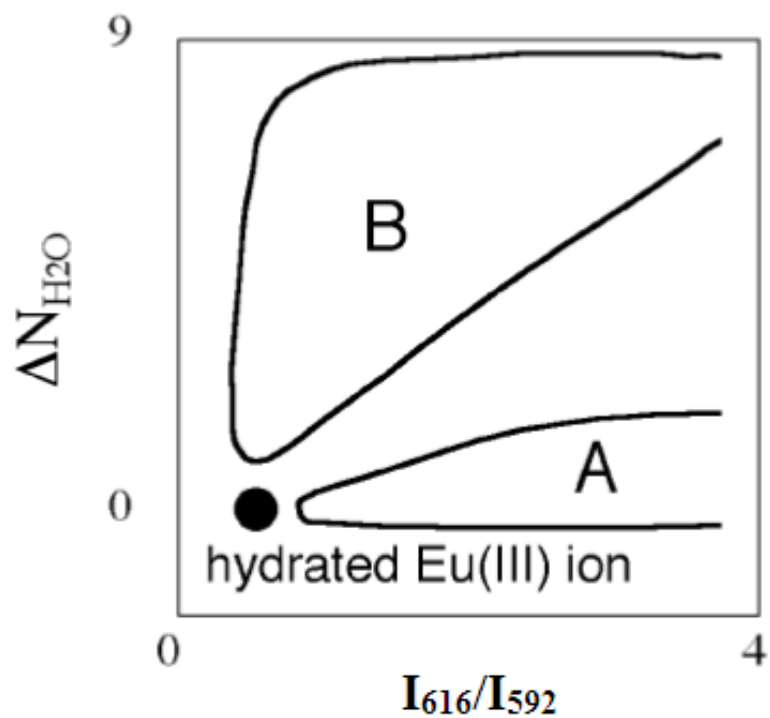


**Figure 3.8** Schematic CE diagram indicating areas corresponding to the characteristics of the interactions between Eu(III) and ligands. Plots in zones A and B are attributable to outer-sphere and inner sphere coordination, respectively (Ozaki *et al.* 2002).

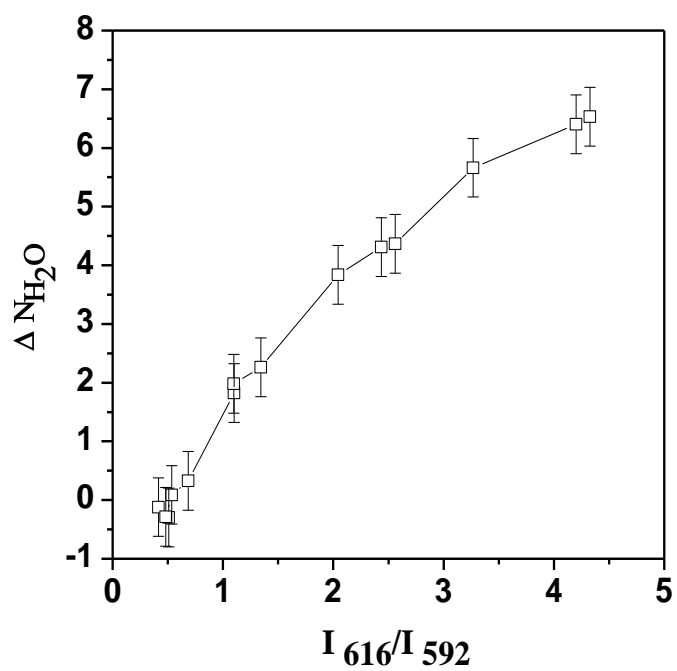


**Figure 3.9** CE diagram for varying [HIBA]/[Eu(III)]

Similar studies were carried out with other LMCA which are discussed below in brief:

### 3.4.2. Eu-PA:

For Eu(III)-PA system, the familiar emission bands at 592 nm and 616 nm due to  $^5D_0 \rightarrow ^7F_1$  and  $^5D_0 \rightarrow ^7F_2$  respectively were obtained. The plot of  $I_{616/592}$  against L/M (figure 3.10) shows that with the increasing L/M, the asymmetric ratio also increases as the result of replacement of water molecules by the chelating ligand. The plot of intensity ratio vs L/M shows two plateaus, first around L/ M ratio 8-20 and second plateau at L/M close to 50, which were used to deduce stability constants of Eu(III)-PA complexes (Table 3.1). These two plateaus are attributed to the formation of 1:1 and 1:2 complexes respectively which are further corroborated from the lifetime data. The information about the stoichiometry of the complex formed was obtained from the lifetime data shown in figure 3.11 (a). From the plot of  $n(H_2O)$  vs. L/M (figure 3.11 (b)), it can be seen that,  $n(H_2O) = 7$  and 5 at L/M around 8-20 and at L/M = 50 respectively. As PA is known to be a bidentate ligand the  $n(H_2O)$  values corroborate formation of 1:1 and 1:2 in respective ranges (*Wang et al., 1999*).

The  $\log \beta$  values for Eu-PA complexes are slightly different than those reported in literature (*Wang et al., 1999*), wherein changes in the  $^5D_0 \rightarrow ^7F_0$  excitation spectra of Eu(III) with increasing PA concentration were used to deduce the stability constant. The observed discrepancies in the stability constant values can be attributed to sensitivity of excitation source used in two studies. In present studies xenon flash lamp has been used whereas in literature the laser was used as an excitation source.

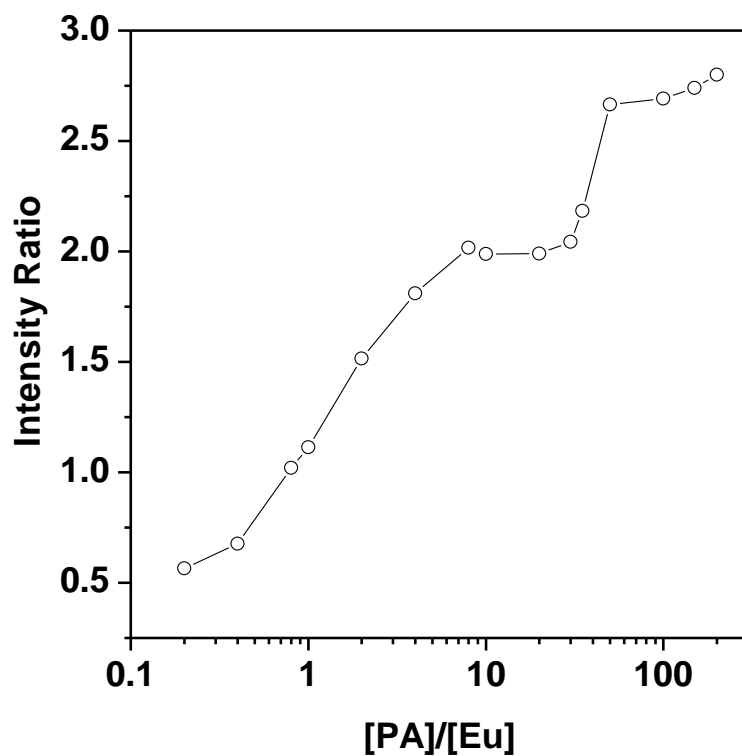


Figure 3.10  $I_{616}/I_{592}$  of Eu vs.  $[PA]/[Eu]$

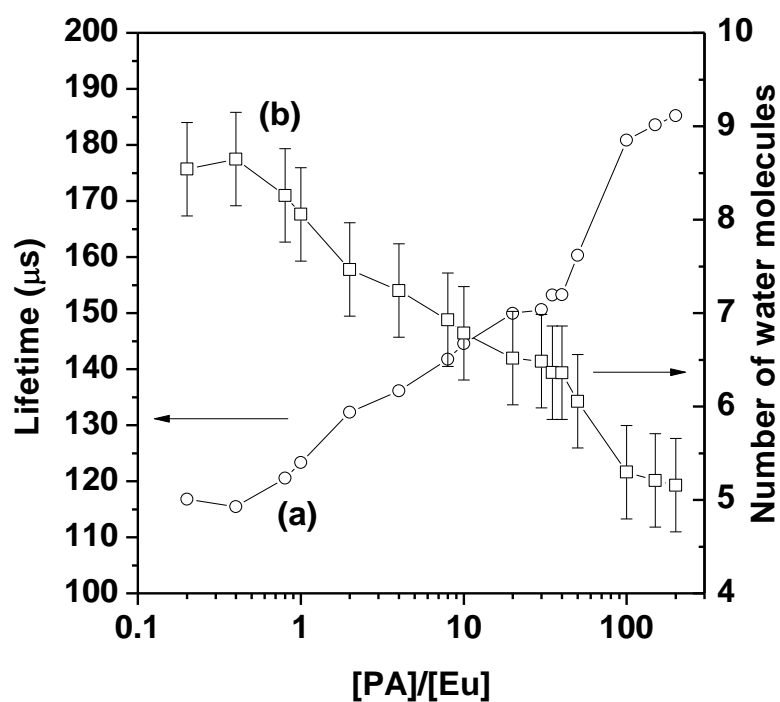


Figure 3.11 (a) Lifetime vs.  $[PA]/[Eu]$ , (b) Number of water molecules vs.  $[PA]/[Eu]$

### 3.4.3. Eu-MA:

The emission spectra of Eu-MA solutions having varying ratio of the concentration of ligand and metal ion showed the familiar rise in the intensity of 616 nm peak with respect to that at 592 nm as shown in figure 3.12. The intensity ratio shows a small plateau at L/M value in the region around 8-10 and a second plateau at L/M close to 75-100 as shown in figure 3.12.

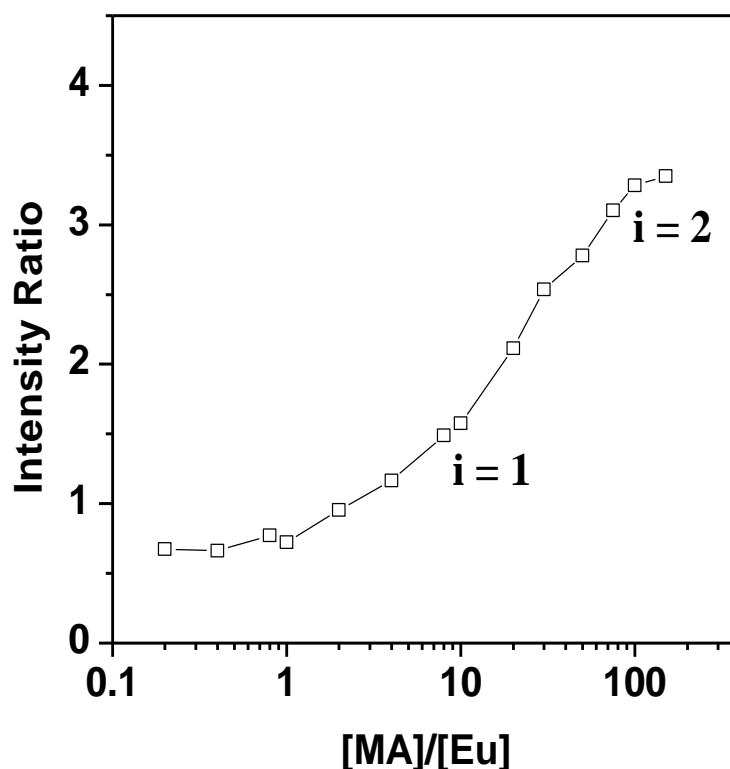
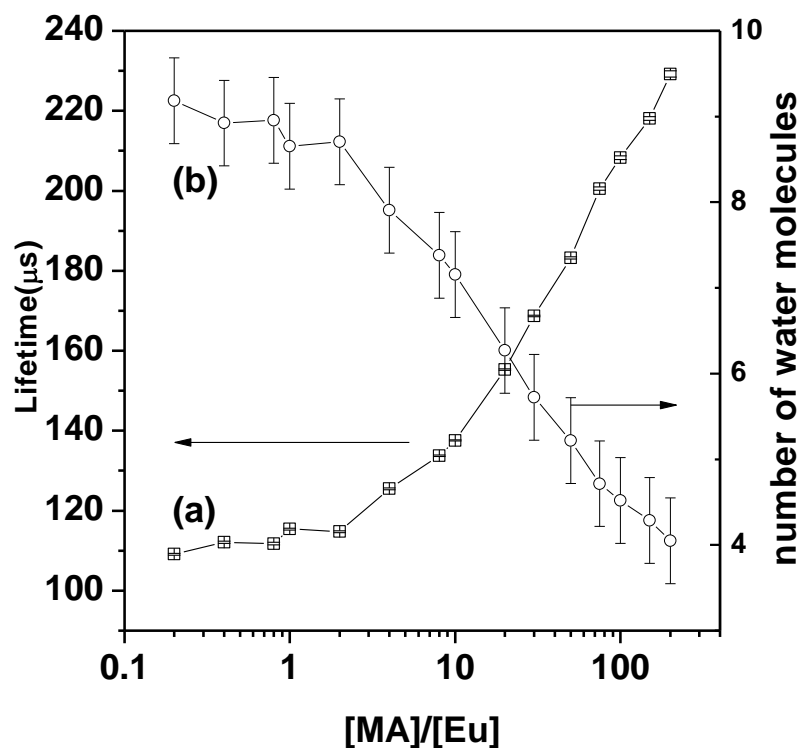


Figure 3.12  $I_{616}/I_{592}$  of Eu vs.  $[MA]/[Eu]$

The life time data follow similar trend with the corresponding  $n(H_2O)$  values being 7 and 5 at L/M value close to 8 and 75 respectively indicating the formation of 1:1 and 1:2 type of complexes between Eu and MA as shown in figure 3.13. The stability constant of  $Eu(MA)$  and  $Eu(MA)_2$  (Table 3.1) were determined from the intensity ratio data which are in conformity with literature data (Manning, 1967). The intensity ratio appears to increase beyond L/M value equal to 200 indicating the formation of

Eu(MA)<sub>3</sub>. However the measurements at higher L/M value than 200 could not be continued due to the limiting solubility of MA and difficulty in maintaining the ionic strength at 0.1 M.



**Figure 3.13** (a) Lifetime vs.  $[MA]/[Eu]$ , (b) Number of water molecules vs.  $[MA]/[Eu]$

#### 3.4.4. Eu-SA:

As in the case of HIBA, PA and MA, similar results were also obtained for Eu-SA system. Figure 3.14 shows the plot of  $I_{616/592}$  (asymmetric ratio) as a function of L/M. The plot shows step wise increase of  $I_{616/592}$  with SA concentration indicating the formation of 1:1 and 1:2 complexes whose stability constant are given in Table 3.1. The  $\log \beta$  values for Eu-SA are in quite a good agreement with the literature data (Wang *et al.*, 2000).

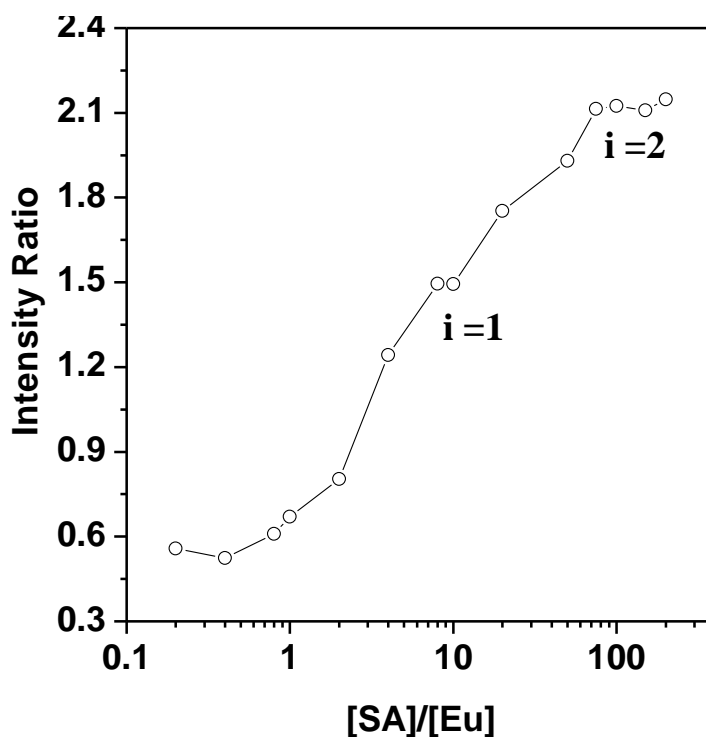


Figure 3.14  $I_{616}/I_{592}$  of Eu vs.  $[SA]/[Eu]$

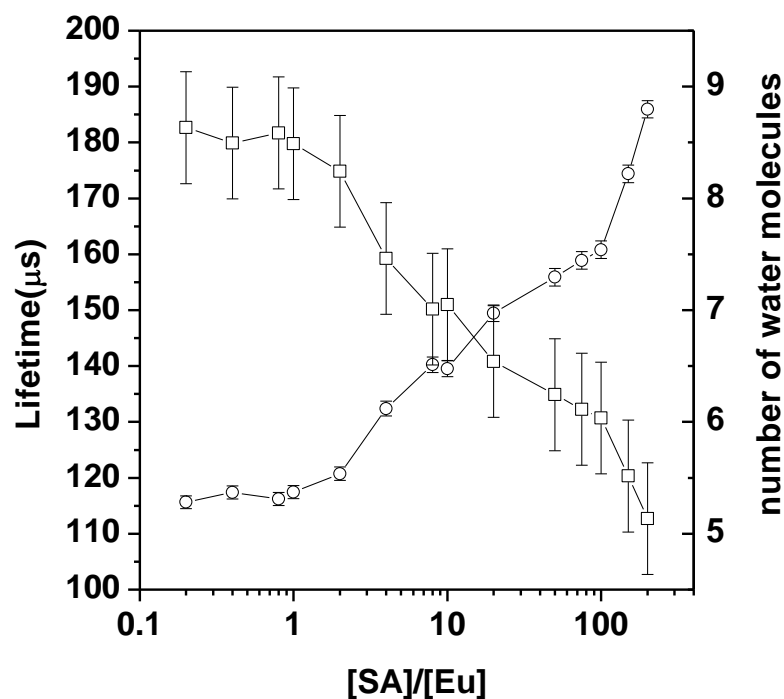


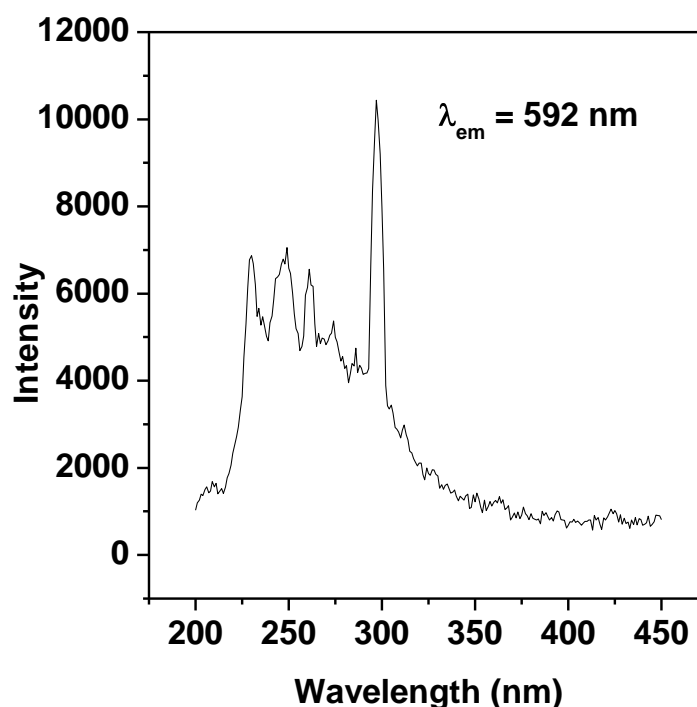
Figure 3.15 (a) Lifetime vs.  $[SA]/[Eu]$  (b) Number of water molecules vs.  $[SA]/[Eu]$

Figure 3.15 (a) shows the plot of life time as a function of L/M. The life-time increases from  $113 \mu\text{s}$  (for  $L/M = 0$  i.e. aquo complex of Eu) to  $186 \mu\text{s}$  for the highest

concentration of SA ( $L/M = 200$ ). Figure 3.15 (b) shows the number of water molecules coordinated to Eu at different values of  $L/M$ . Considering SA as a bidentate ligand at pH 5.5, each SA will replace two water molecules from Eu (aquo) complex. The  $n(\text{H}_2\text{O})$  value for 1:1 complex (7) agrees with that expected for removal of two water molecules, that for 1:2 complex is also as the expected value (5).

### 3.4.5. Eu-HA:

The HA solution has intense and broad excitation spectrum as shown in figure 3.16 owing to large number of chromophores present in HA. In view of this, the concentration of Eu ( $5 \times 10^{-5} \text{ M}$ ) was decreased, so as to work with lower concentration of HA thereby avoid quenching of Eu(III) fluorescence.



**Figure 3.16** Excitation spectrum of HA

The continuous rise of asymmetric ratio,  $I_{616/592}$  as a function of  $L/M$  was observed for Eu(III)-HA system (figure 3.17) which indicates the formation of

Eu(III)-HA complex. In case of Eu(III)-HA system stability constant could not be determined as plateau in the intensity ratio plot was not observed due to the limited range of  $[HA]/[Eu]$  investigated in the present work, owing to the quenching of Eu(III) fluorescence by HA. For  $[HA]/[Eu] = 10$ , the  $I_{616}/I_{592}$  is less than that for  $[HA]/[Eu] = 8$  which implies that the static quenching of Eu(III) fluorescence take place above  $[HA]/[Eu] = 8$ . Since xenon lamp was used as the excitation source in present studies, the concentrations lower than  $5 \times 10^{-5}$  M could not be employed to study Eu(III)-HA system. However in literature, there are reports where binding characteristics of HS with Eu(III)/Cm(III) has been studied at very low concentration ( $\sim 10^{-7}$  M) by employing laser as an excitation source (Chung *et al.*, 2005; Monsallier *et al.*, 2003).

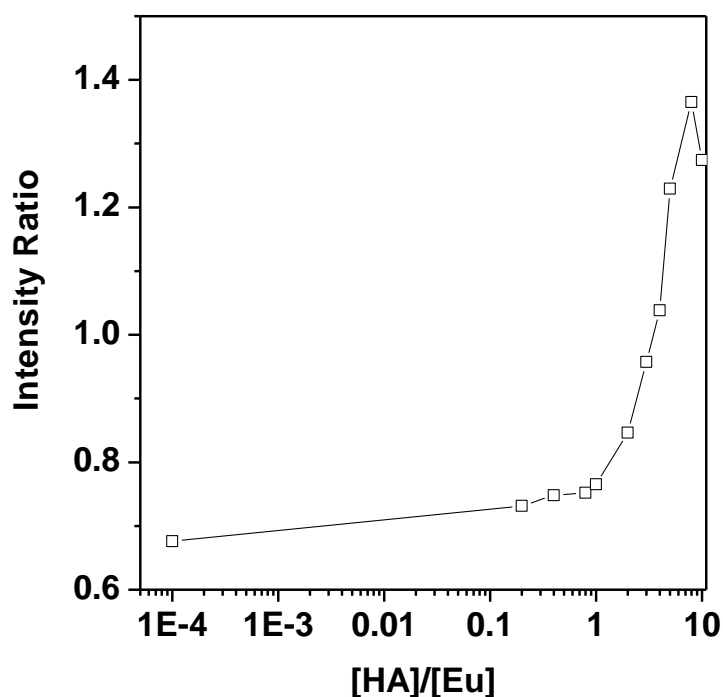
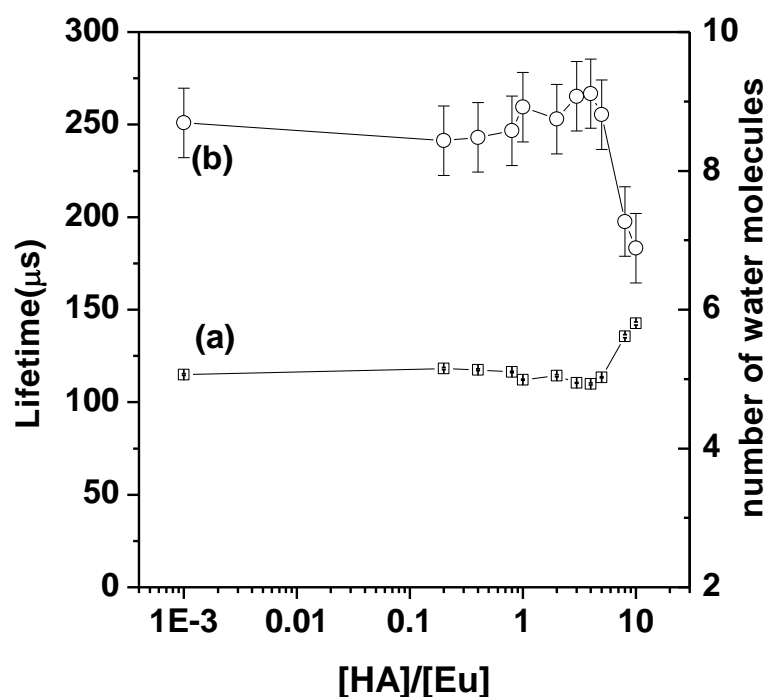


Figure 3.17  $I_{616}/I_{592}$  of Eu vs  $[HA]/[Eu]$

The plot of life-time vs. L/M (figure 3.18 (a)) shows no change in life-time at least up to L/M of 5, above which a slight increase of life time was observed. The constancy of life-time and its closeness to that of Eu aquo complex  $[\text{Eu}(\text{H}_2\text{O})_9]$  indicates the number of coordinated water molecules does not change upon complexation with HA (figure 3.18(b)). Owing to the heterogeneity of the complexing sites in the HA macromolecule, the increase in the life-time value above  $L/M = 8$  indicates the binding of Eu to higher affinity sites when Eu concentration is small as compared to HA concentration.



**Figure 3.18** (a) Lifetime vs  $[\text{HA}]/[\text{Eu}]$ , (b) Number of water molecules vs  $[\text{HA}]/[\text{Eu}]$

The CE diagram for Eu(III)-HA system (figure 3.19) shows that all the points pertaining to different  $[\text{HA}]/[\text{Eu}]$  lie in the zone A (figure 3.8) which correspond to outer sphere complexation. Thus, CE diagram validate the outer sphere complex formation for Eu(III)-HA system predicted from lifetime data.

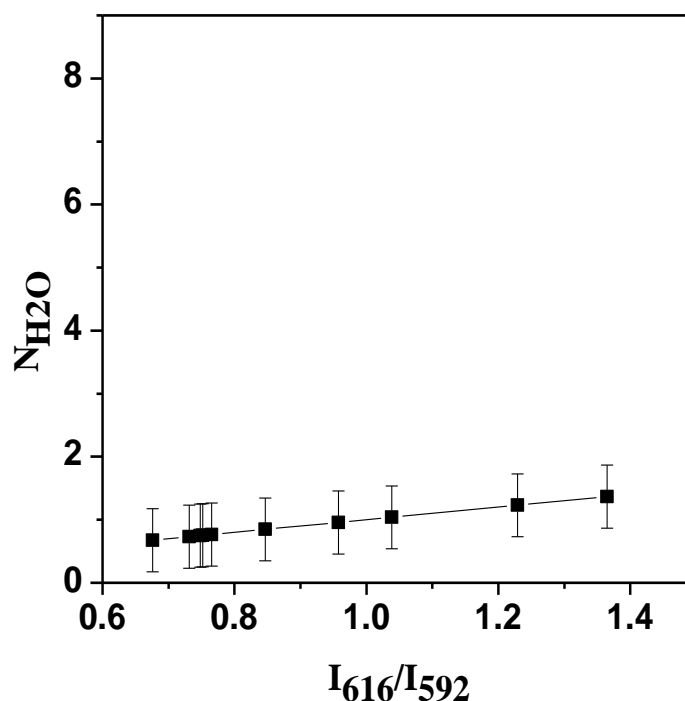


**Figure 3.19** CE diagram for Eu(III)-HA system

The carboxylic and hydroxyl groups are major functional groups in HA which are responsible for its complexing and adsorptive properties. Since HA is a macromolecule of undefined structure with large heterogeneity, initially it was thought that LMCA having carboxyl and hydroxyl moiety can be used as model compounds of HA to understand the binding characteristics of HA. In present work complexation of both LMCA and HA with Eu(III) has been investigated and the formation of outer sphere complex in case of HA, in contrast to LMCA, suggests that the behaviour of LMCA cannot be taken analogues to HA. The drastically different behaviour is the outcome of polyfunctionality and site heterogeneity of HA. On the other hand, even though LMCA have similar functional groups as those found in HA, their well-defined structure and sites as compared to HA preclude their use as model compounds of HA. Although as large variety of LMCA exist in nature, their complexation studies with lanthanides/actinides are important but LMCA should not

be treated as model compounds of HA. Similar observations have been made in the literature (*Kar et al., (communicated)*)

### **3.5. Conclusions:**

In the present work TRFS was used to deduce the stability constant of Eu – LMCA complexes. The  $I_{616}/I_{592}$  and life time increases with increasing ratio of ligand to metal ion concentration. The stability constants of Eu-LMCA complexes were obtained from the ratios of intensity of 616 and 592 nm peaks. The number of water molecules coordinated to Eu(III), obtained from lifetime data, revealed the information about the stoichiometry of the complexes. Eu(III) forms 1:1, 1:2 and 1:3 type of complexes with HIBA but only 1:1 and 1:2 complexes with phthalic, mandelic and SA as the ligand to metal concentration ratio is increased. The stability constants for all the systems are in agreement with the literature data obtained by other methods. The life-time data of Eu-HA solutions are invariant with L/M ratio up to 5 indicating outer sphere complexation. The deviation from the life-time data at the highest values of L/M indicates the binding of Eu(III) to high affinity sites. It was found that binding characteristics of HA are entirely different from LMCA. This suggests that utmost care need to be taken while studying metal ion binding to HA using model systems.

**Chapter IV**

**Sorption of**

**Trivalent Actinides/Lanthanides:**

**Effect of Complexing Anions**

#### 4.1. Introduction:

In the present chapter the effect of HA and HIBA on sorption of Cm(III) by silica colloids was studied by employing batch sorption, LAM (in case of HA) and SCM (in case of HIBA). Moreover, the effect of changing the order of addition of the metal ion and HA/ HIBA on sorption was also investigated. Further, similar sorption studies, using HIBA, were carried out with Eu(III) at higher concentration ( $5 \times 10^{-5}$  M) so as to characterize the surface complexes by TRFS and information obtained from TRFS was used in the SCM. The results obtained for Eu(III) and Cm(III) systems have been compared. Also, the use of small organic molecules as model compounds of HA has been evaluated by comparing the influence of HA and HIBA on sorption of Cm(III) by silica.

Trivalent actinides such as, americium ( $^{241}\text{Am}$ ,  $^{243}\text{Am}$ ) and curium ( $^{245}\text{Cm}$ ,  $^{246}\text{Cm}$ ) constitute a major fraction of the minor actinides present in the high level liquid waste generated during the reprocessing of spent nuclear fuel. Though partitioning and transmutation is being considered as one of the options to incinerate these minor actinides in accelerator driven sub-critical reactor system (ADS), presently the HLW is being managed by immobilizing it in solid form (glass, synroc), which may be buried in deep geological repositories in near future. Thus, these long-lived isotopes, such as,  $^{241}\text{Am}$ ,  $^{243}\text{Am}$ ,  $^{245}\text{Cm}$  and  $^{246}\text{Cm}$  will be present in the earth (deep geological repositories) for thousands of years and over this time period, it is possible that these minor actinides might enter the geosphere, through earthquakes, volcanic eruptions, leaching and corrosion of waste form and underground water movement. The major concern during the release of the minor actinides and long lived fission products from the vitrified waste buried in a deep geological repository is the migration of long lived radionuclides in aquatic environment which is known to be

influenced by the presence of colloids and complexing anions (*Kepak, 1971; Penrose et al., 1990; Kersting et al., 1999*). Moreover, organic complexing anions affect the dissolution of glass containing vitrified waste (*Gin et al., 1994*). Hence it is imperative to know the mechanism of interaction of the radioactive elements with colloids and complexing anions. The complexing anions include simple organic molecules, viz., carboxylic acids, amino polycarboxylic acids as well as complex molecules, such as, FA and HA.

The common colloids present in natural waters are based on oxides of Si, Al and Fe. Extensive studies have been carried out on the sorption of trivalent actinides/lanthanides on different colloids (*Piasecki and Sverjensky, 2008; Rabung et al. 1998, 2000, 2004, 2006; Kumar et al., 2013; Fairhurst et al., 1995a; Takahashi et al., 2006; Pathak et al., 2006, 2007a*). Silica is one of the most common constituents of the mineral oxides, viz., feldspar, quartz, etc. as well as clays, viz., bentonite, which are being proposed as backfill material in the deep geological repositories. The granitic rocks which contain silica rich minerals are preferred host rocks for depositing the immobilized HLW. Various literature reports exist in which sorption of Eu(III) on silica follows typical S shaped sorption profile and role of various parameters such as pH, ionic strength and silica dissolution has been evaluated (*Fairhurst et al., 1995a; Takahashi et al., 2006; Pathak and Choppin, 2006, 2007a*).

The concentration of HA in natural waters is observed to be in the range of few parts per million which is sufficient to affect the sorption behaviour of multivalent cations such as Am(III) and Cm(III). Several studies exist in literature in which the effect of HA on the sorption of Eu(III) and Am(III) on colloids are reported (*Macasek et al., 1999; Ledin et al., 1994; Fairhurst et al. 1995b; Sakuragi et al., 2004; Samadfam et al. 2000*). Presence of HA enhances the sorption of

Eu(III)/Am(III) on colloids at low pH and decrease the same at high pH, compared to the binary metal ion-colloid system.

Although attempts are being made to understand the sorption behaviour of radionuclides in presence of HS (*Macasek et al., 1999; Ledin et al., 1994; Fairhurst et al., 1995b; Sakuragi et al., 2004; Samadfam et al., 2000; Tan et al., 2008, 2009; Wang et al., 2004; Chen et al., 2013*), the complex structure and poly functionality of HS make it extremely difficult to understand the sorption phenomena from fundamental point of view. However, the sorption phenomena in systems containing simple molecules are easier to explain, as complexation of metal ions with such molecules is well understood (*Jain et al., 2008*). Further, the small molecules have well defined structure and thus are helpful in understanding the sorption phenomena from mechanistic point of view. Various literature reports exist in which effect of LMCA on sorption of trivalent lanthanides and actinides have been studied (*Alliot et al., 2005a, 2005b, 2006; Pathak and Choppin, 2007a; Tits et al., 2005*).

The sorption profile is dependent upon the interaction of the complexing anions with the metal ion as well as the surface sites in the case of ternary metal ion-ligand-mineral oxide systems. The formation of synergic surface complexes has also been proposed to explain the sorption profile of Eu(III)/Am(III) sorption on alumina in presence of complexing anions (acetic, oxalic and carbonic acids) (*Alliot et al., 2005a; Alliot et al., 2005b; Alliot et al., 2006*). A synergistic enhancement in the sorption of Eu(III) on suspended silica was observed for oxalate and phosphate ligands and formation of ternary Eu/silica/ligand complexes were confirmed by TRLFS (*Pathak and Choppin, 2007a*). On the other hand the retention of Eu(III), Am(III) and Th(IV) on calcite was not affected by gluconic acid and isosaccharinic acid (*Tits et al., 2005*).

Spectroscopic techniques such as TRLFS and EXAFS have been employed to characterize the sorbed species in both binary and ternary systems containing complexing anions (*Tan et al., 2008, 2009; Wang et al., 2004; Chen et al. 2013, Rabung et al., 2000, 2005; Fouchard et al., 2004a; Hartmann et al., 2008; Ishida et al., 2009; Schlegel et al., 2004; Stumpf et al., 2007*). Though TRLFS and EXAFS are the most widely used spectroscopic techniques for characterization of the sorbed metal ions, other techniques, such as, XPS and SEM-EDS has also been used in a few cases (*Fouchard et al., 2004a; Mercier et al., 2006*). These studies provide valuable information about the structure of the surface complexes and thereby help in validation of SCM hypothesis.

SCMs provide molecular description using equilibrium approach and are designed to calculate the interaction constants mathematically by taking into account the aqueous distribution of species, the reactivity and the electrostatic properties of the surface. SCM has been widely used to model sorption data of actinides and fission products on various mineral oxides and clays (*Kar et al., 2012; Bradbury and Baeyens 2006; Grambow et al., 2006; Bradbury et al., 2005; Gaskova and Bukaty, 2008*). In addition to the modeling of binary systems, the modeling of the sorption data for the ternary, actinide-complexing anions- mineral oxides, systems has also been attempted (*Guo et al., 2009a; Stamberg et al., 2006; Singh et al., 2010*). Recently the sorption of Eu(III) on rectorite in the presence of HA has been successfully modeled by SCM (*Chen et al., 2013*).

The aim of the present work was to study the effect of HA on the sorption of Cm(III) by silica. LAM was used to qualitatively explain the sorption profile. To the best of our knowledge, there are no studies in the literature on the effect of HA on sorption of Cm(III) by silica colloids. The effect of ionic strength and HA

concentration on Cm(III) sorption was also investigated. Further, the studies were also carried out on the effect of addition order of Cm(III) and HA to the silica suspensions.

In addition, the effect of varying concentration of HIBA and addition order of the Cm(III) and HIBA on the sorption of Cm(III) by silica was also studied using batch sorption experiments and SCM. HIBA has been used as a simple organic complexant. SCM for both binary and ternary system was done using the DLM. Though there exist large number of studies in literature in which SCM of effect of complexing anions have been dealt (*Guo et al., 2009a; Stamberg et al., 2006; Singh et al., 2010*), SCM of Cm(III) in presence of small organic molecules has been attempted for the first time. Moreover, the comparison of the effect of HIBA and HA on Cm(III) sorption on to silica has been made so as to ascertain whether simple molecules can be used as analogue of HS when it comes to study the influence of organics on the sorption of metals.

Furthermore, the spectroscopic characterization of the sorbed species was also carried out using TRFS with Eu(III) as a probe. The effect of HIBA on the sorption of Eu(III) by silica was investigated using batch sorption experiments, TRFS and SCM. Both, batch sorption experiments as well as TRFS measurements, were carried out in the case of binary (Eu(III)-Silica) and ternary (Eu(III)-silica-HIBA) systems. The complexation of Eu(III) by HIBA has been studied in our laboratory using TRFS, wherein the fluorescence emission spectra were found to be sensitive to the complexation of Eu(III) by HIBA as described in chapter 3 (*Jain et al., 2008*). The TRFS of sorbed Eu(III) have been used to infer about the surface complexes during the modeling for both binary and ternary system using the DLM.

## 4.2. Experimental:

### 4.2.1 Materials and characterization:

Silica powder (Aerosil Belgium) was used as received. Its surface area and point of zero charge was determined by methods described in Chapter 2. The number of surface sites on the silica powder was determined by titrating the 300 mg of silica in 50 ml 0.1 M NaClO<sub>4</sub> with standard 0.01 M HClO<sub>4</sub> / 0.1 M NaOH.

<sup>244</sup>Cm (T<sub>1/2</sub> = 18.1 years) was used as a tracer for curium so as to attain low concentration (2.2 X 10<sup>-10</sup> M) encountered in natural water conditions. For sorption studies of Eu(III), <sup>152</sup>Eu was used as a radiotracer.

HA (Aldrich) having proton exchange capacity of 7.1 meq/g was used (*Boily and Fein, 2000*). AR grade HIBA (Alfa Aesar) was used as received. All solutions were prepared in low conductivity Millipore water having resistivity of 18 MΩ.cm and HA solutions were stored in dark.

### 4.2.2. Batch Sorption Experiments:

Sorption studies were carried out by using batch sorption method to investigate the sorption of <sup>244</sup>Cm (III) on silica. The sorption of Cm(III) is influenced by several factors such as contact time, pH, ionic strength, HA concentration and order of addition of HA/HIBA and Cm(III). The effect of these different experimental parameters on Cm(III) sorption by silica has been studied. Furthermore, batch sorption studies were also carried out with Eu(III) in presence and absence of HIBA.

The details of the batch sorption experiments have been discussed in Chapter 2. The concentration of silica suspensions was 5 g/L in case of Cm(III) and 10 g/L for experiments with Eu(III). Ionic strength was maintained at 0.1 M using NaClO<sub>4</sub>.

In order to determine the time required to achieve equilibrium in the sorption, kinetic sorption study at pH 6.5 was carried out which showed that the equilibrium in the percentage sorption was achieved in 24 hours. Hence the equilibration time for sorption of  $^{244}\text{Cm}$  by silica was fixed as 24 hours.

In the case of experiments in presence of HA, the suspensions were first equilibrated with 2 mg/L HA for 48 hours and subsequently  $^{244}\text{Cm}$  activity was added for further equilibration for another 24 hours. This order is hereafter referred to as Silica-HA-Cm. The 48 hours of contact time for silica and HA was based on the literature reports for the Eu(III)-silica system (*Fairhurst et al., 1995 b*).

The experiments with the reverse order of addition of  $^{244}\text{Cm}$  and HA (referred to as Silica-Cm-HA) were carried out by first equilibrating the silica suspensions ( 20 mL containing 5 g/L silica) at varying pH with the  $^{244}\text{Cm}$  activity for 24 hours and later adding the HA solution (2 mg/L), which was then equilibrated for another 48 hours. 1 mL aliquots were drawn from the supernatant (after centrifugation) after equilibration with HA to obtain the sorption data for ternary (silica-Cm-HA) system.

The effect of ionic strength was studied by measuring sorption at different ionic strengths, 0.005-0.2 M  $\text{NaClO}_4$  and at a fixed pH of 6.5. This pH value was chosen as the percentage sorption was found to be close to 100% at this pH. Effect of HA concentration (2-20 mg/L) on sorption of Cm by silica was also studied

In the case of experiments in presence of HIBA, the experiments were carried out in similar manner as for HA. Concentration of HIBA was  $1.0 \times 10^{-3}$  M and  $1.0 \times 10^{-5}$  M. The HIBA concentrations  $1.0 \times 10^{-5}$  M and  $1.0 \times 10^{-3}$  M will be hitherto represented as HIBA(I) and HIBA(II) respectively. Ternary system where HIBA was added before Cm are termed as Silica-HIBA-Cm and those with the reverse order of addition of Cm(III) and HIBA are referred to as Silica-Cm-HIBA. For binary silica-

Eu(III) and ternary silica-HIBA-Eu(III) systems, same methodology was followed and HIBA concentration was kept  $2.5 \times 10^{-3}$  M.

#### **4.2.3. Silica dissolution studies:**

For the determination of dissolved silica, silica suspensions (10 g/L) of varying pH were equilibrated with Eu(III) ( $5 \times 10^{-5}$  M) for 4 and 24 hours, respectively, on a mechanical shaker. The suspensions were centrifuged and the supernatant solutions were assayed for dissolved Si content by ICP-AES. The calibration of the instrument was carried out using 1000 mg/L standard Si solution (Merck) after suitable dilution.

#### **4.2.4. Sorption of HIBA by silica:**

In order to determine the sorption of HIBA by silica, the silica suspensions (10 g/L) of varying pH were contacted with HIBA ( $2.5 \times 10^{-3}$  M) for 48 hours in a mechanical shaker. The suspensions were later centrifuged and the supernatant solutions were assayed for TOC.

#### **4.2.5. TRFS measurements:**

For the TRFS measurements 10 ml of silica suspensions (10 g/L) of varying pH (4.0-8.0) were contacted with Eu(III) solutions ( $5.0 \times 10^{-5}$  M) for 24 hours. The suspensions were filtered using 0.1 micron membrane filter to remove any unadsorbed Eu(III). Subsequently the solid samples were vacuum dried and mounted on glass plate for TRFS measurements. Similar exercise was carried out for preparation of sample in the case of ternary Eu(III)-silica-HIBA system.

### 4.3 Results and Discussion:

#### 4.3.1 Characterization of Silica:

The surface area of silica was found to be  $180 \pm 5 \text{ m}^2/\text{g}$ , which corresponds to particle size of  $6.2 \pm 0.2 \text{ nm}$ . The point of zero charge ( $\text{pH}_{\text{PZC}}$ ) of silica was obtained from zeta potential measurements and the value was found to be 2.4 (*Kumar et al., 2006*). The data of acid base titration of silica are shown in figure 4.1. These were analysed by FITEQL 4.0 to obtain the concentration of surface sites and log K for protonation ( $\log K_1$ ) and deprotonation ( $\log K_2$ ) of  $\equiv \text{SiOH}$  groups, which are given in Table 4.4. The  $\log K_2$  obtained in the present work is close to that reported by E.Osthols (*1995*) ( $\log K_2 = -6.9$ ) for Aerosil OX 200 silica.

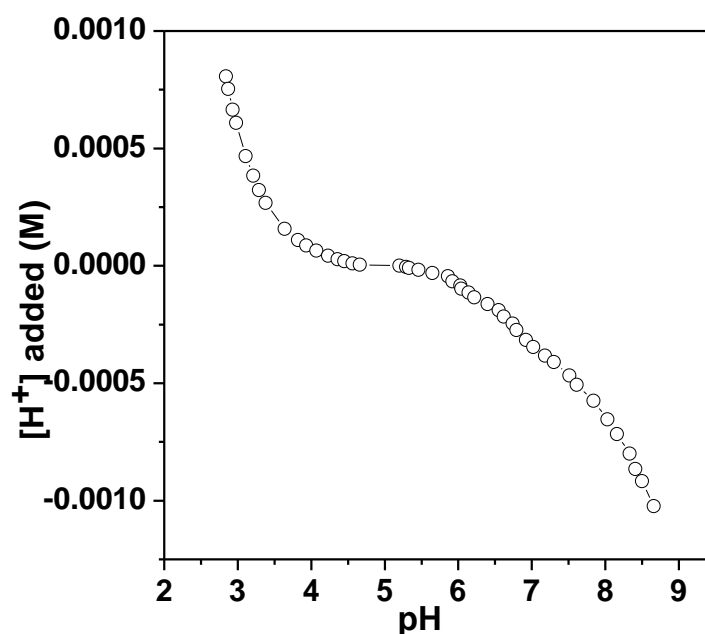


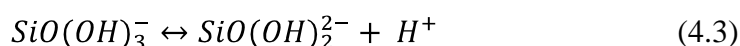
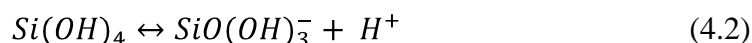
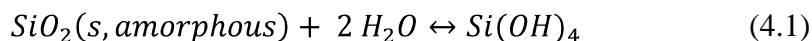
**Figure 4.1** Potentiometric titration of silica suspension (6 g/L) in 0.1 M  $\text{NaClO}_4$ .

#### 4.3.2. Silica Dissolution Studies:

The results of the ICP-AES measurements of Si concentration in the supernatant solutions of Eu(III)-silica systems are given in Table 4.1. The amount of

dissolved Si is more for equilibration time of 4 hours than that of 24 hours, indicating the interaction of the dissolved silica with the solid surface.

Dissolution of silica can be characterized by the following equilibria (*Stumm and Morgan, 1996*):



The dissolution of silica increases with pH. Furthermore, Eu(III) is known to promote the dissolution of silica by facilitating hydrolysis of Si-O-Si bonds (*Takahashi et al., 2006*). The concentration of silicic acid formed owing to the dissolution of silica in presence of Eu(III) is of the order of 10 mM, at which polysilicic acid is dominant (*Panak et al., 2005*). In absence of Eu(III), the concentration of silicic acid formed owing to the dissolution of silica is of the order of 2 mM (*Kar et al., 2012*). It is to be noted that in presence of Cm(III), the concentration of silicic acid has been assumed to be same as in case of bare silica owing to very low concentration of Cm(III) employed in the present work.

**Table 4.1** Dissolved Si (ppm) in silica suspensions (10 g/L) in presence of Eu(III) ( $5.0 \times 10^{-5}$  M) measured after different time of equilibration.

pH	(4 hours)	(24 hours)
4.56	240	200
6	310	240
7.86	510	260

#### 4.3.3. Speciation Calculations:

Speciation of Cm(III) in aqueous solution was calculated using the geochemical equilibrium speciation code MINTQA2 (*Allison et al., 1991*) after

incorporating the stability constants of  $\text{Cm}^{3+}$  complexes with  $\text{OH}^-$  (Wimmer *et al.*, 1992), HIBA (Shalinets, 1971) and silicic acid (Panak *et al.*, 2005; Jensen and Choppin, 1996). The speciation of Cm(III) in presence of silicic acid was generated by considering the formation of  $\text{CmOSi(OH)}_3^{2+}$  and  $\text{Cm(OSi(OH)}_3)_2^+$ . The stability constant for Cm(III) disilicate was not available in literature, thereby necessitating the use of stability constant value of Eu(III) disilicate (Jensen and Choppin, 1996). Deprotonation constant of HIBA (Portanova *et al.*, 2003) was also incorporated in MINTEQA2. Formation of  $\text{Cm}^{3+}$  humate complexes was also considered by making use of the formation constant and site capacities as defined within MINTEQA2. The values of  $\log \beta$  for Cm-HA and site density of HA are  $6.4$  and  $7.6 \times 10^{-3} \text{ eq.g}^{-1}$  respectively (Boily and Fein, 2000; Cornelis, 2005).

Speciation of Eu(III) was calculated after incorporating the  $\log K$  for Eu(III)-HIBA (Jain *et al.*, 2008), Eu(III) silicate complexes (Jensen and Choppin, 1996) and Eu(III) hydroxo complexes (Tetre *et al.*, 2006). In view of the non-availability of the  $\log K$  for interaction of europium and polysilicic acid, we studied the speciation of Eu(III) in presence of silicic acid considering the formation of  $\text{EuOSi(OH)}_3^{2+}$  and  $\text{Eu(OSi(OH)}_3)_2^+$ . The  $\log K$  for the Eu(III)-silicates were taken from Jensen and Choppin (1996). The  $\log K$  of different complexes considered in the calculations are given in Table 4.2. The data was transformed to zero ionic strength before inserting as input in the code.

The carbonate concentration in the suspensions was assumed to be negligible as (i) millipore water was boiled before use, (ii) the sorption was carried out in air tight polypropylene tubes and (iii) the time period for closing the tubes after adjustment of pH was kept as short as possible.

**Table 4.2** Log  $\beta$  used for calculating the aqueous speciation

Reaction	log $\beta$
$\text{Cm}^{3+} + \text{H}_2\text{O} \longrightarrow \text{Cm}(\text{OH})^{2+} + \text{H}^+$	-7.2 <sup>a</sup>
$\text{Cm}^{3+} + 2\text{H}_2\text{O} \longrightarrow \text{Cm}(\text{OH})_2^+ + 2 \text{H}^+$	-15.1 <sup>a</sup>
$\text{Cm}^{3+} + 3\text{H}_2\text{O} \longrightarrow \text{Cm}(\text{OH})_3 + 3 \text{H}^+$	-26.2 <sup>a</sup>
$(\text{CH}_3)_2\text{COHCOO}^- + \text{H}^+ \longrightarrow (\text{CH}_3)_2\text{COHCOOH}$	3.75 <sup>b</sup>
$\text{Cm}^{3+} + (\text{CH}_3)_2\text{COHCOO}^- \longrightarrow (\text{CH}_3)_2\text{COHCOOCm}^{2+}$	2.96 <sup>c</sup>
$\text{Cm}^{3+} + 2(\text{CH}_3)_2\text{COHCOO}^- \longrightarrow ((\text{CH}_3)_2\text{COHCOO})_2\text{Cm}^+$	5.15 <sup>c</sup>
$\text{Cm}^{3+} + 3(\text{CH}_3)_2\text{COHCOO}^- \longrightarrow ((\text{CH}_3)_2\text{COHCOO})_3\text{Cm}$	6.36 <sup>c</sup>
$\text{Cm}^{3+} + \text{H}_4\text{SiO}_4 \longrightarrow \text{Cm}(\text{OSi}(\text{OH})_3)^{2+} + \text{H}^+$	-2.07 <sup>d</sup>
$\text{Cm}^{3+} + 2 \text{H}_4\text{SiO}_4 \longrightarrow \text{Cm}(\text{OSi}(\text{OH})_3)_2^+ + 2 \text{H}^+$	-6.87 <sup>e</sup>
$\text{Eu}^{3+} + \text{H}_2\text{O} \longrightarrow \text{Eu}(\text{OH})^{2+} + \text{H}^+$	-7.8 <sup>f</sup>
$\text{Eu}^{3+} + 2\text{H}_2\text{O} \longrightarrow \text{Eu}(\text{OH})_2^+ + 2 \text{H}^+$	-16.4 <sup>f</sup>
$\text{Eu}^{3+} + 3\text{H}_2\text{O} \longrightarrow \text{Eu}(\text{OH})_3 + 3 \text{H}^+$	-25.2 <sup>f</sup>
$\text{Eu}^{3+} + 4\text{H}_2\text{O} \longrightarrow \text{Eu}(\text{OH})_4^- + 4 \text{H}^+$	-35.3 <sup>f</sup>
$\text{Eu}^{3+} + (\text{CH}_3)_2\text{COHCOO}^- \longrightarrow (\text{CH}_3)_2\text{COHCOOEu}^{2+}$	3.32 <sup>g</sup>
$\text{Eu}^{3+} + 2(\text{CH}_3)_2\text{COHCOO}^- \longrightarrow ((\text{CH}_3)_2\text{COHCOO})_2\text{Eu}^+$	5.50 <sup>g</sup>
$\text{Eu}^{3+} + 3(\text{CH}_3)_2\text{COHCOO}^- \longrightarrow ((\text{CH}_3)_2\text{COHCOO})_3\text{Eu}$	6.62 <sup>g</sup>
$\text{Eu}^{3+} + \text{OSi}(\text{OH})_3^- \longrightarrow \text{Eu}(\text{OSi}(\text{OH})_3)^{2+}$	7.26 <sup>e</sup>
$\text{Eu}^{3+} + 2\text{OSi}(\text{OH})_3^- \longrightarrow \text{Eu}(\text{OSi}(\text{OH})_3)_2^+$	11.7 <sup>e</sup>

(a: Wimmer et al., 1992; b: Portanova et al., 2003; c: Shalinets, 1971; d: Panak et al., 2005; e: Jenson and Choppin, 1996; f: Tetre et al., 2006; g: Kar et al., 2008)

The speciation diagrams in absence and presence of HA are shown in figures 4.2 (a) and 4.2 (b). It is worth mentioning that here the contribution of dissolved silicates is not included. During the interpretation of sorption data of addition order of Cm(III) and HA, it was realized that silica dissolution plays important role in deciding Cm(III) speciation. In absence of HA, hydrolyzed Cm(III) species dominate the

speciation above pH 6, while in presence of HA, the humate complex dominates the speciation in the pH range of 5-8, with the hydrolyzed species concentration increasing above pH 8. However, at higher pH (> 8) values carbonate complexation of Cm(III) cannot be ruled out.

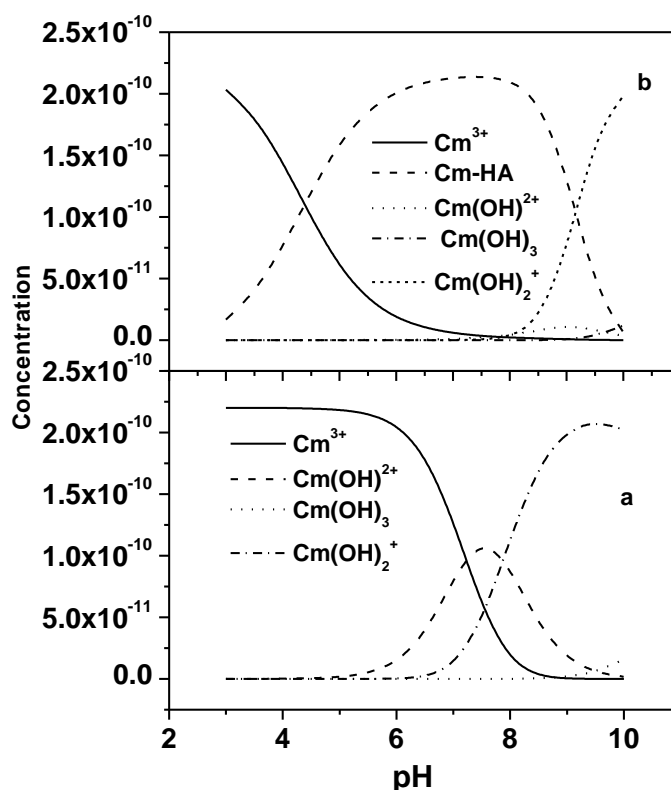


**Figure 4.2** Speciation of Cm(III) in (a) absence and (b) presence of (2 mg/L) HA.

$$[\text{Cm(III)}] = 2.2 \times 10^{-10} \text{ M}, I = 0.1 \text{ M}$$

The speciation diagrams in absence and presence of HIBA are shown in figures 4.3 (a) and 4.3 (b and c) respectively. It can be seen that up to pH 7.0,  $\text{Cm(OSi(OH)}_3)_2^{2+}$  is the dominant species above which  $\text{Cm(OSi(OH)}_3)_3^{2+}$  dominates. In the presence of  $10^{-5}$  M HIBA (figure 4.3 (b)), curium silicate continues to dominate the speciation while in case of  $10^{-3}$  M HIBA (figure 4.3 (c)),  $\text{Cm(HIBA)}_2^{2+}$  and  $\text{Cm(HIBA)}_3^{2+}$  are also present up to pH 4.5 though the speciation is still dominated by silicate complexes.

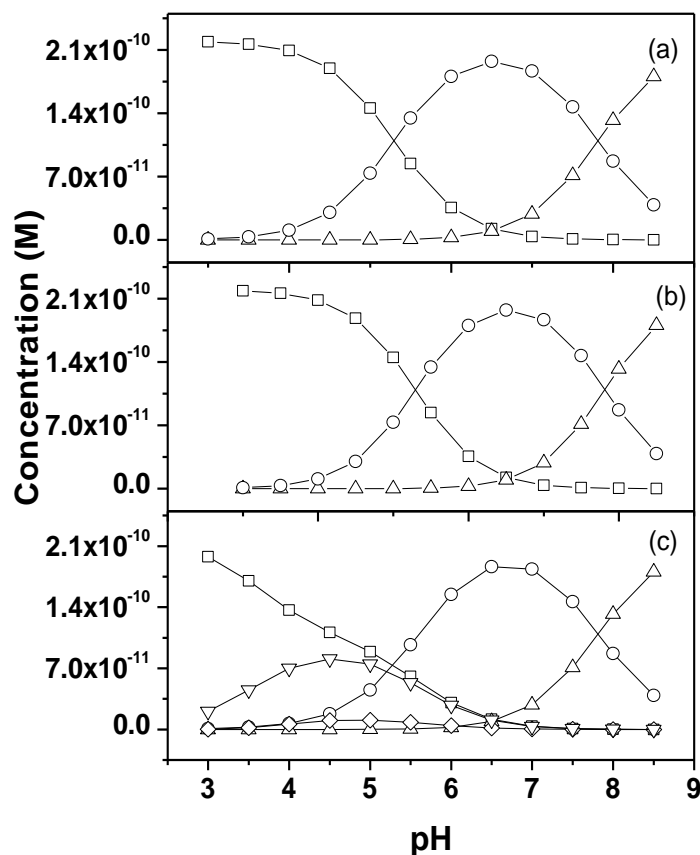


**Figure 4.3** Curium speciation in absence (a) and presence (b and c) of HIBA.

$[Cm(III)] = 2.2 \times 10^{-10}$ ;  $[HIBA] = 1 \times 10^{-5}$  M in (b) and  $1 \times 10^{-3}$  M (c). Ionic strength = 0.1 M  $NaClO_4$ .  $Cm^{3+}$  ( $\square$ ),  $Cm(IBA)^{2+}$  ( $\nabla$ ),  $Cm(IBA)_2^+$  ( $\diamond$ ),  $[Cm(OSi(OH)_3)_2]^+$  ( $\circ$ ) and  $[Cm(OSi(OH)_3)_2]^+$  ( $\Delta$ ).

Figures 4.4 (a) and 4.4 (b) show the speciation of Eu(III) in absence and presence of HIBA respectively. It can be seen that up to pH 7.0,  $Eu(OSi(OH)_3)_2^+$  is the dominant species above which  $Eu(OSi(OH)_3)_2^+$  dominates. In the presence of HIBA,  $Eu^{3+}$ ,  $Eu(HIBA)^{2+}$  and  $Eu(HIBA)_2^+$  are also present up to pH 4.5 but the speciation continues to be dominated by silicate complexes.

Thus, silicates are major species in pH range of study for Cm(III) and Eu(III) irrespective of their concentration.

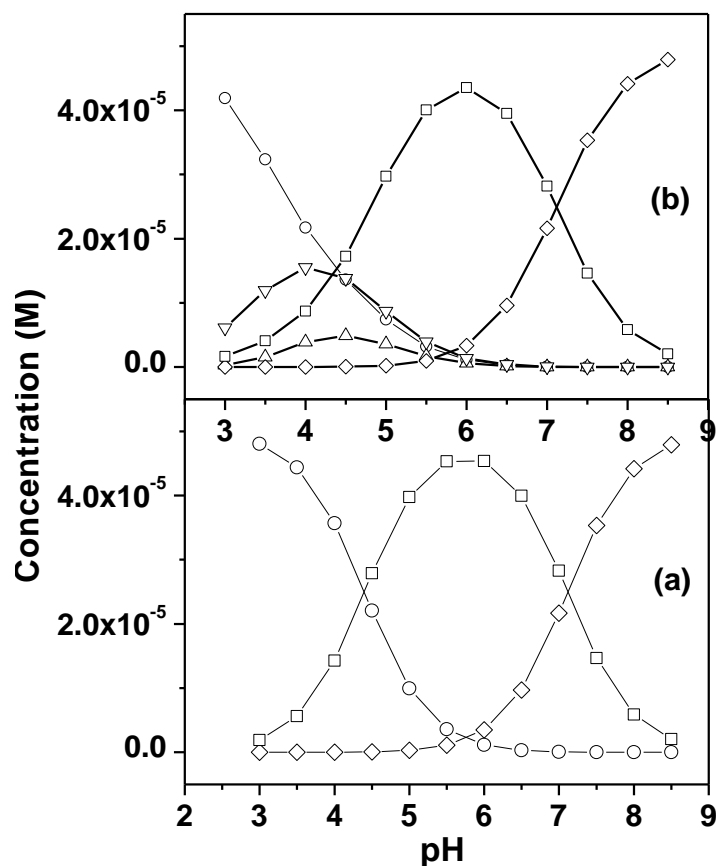


**Figure 4.4** Europium speciation in absence (a) and presence (b) of HIBA.  $[\text{Eu(III)}] = 5.0 \times 10^{-5} \text{ M}$ ;  $[\text{HIBA}] = 2.5 \times 10^{-3} \text{ M}$ . Ionic strength = 0.1 M  $\text{NaClO}_4$ .  $\text{Eu}^{3+}$  (o),  $\text{Eu(IBA)}^{2+}$  ( $\Delta$ ),  $\text{Eu(IBA)}_2^+$  ( $\nabla$ ),  $[\text{Eu(OSi(OH)}_3)_2]^{2+}$  ( $\diamond$ ) and  $[\text{Eu(OSi(OH)}_3)_2]^+$  ( $\square$ ).

#### 4.3.4. Kinetics study of sorption of Cm (III) by silica colloids:

Figure 4.5 shows the temporal profile of the sorption of Cm (III) by silica colloids at pH 6.5. The sorption reaches a equilibrium value in less than 24 hours. Ho. et. al. (1998) did the comparison of various kinetic models and found that pseudo second order equation describes the sorption kinetics better than other models. The sorption kinetics in literature has been modeled by the pseudo second-order rate equation (Fan et al., 2008; Chen et al., 2007)

$$\frac{t}{q_t} = \frac{1}{kq_e^2} + \frac{t}{q_e} \quad (4.4)$$

$k$  ( $\text{g mg}^{-1}\text{h}^{-1}$ ) is the pseudo second-order rate constant of adsorption,  $q_e$  and  $q_t$  are the amounts of metal ion sorbed ( $\text{mg/g}$ ) at equilibrium and at time  $t$  respectively.

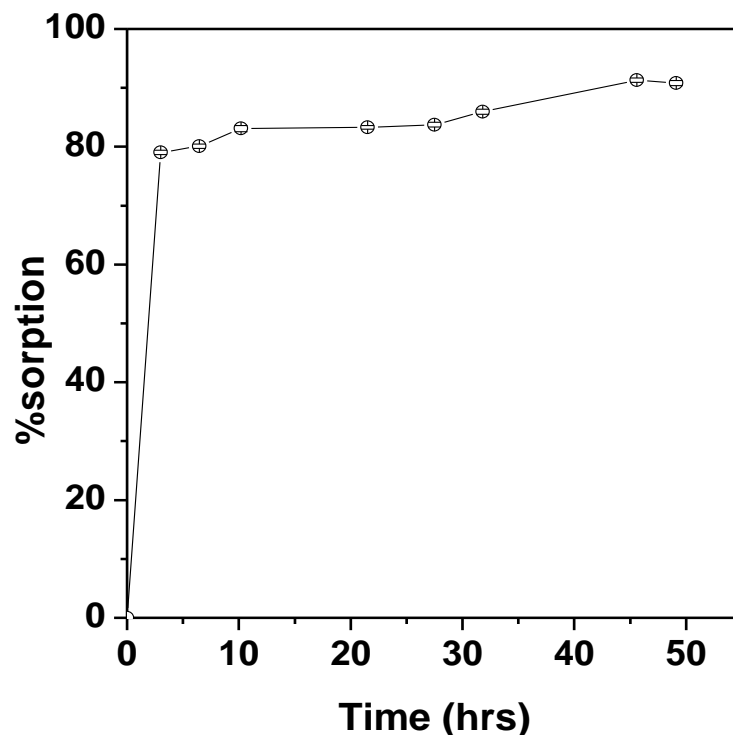


**Figure 4.5** Kinetics of sorption of Cm by silica. pH = 6.5,  $[\text{Cm(III)}] = 2.2 \times 10^{-10}$  M,  $I = 0.1$  M ( $\text{NaClO}_4$ ),  $[\text{Silica}] = 5$  g/l

Figure 4.6 shows the plot of  $t/q_t$  vs  $t$ . The values of  $q_e$  and  $k$  calculated from slope and intercept are  $9.88 \times 10^{-6}$   $\text{mg g}^{-1}$  and  $1.35 \times 10^{-5}$   $\text{g mg}^{-1}\text{h}^{-1}$  respectively. The value of  $q_e$  obtained from slope analysis was found close to  $q_t$  at maximum contact time between curium and silica and low value of  $k$  suggests that sorption equilibrium is attained slowly. The coefficient of regression for linear fitting is close to 1 which signifies that sorption kinetics can be described by pseudo second order rate equation. Similar trends have been observed in case of Th(IV) sorption on attapulgite (*Fan et al., 2008*).

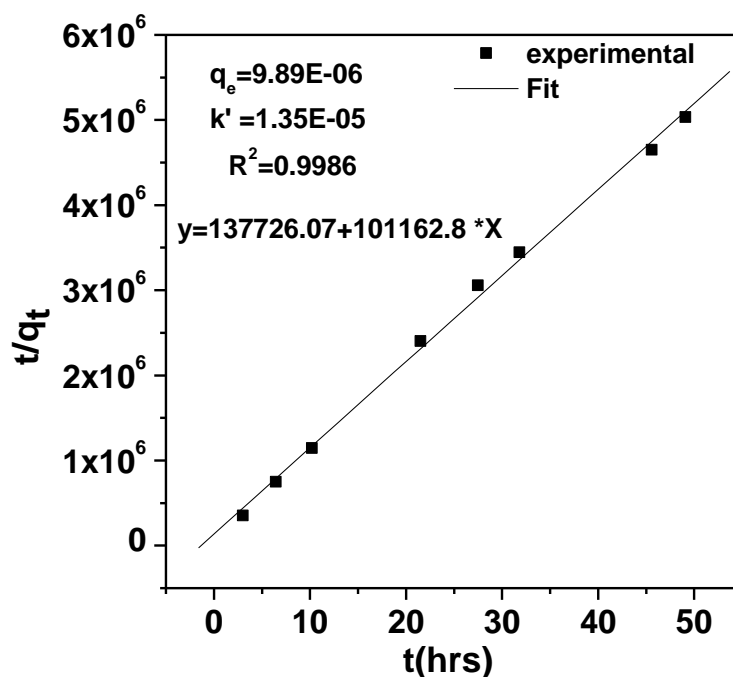


**Figure 4.6** Plot of kinetic data showing pseudo second order kinetics

#### 4.3.5. Sorption of Cm (III) by silica: Effect of HA:

The percentage sorption of curium by silica colloids increases with increasing pH and reaches a saturation value > 95 % at pH 6.5 above which it remains constant as shown in figure 4.7. This is understood in terms of positive charge on silica colloids at low pH (< 2.4) and increasingly negative charge above it. As the pH of the aqueous suspension increases above 2.4, the silica surface becomes more and more negatively charged thus resulting in the sorption of the positively charged Cm<sup>3+</sup> ions. The high percentage sorption at higher pH can be explained in terms of the surface complexation between Cm<sup>3+</sup> and ≡SiO<sup>-</sup> surface sites of silica. The results are in agreement with the literature data for sorption of Am(III) by kaolinite (*Samadfam et al., 2000*) and that of Eu(III) by silica (*Fairhurst et al., 1995 a*).

In the presence of HA, the sorption of Cm(III) on silica is enhanced compared to the binary system of Cm(III)-silica system at lower pH values. The percentage sorption reaches a maximum at pH 6 and then falls to lower value in the pH range 6.5-

8 above which it is found to increase again. The enhancement in the percentage sorption at low pH and reduction at high pH in presence of HA is also observed in the sorption studies with Eu (III) (Fairhurst *et al.*, 1995 a) and Am (III) (Sakuragi *et al.*, 2004) and can be explained in terms of the sorption profile of HA on silica (Kumar *et al.*, 2006). At low pH, the negatively charged HA molecules get sorbed on the positively charged silica surface ( $=\text{Si-OH}_2^+$ ) by electrostatic interaction. With increase in pH the silica particles acquire negative charge due to the deprotonation of the  $\equiv\text{Si-OH}$  surface sites, resulting in repulsion between the anionic HA molecules and the negatively charged silica particles and hence decrease in the sorption of HA by silica. The HA molecules present in the liquid phase, owing to their strong affinity for Cm(III) result in decreased sorption of Cm (III) onto the silica surface.

Figure 4.7 shows that in presence of HA, the decrease in the sorption at intermediate pH is much more in the case of silica-HA-Cm than that in case of silica-Cm-HA system. Further, the percentage sorption at varying length of time of equilibration 24-72 hours was found to be nearly same for the silica-Cm-HA system. The enhancement in the sorption of Cm(III) by silica at low pH is similar to that observed in the previous experiment Silica-HA-Cm. However, the decrease in the sorption of Cm(III) at intermediate pH values is not as high as was observed in the case of Silica-HA-Cm.

Various authors report the influence of addition sequence on metal ions distribution at solid liquid interface (Wang *et al.*, 2000; Xu *et al.*, 2006 a; Reiller *et al.*, 2005; Davis, 1984 ; Fan, 2009) while others rule out its effect on metal sorption (Xu *et al.*, 2006 b; Li *et al.*, 2009; Liu *et al.*, 2001; Wang *et al.*, 2004). Wang. *et al.* (2000) studied the effect of sequence of Yb(III) and FA addition to the alumina and found higher  $K_D$  values when FA addition preceded Yb(III) which was attributed to

different behavior of FA molecules sorbed on alumina and those in solution. Similar effect of addition order was observed in case of copper sorption on alumina (Davis, 1984). The EXAFS studies of Eu(III) sorbed by attapulgite, a hydrated Mg-Al-silicate, in presence of HA showed difference in the structure of the sorbed species when the order of addition of Eu(III) and HA was reversed (Fan, 2009). On the contrary, Wang. et al. (2004) did not observe any effect of addition sequence of alumina and HA in the fluorescence spectra of Cm(III)-alumina-HA system. Thus the effect of the sequence of metal ion and HA addition to the solid sorbent influences the metal ion sorption, has to be investigated in detail.

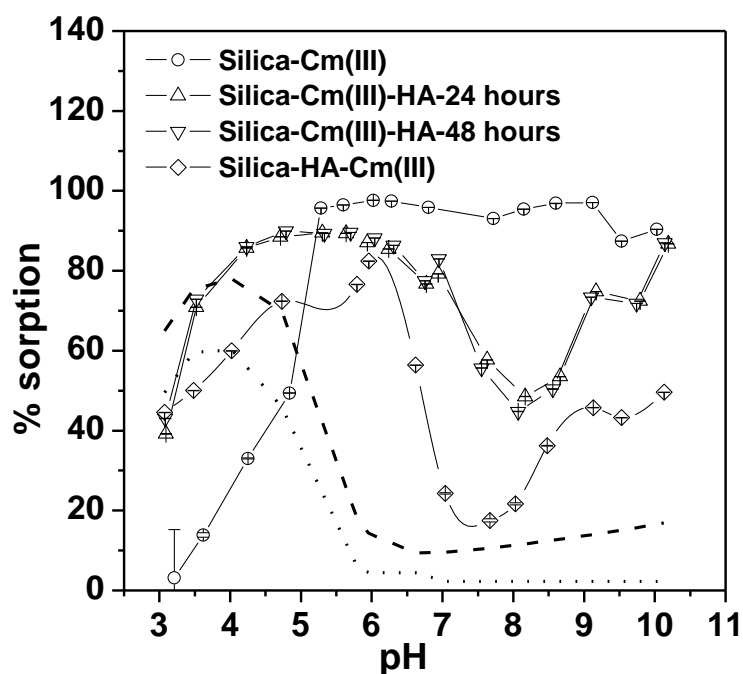


**Figure 4.7** Sorption of Cm by silica: Effect of addition order.  $[Cm(III)] = 2.2 \times 10^{-10}$  M,  $I = 0.1$  M ( $NaClO_4$ ),  $[Silica] = 5$  g/l,  $[HA] = 2$  mg/L. The dash and dotted lines are the LAM fits of silica-HA-Cm(III) systems

In the present study of silica-Cm-HA, initially Cm(III) is sorbed quantitatively onto the silica surface. Addition of HA to this suspension results in complexation of

sorbed Cm(III) by HA. One of the explanations for the decreased desorption of Cm(III) in the Silica-Cm-HA at intermediate pH values, could be the incorporation of Cm(III) in silica matrix following dissolution of silica. The dissolution of silica increases with pH. Furthermore, Takahashi et al. (2006) found that presence of Eu(III) promotes the dissolution of silica by facilitating hydrolysis of Si-O-Si bonds. Chung et al. (1998) studied Cm(III) sorption on silica using TRLFS and obtained two lifetimes 220 $\mu$ s and 740 $\mu$ s. They assigned shorter lifetime component to  $\equiv\text{SiOCm}^{2+}$  and larger lifetime component to co-precipitation of Cm and Si(OH)<sub>4</sub> formed as the result of silica dissolution

#### 4.3.5.1. LAM of ternary system:

With a view to understand the role of HA in influencing the sorption behaviour of Cm(III) by silica, LAM was carried out. This simple model, assumes that the sorption in the case of ternary Cm-silica-HA system can be explained in terms of the additive effect of the binary interactions between the individual components. According to this model, complexation of Cm(III) by mineral bound HA will enhance the sorption of Cm(III), while the HA present in solution will tend to decrease the sorption. The  $K_D$  at any pH in the ternary system is given by the equation 2.19.

The  $K_D^0$  for binary system as a function of pH was obtained from the measured sorption data. The fraction of HA bound to silica as a function of pH was obtained from the experimental data on sorption of Aldrich HA on silica measured by Fairhurst et al. (1995 a). For the stability constant of Cm(III)-HA, the data reported by Silva and Nitsche (1995), for Am(III)-HA as a function of pH was used. The percentage sorption of Cm(III) in the ternary system calculated from the  $K_D$  values are shown as dotted and dashed lines in figure 4.7 for two conditions of  $\beta_1$  and  $\beta_2$ , that is,

(i)  $\beta_2 = \beta_1$  and (ii)  $\beta_2 = 1.05 \beta_1$ . The results show that the linear additive model can explain the observed trend of sorption data, that is, enhancement at lower pH and decrease at intermediate pH values qualitatively. Increasing the stability constant of Cm(III) complex with mineral bound HA by 5%, with respect to that in solution gives the results which are closer to the experimental data. However, the calculated sorption curves are far from the experimental data, indicating that the assumptions in the linear additive model that the  $K_D$  values are additive may not be valid. This is plausible as the sorption of HA onto silica might modify the surface charge characteristics of the silica at lower pH. HA coated silica particles have been found to have more negative surface charge than bare silica particles (*Ledin et al. 1994*). The rise in percentage sorption at higher pH ( $> 8$ ) is in agreement with that observed by Fairhurst et al. (*1995 a*) and could be due to the formation of carbonate complexes or incorporation of Cm in lattice (*Panak et al., 1996; Takahashi et al., 2002*). However, the exact mechanism of the rise is not clear. Speciation calculation of Cm(III) in aqueous system containing both HA and carbonate anions predicts the dominance of  $\text{Cm}(\text{CO}_3)_2^-$  at pH above 9 while humate complexes dominate in the pH range of 7-9 (*Takahashi et al., 2002*). For a clear understanding of the effect of HA on the sorption of Cm(III) by silica, SCM of the ternary system is needed with input about the structure of the surface complexes from the spectroscopic techniques, such as EXAFS and TRLS, which can provide direct signature of the metal ligand complex on the mineral oxides (*Takahashi et al., 2002*).

#### 4.3.6. Sorption of Cm (III) by silica: Effect of ionic strength:

Figure 4.8 shows a plot of percentage sorption of curium by silica colloids as a function of ionic strength at pH 6.5. The percentage sorption remains nearly constant

indicating negligible effect of ionic strength on the sorption process. This suggests that the sorption follows inner sphere complex formation between Cm(III) and surface sites on silica. The small decrease in the percentage sorption with increasing ionic strength (I) up to I = 0.1 M may be due to the ionic strength dependence of the binding constant of Cm(III) with silica (*Reed et al., 1999*).

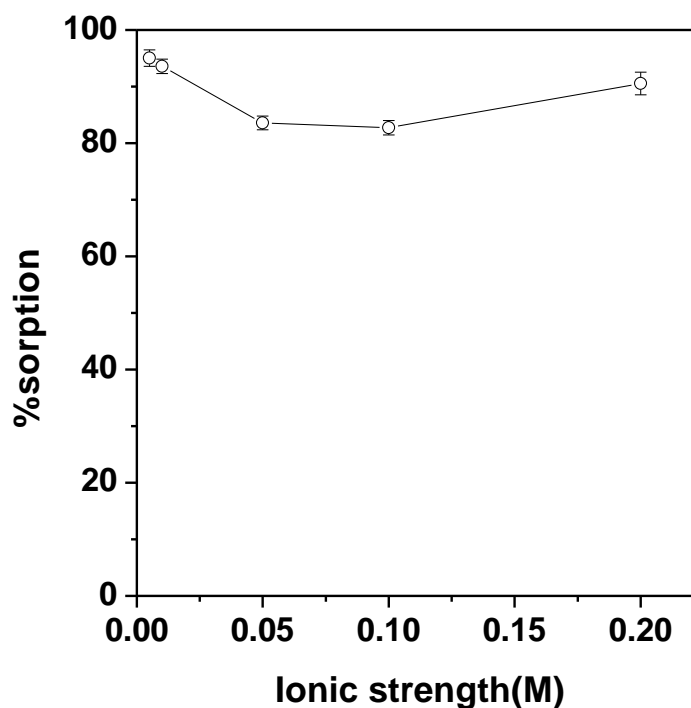


**Figure 4.8** Effect of ionic strength on sorption of Cm by silica colloids. pH = 6.5,

$$[\text{Cm(III)}] = 2.2 \times 10^{-10} \text{ M}, [\text{Silica}] = 5 \text{ g/l}$$

Figure 4.9 shows the speciation of Cm(III) as a function of ionic strength at pH 6.5 obtained using the geochemical code MINTEQA2. The concentration of  $\text{Cm(OH)}^{2+}$  decreases with increase in ionic strength up to I = 0.05 M which is attributed to a decrease in activity coefficient of  $\text{Cm}^{3+}$  and  $\text{Cm(OH)}^{2+}$  with ionic strength. The decrease in activity coefficient of  $\text{Cm}^{3+}$  is higher than that of  $\text{Cm(OH)}^{2+}$ , hence  $\text{Cm(OH)}^{2+}$  concentration decreases initially. Above I = 0.05 M, the

concentration of both the species remains constant. The higher hydrolyzed species are not dominant at pH 6.5.

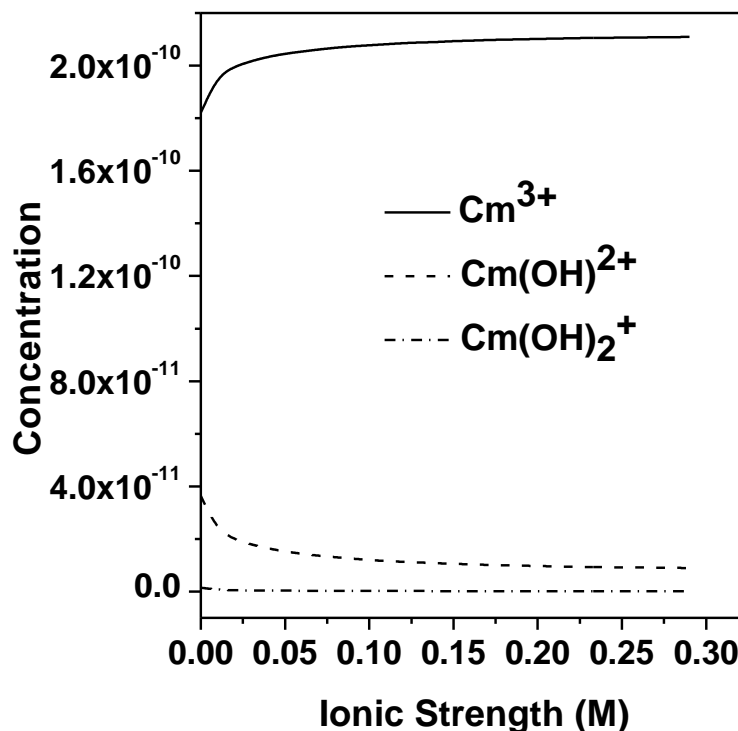


**Figure 4.9** Speciation of Cm(III) as a function of ionic strength at pH = 6.5.

In case of sorption reactions three factors are affected by ionic strength namely (i) Coulombic energy, (ii) dissociation constant of surface sites and (iii) activity coefficient of  $\text{Cm}^{3+}$  in solution. The Coulombic energy and activity coefficient of  $\text{Cm}^{3+}$  in solution decrease with ionic strength and dissociation constant of surface sites increases with ionic strength (*Dzombak and Morel, 1990*). Thus, the first two factors tend to decrease the sorption while third one favours the sorption with increasing ionic strength. The net effect is that there is a slight decrease in sorption initially with ionic strength. Thus, the negligible influence of ionic strength suggests the occurrence of inner sphere complexation between silica surface sites and curium.

#### 4.3.7. Sorption of Cm (III) by silica: Effect of HA concentration:

The variation of the percentage sorption as a function of concentration of HA, at pH = 6.0, is plotted in Figure 4.10. Except for the lowest concentration of HA, the percentage sorption gradually decreases with increasing concentration of HA, which can be explained in terms of strong complexation of Cm(III) by HA in the intermediate pH range. Similar effect of HA concentration has been observed in case of Th(IV) sorption on hematite (Reiller *et al.*, 2005).

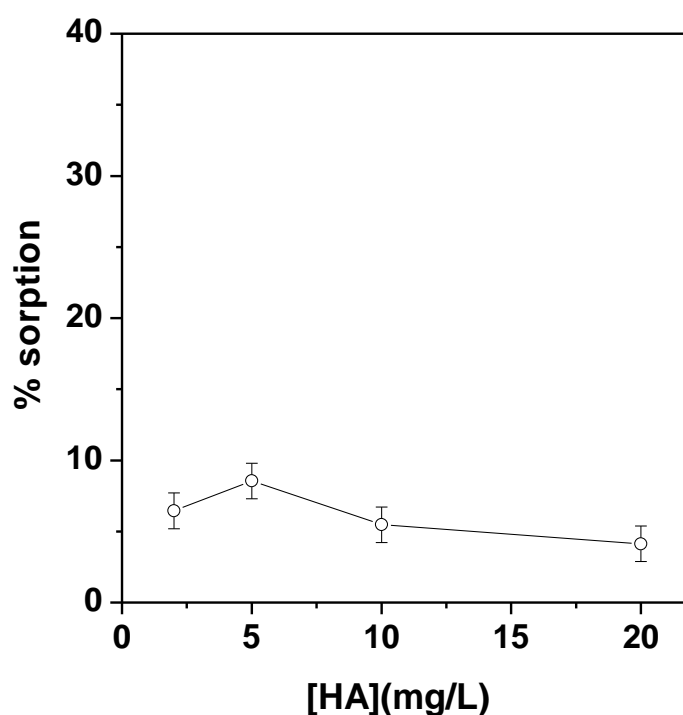
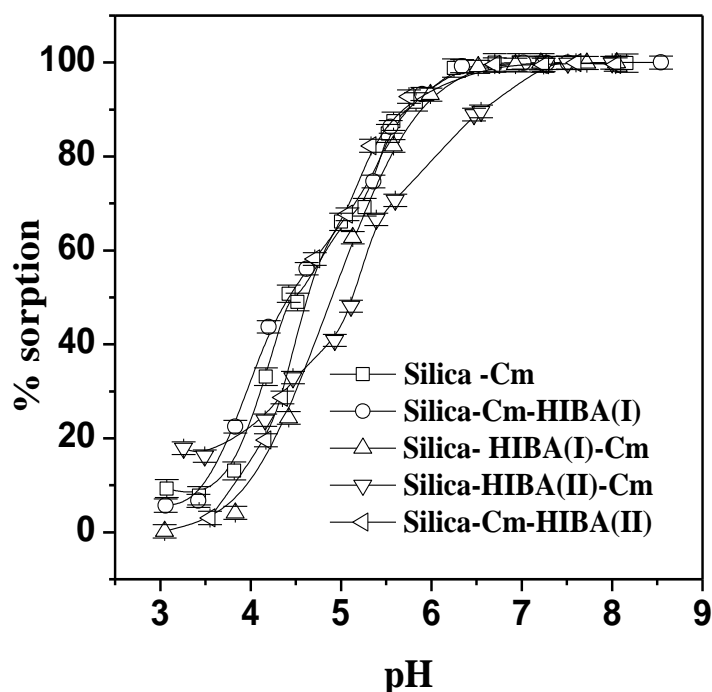


Figure 4.10 Sorption of Cm by silica as a function of [HA]. (pH = 6.0)

#### 4.3.8. Sorption of Cm (III) by silica: Effect of HIBA concentration:

The percentage sorption of curium by silica colloids in absence and presence of HIBA is shown in Figure 4.11. In the case of Silica-Cm-HIBA(I), the sorption data follow that of the binary system whereas the sorption edge is slightly shifted to higher pH for Silica-HIBA(I)-Cm system as compared to the binary Cm(III)-silica system as shown in figure 4.11. Similar trends are observed in Silica-Cm-HIBA(II) and Silica-

HIBA(II)-Cm systems (figure 4.11) but in case of Silica-HIBA(II)-Cm the shift of sorption edge is more pronounced as compared to Silica-HIBA(I)-Cm. This is attributed to higher HIBA concentration in these systems.



**Figure 4.11** Sorption of Cm(III) on silica in presence and absence of HIBA.

[Cm(III)] =  $2.2 \times 10^{-10}$  M; Silica = 5 g/L; [HIBA(I)] =  $1 \times 10^{-5}$  M, ; [HIBA(II)] =  $1 \times 10^{-3}$  M; I = 0.1 M (NaClO<sub>4</sub>).

The effect of HIBA on the sorption of Eu(III) by silica can be understood considering the sorption of HIBA by silica. TOC values in the supernatant solutions were found to be close to that corresponding to the initial HIBA concentration indicating negligible sorption of HIBA by silica at all pH values. The low  $pK_a$  (3.78) of HIBA (Portanova *et al.*, 2003) suggests that its anionic form dominates in the pH range of study in which the silica surface is negatively charged ( $PZC < 2.4$ ) (Kumar *et al.*, 2006), thereby resulting in negligible sorption of HIBA on silica. Thus, HIBA can be treated as a complexing anion present in silica suspension. For Silica-HIBA(I)-Cm

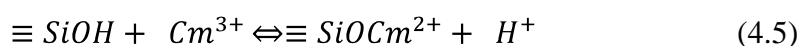
system, with the increase in pH of the suspension, the complexation of Cm(III) by HIBA results in decreased sorption of Cm(III) on silica surface. In the case of Silica-Cm(III)-HIBA(I) system, initially Cm(III) is sorbed quantitatively onto the silica surface. Introduction of HIBA to this suspension should result in complexation of sorbed Cm(III) by HIBA and thereby generation of sorption profile similar to Silica-HIBA(I)-Cm system. However, the decrease in the sorption of Cm(III) as observed in case of Silica-HIBA(I)-Cm is not seen in the case of Silica- Cm-HIBA(I). In most of the cases the effect of addition order of HA and metal ion on sorption to mineral oxides have been studied (*Wang et al., 2000, 2004; Xu et al., 2006 a, 2006 b; Reiller et al., 2005; Davis, 1984; Fan, 2009; Li et al., 2009; Liu et al., 2001*) but there is hardly any literature report dealing with addition order of small complexing anions and metal ions. One of the explanations for the decreased desorption of Cm(III) in the Silica-Cm-HIBA(I), could be the incorporation of Cm(III) in silica matrix following dissolution of silica. The  $\log \beta$  for Cm-HA (*Cornelis, 2005*) is much more than that of Cm-HIBA which is responsible for the higher desorption capacity of HA as compared to HIBA.

#### **4.3.9. SCM:**

SCM was used to analyse the data of Cm(III) sorption on silica in absence and presence of HIBA to infer about the surface reactions governing the sorption process. In present studies DLM has been used which assumes the oxide-water interface to comprise of two charged layers, namely, surface layer and a diffuse layer of counter ions in solution. The Gouy-Chapman distribution of ions was assumed for the diffuse layer.

#### 4.3.9.1. SCM of binary systems:

In Cm(III)-silica system, the most dominant species in the pH range of study are  $\text{Cm}^{3+}$  and  $\text{CmH}_3\text{SiO}_4^+$  as shown in figure 4.3(a). Thus, a model considering monodentate mononuclear curium surface complex  $\equiv\text{SiOCm}^{2+}$  and monodentate mononuclear curium monosilicate surface complex  $\equiv\text{SiOCmH}_3\text{SiO}_4^+$  was tried which successfully fit the sorption data for binary system. The corresponding surface complexation reactions are described in equations (4.5) and (4.6).



Although the above model fit the sorption data quite well, TRLFS of Cm(III) sorption on silica revealed the existence of two species with lifetimes 220  $\mu\text{s}$  and 740  $\mu\text{s}$  which correspond to 2 and 0 water molecules respectively (*Chung et al., 1998*), therefore the sorption data was fitted using monodentate mononuclear curium disilicate surface complex  $\equiv\text{SiOCm}(\text{H}_3\text{SiO}_4)_2$  instead of monodentate mononuclear curium monosilicate surface complex  $\equiv\text{SiOCmH}_3\text{SiO}_4^+$  as  $\equiv\text{SiOCm}(\text{H}_3\text{SiO}_4)_2$  approximates more closely to the species containing no water molecules. The surface complexation reaction for  $\equiv\text{SiOCm}(\text{H}_3\text{SiO}_4)_2$  is given below.



Thus, Cm(III) sorption on silica is described using monodentate mononuclear curium surface complex  $\equiv\text{SiOCm}^{2+}$  and monodentate mononuclear curium disilicate surface complex  $\equiv\text{SiOCm}(\text{H}_3\text{SiO}_4)_2$  as shown in figure 4.12.

#### 4.3.9.2. SCM of ternary systems:

The sorption data for the ternary system of Cm(III)-silica-HIBA systems were modeled using similar analogy as that in case of binary system.

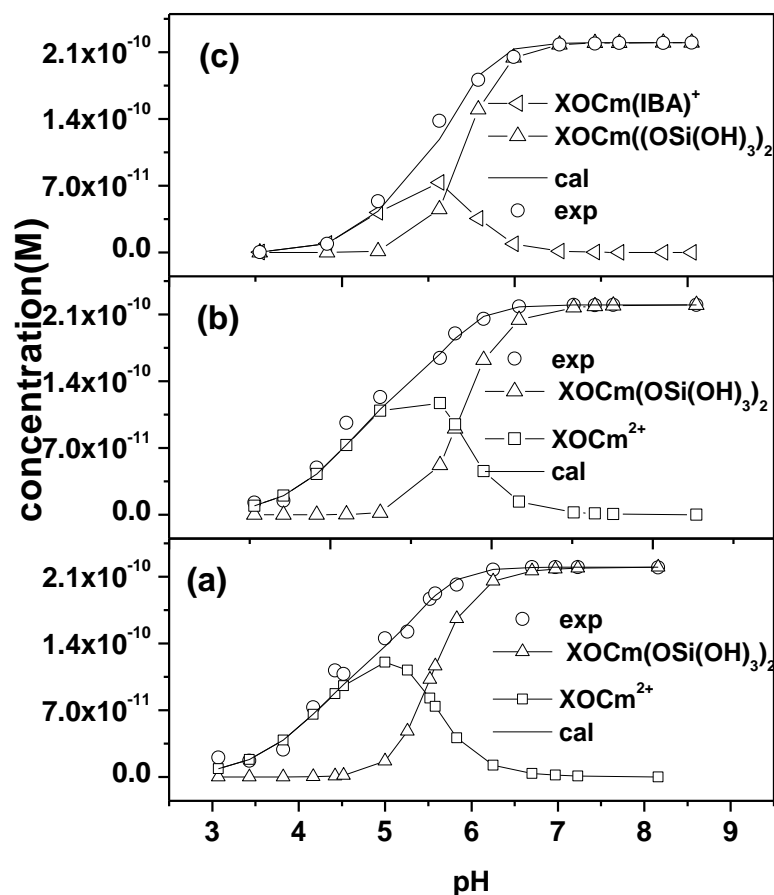


**Figure 4.12** SCM of Cm(III) sorption by Silica in presence of HIBA (a) binary Silica-Cm system; (b) Silica-Cm-HIBA(I) system ; (c) Silica-HIBA(I)-Cm system;

$$[\text{Cm(III)}] = 2.2 \times 10^{-10} \text{ M}; \text{Silica} = 5 \text{ g/L}; [\text{HIBA}] = 1 \times 10^{-5} \text{ M}.$$

#### 4.3.9.2. (a) Silica-Cm-HIBA(I) system ( $[\text{HIBA}] = 10^{-5} \text{ M}$ ) :

In Silica-Cm-HIBA(I) system, the surface complex pertaining to Cm(III) and  $\text{CmH}_3\text{SiO}_4^+$ , the major species in aqueous phase in the pH range of study, were considered while modeling the sorption data of this ternary system. The sorption profile could be explained considering the surface complexes, namely,  $\equiv\text{SiOCm}^{2+}$  and  $\equiv\text{SiOCmH}_3\text{SiO}_4^+$ . However, using the similar hypothesis, as in the case of binary system, that  $\equiv\text{SiOCm}(\text{H}_3\text{SiO}_4)_2$  approximates more closely to the species containing no water molecules,  $\equiv\text{SiOCm}(\text{H}_3\text{SiO}_4)_2$  and  $\equiv\text{SiOCm}^{2+}$  were considered as surface

complexes which gave the best fit as shown in figure 4.12 (b) and corresponding surface reactions are given by equations (4.5) and (4.7).

#### 4.3.9.2. (b) Silica-HIBA(I)-Cm system ([HIBA] = 10<sup>-5</sup> M):

The aqueous speciation is same in both Silica-HIBA(I)-Cm and Silica-Cm-HIBA(I) systems as it is independent of order of addition of HIBA and Cm(III). The surface complexes  $\equiv\text{SiOCm}^{2+}$  and  $\equiv\text{SiOCm}(\text{H}_3\text{SiO}_4)_2$  were evaluated to fit the sorption data but no convergence was obtained which in turn validated that order of addition of HIBA and Cm(III) does influence the surface species responsible for sorption. In case of Silica-HIBA(I)-Cm, when Cm(III) is added to silica suspension containing HIBA, Cm(III) can interact both with HIBA and silica. As the kinetics of complex formation (Cm-HIBA) is much faster than that of sorption, it can be concluded that Cm-HIBA complex is formed instantaneously and get sorbed on to silica surface, even though aqueous speciation calculations do not support their existence. Consideration of surface complexes, namely,  $\equiv\text{SiOCm}(\text{IBA})^+$  and  $\equiv\text{SiOCm}(\text{H}_3\text{SiO}_4)_2$  resulted in successful fitting of sorption data as shown in figure 4.12 (c). The surface complexation reactions for both the sorbates are given by equation (4.7) and (4.8).



#### 4.3.9.2. (c) Silica-Cm-HIBA(II) system ([HIBA] = 10<sup>-3</sup> M):

The speciation of Cm(III) is dominated by  $\text{Cm}^{3+}$ ,  $\text{Cm}(\text{IBA})^+$  and  $\text{Cm}(\text{H}_3\text{SiO}_4)^{2+}$  in the pH range of interest (figure 4.3(c)). As far as curium silicate species are concerned  $\text{Cm}(\text{H}_3\text{SiO}_4)^{2+}$  was considered as sorbate instead of  $\text{CmH}_3\text{SiO}_4^{2+}$ . All the permutations of the surface complexes involving the above

mentioned species were tried in order to fit the sorption profile but no convergence was obtained in any case. Therefore  $\text{Cm(IBA)}_2^+$  complex, though formed in minute amount, was considered as a potential sorbate along with  $\text{Cm(H}_3\text{SiO}_4)_2^+$ . The two surface complexes comprising of these two species were found to fit the sorption data satisfactorily as shown in figure 4.13 (a). The corresponding surface complexation reactions are given by equations (4.7) and (4.9).



#### 4.3.9.2. (d) Silica-HIBA(II)-Cm system ( $[\text{HIBA}] = 10^{-3} \text{ M}$ ):

In Silica-HIBA(II)-Cm(III) system, the aqueous speciation is same as in Silica-Cm(III)-HIBA(II). The surface complexes pertaining to  $\text{Cm(IBA)}_2^+$  and  $\text{Cm(H}_3\text{SiO}_4)_2^+$  were evaluated for fitting the sorption data but satisfactory fit was not obtained as the 10-20 % sorption at low pH could not be explained by considering only these two surface complexes. In order to account for sorption at low pH, outer sphere surface complex  $\equiv \text{SiOHCm(IBA)}^+$  was tested along with the two surface complexes mentioned above which could successfully fit the sorption data as shown in figure 4.13 (b).

The need for an outer sphere complex can be attributed to sorption of HIBA on silica surface which was determined using TOC content in supernatant of the silica suspension after equilibration with HIBA. It is worth mentioning here that sorption of 2-3% HIBA on silica at low pH would not be manifested in the TOC measurement, though it would be sufficient to enhance the sorption of Cm(III) at low pH. The surface complexation reactions for all the three sorbates are given by equation (4.7), (4.9) and (4.10).



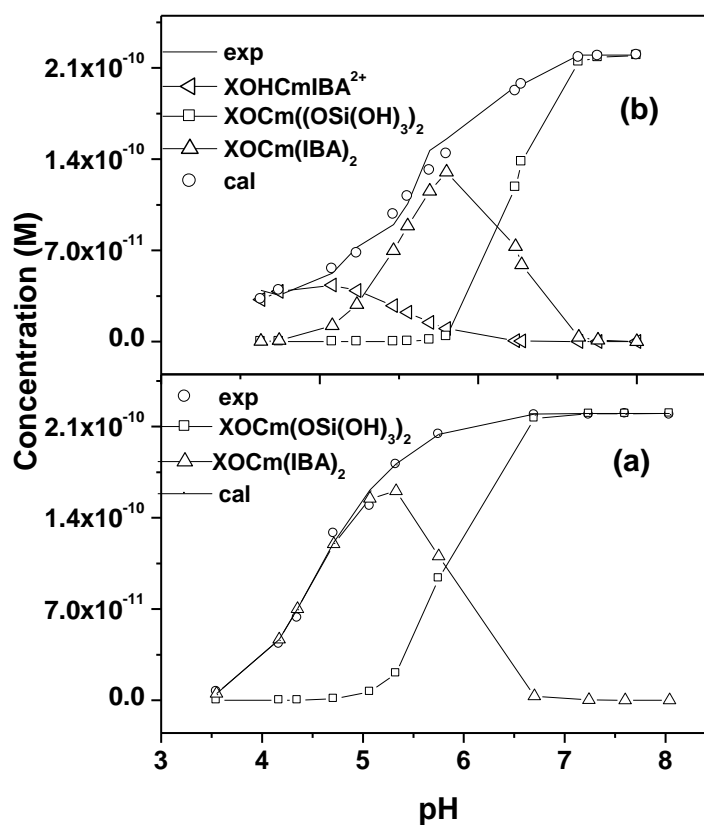


**Figure 4.13** SCM of Cm(III) sorption by Silica in presence of HIBA (a) Silica-Cm-HIBA(II) system ; (b) Silica-HIBA(II)-Cm system;  $[Cm(III)] = 2.2 \times 10^{-10}$  M; Silica = 5 g/L;  $[HIBA] = 1 \times 10^{-3}$  M.

Thus, it appears that not only the aqueous speciation governs the various possibilities of surface complexes, but the addition order of HIBA and Cm(III) is also one of the important parameters influencing the type of surface complex formed at the solid solution interface. The stability constants of the surface complexes for all the systems are given in Table 4.3.

**Table 4.3** Optimized parameter values as obtained from FITEQL for Cm-silica and Cm-silica-HIBA systems

System	Reaction	Log K	WSOS/ DF
Silica-Cm(III)	$\equiv\text{SiOH} + \text{Cm}^{3+} + 2\text{SiO}(\text{OH})_3^- \leftrightarrow \equiv\text{SiOCm}(\text{OSi}(\text{OH})_3)_2 + \text{H}^+$	-7.94	15.1
	$\equiv\text{SiOH} + \text{Cm}^{3+} \leftrightarrow \equiv\text{SiOCm}^{2+} + \text{H}^+$	-2.53	
Silica-Cm(III)- HIBA(I)	$\equiv\text{SiOH} + \text{Cm}^{3+} + 2\text{SiO}(\text{OH})_3^- \leftrightarrow \equiv\text{SiOCm}(\text{OSi}(\text{OH})_3)_2 + \text{H}^+$	-8.04	10.1
	$\equiv\text{SiOH} + \text{Cm}^{3+} \leftrightarrow \equiv\text{SiOCm}^{2+} + \text{H}^+$	-2.48	
Silica-HIBA(I)- Cm(III)	$\equiv\text{SiOH} + \text{Cm}^{3+} + 2\text{SiO}(\text{OH})_3^- \leftrightarrow \equiv\text{SiOCm}(\text{OSi}(\text{OH})_3)_2 + \text{H}^+$	-7.58	2.55
	$\equiv\text{SiOH} + \text{Cm}^{3+} + \text{HIBA} \leftrightarrow \equiv\text{SiOCm}(\text{IBA})^+ + 2\text{H}^+$	2.16	
Silica-Cm(III)- HIBA(II)	$\equiv\text{SiOH} + \text{Cm}^{3+} + 2\text{SiO}(\text{OH})_3^- \leftrightarrow \equiv\text{SiOCm}(\text{OSi}(\text{OH})_3)_2 + \text{H}^+$	-8.21	3.91
	$\equiv\text{SiOH} + \text{Cm}^{3+} + 2\text{HIBA} \leftrightarrow \equiv\text{SiOCm}(\text{IBA})_2 + 3\text{H}^+$	4.25	
Silica-HIBA(II)- Cm(III)	$\equiv\text{SiOH} + \text{Cm}^{3+} + 2\text{SiO}(\text{OH})_3^- \leftrightarrow \equiv\text{SiOCm}(\text{OSi}(\text{OH})_3)_2 + \text{H}^+$	-8.42	3.33
	$\equiv\text{SiOH} + \text{Cm}^{3+} + 2\text{HIBA} \leftrightarrow \equiv\text{SiOCm}(\text{IBA})_2 + 3\text{H}^+$	3.65	
	$\equiv\text{SiOH} + \text{Cm}^{3+} + \text{HIBA} \leftrightarrow \equiv\text{SOHCm}(\text{IBA})^{2+} + \text{H}^+$	5.19	

#### 4.3.10. Sorption of Eu(III) by silica: Effect of HIBA concentration:

Figure 4.14 shows the data on sorption of Eu(III) by silica both in absence and presence of HIBA. The sorption of Eu(III) by silica increases with the pH of the suspension approaching nearly 100% at pH 7.0. In the presence of HIBA, a significant

decrease in the sorption of Eu(III) by silica was observed in the pH range of 5.5 – 7.0. Similar observation was made by Pathak et al. (2007a) in the case of sorption of Eu(III) by silica in presence of citrate.

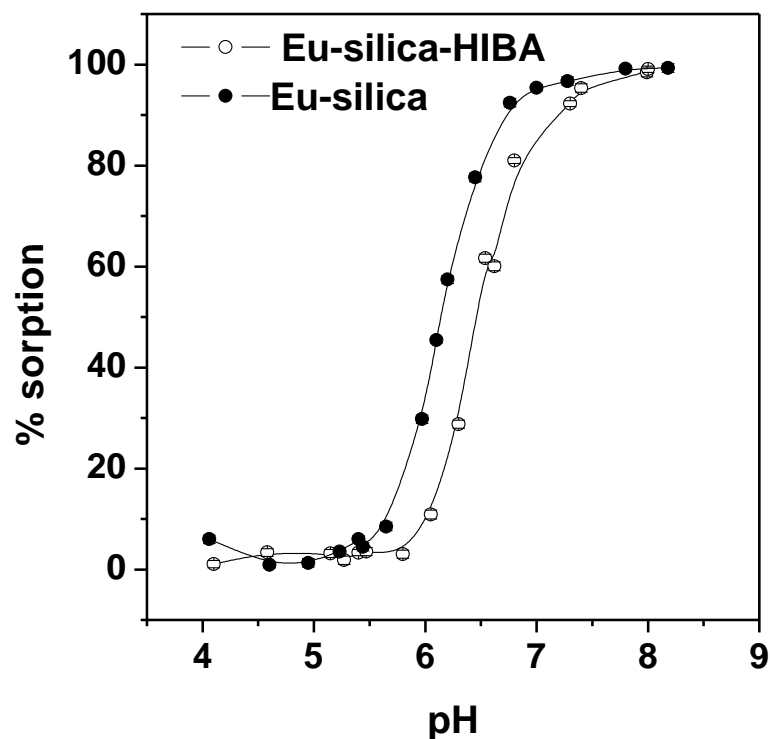


**Figure 4.14** Sorption of Eu(III) on silica in presence and absence of HIBA. [Eu(III)] =  $5.0 \times 10^{-5}$  M; Silica = 10 g/L; [HIBA] =  $2.5 \times 10^{-3}$  M, I = 0.1 M (NaClO<sub>4</sub>).

Sorption of HIBA by silica has been found to be negligible at all pH values, therefore HIBA can be treated as a complexing anion present in silica suspension. With the increase in pH of the suspension, the complexation of Eu(III) by HIBA results in decreased sorption of Eu(III) on silica surface. The similar decrease in the sorption of UO<sub>2</sub><sup>2+</sup> on silica has been observed in presence of citric acid (Kar et al., 2012). At higher pH values, surface precipitation of Eu(OH)<sub>3</sub> is possible. Surface precipitation is likely to occur when metal concentration is more than 1/10 of the

solubility limit and surface coverage is greater than 1/3 of the total surface sites available for sorption (*Dzombak and Morel, 1990*).

In the present work, though, solubility limit is exceeded at pH 6.2, but even at 100% sorption only small fraction of the total surface sites will be occupied and hence surface precipitation is likely to be absent. Further, the TRFS measurements did not show any lifetime component ( $40 \pm 5 \mu\text{s}$ ) (*Plancque et al., 2003*) corresponding to  $\text{Eu}(\text{OH})_3$  which confirms the absence of  $\text{Eu}(\text{III})$  precipitation. Absence of surface precipitation was also reported by Rabung et al. (2000) in the metal ion concentration range  $10^{-8}$  -  $10^{-4}$  M even at pH = 8. TRFS studies with  $2 \times 10^{-4}$  M  $\text{Eu}(\text{III})$  on silica also showed that europium precipitation did not take place even at pH 7.5 (*Takahashi et al., 2006*). Fluorescence studies of  $\text{Eu}(\text{III})$  ( $10^{-3}$  M) on silica revealed the existence of two surface complexes. However, no signature of  $\text{Eu}(\text{OH})_3$  precipitation was observed even at a concentration 20 times higher than that used in present work (*Fouchard et al., 2004a*).

#### 4.3.10. 1. TRFS:

Figures 4.15 (a) and 4.15 (b) show the fluorescence emission spectra of  $\text{Eu}(\text{III})$  sorbed on silica in absence and presence of HIBA respectively. The spectrum shows characteristic fluorescence emission due to the decay of the  $^5\text{D}_0$  excited state of  $\text{Eu}^{3+}$  into  $^7\text{F}_j$  ( $j = 0-4$ ) states. The spectra have been normalized with respect to the intensity at 592 nm, except for pH < 5.5, where no spectral features characteristic of  $\text{Eu}(\text{III})$  were observed. The transition corresponding to 616 nm peak ( $^5\text{D}_0 \rightarrow ^7\text{F}_2$ ) is hypersensitive owing to its electric dipole nature and its intensity is dependent on the symmetry around the metal ion. With the sorption of  $\text{Eu}(\text{III})$  by silica, the chemical environment around the metal ion becomes more and more asymmetric leading to the

increase in the asymmetric ratio ( $R = I_{616}/I_{592}$ ). This is evident from the increase in intensity of the 616 nm peak with respect to that of 592 nm peak as shown in figure 4.15 (a).

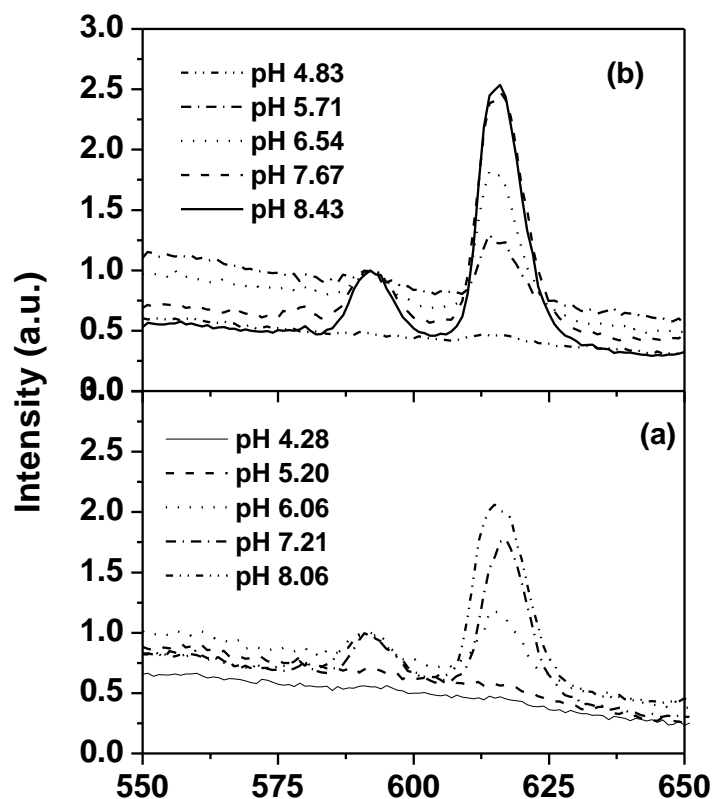


**Figure 4.15** Time resolved fluorescence emission spectra of Eu(III) sorbed on silica in absence (a) and presence (b) of HIBA.  $[Eu(III)] = 5.0 \times 10^{-5} M$ ; Silica = 10 g/L;  $[HIBA] = 2.5 \times 10^{-3} M$ .

Figure 4.16 shows the typical fluorescence decay curve for Eu(III) sorbed on silica at pH 8.06. The fluorescence decay data from 25  $\mu s$  to 2.0 ms were fitted into multi-exponential functions to obtain the lifetime data. The best fit ( $\chi^2 \sim 1.4$ ) was obtained with four life time components. The shortest lived component was found to be of the order of 1  $\mu s$  which is due to instrumental artifact and does not vanish even

if the spectrum is recorded by giving an appropriate delay. The other short lived component is around 20  $\mu\text{s}$  and did not show any signature of Eu(III) characteristic emission when the spectrum was gated with respect to this particular lifetime. Hence in further discussion two lifetime components,  $\tau_1$  and  $\tau_2$ , having characteristic Eu(III) emission have been discussed. The emission spectrum of bare silica showed a broad band with maximum at 450 nm. It was found that silica exhibits a longer lived component (Figure 4.16 (b)) but its fraction is much smaller (4-5%) than that observed (30-70%) in case of europium sorbed on silica.

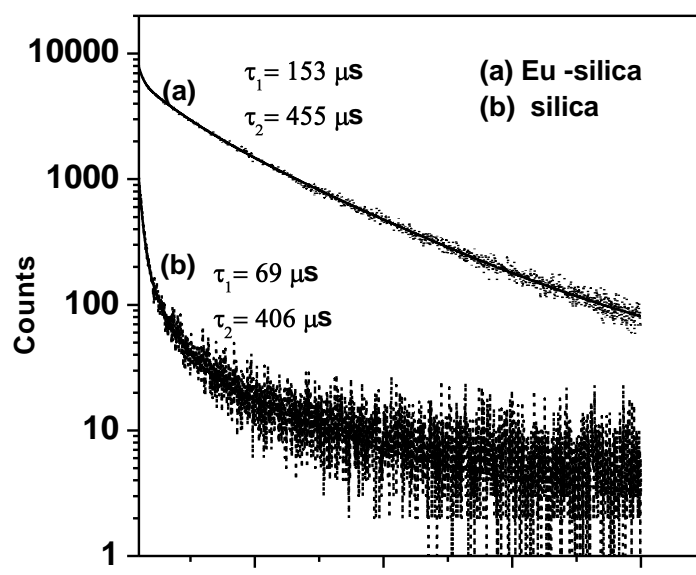


**Figure 4.16** Comparison of the fluorescence decay curve of Eu(III) sorbed on silica at pH = 8.06 to that of bare silica.

Figure 4.17 shows the variation of  $\tau_1$  and  $\tau_2$  as a function of pH both in absence and presence of HIBA. The magnitude of the life times, 150  $\mu\text{s}$  and 400  $\mu\text{s}$ , remains nearly constant at all pH values. The error on the lifetime values is about 10% which arises due to the instrumental drifts, temperature variation and sample

preparation. The magnitude of  $\tau_1$  and  $\tau_2$  is in agreement with the literature reports where in the  $\tau_1$  and  $\tau_2$  values of 130  $\mu\text{s}$  and 350  $\mu\text{s}$  (Fouchard *et al.*, 2004a) and 137  $\mu\text{s}$  and 335  $\mu\text{s}$  (Tetre *et al.*, 2006) have been observed.

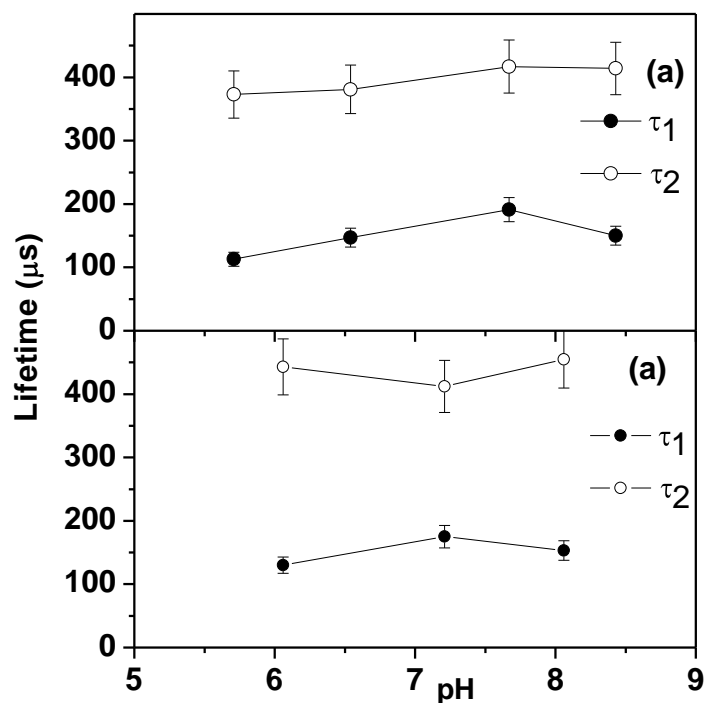


**Figure 4.17** Fluorescence life time data of Eu(III) sorbed on silica in absence (a) and presence (b) of HIBA.  $[\text{Eu(III)}] = 5.0 \times 10^{-5} \text{ M}$ ; Silica = 10 g/L;  $[\text{HIBA}] = 2.5 \times 10^{-3} \text{ M}$ .

The lifetime can be correlated to the number of water molecules by the relationship given in equation 3.2. Though this empirical correlation is applicable to Eu(III) complexes in solution, it can be used as a guide to predict the nature of sorbed Eu(III) species. The short lived component corresponds to 6-7 water molecules indicating that Eu(III) is sorbed onto silica through inner sphere complexation while the long lived component, corresponding to 1-2 water molecules, is attributed to sorbed Eu(III) silicate complexes. The lifetime data are similar in presence of HIBA

indicating negligible effect of HIBA on the fluorescence characteristics of sorbed Eu(III). This further corroborates the negligible sorption of HIBA by silica.

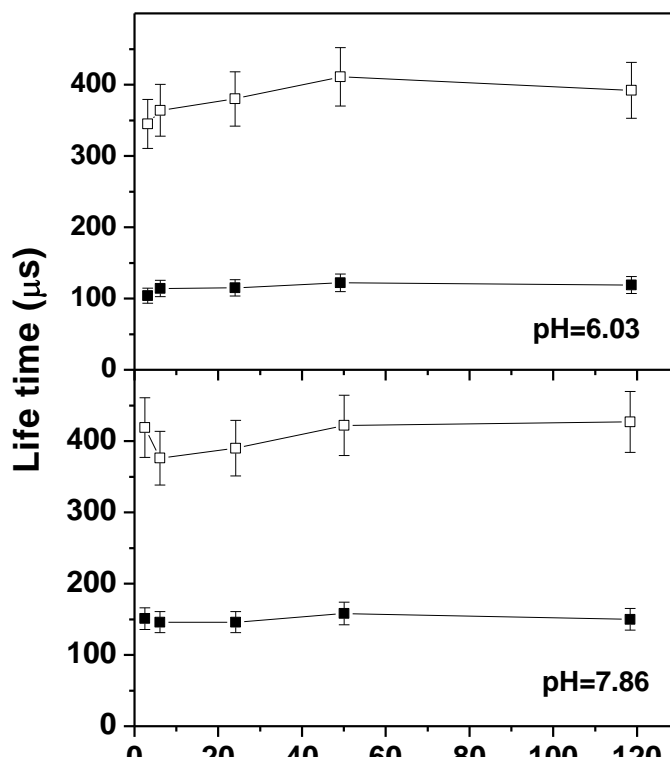


**Figure 4.18** Lifetime data of Eu(III) sorbed on silica as function of equilibration time.

[Eu(III)] =  $5.0 \times 10^{-5}$  M; Silica = 10 g/L.

Takahashi et al. (1998) observed mono-exponential decay with the lifetime increasing with pH, while bi-exponential decay has been reported by many authors (Fouchard et al., 2004a; Tetre et al., 2006), though no comments were made about the nature of species. Similar observations were made by Chung et al. (1998) in the study of Cm(III) sorption on silica by TRFS. They assigned shorter lifetime component (220  $\mu$ s) to  $\equiv$ SiOCm<sup>2+</sup> and the longer lifetime component (740  $\mu$ s) to co-precipitation of Cm and Si(OH)<sub>4</sub> formed as a result of silica dissolution. Thus the

TRFS studies clearly suggest the occurrence of two surface complexes having distinctly different chemical environments.

Figure 4.18 shows the fluorescence decay lifetime of Eu(III) sorbed on to silica as a function of aging time for two pH values (6 and 8). The constancy of the lifetimes over a period of 5 days suggests the absence of any aging effects which has been proposed as a mechanism of the incorporation of Eu(III) into the silica matrix (Takahashi *et al.*, 2006).

#### 4.3.10.2. SCM :

The information obtained from the TRFS measurements and the speciation calculation of Eu(III) in presence of silicic acid and HIBA have been used in the SCM of the binary and ternary systems using FITEQL 4.0. Based on the speciation diagram (figure 4.3), and the life time values, the two surface complexes can be attributed to sorption of  $\text{Eu}^{3+}$  ( $\tau_1$ ) and  $\text{Eu}(\text{OSi}(\text{OH})_3)_2^+$  ( $\tau_2$ ) onto the silica surface. Though  $\text{Eu}(\text{OSi}(\text{OH})_3)_2^+$  is the dominant species in the pH range of study (figure 4.3), considering the inevitable formation of polysilicic acid,  $\text{Eu}(\text{OSi}(\text{OH})_3)_2^+$  has been considered, as a more realistic species, in SCM. Moreover, the two surface complexes owing to sorption of  $\text{Eu}^{3+}$  and  $\text{Eu}(\text{OSi}(\text{OH})_3)_2^+$  onto the silica surface did not yield satisfactory fits which further corroborates the formation of polysilicic acid. The SCM predictions along with experimental data, considering  $\text{Eu}(\text{OSi}(\text{OH})_3)_2^+$ , are shown as continuous curves in figure 4.19 (a) and 4.19 (b) for both binary and ternary systems respectively. The log K values for the surface complexes along with WSOS/DF are given in Table 4.4.

**Table 4.4** Optimised parameter values as obtained from FITEQL for Eu-silica and Eu-silica -HIBA

System	Reaction	log K	WSOS/DF
Potentiometric titration data fitting using DLM	$\text{SiOH} + \text{H}^+ \leftrightarrow \equiv\text{SiOH}_2^+$	0.56	16.68
	$\equiv\text{SiOH} \leftrightarrow \equiv\text{SiO}^- + \text{H}^+$	-6.8	
	Surface sites $\equiv\text{SiOH}$	$2.45 \times 10^{-4}$ mol/g	
Eu-silica	$2(\equiv\text{SiOH}) + \text{Eu}^{3+} \leftrightarrow (\equiv\text{SiO})_2\text{Eu}^+ + 2\text{H}^+$	-6.41	6.79
	$2(\equiv\text{SiOH}) + \text{Eu}^{3+} + 2\text{SiO}(\text{OH})_3^- \leftrightarrow (\equiv\text{SiO})_2\text{Eu}(\text{OSi}(\text{OH})_3)_2^- + 2\text{H}^+$	-14.09	
Eu-silica-HIBA	$2(\equiv\text{SiOH}) + \text{Eu}^{3+} \leftrightarrow (\equiv\text{SiO})_2\text{Eu}^+ + 2\text{H}^+$	-6.78	21.09
	$2(\equiv\text{SiOH}) + \text{Eu}^{3+} + 2\text{SiO}(\text{OH})_3^- \leftrightarrow (\equiv\text{SiO})_2\text{Eu}(\text{OSi}(\text{OH})_3)_2^- + 2\text{H}^+$	-14.93	

Figure 4.19 shows that  $(\equiv\text{SiO})_2\text{Eu}(\text{OSi}(\text{OH})_3)_2^-$  dominates the sorption of Eu(III) by silica in the pH range of 6-8. This is further corroborated by the observation of dominating long lived component in the fluorescence decay data, indicating nearly 1-2 water molecules around the  $\text{Eu}^{3+}$  ion. The bidentate binding of Cm(III) to quartz surface has also been predicted by Stumpf et al. (2004). Since europium silicates are the dominant species in presence of HIBA (figure 4.3), the same surface complexes have been proposed for ternary system. Thus we find that, though presence of HIBA decreases the sorption of Eu(III) by silica in the intermediate pH range of 5.5 – 7.0, Eu-silicate complexes dominate the surface complexation with the un-complexed Eu(III) playing a minor role. The detail understanding of the sorption process would require the study of Eu(III) complexation with polysilicic acid.

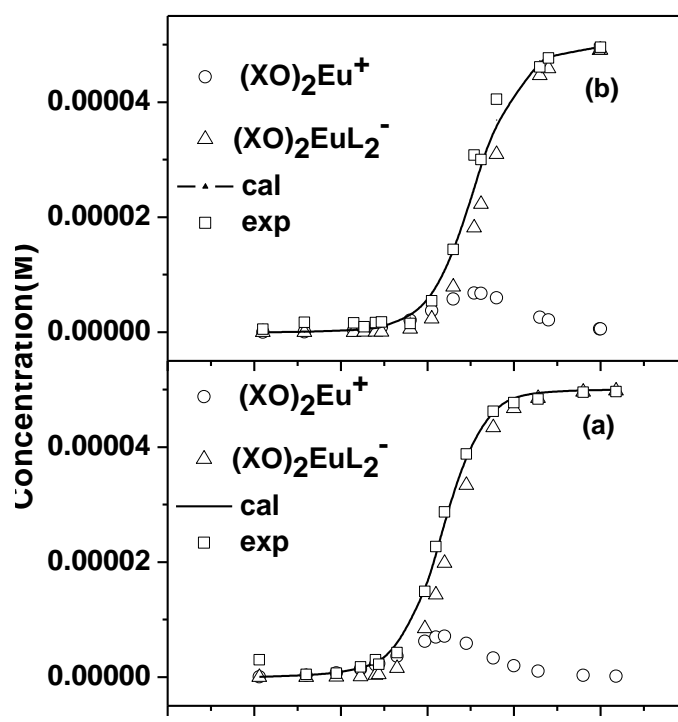


**Figure 4.19** SCM of Eu(III) sorption by Silica in absence (a) and presence of HIBA(b).  $[\text{Eu(III)}] = 5.0 \times 10^{-5} \text{ M}$ ; Silica = 10 g/L;  $[\text{HIBA}] = 2.5 \times 10^{-3} \text{ M}$ .  $\text{L} = \text{OSi(OH)}_3^-$ .

#### 4.3.11. Comparison of Silica-Cm(III) and Silica-Eu(III) systems:

Sorption of Cm(III) and Eu(III) on silica, shown in figure 4.20 (a), follow the typical 'S' shaped curve with the sorption edge at pH 4 and pH 6 respectively. The observed difference in the sorption edge is a manifestation of five order of magnitude difference in concentration of Cm(III) ( $1 \times 10^{-10} \text{ M}$ ) and Eu(III) ( $5 \times 10^{-5} \text{ M}$ ). In the case of Eu(III)-silica system, bidentate mononuclear europium surface complex  $(\equiv\text{SO})_2\text{Eu}^+$  and bidentate mononuclear europium disilicate surface complex  $(\equiv\text{SO})_2\text{Eu}(\text{H}_3\text{SiO}_4)_2^-$  were postulated to fit the sorption profile whereas for the Cm(III)-silica system, satisfactory fits were obtained with monodentate mononuclear curium surface complex  $\equiv\text{SOCm}^{2+}$  and monodentate mononuclear curium disilicate

surface complex  $\equiv\text{SOCm}(\text{H}_3\text{SiO}_4)_2$ . The different kind of binding in both the systems can be attributed to the different ratio of silica sites to metal ion involved, which is 50 for Eu(III)-silica system and about  $10^7$  for Cm(III)-silica system.

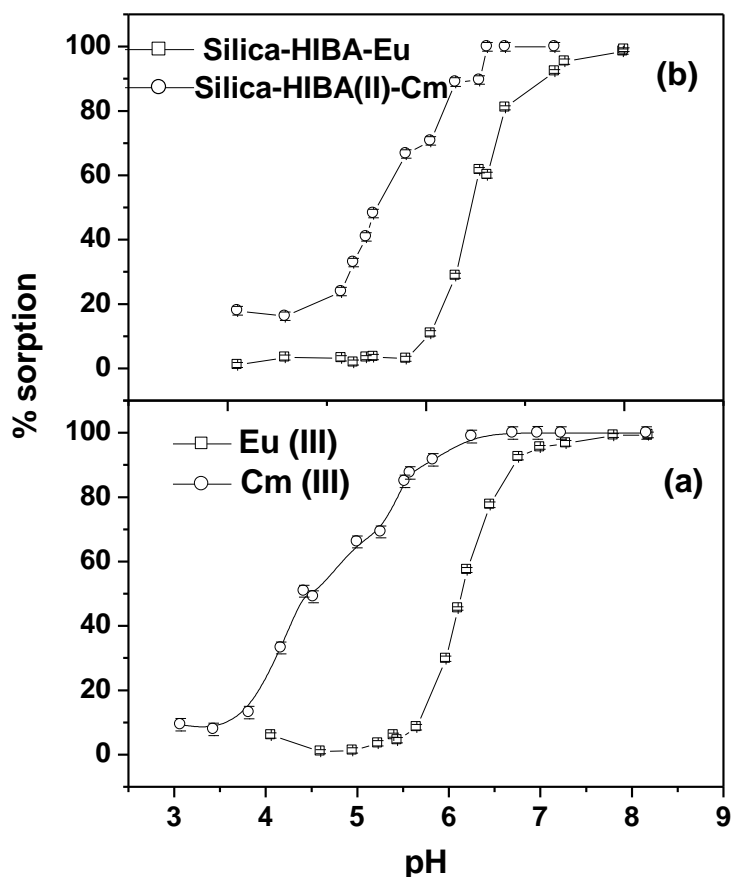


**Figure 4.20** Sorption of Cm(III) and Eu(III) on silica in absence (a) and presence (b)

of HIBA. For Silica-Cm(III) system :Silica = 5 g/L, [Cm(III)] =  $2.2 \times 10^{-10}$  M, [HIBA] =  $1 \times 10^{-3}$  M and I= 0.1 M (NaClO<sub>4</sub>). For Silica-Eu(III) system :Silica = 10 g/L [Eu(III)] =  $5 \times 10^{-5}$  M, [HIBA] =  $2.5 \times 10^{-3}$  M and I=0.1 M (NaClO<sub>4</sub>) (Kar et al. 2011b).

The comparison of sorption data for ternary systems, namely, Silica-HIBA(II)-Cm with Silica-HIBA-Eu is shown in figure 4.20 (b) (Kar et al., 2011 b). Silica-

HIBA(II) -Cm system has been selected as concentration of HIBA and the order of addition of HIBA and metal ion are similar to Silica-HIBA-Eu system.

The shift of sorption edge to higher pH in case of Eu(III) is attributed to the higher concentration of Eu(III) than that of Cm(III). The bidentate mononuclear europium surface complex  $(\equiv\text{SO})_2\text{Eu}^+$  and bidentate mononuclear europium disilicate surface complex  $(\equiv\text{SO})_2\text{Eu}(\text{H}_3\text{SiO}_4)_2$  were able to fit the sorption profile in Silica – HIBA-Eu(III) system. Though presence of HIBA shifts the sorption edge to high pH, the speciation is still dominated by europium silicates in presence of HIBA. Therefore, the same surface complexes have been proposed for ternary system. In case of Silica-HIBA(II)-Cm, apart from the two inner sphere surface complexes  $\equiv\text{SiOCm}(\text{IBA})_2$  and  $\equiv\text{SiOCm}(\text{H}_3\text{SiO}_4)_2$ , which are different from that in Silica-Eu(III) system, an outer sphere complex  $\equiv\text{SiOHCm}(\text{IBA})^{2+}$  is required to reproduce the sorption profile.

In case of Silica-HIBA(II)-Cm system, the surface complexes involving Cm(III)-HIBA also appear to participate in the sorption process in contrast to Silica-HIBA-Eu(III) owing to five order of magnitude higher value of  $[\text{HIBA}]/[\text{M(III)}]$  in case of Cm(III) than that in case of Eu(III). Moreover, the concentration ratio of dissolved silica to HIBA is 2 in case of Silica-HIBA(II)-Cm system where as it is 4 for Silica-HIBA-Eu(III). Thus although stability constants for metal silicate complexes are very high as compared to metal HIBA complexes, due to the comparable concentration of HIBA and dissolved silica the contribution of Cm-HIBA complexes towards the surface speciation cannot be ruled out. However, in order to have detailed understanding about the role of HIBA, its concentration variation over a wide range need to be studied.

**4.3.12. Comparison of Silica-HIBA(I)-Cm and Silica-HA-Cm systems:**

HA is a natural organic matter with large heterogeneity. The high molecular weight with hydrocarbon networks leads to lipophilic interactions and functional groups like carboxylate and phenolate contribute to the lyophilic character of HA (Stevenson, 1982). HA is found to have significant influence on the migration of radio-nuclides in the aquatic environment (Choppin, 1999). The presence of carboxylic and hydroxyl groups, the major functional groups in HA, has attracted the attention of geochemists towards the adsorptive properties of low molecular weight organic acids which are considered building blocks of NOM. However, even if their influence on the adsorption of metal ions can be modeled accurately, the behaviour of these compounds may not be analogues to HA. With this in view, the data for sorption of Cm(III) by silica in presence of HIBA were compared with those in presence of HA. The data are shown in figure 4.21.

Unlike in the case of silica-HA-Cm, wherein strong influence of presence of HA was observed in the pH range 3-8, (enhancement at lower pH and decrease in sorption at higher pH), the effect of HIBA on sorption of Cm(III) by silica was found to be weak. This is partly due to the sorption of HA on silica at lower pH and negligible sorption at higher pH and partly due to the higher stability constant of Cm(III)-HA complexes than that of Cm(III)-HIBA. In the case of Silica-Cm-HIBA(I), the sorption data exhibits similar sorption profile as that observed for the binary Cm(III)-Silica system. This is again quite different from silica-Cm-HA system, wherein the Cm(III) sorption by silica is enhanced at low pH and decreased in the intermediate pH range, though not as much as in the case of silica-HA-Cm system

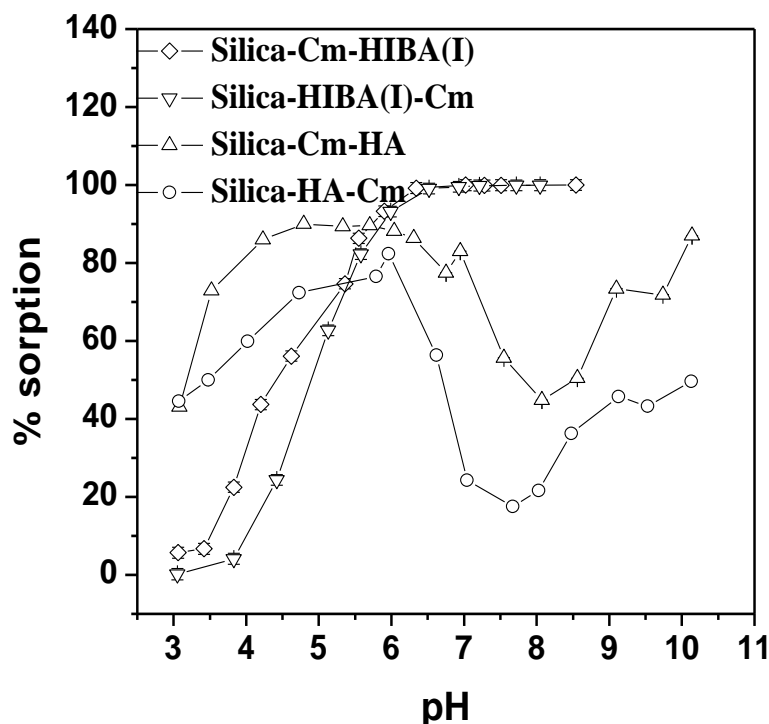


**Figure 4.21** Sorption of Cm(III) on silica in presence of HIBA and HA. Silica = 5 g/L; [Cm(III)] =  $2.2 \times 10^{-10}$  M; I = 0.1 M (NaClO<sub>4</sub>); [HIBA] =  $1 \times 10^{-5}$  M and [HA] = 2 mg/L.

From the above observations, it is evident that the influence of HIBA on sorption of Cm(III) by silica is drastically different from that of HA, which can be attributed to polyfunctionality of HA. Thus, though small molecules can be studied in order to have fundamental understanding of the nature of binding between the different functional groups present in HA and metal ion, they cannot be used as analogues of HA.

#### 4.4. Conclusions:

The present study has shown that the sorption of curium by silica is significantly influenced by the presence of HA in the entire pH range of 4-10. While the sorption is enhanced at lower pH (< 5) it is drastically decreased in the pH range of 6.5-8 in the presence of HA. The addition order of Cm(III) and HA was found to

affect the sorption data in the ternary silica-Cm-HA system. The incomplete desorption of Cm(III) in the case of ternary silica-Cm-HA system could be due to partial incorporation of Cm(III) in the silica matrix. The near independence of the sorption data on ionic strength indicates inner sphere complex formation between  $\text{Cm}^{3+}$  ions and the silica surface sites.

In case of HIBA, Cm(III) sorption is dependent upon the addition order of Cm(III) and HIBA to the silica suspension. Cm(III) sorption by silica is decreased in presence of HIBA, if the HIBA is added before Cm(III), unlike in the case of silica-Cm(III)-HIBA, wherein the sorption follows binary Silica-Cm(III) profile. The observed discrepancies are attributed to partial incorporation of Cm(III) in the silica matrix in binary system and Silica-Cm-HIBA(I). Significant concentration of Si in the supernatant solutions of silica suspensions indicate the presence of dissolved silica that undergoes complexation with Cm(III) and dominates the speciation of Cm(III) even in the presence of HIBA. SCM using DLM showed the evolution of different surface complexes as a function of HIBA concentration as well as order of addition of HIBA and Cm(III).

TRFS of Eu(III) sorbed on silica provided evidence for the existence of two surface complexes which in turn validated the SCM hypothesis. The short lived component was attributed to  $(\equiv\text{SiO})_2\text{Eu}^+$ , while the long lived component was attributed to  $(\equiv\text{SiO})_2\text{Eu}(\text{OSi}(\text{OH})_3)_2^-$ , with the latter dominating the sorption profile of Eu(III) in both in absence and presence of HIBA.

The comparison of effect of HIBA on sorption of Eu(III) and Cm(III) revealed effect of metal ion concentration on the sorption data. While the comparison of influence of HIBA and HA on Cm(III) sorption revealed that the behaviour of small organic molecules could not be considered as analogous to HA.

**Chapter V**

**Sorption of uranium by silica:**

**Effect of Complexing anions**

**5.1. Introduction:**

In the present chapter the effect of pH, ionic strength, U(VI) concentration and complexing anions, namely, carbonate and citrate on sorption of U(VI) by silica has been studied through batch sorption experiments, SCM and TRFS, wherever possible.

One of the challenges faced by the nuclear industry is the possible contamination of the biosphere with radiotoxic elements, due to their release from the concentrated regions, such as, mill tailing ponds, deep geological repositories of high level radioactive wastes, spent fuel storage facilities, etc. In order to evaluate the long term impact of the radioactive contaminants on the living world, it is essential to investigate the mechanism of the pathways through which they might get into the biosphere from their containment. Sorption onto sediments and rock surfaces in the vicinity of the water bodies would retard the migration of the actinides to the far field. However, the presence of complexing anions (inorganic and organic) in the ground water may result in their desorption from the solid surfaces and hence enhance their migration. Thus, role of complexing anions, which are ubiquitous in natural waters, in deciding the fate of radiotoxic elements has to be understood thoroughly in order to precisely predict their migration in environment.

In addition to naturally occurring uranium, a large quantity of uranium is released in the environment owing to its use in nuclear industry. Extensive mining of uranium results in large quantities of uranium in the mill tailing ponds near the uranium mining sites which can potentially come into contact with the environment. Moreover, U(VI) can also be used as an analogue of hexavalent high specific activity actinides, viz., Np(VI) and Pu(VI). Thus, migration of U(VI) in aquatic environment is important and its mobility is dependent upon its chemical properties. Under normal atmospheric conditions, the most stable oxidation state of uranium is +6 and it exists

as uranyl ion which is a hard acid and can interact with wide variety of complexants and sorbents existing in nature.

Silica constitutes almost 60 % mass of the Earth's crust. In silica, Si has tetrahedral coordination with 4 oxygen atoms surrounding a central Si atom. In each of the most thermodynamically stable forms of silica, on average, all 4 oxygen atoms of the  $\text{SiO}_4$  tetrahedra are shared with others, yielding the net chemical formula  $\text{SiO}_2$ . Silica is one of the most common constituents of the minerals viz., feldspar, quartz, etc., (constituents of granitic rocks) as well as clays, such as, bentonite, montmorillonite, etc., which are being proposed as backfill materials in the deep geological repository. As silica constitute a major constituent of the rocks, sediments, soil and clays, understanding the interaction of actinides with simple mineral oxide  $\text{SiO}_2$  will help in getting insight into their migration behaviour in geosphere.

There are numerous literature reports on U(VI) sorption by silica ( *Pathak et al., 2007b; Guo et al., 2009b; Gabriel et al., 2001; Fouchard et al., 2004b; Drot et al., 2007; Batuk et al., 2011; Sylwester et al., 2000; Reich et al., 1996; Wang et al., 2005; Lehmann et al., 2008*). Sorption of U(VI) on hydrous silica at pH 2.5 was found to be dependent on the nature of electrolyte (*Pathak et al., 2007b*). Guo.et.al. (*2009b*) quantitatively interpreted U(VI) sorption on silica using mononuclear inner-sphere surface complex  $\equiv\text{SOUO}_2^+$  and a polynuclear innersphere surface complex  $\equiv\text{SO}(\text{UO}_2)_3(\text{OH})_5$  while TRLIF and XPS measurements revealed the existence of  $\equiv\text{SOUO}_2\text{H}_3\text{SiO}_4$  in addition to the two surface complexes mentioned above (*Gabriel et al., 2001; Fouchard et al., 2004b*). However, three surface complexes, viz.,  $\equiv\text{SO}_2\text{UO}_2$ ,  $\equiv\text{SO}_2\text{UO}_2\text{OH}^-$  and  $\equiv\text{SO}_2\text{UO}_2\text{OHCO}_3^{3-}$  have been identified using TRLIF which has been used in SCM to reproduce the sorption profile (*Drot et al., 2007*) while Batuk.et.al. observed only  $\equiv\text{SO}_2\text{UO}_2$  and  $\equiv\text{SO}_2\text{UO}_2\text{OH}^-$  using TRLIF and EXAFS

(*Batuk et al., 2011*). In other EXAFS studies also, adsorption of the uranyl onto the silica was explained by an inner-sphere, bidentate complexation with the surface, with the formation of polynuclear surface complexes occurring at near-neutral pH (*Sylwester et al., 2000; Reich et al., 1996*). Moreover, uranium(VI) silicate minerals boltwoodite, sodium boltwoodite and uranophane were synthesized, characterized and used for identification purposes of uranyl silicate phases that are formed in the environment (*Wang et al., 2005; Lehmann et al., 2008*).

There exist literature reports in which effect of complexing anions on sorption of U(VI) by mineral oxides has been studied (*Payne et al., 1996; Guo et al., 2009c; Boenisch and Traina, 2006; Hongxia et al., 2002, 2009; Pathak et al., 2007c; Alliot et al., 2005c; Redden et al., 2001; Garcia-Gonzalez et al., 2009, 2012; Nero et al., 2011*). Although, the presence of complexing anions modifies the sorption profile of radionuclides on mineral oxides, no general trend on the sorption of U(VI) by the mineral oxides is observed. Phosphate ions enhanced retention of U(VI) on ferrihydrite was observed in the pH range 2-4 (*Payne et al., 1996*). U(VI) sorption on goethite was not affected by presence of carbonate ions (*Guo et al., 2009 c*) where as U(VI) desorption from goethite was enhanced by oxalic acid (*Boenisch and Traina, 2006*). In the presence of complexing anions, such as, phosphate and fulvate, U(VI) transport was found to be retarded in silica column (*Hongxia et al., 2002*) with the sorption being affected by pH, ionic strength and contact time (*Hongxia et al., 2009*). In presence of carboxylic acids, the inhibition of U(VI) sorption on silicate has been attributed to soluble U(VI) carboxylate complexes (*Pathak et al., 2007c*). The enhancement in sorption in presence of complexing anions can be explained in terms of synergic sorption of cationic complexes of radionuclide and the small organic ligands (*Alliot et al., 2005c*), which has been confirmed by EXAFS for U(VI)-citric

acid and goethite system (Redden *et al.*, 2001). In the presence of citric and oxalic acid, the sorption edge for U(VI) on zirconium diphosphate shifted to higher pH and ternary surface complexes were proposed to explain the sorption data (Garcia-Gonzalez *et al.*, 2009) which was ascertained by TRLFS (Garcia-Gonzalez *et al.*, 2012). In contrast, in the case of U(VI)-alumina system, the enhanced sorption was explained by TRLFS in terms of surface precipitation of uranyl phosphate (Nero *et al.*, 2011). Further, there are few studies on the modeling of the sorption data for the ternary actinide-complexing anions-mineral oxides surface wherein ternary surface complexes were used to explain the sorption profile (Stamberg *et al.*, 2003; Singh *et al.*, 2010).

Although there exist large number of studies in literature in which effect of complexing anions have been dealt (Payne *et al.*, 1996; Guo *et al.*, 2009c; Boenisch and Traina, 2006; Hongxia *et al.*, 2002, 2009; Pathak *et al.*, 2007c; Alliot *et al.*, 2005c; Redden *et al.*, 2001; Garcia-Gonzalez *et al.*, 2009, 2012; Nero *et al.*, 2011), SCM in presence of these anions especially for U(VI)-silica system has not been investigated extensively (Stamberg *et al.*, 2003; Singh *et al.*, 2010). Thus, the aim of the present work was to investigate the mechanism of the interaction between U(VI) and silica in presence of the complexing anions, namely, carbonate and citrate, the two common complexing anions present in ground water, through batch sorption experiments, and SCM. There are very few reports on modeling the effect of carbonate on U(VI)-silica system (Stamberg *et al.*, 2003) but the experimental parameters such as U(VI) concentration, ionic strength were different from those fixed in present work. The modeling of the effect of citrate on U(VI)-silica system has been attempted for first time. The effect of concentration and ionic strength on the sorption of U(VI) by silica has also been studied by batch sorption experiments and

subsequently modeled using SCM. The sorption data, for binary and ternary systems, have been modeled with the help of the SCM using FITEQL software (*Heberlin and Westall, 1994*) and corroborated with TRFS for binary system.

## 5.2. Experimental:

### 5.2.1. Materials:

$^{233}\text{U}$  (Half life =  $1.5 \times 10^5$  years) was used as a radiotracer for U(VI) in the batch sorption experiments. The details of preparation of radiotracer are given in Chapter 2. The specific activity of stock solution of  $^{233}\text{U}$  was found to be  $4.0 \times 10^5$  dpm/mL. Wherever high U(VI) concentrations were used, natural U(VI) was added (0.1 M in 0.1 M  $\text{HClO}_4$ ) along with the radiotracer.

The characterization of silica is discussed in chapter 4. Citric acid (Thomas Baker 99.7%) and sodium bicarbonate (Thomas Baker 99.8%) were used to study the effect of complexing anions.

### 5.2.2. Batch Sorption Studies:

The details of the batch sorption experiments have been discussed in Chapter 2. The concentration of silica suspensions was 5 g/L. U (VI) concentration was varied from  $4.47 \times 10^{-7}$  M to  $4.47 \times 10^{-4}$  M and ionic strength was maintained 0.1 M using  $\text{NaClO}_4$ . The polypropylene tubes containing the suspensions were purged with argon to remove  $\text{CO}_2$  and then capped, sealed in polyvinyl chloride (PVC) bags and kept for incubation in a mechanical shaker for a time period of 24 hours which was found adequate for completion of the sorption process (*Pathak et al., 2007c*).

The experiments on ionic strength variation ( $I = 0.01 - 0.1$  M) and effect of carbonate and citrate were carried out at  $[\text{U(VI)}] = 4.47 \times 10^{-6}$  M. For studying the effect of citrate / carbonate, the silica suspensions were first equilibrated with

carbonate / citrate for 48 hours followed by addition of U(VI) and the suspensions were again subjected to 24 hours equilibration.

### **5.2.3. Silica dissolution studies:**

For the determination of dissolved silica, silica suspensions (5 g/L) of varying pH with and without U(VI) ( $4.47 \times 10^{-4}$  M) were equilibrated for 4 and 24 hours, respectively, on a mechanical shaker. The suspensions were centrifuged and the supernatant solutions were assayed for dissolved Si content by ICP-AES. The calibration of the instrument was carried out by 1000 mg/L standard Si solution (Merck) after suitable dilution.

### **5.2.4. TRFS:**

For fluorescence measurements, the sample preparation was similar to batch sorption experiments. After phase separation, concentrated slurry was taken in cuvette for fluorescent measurements. The U(VI) concentration was maintained at  $5 \times 10^{-5}$  M.

## **5.3. Results and Discussion:**

### **5.3.1. Sorption data:**

#### **5.3.1.1. Effect of U(VI) concentration and ionic strength:**

Figure 5.1 shows the data on sorption of U(VI) by silica as a function of pH at different U(VI) concentrations. The sorption increases with the increasing pH of the suspension and remains constant at 100% after pH 4.5 in the case of  $[U(VI)] = 4.47 \times 10^{-7}$  M -  $4.47 \times 10^{-5}$  M. At  $[U(VI)] = 4.47 \times 10^{-4}$  M, the maximum sorption is reached at pH = 5.3. This suggests that the pH edge shifts to higher pH with increasing metal ion concentration. This shifting of the sorption edge to higher pH

with increasing concentration of the metal ion can be explained on basis of the heterogeneity of surface sites (having different affinity) on silica.

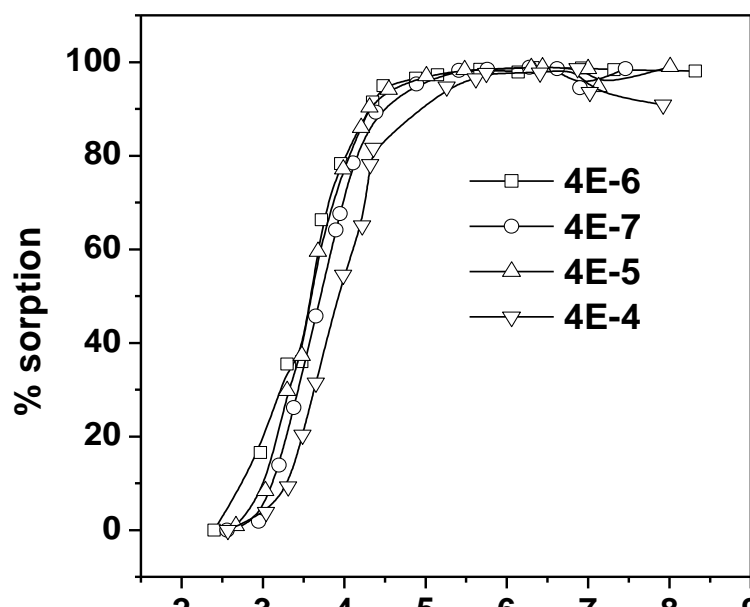


**Figure 5.1** Sorption of U(VI) on silica at varying U(VI) concentration. [U(VI)] =  $4.47 \times 10^{-7}$  M -  $4.47 \times 10^{-4}$  M; Silica = 5 g/L; I = 0.1 M ( $\text{NaClO}_4$ ).

At low initial U(VI) concentration, only high affinity sites (2-3% of total sites) might be occupied (*Dzombak and Morel, 1990*), but with increase in U(VI) concentration both high and low affinity sites may participate in sorption process. Moreover, the total number of silica surface sites available for U(VI) sorption are  $1.2 \times 10^{-3}$  M. Up to U(VI) =  $4.47 \times 10^{-5}$  M, only 3% of the total surface sites are occupied, even when sorption of U(VI) is 100%, and thereby no shift in sorption edge is observed in the concentration range  $4.47 \times 10^{-7}$  to  $4.47 \times 10^{-5}$  as U(VI) sorption takes place preferentially at high affinity sites. However, at U(VI) =  $4.47 \times 10^{-4}$ , 36% of the surface sites are occupied at 100% sorption of U(VI) and thus sorption takes place via both high and low affinity sites which results in shifting of sorption edge to

higher pH. Payne et al. made similar observation for U(VI) sorption on ferrihydrite (Payne, 1999).

Figure 5.2 shows sorption of U(VI) by silica as a function of ionic strength. The ionic strength has negligible effect on percentage sorption which signifies inner sphere complexation. It is worth mentioning that the range in which ionic strength variation has been investigated is limited due to clogging of pH electrode at higher  $\text{NaClO}_4$  concentration.

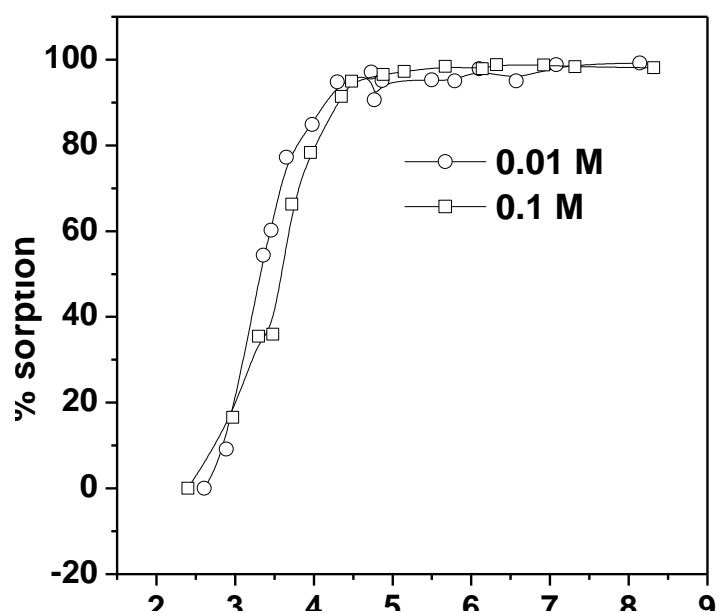


**Figure 5.2** Sorption of U(VI) on silica at varying ionic strength.  $[\text{U(VI)}] = 4.47 \times 10^{-6}$  M; Silica = 5 g/L; I = 0.01, 0.1 M ( $\text{NaClO}_4$ ).

The increase in ionic strength influences three factors, namely, the protonation and de-protonation at the silica surface, the activity of  $\text{UO}_2^{2+}$  in solution and the Coulomb energy. The Coulomb energy and activity coefficient of  $\text{UO}_2^{2+}$  in solution decrease with ionic strength thereby decreasing the sorption. On the other hand, the dissociation constant of surface sites increases with ionic strength and hence will

favour the sorption with increasing ionic strength (*Dzombak and Morel, 1990*). The net effect is that there is a slight decrease in sorption initially with ionic strength. Hongxia et al. also reported that U(VI) sorption on silica is independent of ionic strength in the range 0.002-0.2 M (*Hongxia and Zuyi, 2002*).

### 5.3.1.2. Effect of complexing anions:

Figure 5.3 shows pH dependence of the U(VI) sorption by silica in presence of carbonate and citrate at the ligand concentration equal to  $1.0 \times 10^{-3}$  M. U(VI) sorption remains unaffected by presence of carbonate ions in the pH range studied.

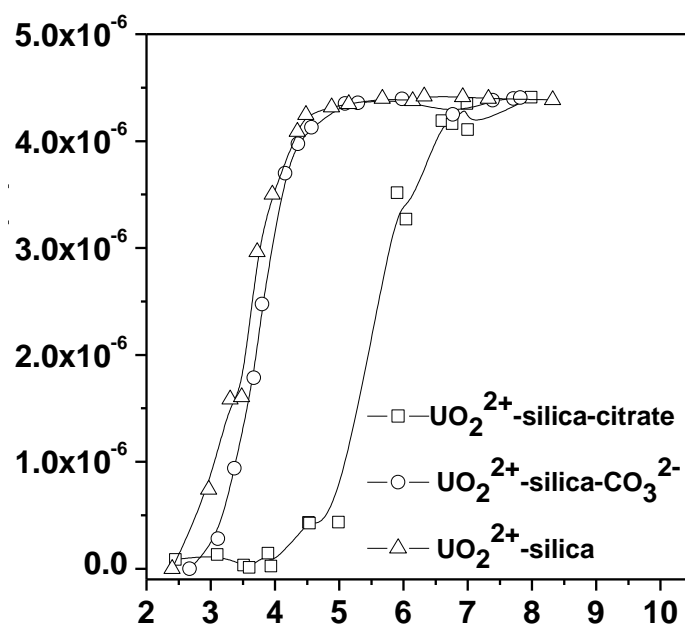


**Figure 5.3** Sorption of U(VI) on silica in presence and absence of citrate/carbonate.

[U(VI)] =  $4.47 \times 10^{-6}$  M; Silica = 5 g/L; [CIT] =  $10^{-3}$  M; [CO<sub>3</sub><sup>2-</sup>] =  $10^{-3}$  M; I = 0.1 M (NaClO<sub>4</sub>).

In presence of carbonate U(VI) forms strong anionic complexes, which are responsible for the drastic reduction in the sorption of U(VI) by mineral oxides

(Payne, 1999). However, such effects are observed at higher pH > 8. In the present work U(VI) sorption has been studied up to pH 8, therefore the effect of carbonate is not evident in present work. Further in some studies the U(VI) sorption is found to decrease only when carbonate concentration is above  $10^{-3}$  M (Stamberg *et al.* 2003; Baik and Hahn, 2001). Stamberg *et al.* (2003) found that in presence of 0.005 M carbonate, U(VI) sorption on mesoporous silica decreased from 100% at pH 6 to 90% at pH 8. However, the carbonate concentration in their case was five times more than that used in present work.

In the presence of citric acid, the sorption is negligible up to pH 5 beyond which it was found to increase sharply reaching close to 100% at pH 6.5. The effect of citric acid on the sorption of U(VI) by silica can be understood by considering the sorption of citric acid on silica. The  $pK_a$  of citric acid (Kantar *et al.*, 2009) suggests that its anionic form dominates in the pH range (3-8), in which the silica surface is negatively charged (PZC < 2.4) (Kumar *et al.*, 2006), thereby resulting in negligible sorption of citric acid on silica. With the increase in pH of the suspension, the complexation of U(VI) by citric acid results in decreased sorption of U(VI) on silica surface. The similar decrease in the sorption of U(VI) on silica and zirconium diphosphate in presence of citric acid has been reported in literature (Pathak *et al.*, 2007c; , Garcia-Gonzalez *et al.*, 2009) which is attributed to U(VI) complexation by citric acid in aqueous phase.

### 5.3.2. Silica dissolution studies:

Figure 5.4 shows Si concentration in the supernatant solutions of silica and U(VI)-silica systems obtained by ICP-AES. The amount of dissolved Si is almost same for equilibration time of 4 and 24 hours in both the systems, indicating that presence of U(VI) has negligible effect on silica dissolution. The U(VI) concentration

$4.47 \times 10^{-4}$  M has been selected as U(VI) assisted silica dissolution, if any, will be maximum in this case. The equilibria characterizing the dissolution of silica is described in chapter 4. The dissolution of silica takes place as a result of hydrolysis of Si-O-Si bonds and increases with pH. The concentration of silicic acid formed owing to the dissolution of silica is of the order of 2 mM, at which mono silicic acid is the dominant species (Panak *et al.*, 2005).

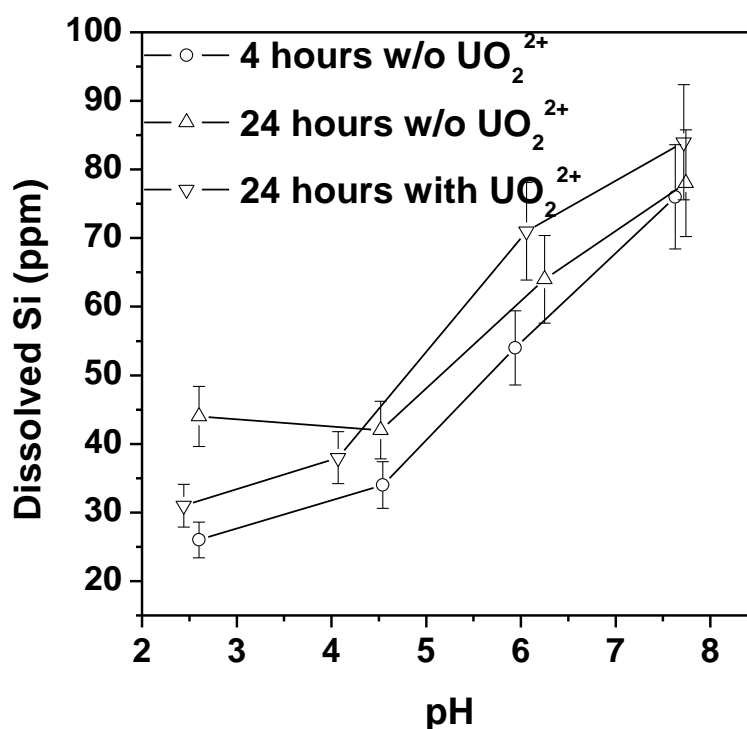


**Figure 5.4** Silica dissolution in presence and absence of U(VI) as function of pH.

$[\text{U(VI)}] = 4.47 \times 10^{-4}$  M; Silica = 5 g/L; I = 0.1 M ( $\text{NaClO}_4$ ).

### 5.3.3. Speciation calculations:

Speciation of U(VI) was calculated using the geochemical code MINTEQA2 (Allison *et al.*, 1999), after incorporating the log K for U(VI) hydroxides, U(VI) carbonate and U(VI) citrate complexes which are listed in Table 5.1.

**Table 5.1** Stability Constants for aqueous complexes

Reaction	$\log \beta^a$
$\text{UO}_2^{2+} + \text{H}_2\text{O} \longrightarrow \text{UO}_2\text{OH}^+ + \text{H}^+$	-5.2 <sup>a,b</sup>
$\text{UO}_2^{2+} + 2\text{H}_2\text{O} \longrightarrow \text{UO}_2(\text{OH})_2 + 2\text{H}^+$	-12.0 <sup>a,b</sup>
$\text{UO}_2^{2+} + 3\text{H}_2\text{O} \longrightarrow \text{UO}_2(\text{OH})_3^- + 3\text{H}^+$	-20.0 <sup>a,b</sup>
$\text{UO}_2^{2+} + 4\text{H}_2\text{O} \longrightarrow \text{UO}_2(\text{OH})_4^{2-} + 4\text{H}^+$	-33.0 <sup>a,b</sup>
$2\text{UO}_2^{2+} + \text{H}_2\text{O} \longrightarrow (\text{UO}_2)_2\text{OH}^{3+} + \text{H}^+$	-2.8 <sup>a,b</sup>
$2\text{UO}_2^{2+} + 2\text{H}_2\text{O} \longrightarrow (\text{UO}_2)_2(\text{OH})_2^{2+} + 2\text{H}^+$	-5.63 <sup>a,b</sup>
$3\text{UO}_2^{2+} + 4\text{H}_2\text{O} \longrightarrow (\text{UO}_2)_3(\text{OH})_4^{2+} + 4\text{H}^+$	-11.9 <sup>a,b</sup>
$3\text{UO}_2^{2+} + 5\text{H}_2\text{O} \longrightarrow (\text{UO}_2)_3(\text{OH})_5^+ + 5\text{H}^+$	-15.56 <sup>a,b</sup>
$3\text{UO}_2^{2+} + 7\text{H}_2\text{O} \longrightarrow (\text{UO}_2)_3(\text{OH})_7^- + 7\text{H}^+$	-31 <sup>a,b</sup>
$4\text{UO}_2^{2+} + 7\text{H}_2\text{O} \longrightarrow (\text{UO}_2)_4(\text{OH})_7^+ + 7\text{H}^+$	-21.9 <sup>a,b</sup>
$\text{UO}_2^{2+} + \text{CO}_3^{2-} \longrightarrow \text{UO}_2\text{CO}_3$	9.7 <sup>a,b</sup>
$\text{UO}_2^{2+} + 2\text{CO}_3^{2-} \longrightarrow \text{UO}_2(\text{CO}_3)_2^{2-}$	17 <sup>a,b</sup>
$\text{UO}_2^{2+} + 3\text{CO}_3^{2-} \longrightarrow \text{UO}_2(\text{CO}_3)_3^{4-}$	21.63 <sup>a,b</sup>
$2\text{UO}_2^{2+} + \text{CO}_3^{2-} + 3\text{H}_2\text{O} \longrightarrow (\text{UO}_2)_2\text{CO}_3(\text{OH})_3^- + 3\text{H}^+$	-1.18 <sup>a,b</sup>
$\text{H}_3\text{CIT} \longrightarrow \text{CIT}^{3-} + 3\text{H}^+$	-14.29 <sup>c</sup>
$\text{H}_2\text{CIT}^- \longrightarrow \text{CIT}^{3-} + 2\text{H}^+$	-11.16 <sup>c</sup>
$\text{HCIT}^{2-} \longrightarrow \text{CIT}^{3-} + \text{H}^+$	-6.39 <sup>c</sup>
$\text{UO}_2^{2+} + \text{CIT}^{3-} \longrightarrow \text{UO}_2\text{CIT}^-$	8.7 <sup>d</sup>
$\text{UO}_2^{2+} + 2\text{CIT}^{3-} \longrightarrow (\text{UO}_2)_2(\text{CIT})_2^{4-}$	21.3 <sup>d</sup>
$\text{H}_4\text{SiO}_4 \longrightarrow \text{H}_3\text{SiO}_4^- + \text{H}^+$	-9.84 <sup>e</sup>
$\text{H}_3\text{SiO}_4^- \longrightarrow \text{H}_2\text{SiO}_4^{2-} + \text{H}^+$	-23.04 <sup>e</sup>
$\text{UO}_2^{2+} + \text{H}_4\text{SiO}_4 \longrightarrow \text{UO}_2\text{H}_3\text{SiO}_4^+ + \text{H}^+$	-1.911 <sup>e</sup>

*a: Grenthe et al.,(1992); b: Guillaumont et al.,(2003); c: Kantar et al.,(2009); d: Payne et al.,(1999); e: Stumm and Morgan, 1996.*

The speciation of U(VI) has been obtained as a function of different parameters viz., U(VI) concentration, pH, ionic strength and presence of complexing anions (carbonate and citrate). As all the solutions were prepared in millipore water which was boiled before use and argon was passed through the suspensions to remove

CO<sub>2</sub>, the carbonate complexation has not been considered in the speciation except when the effect of carbonate was being studied.

Figures 5.5 (a) and 5.6 (a) show that the U(VI) silicate species dominates the U(VI) speciation at low U(VI) concentrations ( $4.47 \times 10^{-7}$  -  $4.47 \times 10^{-6}$  M). It is worth mentioning that at  $[U(VI)] = 4.47 \times 10^{-7}$  M, only mono nuclear hydroxo species  $UO_2OH^+$  are present upto pH 7 along with U(VI) silicate species.

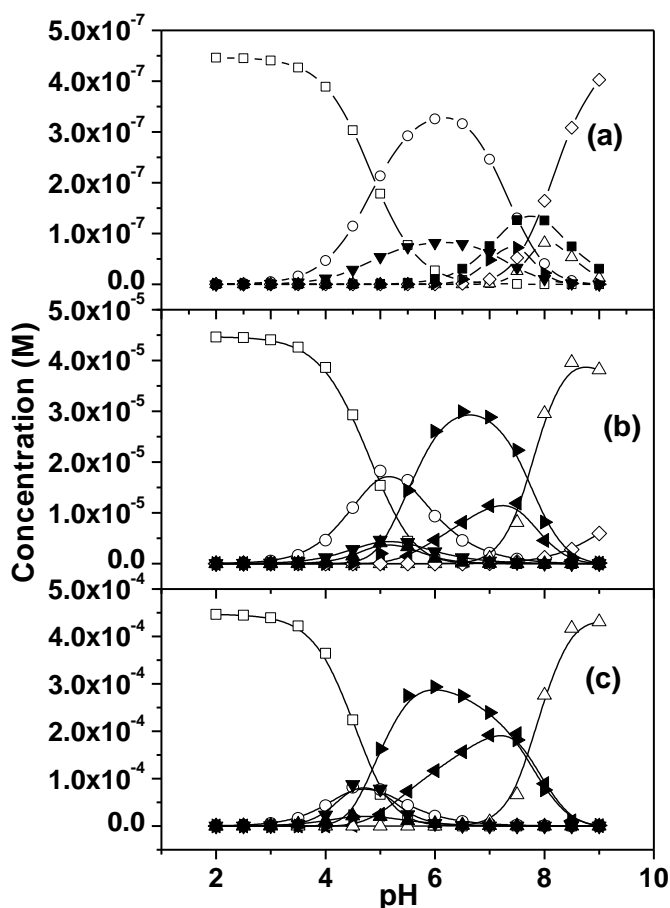


**Figure 5.5** (a) U(VI) speciation in presence of silicic acid as function of pH. (a)  $[U(VI)] = 4.47 \times 10^{-7}$  M;  $I = 0.1$  M NaClO<sub>4</sub>. (b)  $[U(VI)] = 4.47 \times 10^{-5}$  M;  $I = 0.1$  M NaClO<sub>4</sub>. (c)  $[U(VI)] = 4.47 \times 10^{-4}$  M;  $I = 0.1$  M NaClO<sub>4</sub>.  $UO_2^{2+}$  ( $\square$ ),  $UO_2H_3SiO_4$  ( $\circ$ ),  $(UO_2)_4(OH)_7^+$  ( $\blacktriangleleft$ ),  $(UO_2)_3(OH)_7$  ( $\triangle$ ),  $UO_2(OH)_3$  ( $\diamond$ ),  $(UO_2)_2(OH)_2^{2+}$  ( $\blacktriangle$ ),  $UO_2OH^+$  ( $\blacktriangledown$ ),  $(UO_2)_3(OH)_5^+$  ( $\blacktriangleright$ ),  $UO_2(OH)_2$  ( $\blacksquare$ ).

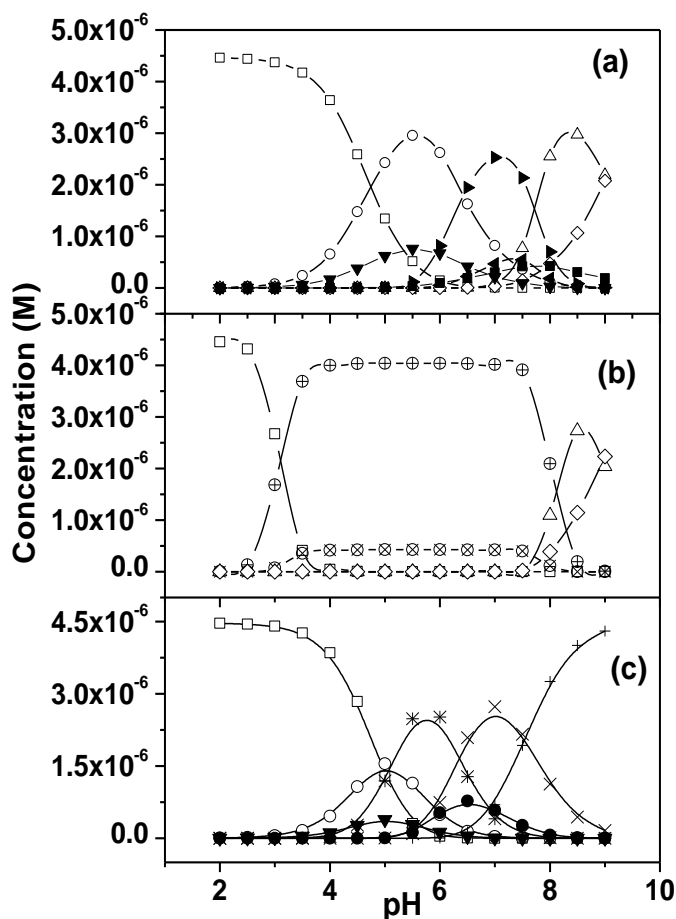


**Figure 5.6** U(VI) speciation in presence of citrate and carbonate as function of pH. (a)

$[U(VI)] = 4.47 \times 10^{-6} \text{ M}$ ;  $I = 0.1 \text{ M NaClO}_4$ . (b)  $[U(VI)] = 4.47 \times 10^{-6} \text{ M}$ ;  $[CIT^{3-}] =$

$10^{-3} \text{ M}$ ;  $I = 0.1 \text{ M NaClO}_4$ . (c)  $[U(VI)] = 4.47 \times 10^{-6} \text{ M}$ ;  $[CO_3^{2-}] = 10^{-3} \text{ M}$ ;  $I = 0.1 \text{ M}$

$\text{NaClO}_4$ .  $UO_2^{2+}$  ( $\square$ ),  $UO_2H_3SiO_4$  ( $\circ$ ),  $(UO_2)_4(OH)_7^+$  ( $\blacktriangleleft$ ),  $(UO_2)_3(OH)_7^-$  ( $\Delta$ ),  $UO_2(OH)_3^-$  ( $\diamond$ ),  $UO_2(OH)_2$  ( $\blacksquare$ ),  $UO_2OH^+$  ( $\blacktriangledown$ ),  $(UO_2)_3(OH)_5^+$  ( $\blacktriangleright$ ),  $UO_2CIT^-$  ( $\oplus$ ),  $UO_2(CIT)_2^{2-}$  ( $\otimes$ ),

$(UO_2)_2CO_3(OH)_3^-$  ( $\bullet$ ),  $UO_2CO_3$  ( $*$ ),  $UO_2(CO_3)_2^{2-}$  ( $\times$ ),  $UO_2(CO_3)_3^{4-}$  ( $+$ ).

However, at  $[U(VI)] = 4.47 \times 10^{-6} \text{ M}$ , the calculations show the existence of trimeric hydroxo species also in addition to the two species present at  $[U(VI)] = 4.47 \times 10^{-7} \text{ M}$ . For higher U(VI) concentrations ( $4.47 \times 10^{-5}$  -  $4.47 \times 10^{-4} \text{ M}$ ), the hydrolysed uranyl species dominate the U(VI) speciation and polynuclear U(VI) complexes  $(UO_2)_4(OH)_7^+$  and  $(UO_2)_3(OH)_5^+$ , become more dominant with increasing

uranyl concentration (figure 5.5 (b) and 5.5 (c)). Moreover at  $[U(VI)] = 4.47 \times 10^{-4}$  M, concentration of  $(UO_2)_4(OH)_7^+$  becomes greater than  $(UO_2)_3(OH)_5^+$ . Thus, with increasing  $[U(VI)]$  concentration, the polynuclear species dominate the U(VI) speciation. The possible precipitation of U(VI) was excluded in the present study, owing to the presence of dissolved silica, which forms strong complexes with U(VI).

In the systems containing complexing anions, the U(VI) speciation is significantly modified owing to complexation of U(VI) by citrate and carbonate. In presence of citrate,  $UO_2CIT^-$  dominates the U(VI) speciation in the pH range 3-8 as shown in figure 5.6 (b), while in presence of carbonate ions U(VI) speciation is dominated by carbonate complexes above pH 5 as depicted by figure 5.6 (c). As carbonate and citrate ions form stronger complexes with U(VI) as compared to hydroxide ion, therefore the hydroxo species of U(VI) are not formed in presence of these complexing anions.

#### 5.3.4. TRFS:

The fluorescence emission spectrum of  $UO_2^{2+}$  originates from the electronic transitions from two excited states at 21,270 and 20,502  $cm^{-1}$  to five vibrational levels in the ground state which have an average spacing of 855  $cm^{-1}$  as shown in Figure 5.7 (*Bells and Biggers, 1968*). The fluorescence spectra are intrinsic property of the U(VI) species in TRFS spectrum, whereas the fluorescence lifetime is dependent on parameters like sample preparation and temperature of the experiment (*Tan et al., 2010*). The fluorescence spectrum of uranyl ions has six characteristic peaks located at around 470, 488, 509, 533, 559, and 585 nm and lifetime is between 1 and 2  $\mu s$  (*Moulin et al., 1998; Kato et al., 1994*).

The excitation spectrum of U(VI) sorbed on silica exhibits maxima at 230 nm, as shown in figure 5.8, which can be attributed to silica assisted excitation of U(VI).

Hence for all the emission spectra and lifetime measurements, the excitation wavelength was fixed at 230 nm.

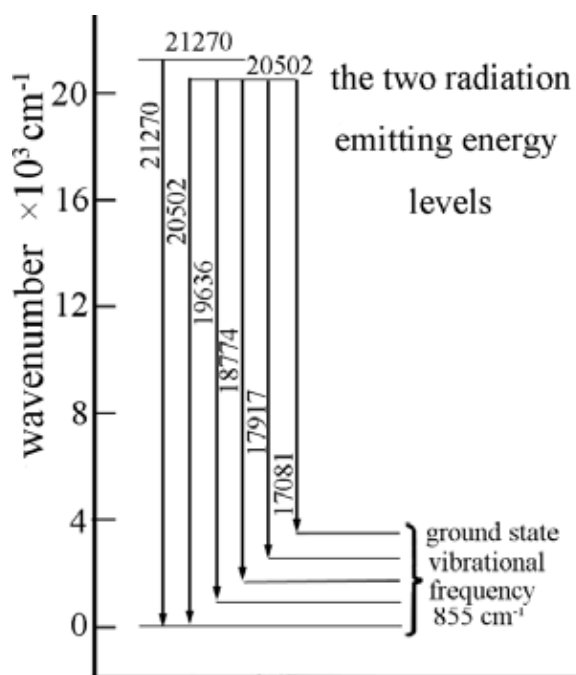


Figure 5.7 Energy level diagram of uranyl ion (Tan et al., 2010)

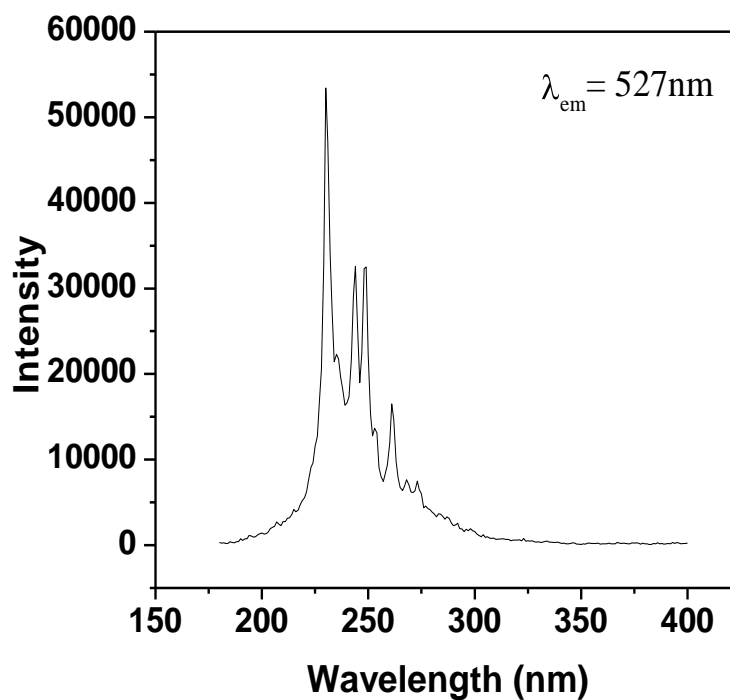
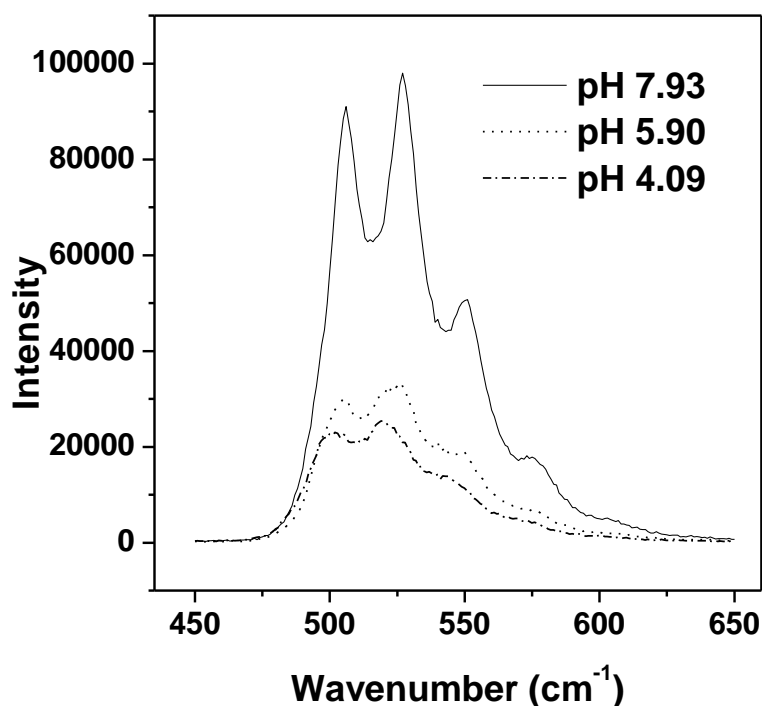


Figure 5.8 Excitation spectra of U(VI) sorbed on silica

Figure 5.9 shows the fluorescence spectrum of U(VI) sorbed onto silica surface at room temperature and varying pH values in the range of 4-8. The spectrum shows several characteristic peaks in 500-600 nm region. The fluorescence intensity increases with pH which is attributed to increase in sorption with pH. The sorbed uranyl species have their peak maxima red shifted (with respect to the uranyl aquo ion) which is attributed to the complexation of the uranyl ion and the surface sites of silica (=Si-OH).



**Figure 5.9** Emission spectra of uranium sorbed on silica at  $\lambda_{\text{ex}} = 230 \text{ nm}$

The lifetime of U(VI) species is dependent on many factors such as sample preparation, presence of quenchers, temperature, in addition to the coordination environment. Therefore, its fluorescence decay profile is only used to gather information about the number of species present. The temporal profile of U(VI) sorbed onto silica showed two lifetimes whose magnitude increases with pH as shown

in table 5.2. Gabriel et al. (2001) observed two decay times values of 170 and 360  $\mu\text{s}$ , for U(VI) sorption on silica, in the entire pH range. In contrast, three lifetimes 65, 180 and 400  $\mu\text{s}$  were identified in the pH range 3-8 for U(VI)-silica system which were attributed to the three different surface species (Drot et al., 2007). In these studies, the observed lifetimes were constant which were assigned to particular species. However, in characterization of uranium(VI) sorbed on calcium silicate hydrate phases, number of lifetime components were used as a signature of number of species present (Tits et al., 2011). Thus, two lifetime values obtained at each pH were used to extract emission spectra of the respective components.

Since the emission characteristics of the two species remained same in the entire pH range, it suggests the existence of two sorbed uranyl species on silica surface. The representative spectra of two components along with the fitted peaks (for each case) are shown in figure 5.10. A pure electronic transition at  $20015\text{ cm}^{-1}$  for short lived species and at  $19912\text{ cm}^{-1}$  for long lived species is followed by a coupling of the O=U=O vibrations resulting in the other peaks in the spectrum. Larger red shift observed for long-lived species suggests a stronger equatorial bonding for the same in comparison to short lived species.

**Table 5.2** Lifetime data of uranium sorbed on silica

pH	$\tau_1$ (%)	$\tau_2$ (%)	$\chi^2$
4.1	120 (64)	237 (36)	5.2
4.6	129 (66)	294 (34)	5.1
5.9	175 (45)	442 (55)	5.2
6.8	231 (31)	547 (69)	3.7
7.9	287 (18)	606 (82)	3.4

The table 5.3 gives the characteristic peak positions of two components along with that for aquo ion for comparison. The information obtained from fluorescence spectra was used to constrain the fitting in SCM for  $U(VI) = 4.47 \times 10^{-5}$  M. As xenon lamp was used as a excitation source, surface complexes with lower  $U(VI)$  concentration could not be investigated.

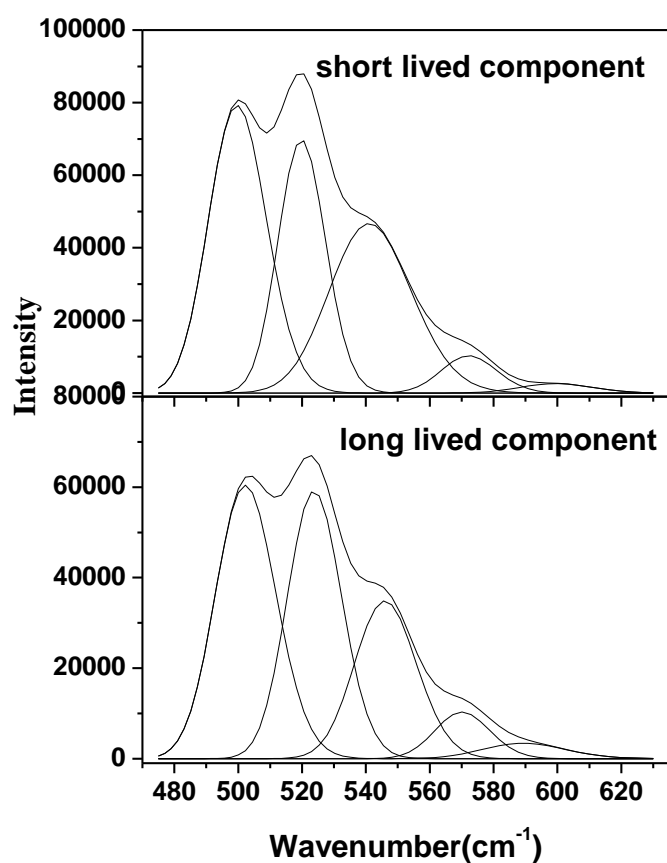


**Figure 5.10** Deconvoluted fluorescence emission spectra of short and long lived component

**Table 5.3** Peak maxima of two components for  $UO_2^{2+}$  sorbed on silica

Sample	$\nu$ ( $cm^{-1}$ )
Short lived species ( $\tau_1$ )	20015,19238,18484,17477,16684
Long lived species( $\tau_2$ )	19912,19092,18316,17542,16973
$UO_2^{2+}$ ion (pH) ( <i>Bells and Biggers, 1968</i> )	21276,20492,19646,18761,17889,17094

### 5.3.4.1. Determination of number of water molecules:

An attempt was made to obtain the information about the structure of the sorbed species by correlating the difference among the frequencies of different peak positions in the emission spectrum, which is equivalent to symmetric stretching vibrational frequency ( $\nu_1$ ), to the number of OH groups in the coordination sphere of  $\text{UO}_2^{2+}$  ion.

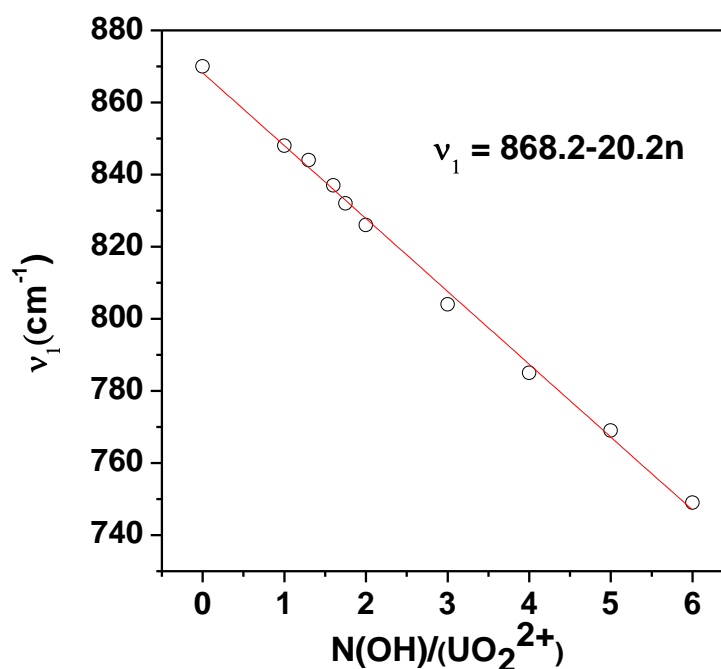


**Figure 5.11** Correlation between  $\nu_1$  and number of OH groups attached to uranyl ion

Bartlett and Cooney (1989) used Raman spectroscopy to determine symmetric stretching frequency ( $\nu_1$ ) for series of uranium containing zeolites having different number of OH groups. In addition,  $\nu_1$  and  $\nu_3$  for uranyl aquo complexes was measured by Lefevre et al. (2008) and made correlation between the  $\nu_1$  and  $\nu_3$ , and the number of OH groups and  $\nu_3$ . Using the above two correlation we constructed relationship between  $\nu_1$  and number of OH groups. The plot of  $\nu_1$  vs the  $N(\text{OH})/ \text{UO}_2^{2+}$ , which essentially gives the information about the number of OH groups around  $\text{UO}_2^{2+}$  ion is shown in figure 5.11.

The symmetric stretching vibrational frequency obtained by subtracting the frequency of peak position in emission spectra was used to deduce the number of OH groups around sorbed uranyl species which were associated with different lifetimes, namely  $\tau_1$  and  $\tau_2$  as shown in table 5.4.

**Table 5.4**  $\Delta\nu$  ( $\text{cm}^{-1}$ ) and  $N(\text{OH}/\text{UO}_2^{+2})$  of uranium sorbed on silica at different pH

pH	Species 1		Species 2	
	$\Delta\nu$ ( $\text{cm}^{-1}$ )	$N(\text{OH}/\text{UO}_2^{+2})$	$\Delta\nu$ ( $\text{cm}^{-1}$ )	$N(\text{OH}/\text{UO}_2^{+2})$
4.1	800	3.5	819	2.5
4.6	768.5	4.9	798	3.5
5.9	786.6	3.9	784.5	4.1
6.8	812	2.8	803.5	3.2
7.93	774	4.6	793	3.7

As is evident from the table, sorbed uranyl species corresponding to  $\tau_1$  has 4-5 OH groups while the species corresponding to  $\tau_2$  has 3-4 OH groups per uranyl ion. The scatter in the value of number of OH groups for same species can be attributed to the broad line width of xenon lamp which has been used as the excitation source for present studies. Thus, the information obtained from TRFS has been used to constrain the SCM as discussed in section 5.3.5.1 (iii).

### 5.3.5. SCM:

The data of U(VI) sorption by silica as a function of pH were analysed in the framework of surface complexation model (SCM) to infer about the mechanism of the sorption process. The fundamentals of SCM are discussed in chapter 2. In making choices for the surface species to be optimized in SCM, the approach adopted has been to assume species which will be formed by the interaction of the dominant aqueous species on silica surface. This approach is based on the Linear Free Energy

Relation observed for a wide variety of solids where a linear correlation between the aqueous complexation constant and surface complexation constant exists (*Dzombak and Morel, 1990; Bradbury and Baeyens, 2009b*). Basically, SCM assumes the sorption process occurring between the surface sites and metal ions similar to the aqueous complexation reaction and applies similar mass balance and mass action conditions to sorption reactions.

Formation of surface species may involve monodentate or bidentate binding of U(VI) with silica sites. In the two models considered for the fitting of the sorption data of the present study, species forming through mononuclear monodentate binding constitute the model 1 while model 2 comprises of species having bidentate mononuclear binding of U(VI) with silica sites. The different types of surface binding (monodentate and bidentate) by U(VI) onto silica surface have been considered in view of the divergent literature reports on U (VI) sorption profiles (*Guo et al.,2009b; Missana et al.,2003*).

### 5.3.5.1. SCM of binary systems:

(i)  $[\text{UO}_2^{2+}] = 4.47 \times 10^{-7} \text{ M}$ :

At  $[\text{UO}_2^{2+}] = 4.47 \times 10^{-7} \text{ M}$ ,  $\text{UO}_2^{2+}$  and  $\text{UO}_2\text{H}_3\text{SiO}_4^+$  are the dominant aqueous species in the pH range 2.0 - 7.5 (figure 5.5 (a)). Surface complexation reactions for these species with silica sites can be described as,



Fitting of the sorption data with model 1 considering monodentate mononuclear uranyl surface  $\equiv\text{SiOUO}_2^{2+}$  and monodentate mononuclear uranyl silicate surface complex  $\equiv\text{SiOUO}_2\text{H}_3\text{SiO}_4$  did not converge. However, good fit was observed

with only silicate surface complex. Fitting carried out as per model 2 considering the bidentate mononuclear uranyl complexes (as in EXAFS studies (*Sylwester et al., 2000*)), could successfully fit the sorption data; but the better fit (based on WSOS/DF) was observed with  $(\equiv\text{SiO})_2\text{UO}_2$  in comparison to (1)  $(\equiv\text{SiO})_2\text{UO}_2$  and  $(\equiv\text{SiO})_2\text{UO}_2\text{H}_3\text{SiO}_4^-$  and (2) only  $(\equiv\text{SiO})_2\text{UO}_2\text{H}_3\text{SiO}_4^-$  cases. Thus, the preferred complexation reaction can be written as

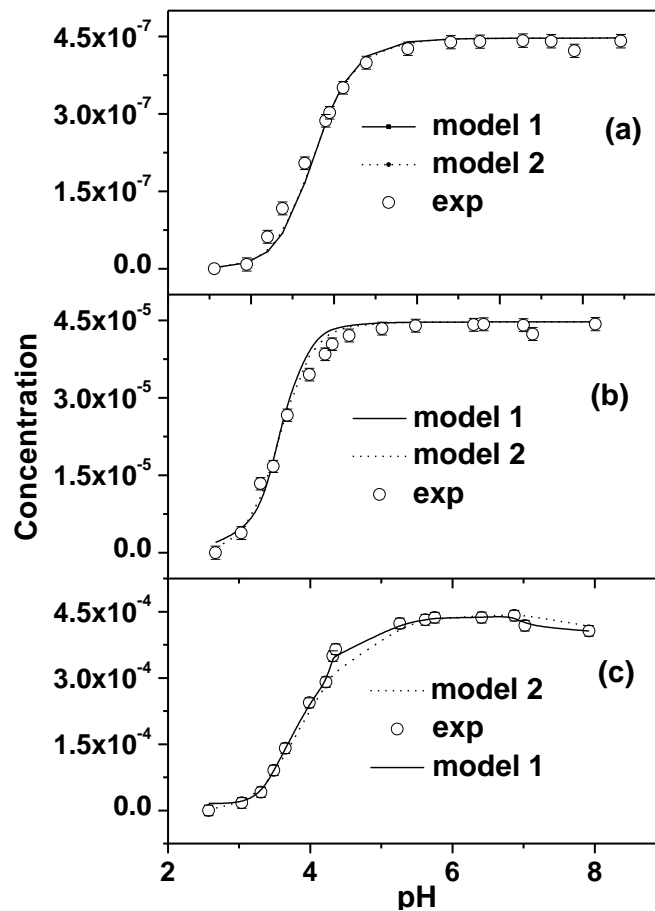
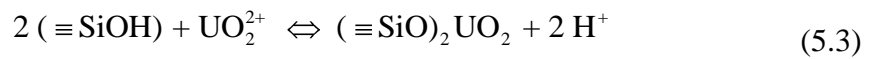


**Figure 5.12** SCM of U(VI) sorption by silica using Model 1 and 2. (a)  $[\text{U(VI)}] = 4.47 \times 10^{-7} \text{ M}$ ;  $m/v = 5 \text{ g/L}$ ;  $I = 0.1 \text{ M NaClO}_4$ . (b)  $[\text{U(VI)}] = 4.47 \times 10^{-5} \text{ M}$ ;  $m/v = 5 \text{ g/L}$ ;  $I = 0.1 \text{ M NaClO}_4$ . (c)  $[\text{U(VI)}] = 4.47 \times 10^{-4} \text{ M}$ ;  $m/v = 5 \text{ g/L}$ ;  $I = 0.1 \text{ M NaClO}_4$ .

Figure 5.12 (a) shows the sorption data along with the surface complexation modeled data using  $\equiv\text{SiOUO}_2\text{H}_3\text{SiO}_4$  and  $(\equiv\text{SiO})_2\text{UO}_2$  surface species in model 1 and 2, respectively for  $[\text{UO}_2^{2+}] = 4.47 \times 10^{-7}$  M. The log K values along with WSOS /DF obtained from FITEQL 4.0 are given in Table 5.5.

**Table 5.5** Optimized parameter values as obtained from FITEQL fit of  $\text{UO}_2^{2+}$ -silica and  $\text{UO}_2^{2+}$ -complexing anion – silica system

System (Ionic Strength)	Species	Log K	WSOS/DF
U(VI)-silica (I = 0.1 M) ( $4.47 \times 10^{-07}$ M) (Model 1)	$\equiv\text{SiOUO}_2\text{OSi}(\text{OH})_3$	-2.86	15.2
U(VI)-silica (I = 0.1 M) ( $4.47 \times 10^{-07}$ M) (Model 2)	$(\equiv\text{SiO})_2\text{UO}_2$	-2.58	2.05
U(VI)-silica (I = 0.1 M) ( $4.47 \times 10^{-06}$ M) (Model 1)	$\equiv\text{SiOUO}_2^+$ $\equiv\text{SiOUO}_2\text{OSi}(\text{OH})_3$ $\equiv\text{SiO}(\text{UO}_2)_3(\text{OH})_5$	-1.90 -2.86 -9.51	1.17
U(VI)-silica (I = 0.1 M) ( $4.47 \times 10^{-06}$ M) (Model 2)	$(\equiv\text{SiO})_2\text{UO}_2$	-2.24	3.26
U(VI)-silica (I = 0.1 M) ( $4.47 \times 10^{-05}$ M) (Model 1)	$\equiv\text{SiOUO}_2^+$ $\equiv\text{SiO}(\text{UO}_2)_3(\text{OH})_5$	-1.90 -12.75	2.57
U(VI)-silica (I = 0.1 M) ( $4.47 \times 10^{-05}$ M) (Model 2)	$(\equiv\text{SiO})_2\text{UO}_2$	-2.29	1.64
U(VI)-silica (I = 0.1 M) ( $4.47 \times 10^{-04}$ M) (Model 1)	$\equiv\text{SiOUO}_2^+$ $\equiv\text{SiO}(\text{UO}_2)_3(\text{OH})_5$	-1.90 -16.59	4.25
U(VI)-silica (I = 0.1 M) ( $4.47 \times 10^{-04}$ M) (Model 2)	$(\equiv\text{SiO})_2\text{UO}_2$	-2.49	1.86
U(VI)-silica (I = 0.2 M) ( $5 \times 10^{-05}$ M) (Model 1) (a)	$\equiv\text{SiOUO}_2^+$ $\equiv\text{SiO}(\text{UO}_2)_3(\text{OH})_5$	-1.92 -12.84	1.55
U(VI)-silica (I = 0.2 M) ( $5 \times 10^{-05}$ M) (Model 2) (a)	$(\equiv\text{SiO})_2\text{UO}_2$	-2.27	1.08
U(VI)-silica (I = 0.1M) ( $4.47 \times 10^{-06}$ M) $10^{-3}$ M $\text{CO}_3^{2-}$	$(\equiv\text{SiO})_2\text{UO}_2$ $(\equiv\text{SiO})_2\text{UO}_2\text{CO}_3^{2-}$	-2.37 -3.82	0.67
U(VI)-silica (I = 0.1M) ( $4.47 \times 10^{-06}$ M) $10^{-3}$ M $\text{Cit}^{3-}$	$(\equiv\text{SO})_2\text{UO}_2\text{Cit}^{3-}$	2.77	2.22

a: Pathak et al., 2007c

(ii)  $[\text{UO}_2^{2+}] = 4.47 \times 10^{-6} \text{ M}$ :

In aqueous speciation for  $[\text{UO}_2^{2+}] = 4.47 \times 10^{-6} \text{ M}$ ,  $\text{UO}_2^{2+}$ ,  $\text{UO}_2\text{H}_3\text{SiO}_4^+$  and  $(\text{UO}_2)_3(\text{OH})_5^+$  are the major species (figure 5.6 (a)) and have been employed to fit the sorption data.

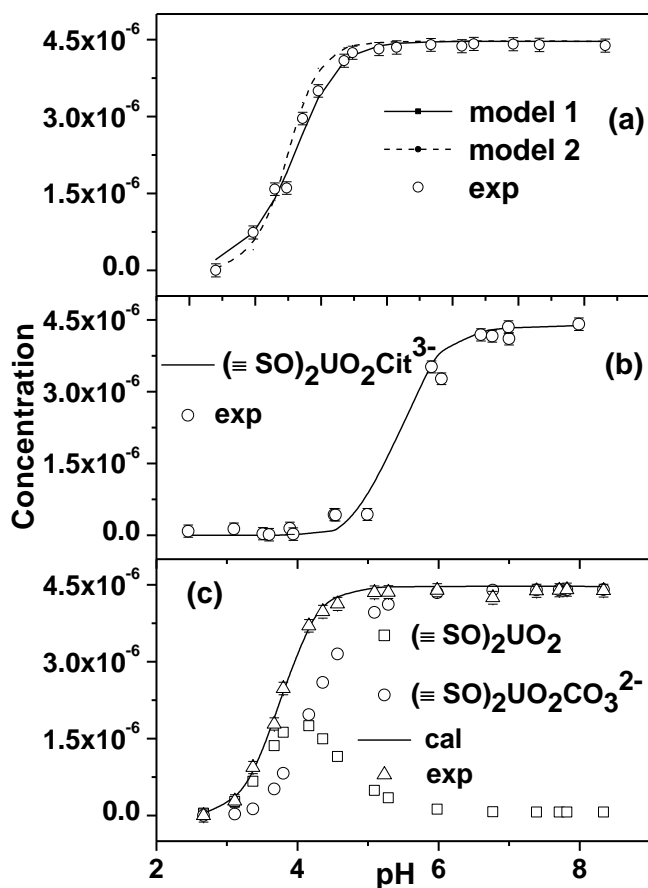


**Figure 5.13** SCM of U(VI) sorption by silica in presence and absence of complexing anions. (a)  $[\text{U(VI)}] = 4.47 \times 10^{-6} \text{ M}$ ;  $m/v = 5 \text{ g/L}$ ;  $I = 0.1 \text{ M NaClO}_4$  using Model 1 and Model 2. (b)  $[\text{U(VI)}] = 4.47 \times 10^{-6} \text{ M}$ ;  $m/v = 5 \text{ g/L}$ ;  $[\text{CO}_3^{2-}] = 1 \times 10^{-3} \text{ M}$ ;  $I = 0.1 \text{ M NaClO}_4$ . (c)  $[\text{U(VI)}] = 4.47 \times 10^{-6} \text{ M}$ ;  $m/v = 5 \text{ g/L}$ ;  $[\text{CIT}] = 1 \times 10^{-3} \text{ M}$ ;  $I = 0.1 \text{ M NaClO}_4$ .

Successful fitting of the sorption data was achieved with  $\equiv\text{SiOUO}_2^+$ ,  $\equiv\text{SiO}(\text{UO}_2)_3(\text{OH})_5$ , and  $\equiv\text{SiOUO}_2\text{H}_3\text{SiO}_4$  as sorbent on silica surface. Choice of only

silicate or hydrolyzed complex along with  $\equiv\text{SiOUO}_2^+$ , while fitting leads to convergence but with higher WSOS/DF value.

It is worth mentioning that while considering the multinuclear species for sorption, the mass action and mass balance coefficients are not the same. The surface complexation reactions for all the species are given by equation (5.1), (5.2) and (5.4).



In model 2, only the bidentate uranyl surface complex ( $(\equiv\text{SiO})_2\text{UO}_2$ ) yielded satisfactory fit at  $[\text{UO}_2^{2+}] = 4.47 \times 10^{-6} \text{ M}$  (figure 5.13 (a)) whereas the inclusion of silicate surface complex in the fitting did not lead to convergence. Since the U(VI) speciation in aqueous phase is same at  $I = 0.1 \text{ M}$  and  $I = 0.01 \text{ M}$ , similar observations were made for  $[\text{UO}_2^{2+}] = 4.47 \times 10^{-6} \text{ M}$  at  $I = 0.01 \text{ M}$ .

**(iii)  $[\text{UO}_2^{2+}] = 4.47 \times 10^{-5} \text{ M}$ :**

At  $[\text{UO}_2^{2+}] = 4.47 \times 10^{-5} \text{ M}$ ,  $\text{UO}_2^{2+}$  and  $(\text{UO}_2)_3(\text{OH})_5^+$  dominate the speciation in pH range of interest (figure 5.5(b)). Uranyl silicate complex ( $\text{UO}_2\text{H}_3\text{SiO}_4^+$ ) forms over pH 4 - 7, and its composition is maximum (~20%) at pH 5. Since from fluorescence studies it was evident that two surface complexes are formed, permutations involving two of above mentioned species were tried at a time and the best fit was obtained with surface species forming with  $\text{UO}_2^{2+}$  and  $(\text{UO}_2)_3(\text{OH})_5^+$  only. The surface complexation reactions for both the species are given by equation (5.1) and (5.4). In model 2, the mononuclear bidentate uranyl surface complex was able to fit sorption data satisfactorily in this case. However, TRFS data supports model 1 as it reveals the presence of two species. The sorption data along with both the fits are shown in figure 5.12 (b). Thus, the mononuclear monodentate uranyl surface complex  $\equiv\text{SiOUO}_2^+$  and polynuclear surface complex will mathematically have 4-5 and 9-12

OH groups. However since  $\equiv\text{SiO}(\text{UO}_2)_3(\text{OH})_5$  is the tri nuclear species, all uranyl ion will not possess same number of OH groups. Thus, one cannot correlate symmetric stretching vibrational frequency with number of OH groups directly in case of polynuclear sorbed species as each of the uranyl will be in different coordination environment.

**(iv)  $[\text{UO}_2^{2+}] = 4.47 \times 10^{-4} \text{ M}$ :**

At  $[\text{UO}_2^{2+}] = 4.47 \times 10^{-4} \text{ M}$ ,  $\text{UO}_2^{2+}$ ,  $(\text{UO}_2)_3(\text{OH})_5^+$  and  $(\text{UO}_2)_4(\text{OH})_7^+$  are the major species present in the aqueous phase (figure 5.5(c)). The  $\equiv\text{SiOUO}_2^+$  and polynuclear surface complex  $\equiv\text{SiO}(\text{UO}_2)_3(\text{OH})_5$  were able to explain the sorption data.

It is evident from Table 5.5 that  $\log K$  for  $\equiv\text{SiOUO}_2^+$  and  $\equiv\text{SiO}(\text{UO}_2)_3(\text{OH})_5$  decrease as U(VI) concentration is increased from  $4.47 \times 10^{-5} \text{ M}$  to  $4.47 \times 10^{-4} \text{ M}$ . Thus even though sorption data for  $4.47 \times 10^{-4} \text{ M}$  is successfully explained by considering one type of surface sites, the decrease in  $\log K$  reflects the involvement of more than one type of surface sites thereby demonstrating the heterogeneous character of silica surface sites. The mononuclear bidentate uranyl surface complex fitted the sorption data better than surface complexes  $\equiv\text{SiOUO}_2^+$  and  $\equiv\text{SiO}(\text{UO}_2)_3(\text{OH})_5$  (figure 5.12(c)).

The sorption data over the varying pH, ionic strength and metal concentration can, thus, be modeled using two approaches, mono-dentate uranyl surface complexes (model 1) and bi-dentate uranyl surface complex (model 2). In the model 1, uranyl surface complexes varied depending upon the predominance of the aqueous uranyl species. At lower metal concentration dissolved silicate participate in the formation of surface complex whereas at higher concentration hydroxide complexes of uranyl bind

with silica surface sites. In the model 2,  $(\equiv\text{SiO})_2\text{UO}_2$  fits the sorption data in all the experimental conditions.

The proposed surface complexation models were evaluated using literature data on sorption of U(VI) by silica. All other parameters, except the surface area and surface site density, were kept same as that used in modeling the data in present work. The data by Pathak et al. (2007c) is referred to as U(VI) ( $5 \times 10^{-5}$  M) sorption on silica (3 g/L) at 0.2 M  $\text{NaClO}_4$ . The SCM fits are closer to the experimental data in case of model 1 as compared to model 2 (figure 5.14). Further, the log K obtained for surface complexes are close to that obtained with  $4.47 \times 10^{-05}$  M (Table 2). Guo et al. (2009 b) modeled U(VI) sorption on silica (50 g/L) as a function of U(VI) concentration ( $5 \times 10^{-5}$  M and  $1 \times 10^{-4}$  M) and found that  $\text{SiOUO}_2^+$  and  $\text{SiO}(\text{UO}_2)_3(\text{OH})_5$  explain the sorption data accurately which are similar to species used in model 1 in present studies.

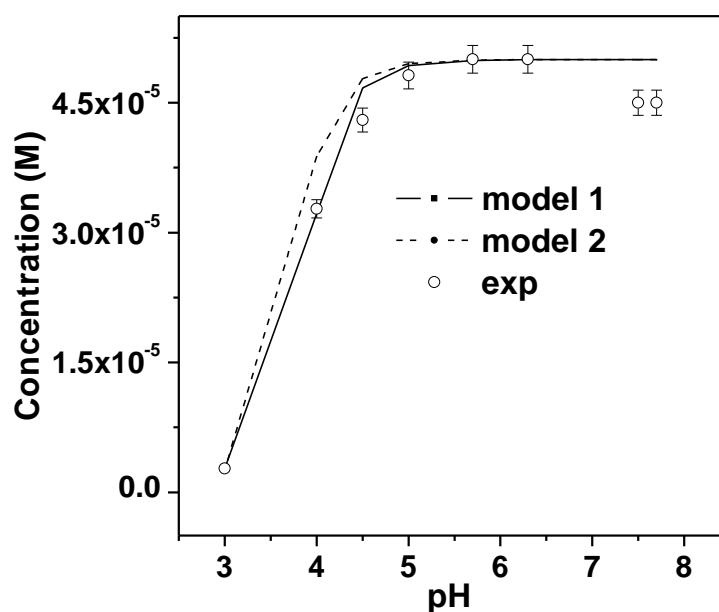


**Figure 5.14** SCM of U(VI) sorption by silica using Model 1 and Model 2 along with sorption data. (a)  $[\text{U(VI)}] = 5 \times 10^{-5}$  M;  $m/v = 3$  g/L;  $I = 0.2$  M  $\text{NaClO}_4$ . Data taken from reference (Pathak et al., 2007c)

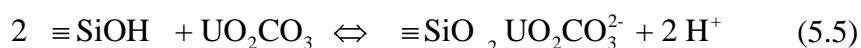
However, the log K values obtained in present studies for mononuclear monodentate uranyl surface complex  $\equiv\text{SiOUO}_2^+$  and polynuclear surface complex  $\equiv\text{SiO}(\text{UO}_2)_3(\text{OH})_5$  are found to be different than those obtained by Guo et al (2009 b). The possible reasons for the observed discrepancies are the differences in surface area and site densities of silica used in the two studies. Moreover, Guo et al. (2009 b) has not taken into account the dissolution of silica which might be responsible for the different values of log K.

In view of present results and those by the evaluation of the literature data, it can be concluded that Model 1 offers a better fit to the different data sets. Thus model 1 is better than model 2 as it reflects more clearly the effects of changing experimental condition on U(VI) sorption. However, more detailed investigations such as EXAFS, TRILIFS are needed to differentiate the applicability of the two models.

#### 5.3.5.2. SCM of ternary systems:

The sorption data for the ternary system of U(VI) – silica – complexing anions were modeled using similar analogy as that in case of binary system. The speciation diagram of  $[\text{UO}_2^{2+}] = 4.47 \times 10^{-6} \text{ M}$  in presence of  $1 \times 10^{-3} \text{ M}$  carbonate (figure 5.6(c)), shows  $\text{UO}_2^{2+}$  and  $\text{UO}_2\text{CO}_3$  as the major species in the aqueous phase in the pH range 2 - 7 and hence these species were considered while fitting the sorption data. The mono-dentate mono-nuclear surface complexes of these species were unable to fit the sorption data. Based on the consideration that some bi-dentate oxy-anions prefer flat hexagonal arrangement in equatorial plane perpendicular to axial bonds in uranyl ions (Payne, 1999), the mono-nuclear bi-dentate surface complexes of the above species were considered. The corresponding surface complexation reactions are given by equations (5.3) and (5.5) and the sorption data along with the modeled data is

shown figure (5.13(c)). The surface complexation constants for these species are given in Table 5.5.



Gabriel et al. (2001) successfully modeled U(VI) sorption on silica in presence of atmospheric CO<sub>2</sub> using bidentate mononuclear surface complexes. However, Stamberg et al. (2003) proposed mono-nuclear mono-dentate carbonate complexes to explain the U(VI) sorption on silica in presence of 0.005 M carbonate in the pH range 6 - 11. Thus, prediction of different kind of species for similar system suggests the need for detailed spectroscopic studies.

The speciation diagram of [UO<sub>2</sub><sup>2+</sup>] = 4.47 X 10<sup>-6</sup> M in presence of 10<sup>-3</sup> M (Figure 5.6 (b)) citrate shows UO<sub>2</sub>CIT<sup>-</sup> as the dominant species with about 5 % contribution from UO<sub>2</sub>(CIT)<sub>2</sub><sup>2-</sup> towards U(VI) speciation. Attempt was made to fit the sorption data with mono-dentate surface complexes pertaining to the two species but no convergence was obtained. Since citric acid is a triprotic acid with carboxylic groups present on each of the carbon, it should also prefer flat hexagonal arrangement in equatorial plane. The mono-nuclear bi-dentate uranyl citrate surface complex (≡SiO)<sub>2</sub>UO<sub>2</sub>CIT<sup>3-</sup> fitted the sorption data quite well. The surface complexation reaction is given by following equation:



Figure 5.13 (b) shows the experimental and modeled data for ternary system and the log K of the fitted species is given in Table 5.5. Thus, sorption equilibria involve uranium(VI) citrate interaction with the surface sites. In U(VI) sorption studies on zirconium diphosphate, a ternary surface complex (Zr)<sub>2</sub>CitUO<sub>2</sub><sup>2+</sup> has been proposed based on SCM and TRLIFS studies (Garcia-Gonzalez et al., 2012)

The above discussion suggests that SCM of the binary and ternary systems can provide insight into the various phenomena which might take place once the actinides are released into the geological media. Of course, the proposed models have to be validated over wider range of experimental conditions so as to attain the predictive capability with respect to migration of any radionuclide in the environment. Further, the SCM predictions need to be validated by spectroscopic investigations, such as, TRLIFS and EXAFS.

#### 5.4. Conclusions:

Sorption of U(VI) by silica as a function of pH follows the typical 'S' shaped curve with the sorption edge at 4.5, which is shifted to higher value (5.3) with increasing U(VI) concentration. This could be due to the heterogeneity of surface sites on silica. U(VI) sorption is independent of ionic strength indicating the inner sphere surface complexation as the dominant mechanism of sorption. Sorption of U(VI) by silica is significantly affected by the presence of citrate in the pH range of 3 - 6, while carbonate anion does not influence the U(VI) sorption by silica at least up to pH 8. SCM using DLM showed the evolution of different surface complexes as a function of U(VI) concentration. The bidentate mono nuclear surface complex was able to fit the sorption data in entire concentration range. The two modeling approaches were applied to some of the literature data for their evaluation and mononuclear monodentate complexes were able to explain the sorption data better than mononuclear bidentate complexes. Moreover, TRFS revealed the existence of two surface complexes at  $[U] = 5 \times 10^{-5}$  M, which was used to constrain the SCM. In case of ternary systems, U(VI) is sorbed as  $(\equiv\text{SiO})_2\text{UO}_2$  and  $(\equiv\text{SiO})_2\text{UO}_2\text{CO}_3^{2-}$  in presence of carbonate and as  $(\equiv\text{SiO})_2\text{UO}_2\text{Cit}^{3-}$  in presence of citrate.

## **Chapter VI**

# **Sorption of Neptunium on Hematite: Effect of HA**

## 6.1. Introduction:

In this chapter the results of the sorption of neptunium on hematite colloids have been described at varying pH values in absence and presence of HA. Sorption studies were carried out under aerobic and anaerobic conditions. The stability constant of Np(V)-humate complex ( $\log \beta$ ) and sorption of HA on hematite was also determined which was used to interpret the neptunium sorption profile on hematite.  $^{239}\text{Np}$ ,  $\beta/\gamma$  emitting radioisotope, was used as a tracer for neptunium.

Migration behaviour of actinides in aquatic environment is related to the form in which these are introduced into the environment, which in turn depend upon their concentration, oxidation state, pH, Eh, ionic strength and presence of complexing anions (inorganic and organic) (*Choppin, 2006*). Owing to the small difference in the redox potential of the different oxidation states of actinides, more than one oxidation state of U, Np and Pu can coexist in solution, which makes their chemistry quite complex (*Choppin, 2005*). One of the important components of aquatic environment which influence the metal ion speciation is natural colloids (*Kersting et al., 1999*). Actinides when released into the environment may form colloids by themselves (true colloids) or may get sorbed onto the inorganic colloids present in the aquatic system and thus form pseudo colloids (*Silva and Nitsche, 1995*). Colloid facilitated transport of actinides is further affected by the presence of HS, which can enhance actinide migration (*Choppin, 1999*). Formation of true colloids of actinides during their release in the environment is unlikely, owing to the extremely low concentration in nature. Hence the most likely process of colloid formation is the sorption of actinides on natural oxyhydroxide colloids of silicon, iron, aluminum, etc. The formation of these radionuclides bearing natural colloids (e.g., hematite, magnetite, goethite, etc) is one of the common modes of transport in the aquatic environment (*Marmier, 2002*).

$^{237}\text{Np}$  is one of the most important radionuclides present in HLW left after the reprocessing of spent nuclear fuel. The long half life ( $T_{1/2} = 2.14 \times 10^6$  y) and alpha activity of  $^{237}\text{Np}$  make it one of the most hazardous contaminants in the geosphere in the long term. This is particularly due to the fact, unlike plutonium and americium, which exist as Pu(IV) and Am(III), respectively, neptunium as Np(V) is not hydrolysed under the conditions of aquatic environment and hence is more mobile (Kim, 1986).

Hematite occurs as a secondary mineral formed by weathering processes in soil, along with other iron oxides or oxyhydroxides such as goethite, is responsible for the red color of many tropical, ancient, and highly weathered soils. It can precipitate out of water and is thus found in form of layers at the bottom of a lake, spring, or other standing water. Hematite ( $\text{Fe}_2\text{O}_3$ ) has hexagonal (rhombohedral) crystal system constructed of  $\text{Fe}^{3+}$  ion surrounded by six oxygen atoms not at the corners of a regular octahedron.

Several studies on the sorption of neptunium on naturally occurring iron minerals (hematite, magnetite, goethite) have been published in the past (Nakayama and Sakamoto, 1991; Tochiyama et al., 1995; Sakamoto et al., 1994; Neroa et al., 2004; Runde et al., 2002; Tinnacher et al., 2012; Nagasaki et al., 1998; Nakata et al., 2001, 2002, 2004; Snow et al., 2013; Li and Kaplan, 2012). These iron bearing minerals show varying sorption properties over a wide pH range, including in some cases the reduction of Np(V) to Np(IV). It was also found that the sorption of neptunium depends on the crystallinity of mineral and is more in case of goethite as compared to hematite and magnetite (Nakayama and Sakamoto, 1991; Tochiyama et al., 1995). Moreover, redistribution studies of neptunium during the alteration of amorphous ferrihydrite to hematite revealed the drastic decrease in sorption due to

increasing crystallinity (Sakamoto *et al.*, 1994). In contrast, sorption of neptunium on iron rich silicates was found to be independent of Fe/Si ratio (Neroa *et al.*, 2004). Runde *et al.* (2002) found Np(V) uptake on hematite to be much less than Pu(V) uptake indicating the involvement of Pu(V) - Pu(IV) reductive sorption process. Kinetics of sorption and desorption of neptunium on hematite and magnetite showed that equilibrium was attained in 1 h while the equilibrium between various chemical forms of sorbed Np was achieved in about 1 week (Nakata *et al.*, 2002). Moreover modeling of the kinetics data revealed that aging process plays a major role in attainment of equilibrium (Tinnacher *et al.*, 2012) and surface diffusion coefficient determination showed that the sorption equilibrium of neptunium on the internal surface sites was very slow process (Nagasaki *et al.*, 1998). Surface assisted reduction of neptunium takes place on magnetite under anaerobic conditions (Nakata *et al.*, 2002) which was found to be 1000 times faster than the Np(V) reduction by Fe(II) ions in homogeneous solution (Nakata *et al.*, 2001, 2004). Neptunium sorption on goethite from attomolar to micromolar concentrations was found to be linear below  $10^{-11}$  M, above which non-linear behaviour was observed which was modeled using 2-site and 3-site Langmuir models (Snow *et al.*, 2013). Recently, Li. and Kalpan (2012) reviewed the sorption studies of neptunium on iron (hydr)oxides. Further, there are few studies on the modeling and spectroscopic investigations of neptunium sorption on iron oxides and hydroxides (Girvin *et al.*, 1991; Kohler *et al.*, 1999; Combes *et al.*, 1992; Teterin *et al.*, 2006; Arai *et al.*, 2007). SCM (SCM) of neptunium sorption on amorphous iron oxyhydroxide showed that  $\text{NpO}_2\text{OH}$  was able to reproduce the sorption profile successfully (Girvin *et al.*, 1991). In contrast, Kohler *et al.* (1999) used surface complex pertaining to  $\text{NpO}_2^+$  to explain the neptunium sorption at low site occupancy. However, EXAFS and XPS studies of neptunium sorbed on goethite

showed inner-sphere surface complex of  $\text{NpO}_2^+$  but the authors did not rule out the possibility of surface complex of neptunium hydroxide or carbonate ligands (*Combes et al., 1992; Teterin et al., 2006*). SCM using ternary neptunyl-carbonato surface complex were able to fit neptunium sorption on goethite and hematite for all partial pressures of  $\text{CO}_2$  which was validated by EXAFS (*Arai et al., 2007*).

HS are known to greatly influence the sorption of actinides on colloids. There exists few literature reports in which effect of HS on neptunium sorption on to different mineral oxides and clays have been investigated (*Niitsu et al., 1997; Schmeide and Bernhard, 2010; Artinger et al., 2000; El-Naggar et al., 2000; Pathak and Choppin, 2007 d; Li and Tao, 2003; Perminova et al., 2007; Chunli et al., 2001; Sakamoto et al., 2000; Khasanova et al., 2007; Kalmykov et al., 2008*). Niitsu et al. (1997) studied the effect of HA on the sorption of Np(V) on kaolinite and found that at  $\text{pH} < 8$  the sorption of Np(V) on kaolinite increased in presence of HA while at  $\text{pH} > 8$  no such effect was observed. On contrary, synthetic HA, with pronounced reducing properties, effectively reduces Np(V) to Np(IV) and neptunium uptake was found to be very low in the presence of HA due to Np(IV) humate complexation in solution (*Schmeide and Bernhard, 2010*). The transport of neptunium as humic colloid bound species was facilitated by presence of HA which was also attributed to neptunium reduction followed by formation of Np(IV)-HA complexes (*Artinger et al., 2000*). Similar results were obtained by El Naggar et al. (2000) suggesting the role of HA in influencing the migration of Np in aquatic environment. The presence of HA enhanced the sorption of neptunium on suspended silicates at low pH and decreased the same at  $\text{pH} > 8$  (*Pathak and Choppin, 2007 d*). In contrast, sorption of neptunium on silica and alumina was not affected by HS, which was attributed to low concentrations of HS and relatively higher concentrations of carbonate owing to

relatively strong complexation of carbonate (*Li and Tao, 2003*). Sequestration of aqueous Np(V) and Pu(V) under anaerobic conditions was achieved by using silica gel coated with covalently bound HA (*Perminova et al., 2007*). In an attempt to simulate the migration of actinides through an aquifer, Chunli et al. (*2001*) studied the influence of HA on migration of actinides using the column of soil and showed that introduction of HA into the aquifer enhanced the mobility of Np and Pu while migration of Np(V) in sandy soil and granite was retarded in the presence of HA and enhanced in case of FA. The observed differences may be caused by the difference in the molecular size distribution of the HS (*Sakamoto et al., 2000*). Khasanova et al. (*2007*) demonstrated that addition of HA to the Np(V)-hematite or Np(V)-goethite systems can markedly increase the Np(V) sorption percentage at pH 2–5.5, but has little effect on the Np(V) sorption rate at pH 5.5–10 while the reduction of Np(V) at low pH has been observed by XPS in the ternary system of goethite–HA–neptunium (*Kalmykov et al., 2008*).

No literature existed on the effect of HA on the sorption of neptunium on hematite colloids at the time of commencement of this work. Till date, only one study, other than the present work, on effect of HA on sorption of neptunium on to hematite has been reported in which neptunium concentration is six orders of magnitude higher than that employed in present work (*Khasanova et al., 2007*). With this view, the influence of HA on the sorption of neptunium on hematite colloids both in absence and presence of HA at varying pH values (3-10) was studied. Moreover, ternary system, neptunium-HA-hematite under anaerobic conditions was investigated for the first time by us. The measurements were also carried out under reducing conditions by using sodium dithionite (as a reducing agent). Moreover, stability constants for

Np(V)-HA was determined using Schubert's method and sorption of HA on hematite was ascertained using UV-visible spectrophotometry.

## 6.2. Experimental:

### 6.2.1. Synthesis and characterization of hematite colloids:

The procedure of hematite synthesis is described in chapter 2. The surface charge density of the colloidal suspension of hematite in 0.01 M NaClO<sub>4</sub> was measured by zeta analyzer (Malvern, Zetasizer Nano ZS) based on dynamic light scattering (DLS). The number of surface sites on the hematite powder was determined by titrating the 300 mg of hematite in 50 ml 0.1 M NaClO<sub>4</sub> with standard 0.01M HClO<sub>4</sub> / 0.01 M NaOH. In another experiment titration of the electrolyte (0.1 M NaClO<sub>4</sub>) was carried out. The plots of [H<sup>+</sup>] / [OH<sup>-</sup>] added versus free [H<sup>+</sup>] / [OH<sup>-</sup>] were used to deduce the total number of surface sites (*Marmier and Fromage, 1999*).

### 6.2.2. Characterization of HA:

HA from ACROS (Belgium) was used for present studies. The characterization of HA has been described elsewhere (*Kumar, 2012*).

### 6.2.3. Preparation of <sup>239</sup>Np tracer:

<sup>239</sup>Np (Half-life =2.35 days) was used as a radiotracer for neptunium in the batch sorption experiments. The details of preparation of radiotracer are given in Chapter 2. Figure 6.1 shows the gamma spectrum of pure <sup>239</sup>Np.

Solvent extraction with 0.5 M thenoyl trifluoro acetone (TTA) in xylene showed negligible extraction of neptunium indicating that the predominate oxidation state was Np(V). 100 μL of the stock solution (10<sup>-11</sup> M) was used in the sorption studies so as to give the neptunium concentration of 10<sup>-13</sup> M.

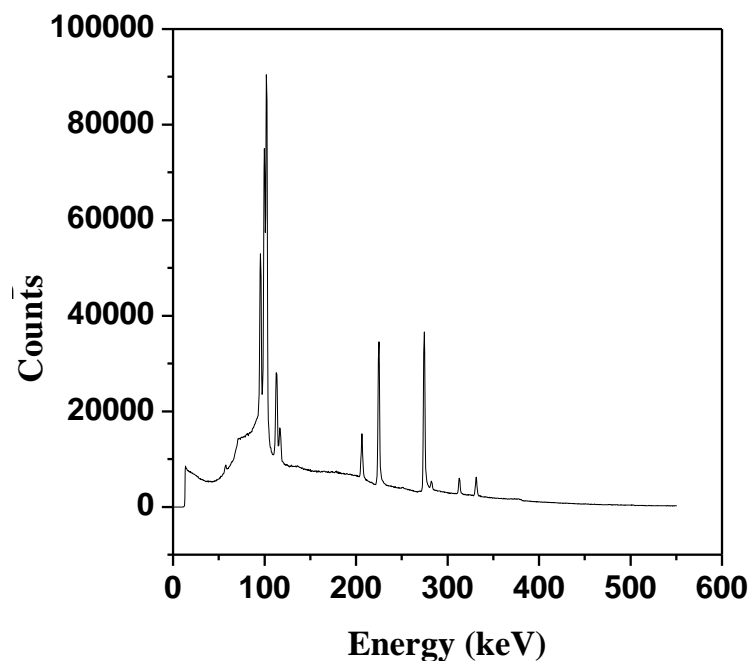


**Figure 6.1** Gamma Spectrum of  $^{239}\text{Np}$

#### 6.2.4. Measurement of the stability constant of Np-HA complex:

The stability constant of the Np(V)-humate complex ( $\beta$ ) was determined by solvent extraction method.  $^{239}\text{Np}$  tracer solution in pH 8 (TRIS buffer) was contacted with the organic phase containing (TTA) and 1, 10 o-phenanthroline in xylene (*Tochiyama et al., 2000*) whereby Np(V) was synergistically extracted quantitatively into the organic phase. 2 mL of the,  $^{239}\text{Np}$  loaded, organic phase was contacted with 2 ml of aqueous solution (pH 8 TRIS) containing varying concentration of HA (0-200 mg/L). Eight sets of samples were prepared. Kinetic experiments showed that the distribution ratio reached the equilibrium value in 4 hours. Hence the contact time with the aqueous phase was kept four hours for all the eight sets. After the equilibration, the aqueous and organic phases were separated and duplicate 100  $\mu\text{L}$  aliquots from both phases were counted for the gamma activity of  $^{239}\text{Np}$  on a well type 3" X 3" NaI(Tl) detector coupled to a 1k channel analyzer. The distribution ratio

(D) of  $^{239}\text{Np}$  was measured in all eight sets with varying concentration of HA in aqueous phase.

### **6.3 Sorption Experiments:**

#### **6.3.1. Sorption of Np(V) on hematite under aerobic condition:**

The detailed procedure of batch sorption experiments has been described in Chapter 2. 3 g/L of hematite suspensions were equilibrated with  $^{239}\text{Np}$  ( $10^{-13}\text{ M}$ ) in the pH range 3-10 for 48 hours, which was fixed considering the literature report on sorption kinetics of neptunium on iron bearing minerals (*Nakayama and Sakamoto, 1991*). After equilibration, the suspensions were centrifuged at 7000 rpm for 45 minutes in order to achieve phase separation. The percentage sorption was calculated, from initial activity ( $A_0$ ) and the activity ( $A$ ) left in the liquid phase after centrifugation, using the equation (2.9) given in chapter 2.

In the case of experiments in presence of the HA, 100  $\mu\text{L}$  of the HA stock solution (200 mg/L) was added to the hematite suspension prior to adjustment of pH. The suspensions were equilibrated for 48 hours before the addition of  $^{239}\text{Np}$ .

#### **6.3.2 Sorption of HA on hematite:**

In order to study the sorption of HA on hematite as function of pH, 100  $\mu\text{L}$  of the HA stock solution (200 mg/L) was added to the hematite suspension (3 g/L), having varying pH in the range of 3-10. After equilibration for 48 hours, the suspensions were centrifuged. The absorbance of the supernatant solutions was measured by a UV - visible spectrophotometer (JASCO-530) in quartz cuvette (1 cm) with the supernatant of a hematite suspension without HA as blank in order to take into consideration the absorbance due to any dissolved hematite. For the

determination of HA concentration in the supernatant solution the absorbance at 288 nm was used as hematite had minimum absorbance at this wavelength.

### **6.3.3. Sorption of neptunium on hematite under anaerobic condition:**

In another set of experiments, the batch sorption experiments on binary system of Np - hematite and ternary system of Np - HA - hematite were carried out under reducing conditions using  $^{239}\text{Np}$  tracer. 100  $\mu\text{L}$  of 0.5 M sodium dithionite solution was added to the hematite suspension (3 g/L) so as to maintain the dithionite concentration as  $5 \times 10^{-3}$  M. The suspensions were purged with  $\text{N}_2$  after the adjustment of pH and immediately thereafter the polypropylene tubes were sealed and kept for equilibration for 48 hours. Rest of the procedure was the same as described above for experiments under aerobic conditions. Similar experiments were carried out in presence of 2 mg/L HA. Np(V) is expected to be reduced to Np(IV) under these reducing conditions which may further be facilitated by the presence of HA.

## **6.4 Results and Discussion:**

### **6.4.1. Characterization of hematite:**

The crystal structure of the hematite powder was confirmed by XRD. The surface area was determined to be 36  $\text{m}^2/\text{g}$  by BET analysis. Figure 6.2 shows the variation of zeta potential of hematite colloids as a function of pH. The errors on the data are  $\pm 1\sigma$  of 5 measurements. The point of zero charge (PZC) of hematite colloids was found to be 6.57, which is close to average value of PZC i.e.  $7.58 \pm 1.51$  for iron (hydro)oxides (*Kosmulski et al., 2003*). The dissolution of hematite in the aqueous suspension was studied through determination of iron concentration in the supernatant solution, after centrifugation of the suspension, using ICP-AES. The highest iron concentration was found to be 50 ppb at pH 4.

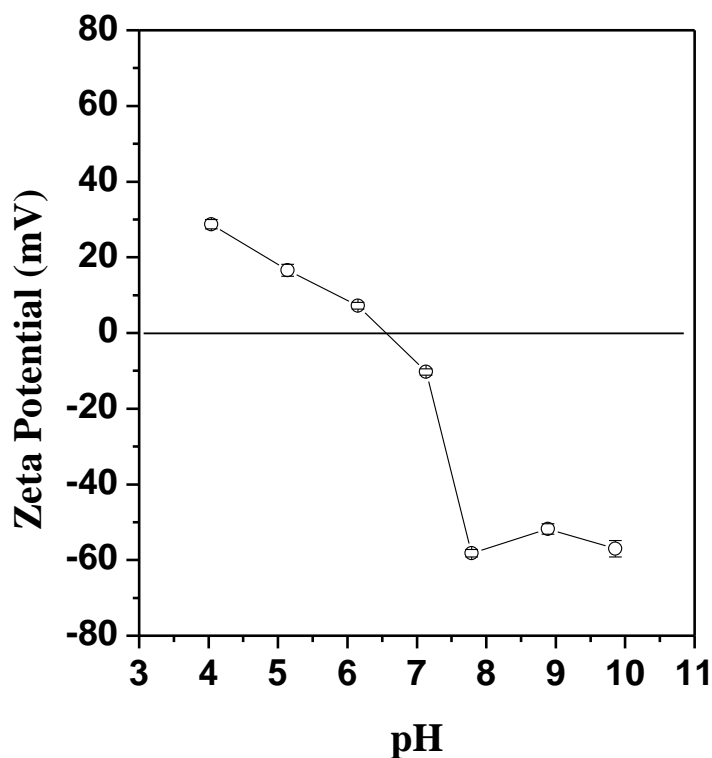


**Figure 6.2** Plot of zeta potential of hematite colloids as a function of pH

Depending upon the pH of the suspension the colloidal particles may be positively or negatively charged as explained by following hydrolysis reactions



where,  $\equiv\text{S-OH}$  represents the hematite surface site. The titration data of hematite with acid and base are shown in Figure 6.3.

The plot of  $[\text{H}^+]$  added vs free  $[\text{H}^+]$  and that of  $[\text{OH}^-]$  added vs free  $[\text{OH}^-]$  reached a saturation value with respect to blank. From the saturation value of  $[\text{H}^+]$  and  $[\text{OH}^-]$  for both acid and base legs respectively, the total number of active sites were calculated as,

$$[\equiv\text{S-OH}] = ([\text{H}^+]_{\text{sat.}} + [\text{OH}^-]_{\text{sat.}})/2 \quad (6.3)$$

The concentration of surface sites was found to be  $2.30 (\pm 0.26) \times 10^{-4}$  mol/L for 300 mg of hematite in 50 ml of solution or  $3.8 (\pm 0.4) \times 10^{-5}$  mol/g of hematite.

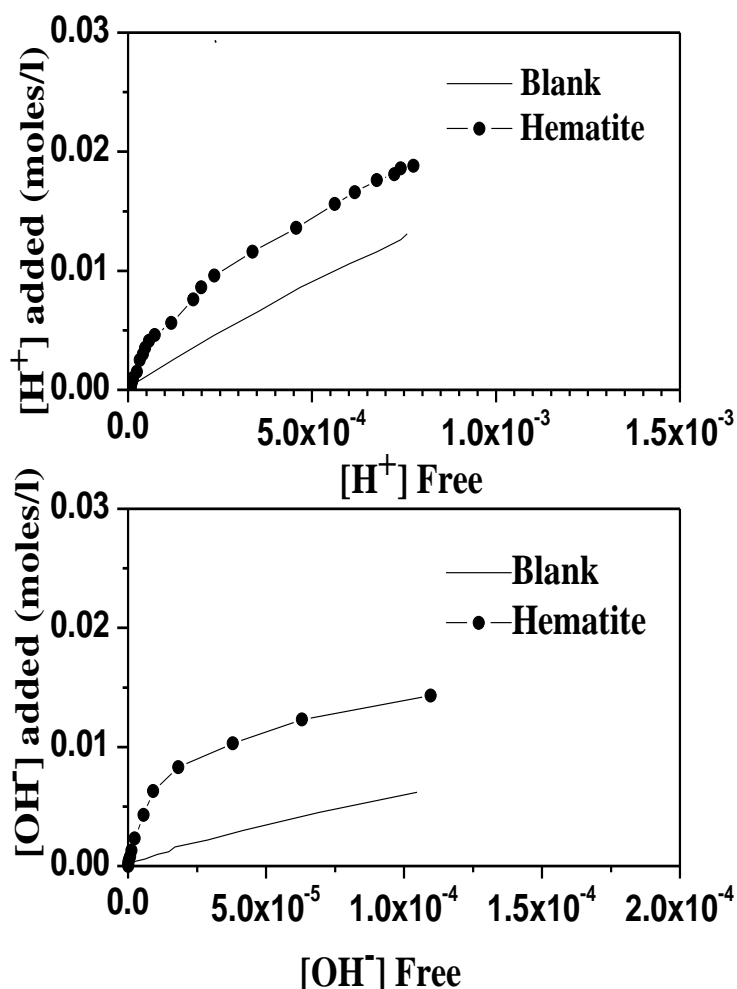


**Figure 6.3** Surface saturation of hematite by H<sup>+</sup> (top) and OH<sup>-</sup> (bottom)

#### 6.4.2. Determination of stability constant of Np-HA complex:

The stability constant of Np(V)-HA complex was determined using Schubert's method (Lenhart *et al.*, 2000). Schubert's method is based on the measurement of distribution ratio of metal ion between organic and aqueous phases, in absence and presence of metal complexing ligands.

The relationship between distribution ratio (D value) and ligand concentration [HA] is given by following equation:

$$\log[(D_0/D)-1] = \log\beta + n \log[HA]_f \quad (6.4)$$

where  $D_0$  is the value of the distribution ratio in the case of aqueous phase without HA.  $[HA]_f$  is the free HA concentration. Since the concentration of Np(V) is

negligible compared to  $[\text{HA}]_f$ , it was assumed to be equal to the total HA concentration  $[\text{HA}]_T$ . The slope of the line gave the stoichiometry ( $n$ ) of the complex (ligand to metal ion ratio) while the intercept gave the  $\log \beta$  value.

The complexation of Np(V) by HA is presented in figure 6.4, which shows the plot of  $\log [(D_0/D)-1]$  as a function of total HA concentration. The slope of the line was found to be 1.03 indicating the formation of a 1:1 complex between  $\text{NpO}_2^+$  and HA. Though complexation of metal ions by HA is assumed to occur mainly through carboxylic acid groups, the role of phenolic groups cannot be ruled out (*Sachs and Bernhard, 2005*). The  $\log \beta$  was found to be  $3.9 \pm 0.2$ , which after correcting for degree of ionization  $\alpha = 0.45$  at pH 8 (*Kumar, 2012*), resulted in a  $\log \beta$  value of  $4.2 \pm 0.2$ . This value is in agreement with the literature value of Np(V)-HA complex as determined by Marquardt et al. (*1996*).

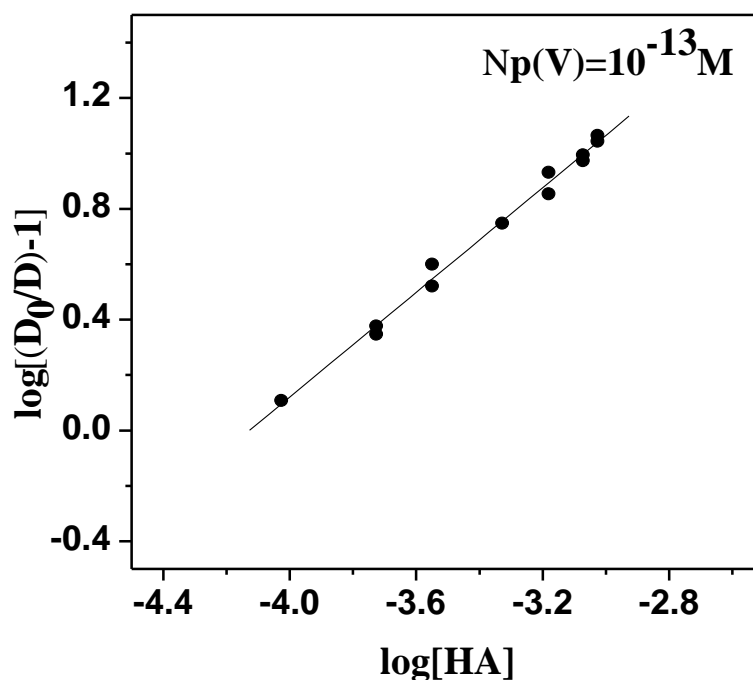


**Figure 6.4** Complexation of Np(V) by HA at pH 8 (TRIS buffer)

### 6.4.3. Sorption of HA on hematite:

Figure 6.5 shows the fraction of HA sorbed on hematite colloids as a function of pH. HA sorption on hematite decreases with increase in pH. The high sorption values for HA in low pH range can be explained in terms of the electrostatic attraction between positively charged hematite surfaces (below  $\text{pH}_{\text{pzc}}$ ) and negatively charged HA. With increasing pH, the surface charge decreases and become negative above its  $\text{pH}_{\text{pzc}}$ . Moreover, ionization of functional groups, mainly carboxyl and phenolic groups, of HA increases with pH which result in huge amount of negative charge on HA. Thus, electrostatic repulsion between HA and hematite is responsible for reduced sorption at high pH. Similar results were obtained by Fairhurst et al. (1995 a).

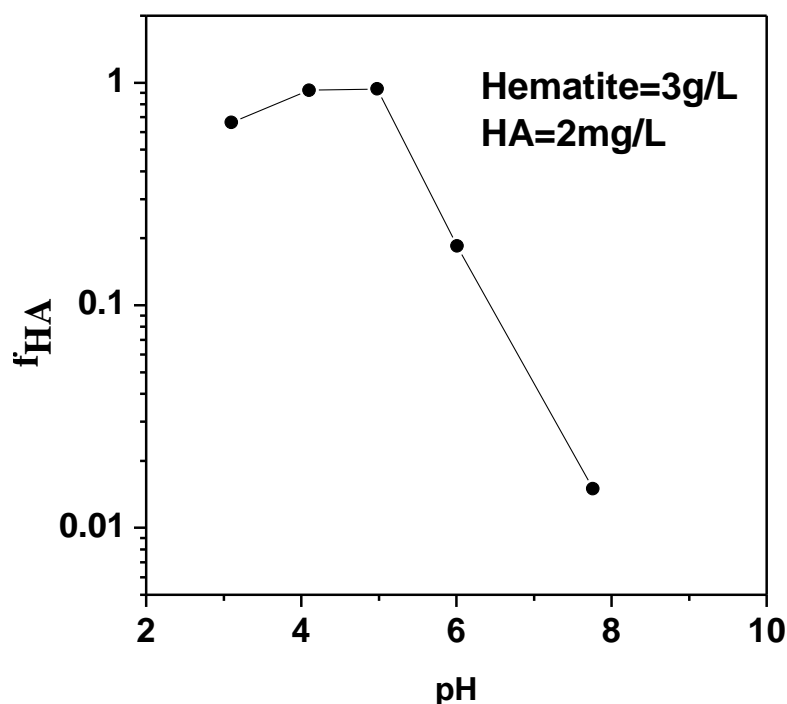


**Figure 6.5** Fraction of mineral bound HA as a function of pH

### 6.4.4. Sorption of Neptunium on hematite colloids in aerobic conditions: Effect of HA:

Figure 6.6 shows the sorption data of Np(V) on hematite colloids as a function of pH under aerobic conditions. The errors shown on the sorption data are

due to counting statistics of  $A$  and  $A_0$ . The percentage sorption is very low till pH 5 (~10%), above which it increases sharply apparently reaching a constant value of 90% at pH 9. The trend of increasing sorption of Np(V) on inorganic colloids with pH has been reported in the case of silica, alumina (Clark *et al.*, 1996) and hematite (Khasanova *et al.*, 2007; Nakayama and Sakamoto, 1991). In all the cases the sorption was found to increase with pH beyond 6. The apparent saturation of percentage sorption at 90% may be due to the formation of negatively charged carbonate complexes, such as  $\text{NpO}_2(\text{CO}_3)_n^{(2n-1)-}$ , where  $n = 1, 2, 3$  (Righetto *et al.*, 1991) as in carbonate-free solution systems containing Np(V)  $4.5 \times 10^{-13}$  to  $4.5 \times 10^{-11}$  M, Np(V) was almost completely sorbed by ferrihydrite between pH 8 and 10 (Girvin *et al.*, 1991).

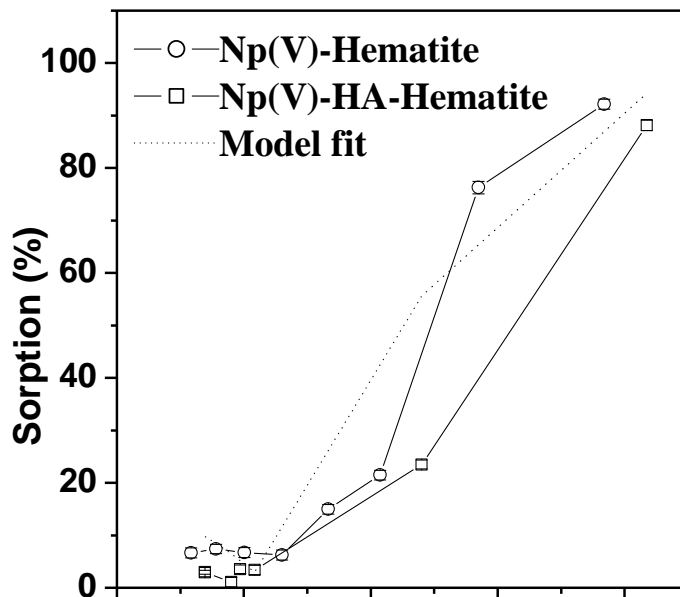


**Figure 6.6** Sorption of Np(V) on hematite: Effect of HA

As seen in Figure 6.6 in presence of HA, the sorption is marginally lower in the pH range 3-6. On the other hand, at pH > 7.0 the significant decrease in sorption

in presence of HA has been observed which is in agreement with the literature reports (Fairhurst *et al.*, 1995a; Righetto *et al.*, 1991; Sakuragi *et al.*, 2004). Sorption behaviour of actinides on minerals has been explained on the basis of hard - soft, acid - base behaviour. Np(V) being a softer acid has lesser affinity for mineral oxides as compared to Th(IV), Pu(IV) and Am(III). The electrostatic attraction between actinyl ion and mineral oxide is less compared to trivalent / tetravalent actinides.

HA enhances Np(V) sorption on goethite and hematite at low pH but at total HA concentration higher than 20 ppm (Khasanova *et al.*, 2007). In present work HA concentration was 2 ppm, hence the increase in Np (V) sorption was not observed at low pH. Sakuragi *et al.* (2004) observed that HA enhances the sorption of Am (III) on hematite colloids at lower pH and lowers the sorption at higher pH. This observation was attributed to the strong sorption of HA on hematite at lower pH, which decreased with increasing pH. Similar observations were made by Fairhurst *et al.* (1995a) in their study on the effect of HA on the sorption of Eu(III) on hematite colloids. Payne *et al.* (1996) studied the effect of HA on uranium sorption on ferrihydrite. Their study showed that addition of HA increased uranium uptake at pH < 7 with little effect at higher pH values. The effect of CO<sub>2</sub> on sorption of Np(V) on hematite was studied by Kohler *et al.* (1999). No effect of CO<sub>2</sub> was observed at lower pH (< 7), while at higher pH values the sorption was found to decrease in presence of CO<sub>2</sub>. This was attributed to the formation of neptunyl carbonato complexes. Thus the observations made in the present study about the suppression of Np(V) sorption by HA at higher pH values can be explained by the formation of Np(V)-HA complex. However the formation of Np(V) carbonato complexes such as  $\text{NpO}_2(\text{CO}_3)_n^{(2n-1)-}$ , where n=1,2,3 can also not be ruled out.

#### 6.4.4.1. LAM of sorption data:

In order to simulate the sorption data of the ternary system involving Np(V), hematite and HA we used the LAM modified by Samadfam et al. (2000). The fundamentals of LAM are described in Chapter 2. The stability constant of Np-HA complex and fraction of HA sorbed on hematite was used as input in LAM to predict the sorption behaviour of ternary Np(V)-HA-hematite system. The prediction of the LAM are shown in figure 6.6 as dotted line, which shows increased sorption of Np(V) at intermediate pH with a slight decrease at higher pH values. The decrease in sorption at higher pH is in agreement with the experimental results, though the decrease is not as much as the experimentally observed. However, the predicted increase at pH 5-6 is not observed in the experiment, which suggests the influence of non-additive factors, such as, change in the surface charge density of HA coated hematite particles with respect to bare hematite particles, or different value of stability constant for Np(V)-HA complex involving mineral bound and aqueous HA.

#### 6.4.5. Sorption of Neptunium on hematite colloids in anaerobic conditions: Effect of HA:

Figure 6.7 shows the sorption data of neptunium on hematite under anaerobic conditions in presence and absence of HA. The sorption of Np on hematite is significantly enhanced at all pH values with respect to the aerobic conditions. Under anaerobic conditions, Np(V) may be reduced to Np(IV) which being a hard acid, is expected to behave similar to Th(IV) and hence the sorption at lower pH is increased compared to that in the case of Np(V). In the presence of HA, the sorption at lower pH values is further enhanced, which may be due to the complexation of Np(IV) by HA, which in turn is strongly sorbed on hematite. At higher pH values, the percentage sorption is same (~100%) in the both the cases, indicating that HA does not affect the

sorption of Np(IV) on hematite. The sorption of Th(IV) on bentonite has been studied by Xu. et al (2006b) who also observed similar observations, that is, there was no effect of HA on sorption of Th(IV) at higher pH values. As Np(IV)-HA complex has a much higher stability constant than Np(V)-HA, it is expected that the sorption of Np(IV) on hematite will reduce at higher pH, contrary to the observations of this work. This indicates that reduction of Np(V) to Np(IV) may not be complete at alkaline pH.

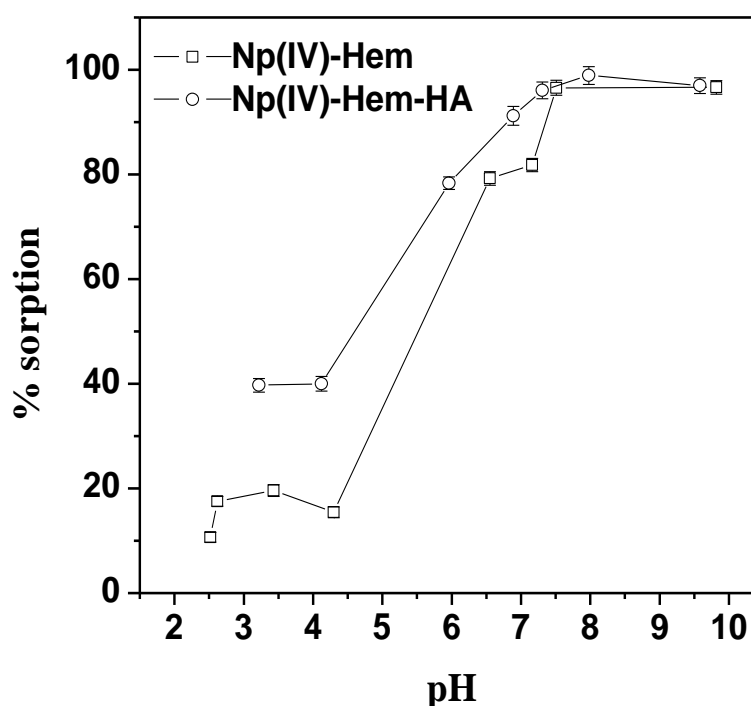


**Figure 6.7** Sorption of neptunium on hematite in presence of HA under reducing conditions

Reduction of Np(V) to Np(IV) has been observed only in case of Fe(II) bearing iron oxide surfaces under anaerobic conditions where Fe(II) itself may act as a reducing agent (Nakata et al., 2002). In the present case, it is possible that Fe<sup>3+</sup> obtained by dissolution of hematite may be reduced to Fe<sup>2+</sup> there by limiting the reduction of Np(V) to Np(IV).

The  $pH_{50}$ , that is, the pH corresponding to 50% of saturation value, obtained from figures 6.6 and 6.7 for Np(V) and Np(IV), were found to be 6.8 and 5.5 respectively, which changed to 8 and 4.6 respectively in the presence of HA. Thus the presence of HA results in significant change in the  $pH_{50}$  value. The decrease in the  $pH_{50}$  value was also observed by Payne (1999) for sorption of  $UO_2^{2+}$  on ferrihydrite. These observations suggest significant effect of HA on sorption of neptunium on hematite colloids both under aerobic as well as anaerobic conditions. While in the case of Np(V), the sorption is decreased in the higher pH range of 7-9, it is enhanced in the lower pH range of 4-7 in the case of Np(IV).

### **6.5. Conclusions:**

The present study showed that Np(V) sorption on hematite colloids at ionic strength of 0.1 M ( $NaClO_4$ ) is negligible up to pH 5, above which it increases sharply with pH. In the presence of HA a decrease in the percentage sorption was observed at higher pH, which has been attributed to the complexation of Np(V) by HA. The  $\log \beta$  for Np(V) - HA was found to be  $4.2 \pm 0.2$ . Under reducing conditions ( $5 \times 10^{-3}$  M sodium dithionite) and  $N_2$  atmosphere, neptunium sorption on hematite was found to be enhanced at all pH values due to reduction of Np(V) to Np(IV). HA was found to further enhance the sorption at low pH values, though no effect was observed at higher pH, which could be due to competition from ferric ions for dithionite. Thus, under anaerobic conditions HA will enhance the sorption of neptunium colloids, as compared to aerobic conditions.

## **Chapter VII**

# **Summary & Conclusions**

In the present thesis complexation and sorption behaviour of actinides/lanthanides on oxide surfaces have been investigated using batch sorption, molecular level spectroscopic techniques, LAM and SCM. The work presented in this thesis is divided into three parts: (i) the complexation of lanthanides with LMCA of environmental relevance and naturally occurring HA (ii) sorption of actinides/lanthanides onto mineral oxides (iii) the effect of complexing anions on sorption of actinides/lanthanides onto mineral oxides. The results of these studies are summarized in this chapter.

1. Complexation of Eu(III) by different complexing anions, viz., HIBA, SA, PA and MA has been studied using TRFS as a tool. The results have been compared with the observations obtained with Eu(III)-HA complexation. The small organic molecules, such as, HIBA, SA, PA and MA form 1: n complexes with Eu(III), with the values of 'n' varying depending upon the denticity of the ligand. The formation of different stoichiometric complexes between Eu(III) and these small organic molecules was evident from the increase in the asymmetric ratio ( $I_{616}/I_{592}$ ) in the emission spectra with increasing ligand to metal ion concentration ratio. These observations were further corroborated with the life time data which showed increase in the life time with increasing ligand to metal ion concentration ratio. The stoichiometry of the complexes was obtained from the life time data using an empirical relation, between the life time and the number of water molecules coordinated to  $\text{Eu}^{3+}$  ion, available in the literature. The stability constant of the different Eu(III) complexes was obtained from the measured asymmetry ratio as a function of ligand to metal ion concentration ratio. Similar experiments were also carried out with the Eu(III)-HA system. In this case the life time values

were found to remain constant at least upto the HA/Eu(III) ratio of 8, above which quenching of the fluorescence was observed as evident from the reduced emission intensity. Thus the stability constant for Eu(III)-HA complexes could not be obtained. Nevertheless, these studies provided the information that the large macromolecular anions, such as, behave differently from the small organic anions.

2. Sorption of Cm(III) by silica was found to be greatly influenced by the presence of HA in the suspension. The sorption of Cm(III) by silica increases with the pH of the suspension, which can be explained in terms of the electrostatic attraction between the positively charged  $\text{Cm}^{3+}$  ions and the negatively charged surface sites of the type  $\equiv\text{Si-O}^-$  on silica, as well as the surface complexation of the metal ion by the surface sites. In presence of HA, the sorption of Cm(III) by silica is enhanced at lower pH values (3-5) and decreased at higher pH values (6-8), and thereafter the sorption was found to increase with pH. These observations could be explained in terms of the sorption of HA by silica. HA is strongly sorbed by the silica at lower pH and the sorption decreases with increasing pH of the suspension becoming negligible at  $\text{pH} > 6$ . Thus the surface bound HA at lower pH results in increased sorption of Cm(III) by silica. On the other hand, in the intermediate pH range the HA is predominantly present in the solution and hence strong complexation of Cm(III) by HA in the solution results in decreased sorption. At higher pH values ( $> 8$ ), the increases in the sorption with pH could plausibly be due to the formation of hydrolysed Cm(III) species which might have higher sorption tendency towards the silica surface. The above observation of the effect of HA on the sorption of Cm(III) by silica could be

quantitatively explained in terms of the linear additive model, by incorporating the modifications to take into account the different binding affinity of surface bound HA from the HA in solution. With a view to obtain more insight into the mechanism of the sorption of Cm(III) by silica in presence of HA, TRFS studies were carried out using Eu(III) as the chemical analogue of Cm(III) and alpha hydroxy iso-butyric acid (HIBA) as a small organic molecule to study if it could be used as an analogue of HA. The TRFS measurements helped in identifying the surface complexes. Further the sorption data could be modeled successfully with the help of SCM. It was observed that the effect of small organic molecules like HIBA was quite different from that of HA, indicating the different binding characteristics of the two complexing anions.

3. Sorption of U(VI) by silica has been studied in presence of two important complexing anions, namely, carbonate and citrate, which are ubiquitous in geosphere. U(VI) sorption by silica increases with the pH of the suspension, with the sorption edge, that is, the pH at 50% sorption, shifting to higher pH with increasing concentration of the metal ion. In presence of carbonate, there was negligible change in the sorption profile, while citrate was found to have significant effect on the sorption of U(VI) by silica, with the sorption decreasing in presence of citrate at higher pH values compared to the binary U(VI)-silica system. The sorption profile for the binary U(VI)-silica and ternary U(VI)-silica-citrate system were fitted using the surface complexation model. SCM using DLM showed the evolution of different surface complexes as a function of U(VI) concentration. The bidentate mono nuclear surface complex was able to fit the sorption data in entire concentration range. The two modeling approaches were applied to some of the literature data for their

evaluation and mononuclear mono-dentate complexes were able to explain the sorption data better than mononuclear bidentate complexes. Moreover, TRFS revealed the existence of two surface complexes at  $[U] = 5 \times 10^{-5}$  M, which was used to constrain the SCM. In case of ternary systems, U(VI) is sorbed as  $(\equiv\text{SiO})_2\text{UO}_2$  and  $(\equiv\text{SiO})_2\text{UO}_2\text{CO}_3^{2-}$  in presence of carbonate and as  $(\equiv\text{SiO})_2\text{UO}_2\text{Cit}^{3-}$  in presence of citrate.

4. Sorption of neptunium by hematite colloids was studied both in absence and presence of HA. Hematite colloids were prepared by precipitation of hydroxide from aqueous solution of ferric chloride followed by heating of the precipitate at high temperatures and grinding in a ball mill. Sorption experiments were carried out using  $^{239}\text{Np}$ , the short lived gamma emitting isotope of neptunium. Under aerobic conditions, Np(V) is the dominant species and its sorption by hematite increases slowly with the pH of the suspension, which could be explained in terms of the low ionic potential of the  $\text{NpO}_2^+$  ions. The stability constant of Np(V)-humate complex was determined using the Schubert's method. Under reducing conditions, Np(IV) is the dominant species and its sorption increases significantly with the pH of the suspension. In presence of HA the sorption was found to increase at lower pH with respect to the binary Np(IV)-hematite system. These studies showed that the migration of neptunium on hematite is greatly influenced in presence of HA under anaerobic conditions.

The work carried out as a part of this thesis has shown that colloids based on mineral oxides of Si, Fe, etc., greatly influence the speciation of actinides under the conditions prevailing in natural waters. Presence of complexing anions, such as, HA has drastic effect on the sorption of trivalent actinides, which in turn is influenced by

the presence of natural organic matter containing HS. TRFS provided valuable information on the complexation of trivalent rare earths by small organic molecules, which can be used to infer about the complexation of trivalent actinides by the small organic molecules present in natural waters. This technique could also provide information about the sorbed metal ions on the surface of mineral oxides, and thereby help in validating the predictions of the SCM. Attempt has also been made to understand the sorbed uranyl species on the surfaces of silica, though the information obtained was limited owing to the lower sensitivity of the TRFS system based on xenon flash lamp as the excitation source. With the induction of dye laser based TRLFS system, it would be possible to study the uranium speciation on the surface of mineral oxides at much lower metal ion concentrations. In the case of neptunium, the studies provided information about the speciation of the metal ion under aerobic and anaerobic conditions in absence and presence of HA. The modeling of the sorption data by SCM needs to be carried out for which the spectroscopic information has to be obtained using techniques, such as LIPAS.

The present work is a small step towards understanding the migration behaviour of actinides and long lived fission products in the geosphere, which is a frontier area of research by the radiochemists worldwide. With the availability of intense synchrotron sources and laser based spectroscopic instruments, the molecular structure of the actinides can be obtained, which in turn would help in validating the models proposed to predict the migration pathways of these long lived radionuclides in the geosphere upon their release from the deep geological repository.

# **Bibliography**

A

- Abdel daiem, M. M., Rivera-Utrilla, J., Ocampo-Pérez, R., Méndez-Díaz, J. D., Sánchez-Polo, M.(2012) Environmental impact of phthalic acid esters and their removal from water and sediments by different technologies : A review, *J. Environ. Manage.* **109**, 164.
- Ahrland, S., Liljenzin, J.O., Rydberg, J. (1973) Solution chemistry, in *Comprehensive Inorganic Chemistry*, J.C. Bailar Jr., H.J. Emeleus, R. Nyhlom and A.F.T. Dickenson(Eds.), Pergamon Press, Oxford, 465.
- Alexander, W. R., McKinley, L. E. (2007) *Deep geological disposal of radioactive waste*, Elsevier, Amsterdam, The Netherlands.
- Alliot, C., Bion, L., Mercier, F., Toulhoat, P. (2005 a) Sorption of aqueous carbonic, acetic and oxalic acids onto  $\alpha$ -alumina, *J. Colloid Interface Sci.* **287**, 444.
- Alliot, C., Bion, L., Mercier, F., Toulhoat, P. (2006) Effect of aqueous acetic, oxalic and carbonic acids on the adsorption of europium onto  $\alpha$ -alumina, *J. Colloid Interface Sci.* **298**, 573.
- Alliot, C., Bion, L., Mercier, F., Vitorge, P., Toulhoat, P. (2005 b) Effect of aqueous acetic, oxalic and carbonic acids on the adsorption of americium into  $\alpha$ -alumina, *Radiochim. Acta* **93**, 435.
- Alliot, C., Vitorge, P., Bion, L., Mercier, F. (2005c) Effect of aqueous acetic, oxalic and carbonic acids on the adsorption of U(VI) into  $\alpha$ -alumina, *New J. Chem.* **29**, 1409.

Allison, J.D., D.S. Brown, and K.J. Novo-Gradac (1991) *MINTEQA2/PRODEFA2, A Geochemical Assessment Model for Environmental Systems: Version 3.0 User's Manual*. United States Environmental Protection Agency, Office of Research and Development, Washington, DC.

Altmaier, M., Neck, V., Fanghanel, T. (2004) Solubility and colloid formation of Th (IV) in concentrated NaCl and MgCl<sub>2</sub> solution, *Radiochim. Acta*, **92**, 537.

Amano, Y. (2012) International Status and Prospects for Nuclear Power 2012 *GOV/INF/2012/12-GC(56)/INF/6 (IAEA)* 15 August.

Aoyagi, N., Toraishi, T., Geipel, G., Hotokezaka, H., Nagasaki, S., Tanaka, S. (2004) Fluorescence characteristics of complex formation of europium(III)-salicylate *Radiochim. Acta* **92**, 589.

Arai, Y., Moran, P.B., Honeyman, B.D., Davis, J.A. (2007) In situ spectroscopic evidence for neptunium(V)-carbonate inner-sphere and outer-sphere ternary surface complexes on hematite surfaces, *Environ. Sci. Technol.* **41**, 3940.

Artinger, R., Marquardt, C.M., Kim, J.I., Seibert, A., Trautmann, N., Kratz, J.V. (2000) Humic colloid-brone Np migration: influence of the oxidation state. *Radiochim. Acta* **88**, 609.

## **B**

Baik, M.H. and Hahn, P.S. (2001) Experimental study on uranium sorption onto silica colloids: Effect of geochemical parameters, *J. Korean Nucl. Soc.* **33**, 261.

- Banerjee, D., Rao, M. A., Samanta, S. K. (2006), Development of a combined chemical treatment process for removal of  $^{106}\text{Ru}$ ,  $^{125}\text{Sb}$  and  $^{137}\text{Cs}$  from alkaline low level reprocessing waste, *DAE. BRNS Symposium on Emerging Trends in Separation Science and Technology, (SESTEC)* 264.
- Barthelemy, P.P., Choppin, G.R., Pierre, P. (1989) Luminescence study of complexation of europium and dicarboxylic Acids, *Inorg. Chem*, **28**, 3354.
- Bartlett, J. R., Cooney, R. P. (1989) On the determination of uranium oxygen bond lengths in dioxouranium(VI) compounds by Raman spectroscopy, *J. Mol. Struct.*, **193**, 295.
- Batuk, D.N., Shiryaev, A.A., Kalmykov, S. N., Batuk, O .N., Romanchuk, A.Y., Shirshin, E.A. Zubavichus, Y.V. (2011) Sorption and speciation of uranium on silica colloids in *Actinide Nanoparticle Research*, Springer- Verlag Berlin Heidelberg, 315.
- Bell, J.T.; Biggers, R.E. (1968) Absorption spectrum of the uranyl ion in perchlorate media III. Resolution of the ultraviolet band structure; some conclusions concerning the excited state of  $\text{UO}_2^{2+}$ . *J. Mol. Spectrosc.*, **25**, 312.
- Bhattacharyya, A., Mohapatra, P. K., Manchanda, V. K. (2006) Separation of americium(III) and europium(III) from nitrate medium using a binary mixture of cyanex-301 with N-donor ligands *Solv. Extr. Exch.*, **24(1)**, 1.
- Boenisch, D.W., Traina, S.J. (2006) A comparative study of the effect of desferrioxamine B, oxalic acid, and Na- alginate on the desorption of U(VI) from goethite at pH 6 and  $25^\circ\text{C}$  , *Geochim. Cosmochim. Acta* **70**, 4356.

- Boggs, B., Livermore, D., Seitz, M. G. (1985) *Humic substances in natural waters and their complexation with trace metals and radionuclides: A review*, U. S. Department of Energy, ANL--84-78.
- Boily, J.F., Fein, J.B. (2000) Proton binding to humic acids and sorption of Pb(II) and humic acid to the corundum surface, *Chem. Geol.* **168**, 239.
- Bradbury, M. H., Baeyens, B. (2002) Sorption of Eu on Na- and Ca-montmorillonites: experimental investigations and modelling with cation exchange and surface complexation. *Geochim. Cosmochim. Acta* **66**, 2325.
- Bradbury, M. H., Baeyens, B. (2006) Modelling sorption data for the actinides Am(III), Np(V) and Pa(V) on montmorillonite. *Radiochim. Acta* **94**, 619.
- Bradbury, M. H., Baeyens, B. (2009 a) Experimental and modelling studies on the pH buffering of MX-80 bentonite porewater. *Appl. Geochem.* **24**, 419.
- Bradbury, M.H., Baeyens, B. (2009 b) Sorption modelling on illite Part II: Actinide sorption and linear free energy relationships, *Geochim. Cosmochim. Acta* **73**, 1004.
- Bradbury, M. H., Baeyens, B. (2011) Predictive sorption modelling of Ni(II), Co(II), Eu(III), Th(IV) and U(VI) on MX-80 bentonite and opalinus clay: A “bottom-up” approach. *Appl. Clay Sci.* **52**, 27.
- Bradbury, M. H., Baeyens, B., Geckeis H., Rabung, Th. (2005) Sorption of Eu(III)/Cm(III) on Ca-montmorillonite and Na-illite Part 2: Surface complexation modelling, *Geochim. Cosmochim. Acta* **69**, 5403.

**C**

- Carnall, W.T., (1979) The absorption and fluorescence spectra of rare earth ions in solution in *Handbook on the Physics and Chemistry of Rare Earths*, (Eds.) K.A. Gschneidner, L. Eyring, Elsevier, Amsterdam, 171.
- Chen, C., Li, X., Zhao, D., Tan, X., Wang, X. (2007) Adsorption kinetic, thermodynamic and desorption studies of Th(IV) on oxidized multi-wall carbon nanotubes, *Colloids Surf., A*, **302**, 449.
- Chen, C., Yang, X., Wei, J., Tan, X., Wang, X. (2013) Eu(III) uptake on rectorite in the presence of humic acid: A macroscopic and spectroscopic study, *J. Colloid Interface Sci.* **393**, 249.
- Choppin, G. R. (1999) Role of humics in actinide behaviour in ecosystem, in: *Chemical Separation technologies and related methods of nuclear waste management* (Eds.) G.R. Choppin and M.Kh Khankhasayev, Kluwer Academic Publishers, Dordrecht, 247.
- Choppin, G. R. (2005) Actinide science: fundamental and environmental aspects, *J. Nucl. Radiochem. Sci.*, **6**, 1.
- Choppin, G. R. (2006) Actinide speciation in aquatic systems. *Mar. Chem.* **99**, 83.
- Choppin, G. R. (2007) Actinide speciation in the environment, *J. Radioanal. Nucl. Chem.*, **273**, 695.
- Choppin, G.R., Allard, B. (1985) Complexes of actinides with naturally occurring organic compounds in *Handbook on the physics and chemistry of the Actinides* (Eds.) A.J. Freeman and C. Keller, Elsevier Science Publ, 407.

- Choppin, G.R., Harvey, B.G., Thompson, S.G. (1956) *J. Inorg. Nucl. Chem.* **2**, 66.
- Choppin, G. R., Jensen, M. P., (2006). Actinides in solution: complexation and kinetics, in *The Chemistry of Actinide and Transactinide Elements (Eds.) L.R.Morss, N.K.Edelstein, and J.Fuger*, Springer, 2524.
- Choppin, G. R., Peterman, D.R. (1998 a) Applications of lanthanide luminescence spectroscopy to solution studies of coordination chemistry, *Coord. Chem. Rev.* **174**, 283
- Choppin, G. R., Wong, P.L. (1998 b) Chemistry of actinide behaviour in marine system, *Aquatic Geochem* **4**, 77.
- Christl, I., Kretzschmar, R. (2001) Interaction of copper and fulvic acid at the hematite water interface, *Geochim. Cosmochim. Acta* **65**, 3435.
- Chung, K. H., Klenze, R., Park, K. K., Paviet-Hartmann, P., Kim, J. I. (1998) A study of the surface sorption process of Cm(III) on silica by time resolved laser induced fluorescence spectroscopy, *Radiochim. Acta*, **82**, 215.
- Chung, K.H., Lee, W., Cho, Y.H., Choi, G.S., Lee, C.W (2005) Comparison of synchronous and laser-induced fluorescence spectroscopy applied to the Eu(III)-fulvate complexation, *Talanta* **65**, 389.
- Chunli, L., Yuae, Y., Zhiming, W., Shushen, L., Zede, G., Bing, L., Ling, J., Hong, J., Ling, W., Dan, L., Zhongde, D. (2001) Influence of humic substances on the migration of  $^{237}\text{Np}$ ,  $^{238}\text{Pu}$  and  $^{241}\text{Am}$  in a weak loess aquifer. *Radiochim. Acta* **89**, 387

Clark, D.L., Conradson, S.D., Ekberg, S.A., Hess, N.J., Janecky, D.R., Neu, M.P., Palmar, P.D., Tait, C.D. (1996) A multi-method approach to actinide speciation applied to pentavalent neptunium carbonate complexation *New. J. Chem.* **20**, 211.

Combes, J.M., Chisholmbrase, C.J., Brown, G.E., Parks, G.A., Conradson, S.D., Eller, P.G., Triay, I.R., Hobart, D.E., Meijer, A. (1992) "EXAFS spectroscopic study of neptunium(V) sorption at the alpha-FeOOH water interface", *Environ. Sci. Technol.* **26**, 376.

Cornelis, R. (2005) *Handbook of elemental speciation II: Species in the environment, food medicine and occupational health*, John Wiley & Sons.

Couston, L., Charbonnel, M.C., Flandin, J.L., Moulin, C., Rancier, F. (2004) TRLIFS study of Eu(III) spectroscopic properties to obtain structural and thermodynamic informations on lanthanide-malonamide complexes in the Eu(III) / NaNO<sub>3</sub>/ Tetra ethyl malonamide system, *Radiochim. Acta* **92**, 411.

CRWMS (2000) Commercial spent nuclear fuel degradation in unsaturated drip tests, Report ACC: MOL.20000107.0209, *Civilian Radioactive Waste Management. System Management and Operating Contractor*, Las Vegas, NV.

## **D**

Davis, J. A. (1984) Complexation of trace metals by adsorbed natural organic matter, *Geochim. et Cosmochim. Acta*, **48**, 679.

Degueldre, C. (2006) Identification and speciation of actinides in the environment in *The Chemistry of Actinide and Transactinide Elements (eds) L.R.Morss, N.K.Edelstein, and J.Fuger*, Springer, 3013.

- Degueldre, C., Triay, I., Kim, J. I., Vilks, P., Laaksoharju, M., Miekeley, N. (2000) Groundwater colloid properties: A global approach *Appl. Geochem.*, **15**, 1043.
- Denecke, M. A. (2006) Actinide speciation using X-ray absorption fine structure spectroscopy, *Coordin. Chem. Rev.* **250**, 730.
- Dey, P.K., Bansal, N.K. (2006) Spent fuel reprocessing: A vital link in Indian nuclear power program, *Nucl. Eng. Des.* **236**, 723.
- Dobbs, J.C., Susetyo, W., Knight, F.E., Castles, M.A., Carreira, L.A., Azarraga, L.V. (1989) Characterization of metal binding sites in fulvic acids by lanthanide ion probe spectroscopy, *Anal. Chem.* **61**, 483
- Dozol, M., Hagemann, R. (1993) Radionuclide migration in groundwaters; review of the behavior of actinides, *Pure & Appl. Chem.*, **65(5)** 1081.
- Drot, R., Roques, J., Simoni, É (2007) Molecular approach of the Uranyl/mineral interfacial phenomena. *C. R. Chimie* **10**, 1078.
- Dzombak, D. A., Morel, F. M. M. (1990) *Surface Complexation Modeling: Hydrous Ferric Oxide*. John Wiley & Sons.

**E**

- Edelstein, N. M., Fuger, J., Katz, J. J., Morss, L. R. (2006 a) Summary and comparison of properties of the actinide and transactinide elements in *The Chemistry of Actinide and Transactinide Elements (Eds.) L.R. Morss, N. K. Edelstein, and J. Fuger*, Springer, 1753.

Edelstein, N. M., Klenze, R., Fanghänel, T., Hubert, S. (2006 b) Optical properties of Cm(III) in crystals and solutions and their applications to Cm(III) speciation, *Coordin. Chem. Rev.* **250**, 948.

El-Naggar, H.A., Ezz El-Din, M.R., Shaha, R. R. (2000) Speciation of neptunium migration in under groundwater, *J.Radioanal. Nucl. Chem.* **246**, 493.

**F**

Fairhurst, A. J., Warwick, P., Richardson (1995 a) The influence of humic acid on the adsorption of europium onto inorganic colloids as a function of pH. *Colloids Surf. A* **99**, 187.

Fairhurst, A.J., Warwick, P., Richardson, S. (1995 b) The effect of pH on europium – mineral interaction in the presence of humic acid, *Radiochim. Acta* **69**, 103.

Fan, Q.H. (2009) Sorption of Eu(III) on attapulgite studied by batch, XPS and EXAFS techniques, *Environ. Sci. Technol.* **43**, 5776.

Fan, Q. H., Wu, W. S., Song, X. P., Xu, J. Z., Hu, J., Niu, Z. W. (2008) Effect of humic acid, fulvic acid and temperature on the sorption-desorption of Th(IV) on attapulgite, *Radiochim. Acta* **96**, 159.

Fanghanel, T., Kim, J.I., Paviet, P., Klenze, R., Hauser, W. (1994) Thermodynamics of radioactive trace elements in concentrated electrolyte solutions: Hydrolysis of Cm<sup>3+</sup> in NaCl Solutions, *Radiochim. Acta* **66/67**, 81.

Farr, J. D., Schulze, R. K., Honeyman, B. D. (2000) Aqueous Pu(IV) sorption on brucite. *Radiochim. Acta* **88**, 675.

Fernandes, M. M., Stumpf, T., Baeyens, B., Walther, C., Bradbury, M. H. (2010) Spectroscopic identification of ternary Cm-carbonate surface complexes, *Environ. Sci. Technol.* **44**, 921.

Fischer, K. (2002) Environmental analysis of aliphatic carboxylic acids by ion-exclusion chromatography, *Analytica Chim. Acta* **465**, 157.

Fouchard, A. K., Drot, R., Simoni, E., Marmier, N., Fromage, F., Ehrhardt, J.J. (2004 a) Structural identification of europium (III) adsorption complexes on montmorillonite, *New J. Chem.* **28**, 864.

Fouchard, A. K., Drot, R., Simoni, E., Ehrhardt, J. J. (2004 b) Use of Spectroscopic Techniques for Uranium(VI)/Montmorillonite Interaction Modeling, *Environ. Sci. Technol.*, **38**, 1399.

## **G**

Gabriel, U., Charlet, L., Schläpfer, C.W., Vial, J.C., Brachmann, A., Geipel, G. (2001) Uranyl surface speciation on silica particles studied by time-resolved laser-induced fluorescence spectroscopy, *J. Colloid Interface Sci.*, **239**, 358.

García-Gonzalez, N., Ordonez-Regil, E., Simoni, E., Barrera-Díaz, C. E. (2009) Effect of organic acids on sorption of uranyl ions in solution onto  $ZrP_2O_7$ . *J. Radioanal. Nucl. Chem.* **283**, 409.

García-Gonzalez, N., Ordonez-Regil, E., Almazan-Torres, M. G., Solis, D., Simoni, E. (2012) Speciation of U(VI) sorbed onto  $ZrP_2O_7$  in the presence of citric and oxalic acid *Radiochim. Acta* **100**, 305.

- Gaskova, O. L., Bukaty, M. B. (2008) Sorption of different cations onto clay minerals: Modelling approach with ion exchange and surface complexation, *Phys. Chem. Earth* **33**, 1050.
- Geckeis, H., Rabung, T. (2008) Actinide geochemistry: From the molecular level to the real system, *J. Contam. Hydrol.* **102**, 187.
- Geipel, G (2006) Some aspects of actinide speciation by laser-induced spectroscopy, *Coordin. Chem. Rev.* **250**, 844.
- Gin, S., Godon, N., Mestre, J.P., Vernaz, E.Y., Beaufort, D. (1994) Experimental Investigation of Aqueous Corrosion of R7T7 Nuclear Glass at 90-Degrees-C in the Presence of Organic-Species. *Appl. Geochem.* **9**, 255.
- Girvin, D.C., Ames, L. L., Schwab, A. P., Mcgarrah, J. E. (1991) Neptunium Adsorption on Synthetic Amorphous Iron Oxyhydroxide, *J. Colloid. Interface Sci.* **14**, 167.
- Grambow, B., Fattahi, M., Montavon, G., Moisan, C., Giffaut, E. (2006) Sorption of Cs, Ni, Pb, Eu(III), Am(III), Cm, Ac(III), Tc(IV), Th, Zr, and U(IV) on MX 80 bentonite: An experimental approach to assess model uncertainty, *Radiochim. Acta* **94**, 627.
- Grenthe, I., Fuger, J., Konings, R.J.M., Lemire, R.J., Muller, A.B., Nguyen-Trung, C., Wanner, H. (1992) *Chemical Thermodynamics of Uranium*, Elsevier Science Publishers, North Holland, Amsterdam.
- Guillaumont, R., Fanghanel, T., Fuger, J., Grenthe, I., Neck, V., Palmer, D.A., Rand, M.H. (2003) *Update on the Chemical Thermodynamics of Uranium, Neptunium,*

- Plutonium, Americium and Technetium*, Elsevier Science Publishers, North Holland, Amsterdam.
- Guo, Z., Li, Y., Wu, W. (2009 c) Sorption of U(VI) on goethite: Effects of pH, ionic strength, phosphate, carbonate and fulvic acid, *Appl. Radiat. Isot.* **67**, 996.
- Guo, Z.J., Su, H.Y., Wu, W.S. (2009 b) Sorption and desorption of U(VI) on silica :experimental and modeling studies, *Radiochim. Acta* **97**, 133.
- Guo, Z., Yan, C., Xu, J., Wu, W. (2009 a) Sorption of U(VI) and phosphate on  $\gamma$ -alumina: binary and ternary sorption systems. *Colloids Surf., A* **336**, 123.
- H**
- Hartmann, E., Baeyens, B., Bradbury, M.H., Geckeis, H., Stumpf, Th. (2008) A spectroscopic characterization and quantification of M(III)/Clay mineral outer – sphere complexes, *Environ. Sci. Technol.* **42**, 7601.
- Hass, Y., Stein, G. (1971) Pathways of radiative and radiationless transitions in europium(III) solutions: role of solvents and anions, *J. Phys .Chem*, **75**, 3688.
- Hayes, K. F., Redden, G., Wendell, E., Leckie, J. O. (1991) Surface complexation models: an evaluation of model parameter estimation using FITEQL and oxide mineral titration data. *J. Colloid Interface Sci.* **142**, 448.
- Herbelin, A., Westall, J. (1994). FITEQL – A Computer Program for Determination of Chemical Equilibrium Constants from Experimental Data. Oregon State University, Corvallis.

Ho, Y. S., McKay, G. (1998) A comparison of chemisorption kinetic models applied to pollutant removal on various sorbents, *Trans I ChemE*, **76 B**, 332.

Hongxia, Z., Chao, Y., Zuyi, T. (2009) Effects of phosphate and fulvic acid on the sorption and transport of U(VI) on silica column, *J.Radioanal. Nucl. Chem.* **279**, 317.

Hongxia Z., Zuyi, T. (2002) Sorption of uranyl ions on silica: Effects of contact time, pH, ionic strength, concentration and phosphate, *J.Radioanal. Nucl. Chem.* **254**, 103.

Horrocks, D.L., Peng L.T. (1971) *Organic scintillators and liquid scintillation counting*, Academic Press, Inc., New York.

Horrocks, W., Sudnick, D. R. (1979) Lanthanide ion probes of structure in Biology. Laser induced luminescence decay constants provide a direct measure of the number of metal-coordinated water molecules. *J. Am. Chem. Soc.* **101**, 334.

Huheey, J. E., Keiter, E.A., Keiter, R.L., Medhi, O.K. (2006) *Some Descriptive Chemistry of the Metals in Inorganic Chemistry Principles of Structure and Reactivity*, Dorling Kindersley, 369.

## **I**

Ishida, K., Kimura, T., Saito, T., Tanaka, S. (2009) Adsorption of Eu(III) on a Heterogeneous Surface studied by Time resolved Laser Fluorescence Microscopy (TRLFM), *Environ. Sci.Technol.* **43**, 1744.

Ishida, K., Saito, T., Aoyagi, N., Kimura, T., Nagaishi, R., Nagasaki, S., Tanaka, S. (2012) Surface speciation of  $\text{Eu}^{3+}$  adsorbed on kaolinite by time-resolved laser fluorescence spectroscopy (TRLFS) and parallel factor analysis (PARAFAC) ,*J. Colloid Interface Sci.* **374**, 258.

**J**

Jain, A., Mohapatra, M., Godbole, S.V., Tomar, B.S. (2008) Time resolved fluorescence spectroscopy of Eu(III) complexation with  $\alpha$  -hydroxyisobutyric acid, *Spectrochim. Acta A* **71**, 1007.

Jain, A., Rawat, N., Kumar, S., Tomar, B. S., Manchanda, V. K., Ramanathan, S. (2007) Effect of humic acid on sorption of neptunium on hematite colloids, *Radiochim. Acta* **95**, 501.

Jain, A., Yadav, K., Mohapatra, M., Godbole, S.V., Tomar, B.S.(2009) Spectroscopic investigation on europium complexation with humic acid and its model compounds, *Spectrochim. Acta A* **72**, 1122.

Jensen, M. P., Choppin, G. R. (1996) Complexation of europium (III) by aqueous orthosilicic acid. *Radiochim. Acta* **72**, 143.

**K**

Kalmykov, S. N., Kriventsov, V. V., Teterin, Y. A., Novikov, A. P. (2007) Plutonium and neptunium speciation bound to hydrous ferric oxide colloids *C.R. Chim.*, **10**, 1060.

- Kalmykov, S. N., Schäfer, T., Claret, F., Perminova, I. V., Petrova (Khasanova), A. B., Shcherbina, N. S., Teterin, Y. A. (2008). Sorption of neptunium onto goethite in the presence of humic acids with different hydroquinone group content *Radiochim. Acta* **96**, 685.
- Kantar, C., Ikizoglu, G., Koleli, N., Kaya, O. (2009) Modeling Cd(II) adsorption to heterogeneous subsurface soils in the presence of citric acid using a semi-empirical surface complexation approach *J. Contam. Hydrol.*, **110**, 100.
- Kar, A. S., Kumar, S., Tomar, B.S. (2012) U(VI) sorption by silica: Effect of complexing anions, *Colloids Surf., A* **395**, 240.
- Kar, A. S., Kumar, S., Tomar, B. S., Manchanda, V. K. (2011 a) Sorption of curium by silica colloids: Effect of humic acid. *J. Hazard. Mater.* **186**, 1961.
- Kar, A. S., Tomar, B. S., Godbole, S. V., Manchanda, V. K. (2011 b) Time resolved fluorescence spectroscopy and modelling of Eu(III) sorption by silica in presence and absence of alpha hydroxyl isobutyric acid. *Colloids Surf. A*: **378**, 44.
- Kar A. S., Tomar, B. S. (communicated) Cm(III) sorption by Silica: Effect of Alpha HydroxyIsobutyric Acid, *Radiochim. Acta*.
- Kato, Y., Meinrath, G., Kimura, T., Yoshida, Z. (1994) A study of U(VI) hydrolysis and carbonate complexation by time-resolved laser-induced fluorescence spectroscopy (TRLFS). *Radiochim. Acta*, **64**, 107.
- Kaushik, C.P., Mishra, R.K., Sengupta, P., Kumar A., Das, D., Kale, G.B., Raj, K. (2006) Barium borosilicate glass – a potential matrix for immobilization of sulfate bearing high-level radioactive liquid waste, *J. Nucl. Mater.* **358**, 129.

- Keeney-Kennicutt, W. L., Morse, J. W. (1985) The redox chemistry of  $\text{Pu(V)O}_2^+$  intercation with common mineral surfaces in dilute solutions and seawater. *Geochim. Cosmochim. Acta.* **49**, 2577.
- Kepak, F. (1971) Adsorption and colloidal properties of radioactive elements in trace concentrations, *Chem. Rev.* **71**, 357.
- Kersting, A. B., Efurud, D. W., Finnegan, D. L., Rokop, D. J., Smith, D. K., Thompson, J. L. (1999) Migration of plutonium in ground water at the Nevada Test Site. *Nature* **397**, 56.
- Kessler, J., (1999) *Colloids in saturated and partially saturated porous media: Approaches to the treatment of colloids in Yucca mountain total system performance assessment* TR112135.
- Khasanova, A.B., Kalmykov S. N., Perminova, I.V., Clark, S.B. (2007) Neptunium redox behavior and sorption onto goethite and hematite in the presence of humic acids with different hydroquinone content, *J. Alloys Compd.* **444**, 491.
- Kim, J. I. (1986) Chemical behaviour of transuranic elements in natural aquatic elements in *Handbook on the physics and chemistry of the actinides*, (Eds.) Freeman, A. J., Keller, C. Elsevier Science, 413.
- Kim J.I. (2006) Significance of actinide chemistry for long term safety of waste disposal, *Nucl. Eng, Technol*, **38(6)**, 459.
- Kimura, T., Choppin, G.R. (1994) Luminescence study on determination of the hydration number of Cm(III), *J. Alloys Compd*, **213**, 313.

- Kimura, T., Kato, Y. (1998) Luminescence study on hydration states of lanthanide (III)–polyaminopolycarboxylate complexes in aqueous solution *J. Alloys Compd*, **275**, 806.
- Klenze, R., Kim, J. I., Wimmer, H. (1991) Speciation of aquatic actinide ions by pulsed laser spectroscopy, *Radiochim. Acta*, **52/53**, 97.
- Klenze, R., Panak, P., Kim, J.I. (1998) A complexation study of Cm(III) and Tb(III) with chelating aromatic ligands by time-resolved laser fluorescence spectroscopy, *J. Alloys Compd*, **271**, 746.
- Knoll, G.F. (2000) *Radiation detection and measurement*, John Willy & sons, New York.
- Kohler, M., Honeyman, B.D., Leckie, J.O. (1999) Neptunium(V) sorption on hematite ( $\alpha$ -Fe<sub>2</sub>O<sub>3</sub>) in aqueous suspension :The effect of CO<sub>2</sub>. *Radiochim. Acta* **85**, 33.
- Kosmulski, M., Maczka, E., Jartych, E., Rosenholm, J.B. (2003) Synthesis and characterization of goethite and goethite – hematite composite: Experimental study and literature survey, *Adv. Colloid Interface Sci.* **103**, 57.
- Krepelova, A.; Brendler, V.; Sachs, S.; Baumann, N.; Bernhard, G. (2007) U(VI)-kaolinite surface complexation in absence and presence of humic acid studied by TRLFS. *Environ. Sci. Technol.*, **41**, 6142.
- Kumar, S. (2012) *Equilibrium and kinetic studies of sorption of actinides and fission products at solid/liquid interface*, Ph.D thesis, Homi Bhabha National Institute, Mumbai, India.

Kumar, S., Godbole, S. V., Tomar, B. S. (2013) Speciation of Am(III)/Eu(III) sorbed on  $\gamma$ -Alumina: Effect of metal concentration, *Radiochim. Acta*.**101**, 73.

Kumar, S., Tomar, B.S., Ramanathan, S., Manchanda, V.K. (2006) Effect of humic acid on cesium sorption on silica colloids, *Radiochim. Acta* **94**, 369.

Kumar, A., Varshney, L., Bhalerao, P., Kaushik C. P., Raj, K. (2008), Evaluation of ALIX as an ion exchanger for selective separation of Cs from acidic solution. *Emerging Trends in Separation Science and Technology, (SESTEC)* 179.

**L**

Lakowicz, J. R. (2006) *Principles of fluorescence spectroscopy*, Springer Science Business Media LLC, New York, USA.

Ledin, A., Karlsson, S., Duker, A., Allard, B. (1994) The adsorption of europium to colloidal iron oxyhydroxides and quartz- the impact of pH and an aquatic fulvic acid, *Radiochim. Acta* **66**, 213.

Lefevre, G., Kneppers, J., Fedoroff, M. (2008) Sorption of uranyl ions on titanium oxide studied by ATR-IR spectroscopy, *J. Colloid Interface Sci.*,**327**, 15.

Lehmann, S., G. Geipel, H. Foerstendorf, G. Bernhard (2008) Syntheses and spectroscopic characterization of uranium(VI) silicate minerals, *J. Radioanal. Nucl. Chem*, **275**, 633.

Lenhart, J. J., Cabaniss, S. E., MacCarthy, P., Honeyman, B. D. (2000) Uranium (VI) complexation with citric, humic and fulvic acids. *Radiochim. Acta* **88**, 345.

- Li, D., Kaplan, D. I. (2012) Sorption coefficients and molecular mechanisms of Pu, U, Np, Am and Tc to Fe (hydr)oxides: A review, *J.Hazard. Mater.* **243**, 1.
- Li, W., Tao, Z. (2003) Comparative study on Np(V) sorption on oxides of aluminum and silicon: effects of humic substance and carbonate in solution, *J. Colloid Interface Sci.* **267**, 25.
- Li, X.L., Chen, C.L., Chang, P.P., Yu, S.M., Wu, W.S., Wang, X.K. (2009) Comparative studies of cobalt sorption and desorption on bentonite, alumina and silica: effect of pH and fulvic acid, *Desalination* **244**, 283.
- Liu, A., Gonzalez, R. D. (2001) Adsorption/Desorption in a System Consisting of Humic Acid, Heavy Metals, and Clay Minerals, *J. Colloid Interface Sci.* **238**, 219.
- Lu, N., Reimus, P. W., Parker, G. R., Conco, J. L., Triay, I. R. (2003) Sorption kinetics and impact of temperature, ionic strength and colloid concentration on the adsorption of plutonium-239 by inorganic colloids. *Radiochim. Acta* **91**, 713.

**M**

- Macasek, F., Shaban, I.S., Matel, L. (1999) Cesium, strontium, europium(III) and plutonium (IV) complexes with humic acid in solution on montmorillonite surface, *J.Radioanal. Nucl. Chem* **241**, 627.
- Manning, P. G. (1967), Europium tartronate and mandelate ion association in water, *Canadian. J. Chem*, **45**, 1643.
- Marmier, N. (2002) *Metal ion adsorption on silica, alumina and related surfaces*, Encyclopedia of Colloids and Surfaces, Marcel Dekker, Inc, 3265.

- Marmier, N., Fromage, F. (1999) Comparing electrostatic and nonelectrostatic surface complexation modelling of the sorption of Lanthanum on hematite. *J. Colloid Int. Sci.* **212**, 252 .
- Marquardt, C., Hermann, G., Trautmann, N. (1996) Complexation of neptunium (V) with humic acids at very low metal concentrations. *Radiochim. Acta* **73**, 119.
- Martell, A.E., Smith, R.M. (1977) *Critical Stability Constants: Other Organic Ligands*, vol.3, Plenum Press, New York.
- Mercier, F., Alliot, C., Bion, L., Thromat, N., Toulhoat, P. (2006) XPS study of Eu(III) coordination compounds: Corelevels binding energies in solid mixed-oxo-compounds  $\text{Eu}_m\text{X}_x\text{O}_y$ . *J. Electron Microsc. Rel. Phenom.* **150**, 21.
- Missana, T., Gutiérrez, M. G., Maffiotte, C. (2003) Experimental and modeling study of the uranium (VI) sorption on goethite, *J. Colloid Interface Sci.* **260**, 291.
- Monsallier, J.M., Artinger, R., Denecke, M.A., Scherbaum, F.J., Buckau, G., Kim, J.I. (2003) Spectroscopic study (TRLFS and EXAFS) of the kinetics of An(III)/Ln(III) humate interaction *Radiochim. Acta* **91**, 567.
- Montavon, G., Markai, S., Billard, I., Nehlig, A., Grambow, B. (2002) Complexation and luminescence spectroscopic studies of europium(III) with polymaleic acid, *Radiochim. Acta* **90**, 289.
- Morel, F. M. M. (1983) *Principles of aquatic chemistry*. Wiley, New York.
- Morel, F. M. M., Morgan, J. J. (1971) A Numerical method for computing equilibria in aqueous chemical systems. *Environ. Sci. Technol.* **6**, 58 - 67.

Moulin, C., Larpent, C., Gazeau, D. (1999) Interaction studies between europium and a surfactant cage "TAC8" by time-resolved laser-induced fluorescence, *Anal. Chim. Acta* **378**, 47.

Moulin, C., Laszak, I., Moulin, V., Tonder, C. (1998) Time-resolved laser-induced fluorescence as a unique tool for low-level uranium speciation. *Appl. Spectrosc.*, **52**, 528.

N

Nagasaki, S., Tanaka, S., Suzuki, A. (1997) Interfacial behavior of actinides with colloids in the geosphere, *J. Nucl. Mater.* **248**, 323.

Nagasaki, S., Tanaka, S., Todoriki, M., Suzuki, A. (1998) Surface sorption and surface diffusion of  $\text{NpO}_2^+$  with poorly crystallized ferric oxide, *J. Alloys Compd* **271–273**, 252.

Nakata, K., Nagasaki, S., Tanaka, S., Sakamoto, Y., Tanaka, T., Ogawa, H. (2001) Sorption of neptunium on surface of magnetite, *Stud. Surf. Sci. Catal.*, **132**, 885.

Nakata, K., Nagasaki, S., Tanaka, S., Sakamoto, Y., Tanaka, T., Ogawa, H. (2002) Sorption and reduction of neptunium(V) on the surface of iron oxides. *Radiochim. Acta* **90**, 665.

Nakata, K., Nagasaki, S., Tanaka, S., Sakamoto, Y., Tanaka, T., Ogawa, H. (2004) Reduction rate of neptunium(V) in heterogeneous solution with magnetite. *Radiochim. Acta* **92**, 145.

- Nakayama, S., Sakamoto, Y. (1991) Sorption of neptunium on naturally- occurring iron -containing minerals. *Radiochim. Acta* **52/53**, 153.
- Nash, K. L., Madic, C., Mathur, J. N., Lacquement, J. (2006) Actinide Separation Science and technology, in *The Chemistry of Actinide and Transactinide Elements*, (Eds.) L.R.Morss, N.K.Edelstein, and J.Fuger, Springer, 2622.
- Neck, V., Altmaier, M., Fanghanel, T. (2007) Solubility of plutonium hydroxides/hydrous oxides under reducing conditions and in the presence of oxygen, *C R Chim.*, **10**, 959.
- Neck, V., Kim, J. I., Seidel, B. S., Marquardt, C. M., Dardenne, K., Jensen, M. P., Hauser, W. A. (2001) Spectroscopic study of the hydrolysis, colloid formation and solubility of Np(IV) *Radiochim. Acta*, **89**, 439.
- Nero, M. D., Galindo, C., Barillon, R., Benoit, M. (2011) TRLFS evidence for precipitation of uranyl phosphate on the surface of alumina: environmental implications *Environ. Sci. Technol.*, **45**, 3982.
- Neroa, M.D., Assadaa, A., Made, B., Barillona, R., Duplatrea, G. (2004) Surface charges and Np(V) sorption on amorphous Al and Fe silicates, *Chem. Geol.* **211**, 15.
- Niitsu, Y., Sato, S., Ohashi, H., Sakamoto, Y., Nagao, S., Ohnuki, T., Muraoko, S. (1997) Effects of humic acid on the sorption of neptunium (V) on kaolinite. *J. Nucl. Mat.* **248**, 328.
- Novikov, A. P., Kalmylov, S. N., Utsunomiya, S., Ewing, R. C., Horreard, F., Merkulov, A., Clark, S. B., Tkachev, V. V., Myasoedov, B. F. (2006) Colloid

transport of plutonium in the far-field of the Mayak production association, Russia.  
*Science*, **314**, 638.

**Q**

Osthols, E. (1995) Thorium sorption on amorphous silica, *Geochim. Cosmochim. Acta* **59**, 1235 -1249.

Ozaki, T., Arisaka , M., Kimura , T., Francis , A. J., Yoshida, Z. (2002) Empirical method for prediction of the coordination environment of Eu(III) by time-resolved laser-induced fluorescence spectroscopy, *Anal. Bioanal. Chem* **374**, 1101.

**P**

Panak, P. J., Kim, M.A., Klenze, R., Kim, J.I., Fanghanel, Th. (2005) Complexation of Cm(III) with aqueous silicic acid, *Radiochim. Acta* **93**, 133.

Panak, P., Klenze, R., Kim, J.I. (1996) A study of ternary complexes of Cm (III) with humic acid and hydroxide or carbonate in neutral pH range by time resolved laser fluorescence spectroscopy, *Radiochim. Acta*.**74**, 141.

Pathak, P.N., Choppin, G.R. (2006) Sorption studies of europium(III) on hydrous silica, *J.Radioanal. Nucl. Chem.* **270**, 277.

Pathak, P.N., Choppin, G.R. (2007 a) Effect of complexing anions on Europium sorption on suspended silica: a TRLFS study for ternary complex formation, *Radiochim. Acta.* **95** ,267.

- Pathak P.N., Choppin, G.R. (2007 b) Kinetics and thermodynamics of U(VI)(VI) sorption on hydrous silica, *Radiochim. Acta* **98**, 507.
- Pathak, P.N., Choppin, G.R. (2007 c) Sorption of uranyl(VI) cations on suspended silicate: effects of N-donor ligands, carboxylic acids, organic cosolvents, and metal ions, *Radiochim. Acta* **95**, 245.
- Pathak, P. N., Choppin, G. R. (2007 d) Sorption of neptunyl(V) cations on suspended silicate: Effects of pH, ionic strength, complexing anions, humic acid, and metal ions, *J. Radioanal. Nucl. Chem.*, **274**, 53.
- Patra, C. Mohapatra, S., Sahoo, S. K., Lenka, P., Dubey, J. S., Tripathi R. M., Puranik V. D. (2013) Age-dependent dose and health risk due to intake of uranium in drinking water from Jaduguda, India, *doi:10.1093/rpd/ncs328*
- Payne, T.E. (1999) *U(VI) interactions with mineral surfaces: controlling factors and surface complexation modeling*, Ph. D Thesis, University of South Wales.
- Payne, T.E, Davis, J.A, Waite, T.D (1996) U(VI) Adsorption on Ferrihydrite - Effects of Phosphate and Humic Acid, *Radiochim. Acta* **74**, 239.
- Peña-Méndez, E. M., Havel, J., Patočka, J. (2005) Humic substances: compounds of still unknown structure: applications in agriculture, industry, environment, and biomedicine, *J. Appl. Biomed.* **3**, 13.
- Penrose, W.R., Polzer, W.L., Essington, E.H., Nelson, D.M., Orlandini, K.A. (1990) Mobility of plutonium and americium through a shallow aquifer in a semiarid region, *Environ. Sci. Technol.* **24**, 228.

- Perminova, I.V., Karpiouk, L.A., Shcherbina, N.S., Ponomarenko, S.A., Kalmykov, S.N., Hatfield, K. (2007) Preparation and use of humic coatings covalently bound to silica gel for Np(V) and Pu(V) sequestration, *J. Alloys Compd* **444–445**, 512.
- Piasecki, W., Sverjensky, D. A. (2008) Speciation of adsorbed yttrium and rare earth elements on oxide surfaces. *Geochim. Cosmochim. Acta* **72**, 3964.
- Plancque, G., Maurice, Y., Moulin, V., Toulhoat, P., Moulin, C. (2005) On the use of spectroscopic techniques for interaction studies, Part I: Complexation between europium and small organic ligands, *Appl. Spectrosc.* **59**, 432.
- Plancque, G., Moulin, V., Toulhoat, P., Christophe, M. (2003) Europium speciation by time-resolved laser-induced fluorescence, *Anal. Chim. Acta*, **478**, 11.
- Portanova, R., Lajunen, L.H., Tolazzi, M., Piispanen, J. (2003) Critical evaluation of stability constants for  $\alpha$ -hydroxycarboxylic acid complexes with protons and metal ions and the accompanying enthalpy changes\*\*Part II. Aliphatic 2-hydroxycarboxylic Acids\*\*\* (iupac technical report). *Pure Appl. Chem.* **75**, 495.
- Pusch, R. (1998) “Backfilling with mixture of bentonite/ballast materials or natural smectite clay”. Swedish Nuclear Fuel and Waste management Co. (SKB), Stockholm. Technical report, Tr-98-16.

**R**

- Rabung, Th., Geckeis, H., Kim, J., Beck, H. P. (1998) Sorption of Eu(III) on a natural hematite: application of a surface complexation model. *J. Colloid Int. Sci.* **208**, 153-161.

- Rabung, Th., Geckeis, H., Wang, X. K., Rothe, J., Denecke, M. A., Klenze, R. (2006) Th. Fanghanel, Cm(III) sorption onto  $\gamma$ -Al<sub>2</sub>O<sub>3</sub>: New insight into sorption mechanism by time-resolved laser fluorescence spectroscopy and extended X-ray absorption fine structure. *Radiochim. Acta.* **94**, 609 - 618.
- Rabung, Th., Pierret, M.C., Bauer, A., Geckeis, H., Bradbury, M.H., Baeyens, B. (2005) Sorption of Eu(III) / Cm(III) on Ca-montmorillonite and Na-illite. Part 1: Batch sorption and time-resolved laser fluorescence spectroscopy experiments, *Geochim. Cosmochim. Acta* **69**, 5393.
- Rabung, Th., Schild, D., Geckeis, H., Klenze, R., Fanghanel, Th. (2004) Cm(III) sorption onto sapphire ( $\alpha$ -Al<sub>2</sub>O<sub>3</sub>) single crystals. *J. Phys. Chem. B* **108**, 17160 - 17163.
- Rabung, Th., Stumpf, Th., Geckeis, H., Klenze, R., Kim, J. I. (2000) Sorption of Am(III) and Eu(III) onto  $\gamma$ -alumina: experiment and modelling. *Radiochim. Acta* **88**, 711.
- Rai, D., Ryan, J. L. (1982) Crystallinity and solubility of Pu(IV) oxide and hydrous oxide in aged aqueous suspensions, *Radiochim. Acta* **30**, 213.
- Rai, D., Serne, R. J., Swanson, J. L. (1980) Solution species of plutonium in the environment, *J. Environ. Qual.* **9**, 417.
- Raj, K., Prasad, K.K., Bansal, N.K. (2006) Radioactive waste management practices in India, *Nucl. Eng. Des.* **236**, 914.
- Ramsay, D.A. (1988) The role of colloids in the release of radionuclides from nuclear waste, *Radiochim. Acta* **44/45**, 165.

- Rattan, S.S., Reddy, A.V.R., Mallapurkar, V.S., Singh, R.J., Prakash, S. (1981) A method for the simultaneous estimation of  $^{228}\text{Th}$  and  $^{229}\text{Th}$ , *J. Radioanal. Nucl.Chem.* **67**, 95.
- Redden, G., Bargar, J., Latmani, R.B. (2001) Citrate enhanced uranyl adsorption on goethite, *J. Colloid Interface Sci.* **244**, 211.
- Reed, D.T., Clark, S.B., Rao, L.F. (1999) *Actinide Speciation in High Ionic Strength Media: Experimental and Modeling approaches to predicting Actinide Speciation*, Kluwer Academic/ Plenum Publishers, New York.
- Reich, T.; Moll, H.; Denecke, A.; Geipel, G.; Bernhard, G.; Mitche, H; Allen, P.G.; Bucher, J.J.; Kaltsoyannis, N.; Edelstein, N.M.; Shuh, D.K. (1996) Characterization of hydrous uranyl silicate by EXAFS. *Radiochim. Acta*, **74**, 219.
- Reiller, P., Casanova, F., Moulin, V. (2005) Influence of addition order and contact time on thorium(IV) retention by hematite in the presence of humic acids. *Environ. Sci. Technol.* **39**, 1641.
- Righetto, L., Bidoglio, G., Aziminoti, G., Bellobono, I. R. (1991) Competitive actinide interactions in colloidal humic acid-mineral oxide systems. *Environ. Sci. Technol.* **25**, 1913.
- Runde, W. (2000) *The Chemical Interactions of Actinides in the Environment*. In Los Alamos Science (ed.) N. G. Cooper, Los Alamos National Laboratory, Los Alamos, NM.
- Runde, W., Conradson, S.D., Wes Efur, D., Lu, N., Vanpelt, C.E., Drew Tait, C. (2002) Solubility and sorption of redox –sensitive radio nuclides (Np, Pu) in J-13

- water from the Yucca Mountain Site: comparison between experiment and theory. *Appl. Geochem.* **17**, 837.
- Runde, W., Neu, M. P. (2006) Actinides in geosphere in *The chemistry of the actinide and transactinide elements*, (ed.) Morss, L. R., Edelstein, N. K., Fuger, J., Springer, 3475.
- S**
- Sachs, S., Bernhard, G. (2005) NIR spectroscopic Study of complexation of neptunium(V) with humic acids: influence of phenolic OH groups on the complex formation, *Radiochim. Acta* **93**, 141.
- Sakamoto, Y., Nagao, S., Ogawa, H., Rao, R.R. (2000) The migration behavior of Np(V) in sandy soil and granite media in the presence of humic substances. *Radiochim. Acta.* **88**, 651.
- Sakamoto, Y., Toshihiko, O., Senoo, M. (1994) Redistribution of neptunium(V) during the alteration of ferrihydrite. *Radiochim. Acta* **66/67**, 285.
- Sakuragi, T., Sato, S., Kozaki, T., Mitsugashira, T., Hara, M., Suzuki, Y. (2004) Am(III) and Eu(III) uptake on hematite in the presence of humic acid. *Radiochim. Acta* **92**, 697.
- Samadfam, M., Jintoku, T., Sato, S., Ohashi, H., Mitsugashira, T., Hara, M., Suzuki, Y. (2000) Effects of humic acid on the sorption of Am(III) and Cm(III) on kaolinite. *Radiochim. Acta* **88**, 717.

- Samadfam, M., Sato, S., Ohashi, H. (1998) Effects of humic acid on the sorption of Eu(III) onto kaolinite, *Radiochim. Acta* **82**, 361.
- Sanchez, A. L., Murray, J. W., Sibley, T. H. (1985) The adsorption of plutonium IV and V on goethite. *Geochim. Cosmochim. Acta* **49**, 2297.
- Schafer, T., Huber, F., Seher, H., Missana, T., Alonso, U., Kumke, M., Eidner, S., Claret, F., Enzmann, F. (2012) Nanoparticles and their influence on radionuclide mobility in deep geological formations, *Appl. Geochem.* **27**, 390.
- Schlegel, M. L., Pointeau, I., Coreau, N., Reiller, P. (2004) Mechanism of europium retention by calcium silicate hydrate: An EXAFS study. *Environ. Sci. Technol.* **38**, 4423 - 4431.
- Schmeide, K., Bernhard, G. (2010) Sorption of Np(V) and Np(IV) onto kaolinite: Effects of pH, ionic strength, carbonate and humic acid, *Appl. Geochem.* **25**, 1238.
- Seaborg G.T. (1949) Place in periodic system and electronic structure of the heaviest elements, *Nucleonics* **5**, 16.
- Seaborg G. T., Katz J. J. (1954) *The Actinide elements*, McGraw – Hill book company, Inc.
- Shalinets, A. B. (1971) Complexing of trivalent actinide and lanthanide elements studied by electromigration. XI. Stability of complexes to strong acid. *Radiokhimiya* **13**, 566.
- Silva, R. J., Nitsche, H. (1995) Actinide environmental chemistry, *Radiochim. Acta* **70/71**, 377.

- Simoni, E. (2002) Radionuclides retention: from macroscopic to microscopic, *C. R. Phys.* **3**, 987.
- Singh, A., Ulrich, K.U., Giammar, D. E. (2010) Impact of phosphate on U(VI) immobilization in the presence of goethite. *Geochim. Cosmochim. Acta* **74**, 6324.
- Snow, M. S., Zhao, P., Dai, Z., Kersting, A. B., Zavarin, M. (2013) Neptunium(V) sorption to goethite at attomolar to micromolar concentrations, *J. Colloid Interface Sci.* **390**, 176.
- Srinivasan, N., Nadkarni, M.N., Balasubramanian, G.R., Chitnis R.T., Siddiqui, H.R. (1972). *Pilot plant for separation of U-233 at Trombay*, BARC Report, Report-643, Bhabha Atomic Research Centre, Mumbai, India.
- Stamberg, K., Venkatesan, K.A., Rao, P.R.V. (2003) Surface complexation modeling of uranyl ion sorption on mesoporous silica. *Colloids Surf., A* **221**, 149.
- Stevenson, F. J. (1982) *Humus Chemistry: Genesis, Composition, Reactions*. John Wiley & Sons.
- Strickland, E. (2011) *Explainer "What went wrong in Japan's nuclear reactors"* IEEE Spectrum. 4 April
- Strobel, B. W. (2001) Influence of vegetation on low-molecular-weight carboxylic acids in soil solution—a review, *Geoderma* **99**, 169
- Stumm, W., Huang, C. P., Jenkins, S. R. (1970) Specific chemical interactions affecting the stability of dispersed system, *Croat. Chem. Acta* **42**, 223.

Stumm, W., Morgan, J. J. (1996) *Aquatic chemistry: Chemical Equilibria and rates in natural waters*. Wiley, New York.

Stumpf, S., Stumpf, Th., Lutzenkirchen, J., Walther, C., Fanghanel, Th. (2004) Immobilization of trivalent actinides by sorption onto quartz and incorporation into siliceous bulk: investigations by TRLFS, *J. Colloid Interface Sci.* **318**, 5.

Stumpf, T., Curtius, H., Walther, C., Dardenne, K., Ufer, K., Fanghanel, T. (2007) Incorporation of Eu(III) into hydrotalcite: A TRLFS and EXAFS study, *Environ. Sci. Technol.* **41**, 3186.

Stumpf, T., Fanghanel, T., Grenthe, I. (2002) Complexation of trivalent actinide and lanthanide ions by glycolic acid: a TRLFS study *Dalton Trans.* **20**, 3799.

Sylwester, E.R., Hudson, E.A., Allen, P.G. (2000) The structure of U(VI) sorption complexes on silica, alumina and montmorillonite, *Geochim. Cosmochim. Acta* **64**, 2431.

## T

Takahashi, Y., Kimura, T., Kato, Y., Minai, Y., Tominaga, T. (1998) Characterization of Eu(III) species sorbed on silica and montmorillonite by laser induced fluorescence spectroscopy. *Radiochim. Acta* **82**, 227.

Takahashi, Y., Kimura, T., Minai, Y. (2002) Direct observation of Cm(III)-fulvate species on fulvic acid – montmorillonite hybrid by laser- induced fluorescence spectroscopy, *Geochim. et Cosmochim. Acta*, **66**, 1.

- Takahashi, Y., Murata, M., Kimura, T. (2006) Interaction of Eu(III) ion and non porous silica: Irreversible sorption of Eu(III) on silica and hydrolysis of silica promoted by Eu(III), *J. Alloys Compd.* **408-412**, 1246.
- Tan, X., Fan, Q., Wang, X., Grambow, B. (2009) Eu(III) sorption to TiO<sub>2</sub> (anatase and rutile): Batch, XPS, and EXAFS studies, *Environ. Sci. Technol.* **43**, 3115.
- Tan, X., Fang, M., Wang, X. (2010) Sorption Speciation of Lanthanides/Actinides on Minerals by TRLFS, EXAFS and DFT Studies: A Review, *Molecules* **15**, 8431.
- Tan, X. L., Wang, X. K., Geckeis, H., Rabung, Th. (2008) Sorption of Eu(III) on Humic Acid or Fulvic Acid Bound to Hydrous Alumina Studied by SEM-EDS, XPS, TRLFS, and Batch Techniques, *Environ. Sci. Technol.* **42**, 6532.
- Teterin, A.Y., Maslakov, K.I., Teterin, Y.A., Kalmykov, S.N., Ivanov, K.E., Vukcevic, L., Khasanova, A.B., Shcherbina, N.S. (2006) Interaction of neptunyl with goethite (alpha-FeOOH), maghemite (gamma-Fe<sub>2</sub>O<sub>3</sub>), and hematite (alpha-Fe<sub>2</sub>O<sub>3</sub>) in water as probed by X-ray photoelectron spectroscopy, *Russ. J. Inorg. Chem.* **51**, 1937.
- Tertre, E., Berger, G., Simoni, E., Castet, S., Giffaut, E., Loubet, M., Catallete, H. (2006) Europium retention onto clay minerals from 25 to 150<sup>0</sup>C: Experimental measurements, spectroscopic features and sorption modeling, *Geochim. Cosmochim Acta* **70**, 4563.
- Thomason, J.W., Susetyo, W., Carreira, L.A. (1996) Fluorescence Spectroscopy of metal humic complexes with the use of lanthanide ion probe spectroscopy, *Appl. Spectrosc.* **50**, 401.

- Tinnacher, R. M., Zavarin, M., Powell, B. A., Kersting, A. B. (2011) Kinetics of neptunium(V) sorption and desorption on goethite: An experimental and modeling study, *Geochim. Cosmochim. Acta* **75**, 6584.
- Tits, J., Geipel, G., Macé, N., Eilzer, M., Wieland, E. (2011) Determination of uranium(VI) sorbed species in calcium silicate hydrate phases: A laser-induced luminescence spectroscopy and batch sorption study, *J. Colloid Interface Sci.* **359**, 248.
- Tits, J., Wieland, E., Bradbury, M. H. (2005) The effect of isosaccharinic acid and gluconic acid on the retention of Eu(III), Am(III) and Th(IV) by calcite. *Appl. Geochem.* **20**, 2082.
- Tochiyama, O., Endo, S., Inoue, Y. (1995) Sorption of Neptunium(V) on various iron oxides and Hydrrous iron oxides, *Radiochim. Acta* **68**, 105.
- Tochiyama, O., Yoshino, H., Kubota, T., Sato, M., Tanaka, K., Niibori, Y., Mitsugashira, T.: (2000) Complex formation of Np(V) with humic acid and polyacrylic acid. *Radiochim. Acta* **88**, 547.
- Toraishi, T., Aoyagi, N., Nagasaki, S., Tanaka, S. (2004) Stoichiometry, stability constants and coordination geometry of Eu(III) 5-sulfosalicylate complex in aqueous system—A TRLIFS study, *Dalton Trans.*, **21**, 3495.

**W**

- Wang, X. K., Dong, W. M., Dai, X. X., Wang, A. X., Du, J. Z., Tao, Z. Y. (2000) Sorption and desorption of Eu and Yb on alumina: mechanisms and effect of fulvic acid. *Appl. Radiat. Isot.* **52**, 165.

Wang, X. K., Rabung, Th., Geckeis, H., Panak, P. J., Klenze, R., Fanghänel, Th. (2004) Effect of humic acid on the sorption of Cm(III) onto  $\gamma$ -Al<sub>2</sub>O<sub>3</sub> studied by the time-resolved laser fluorescence spectroscopy, *Radiochim. Acta*, **92**, 691.

Wang, Z.M., Van de Burgt, L. J., Choppin, G.R. (1999) Spectroscopic study of lanthanide(III) complexes with carboxylic acids, *Inorg. Chim. Acta*, **293**, 167.

Wang, Z.M., Van de Burgt L.J., Choppin, G.R. (2000) Spectroscopic study of lanthanide(III) complexes with aliphatic dicarboxylic acids, *Inorg. Chim. Acta* **310**, 248.

Wang, Z., Zachara, J. M., Gassman, P. L., Liu, C., Qafoku, O., Yantasee, W., Catalano, J. G. (2005) Fluorescence spectroscopy of U(VI)-silicates and U(VI)-contaminated Hanford sediment, *Geochim. Cosmochim. Acta*, **69**, 1391.

Wimmer, H., Kim, J.I., Klenze, R. (1992) A direct speciation of Cm (III) in natural aquatic system by time resolved laser induced fluorescence spectroscopy, *Radiochim. Acta*, **58/59**, 165.

## X

Xu, D., Shao, D.D., Chen, C.L., Ren, A.P., Wang, X.K. (2006 a) Effect of pH and fulvic acid on sorption and complexation of cobalt onto bare and FA bound MX-80 bentonite, *Radiochim. Acta* **94**, 97.

Xu, D., Wang, X. K., Chen, C. L., Zhou, X., Tan, X. L. (2006 b) Influence of soil humic acid and fulvic acid on sorption of thorium(IV) on MX-80 bentonite, *Radiochim. Acta* **94**, 429.

**Z**

- Zachara, J. M., Resch, C. T., Smith, S. C. (1994) Influence of humic substances on  $\text{Co}^{2+}$  sorption by a subsurface mineral separate and its minealogenic components. *Geochim. Cosmochim. Acta* **58(2)**, 553.
- Zaera, F. (2012) Probing liquid/solid interfaces at the molecular level. *Chem. Rev.* **112**, 2920.